STUDIA UNIVERSITATIS
BABEŞ-BOLYAI

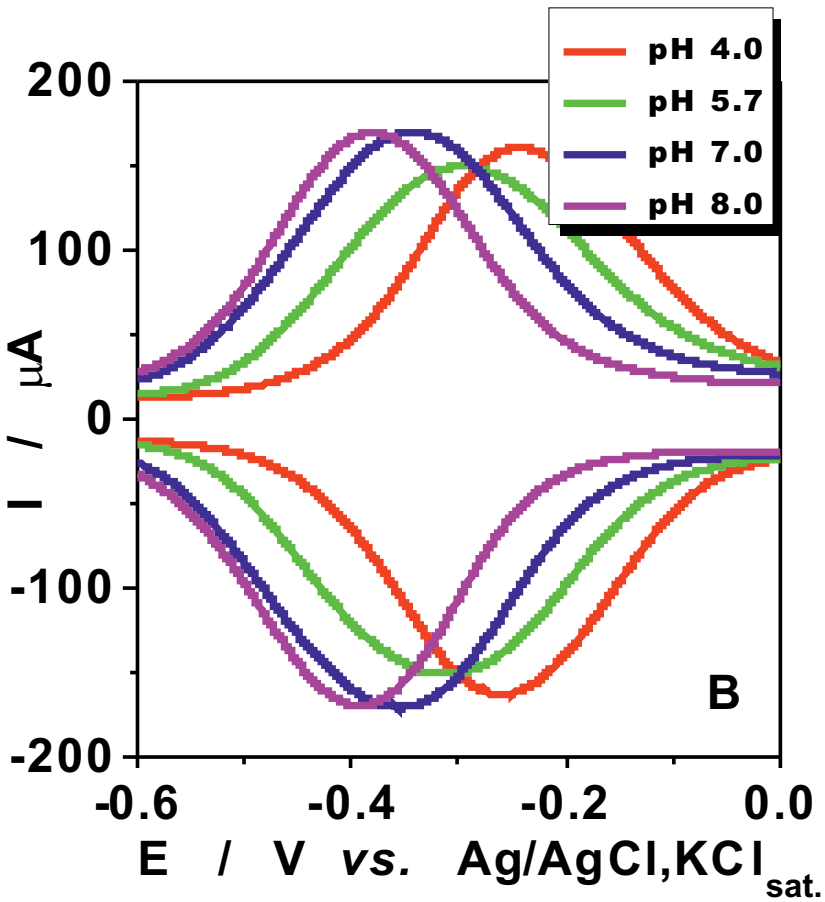

CHEMIA

2/2013

STUDIA
UNIVERSITATIS BABEŞ-BOLYAI

CHEMIA

2/2013

http://chem.ubbcluj.ro/~studiachemia/; studiachemia@chem.ubbcluj.ro
http://www.studia.ubbcluj.ro/serii/chemia/index_en.html

YEAR **Volume 58 (LVIII) 2013**
MONTH **JUNE**
ISSUE **2**

S T U D I A
UNIVERSITATIS BABEŞ–BOLYAI
CHEMIA
2

Desktop Editing Office: 51ST B.P. Hasdeu, Cluj-Napoca, Romania, Phone + 40 264-40.53.52

CUPRINS – CONTENT – SOMMAIRE – INHALT

Studia Universitatis Babes-Bolyai Chemia has been selected for coverage in Thomson Reuters products and custom information services. Beginning with V. 53 (1) 2008, this publication is indexed and abstracted in the following:

- Science Citation Index Expanded (also known as SciSearch®)
- Chemistry Citation Index®
- Journal Citation Reports/Science Edition

STUDIA UBB CHEMIA, LVIII, 2, 2013 (p. 7 – 22)
(RECOMMENDED CITATION)

SYNTHESIS OF TRIPROPIONIN FROM CRUDE GLYCEROL THE BY-PRODUCT OF BIODIESEL PRODUCTION

ZSANETT HERSECZKI[a], GYULA MARTON[a], ANDRAS DALLOS[a]

ABSTRACT. Glycerol is a by-product obtained during the production of biodiesel. An increase in biodiesel production would decrease the market price of glycerol. The objective of this study was to investigate glycerol purification, esterification of glycerol by propionic acid and the field of application of the product. Crude glycerol from a Hungarian biodiesel factory was partly refined, soaps, water, methanol and pigments were removed and glycerol still containing inorganic salts was used for certain esterification reactions. A cost effective process for utilization of crude glycerol was created, which can be applied not only for tripropionin production but preparation of other glycerol esters like glyceryl triacetate, glyceryl tributyrate. Moreover, effect of tripropionin blending on engine performance characteristics and environmental repercussions were studied.

Keywords: *glycerol, biodiesel, tripropionin, fuel additives, oxygenate*

INTRODUCTION

Biodiesel produced by the transesterification of vegetable oils or animal fats with short-chain alcohols (typically methanol) is a promising alternative fuel for diesel engines, because of the limited resources of fossil fuels and environmental concerns [1].

Ideally, three molecules of fatty acid methyl esters (FAME) and one molecule of glycerol are formed when starting from any molecule of a triglyceride (TG) and three moles of methanol [2].

Crude glycerol (G-phase) as an unrefined residue of the biodiesel synthesis shows usually a content of glycerol varying between 30 wt% and 60 wt%. The larger biodiesel plants tend to give the highest “purities”, often around 75 wt% to 90 wt% [3]. The rest of the “crude glycerol” consists primarily of remaining, unconverted triglycerides, unreacted methanol, some dissolved biodiesel, fatty acids, alkali hydroxides, different semi-saponified triglycerides,

[a] *University of Pannonia, H-8200 Veszprem, POB 158, Hungary, herseczki@freemail.hu*

alkali salts of fatty acids, water, pigments and some other remains of the vegetables originated by the oil production.

Fact is that approximately 15-20% of the converted feedstock is released as crude glycerol. The accumulation of crude glycerol not only hampers the development of the biodiesel industry, but it also creates economic and environmental problems [4].

It was projected that the world biodiesel market would reach 168 million tons by 2016, which implied that approximately 25 million tons of crude glycerol would be produced [5]. Too much surplus of crude glycerol from biodiesel production will impact the refined glycerol market [6]. For example, in 2007, the refined glycerol's price was rather low, approximately $0.66 per kg (compared to $1.55 before the expansion of biodiesel production) in the United States. Accordingly, the price of crude glycerol decreased from about $0.55 per kg to $0.11 per kg [7].

Glycerol from biodiesel production is widely recognized as a waste stream, the disposal of which has become a heavy load for the biodiesel plants.

The application of common base technologies like distillation, filtration, extraction, incineration, but even biologically waste treatment of “crude glycerol” is becoming hampered for numerous reasons. These processes are very expensive and exhibit a low yield [8].

Therefore, to release the pressure from the flooded glycerol market nowadays, the development of processes to convert glycerol to commodity chemicals with larger markets than traditional ones capable of absorbing a great part of the newly produced glycerol is becoming increasingly urgent. Some of these strategies include selective reduction – hydrogenolysis to propylene glycol, dehydroxylation to 1,3-propanediol-, halogenation to obtain epichlorohydrin, dehydration to produce acrolein, acrylic acid or 3-hydroxypropionaldehyde and selective oxidation [9]. Meanwhile developing the technology of glycerol conversion to high value products will also add value to the production of biodiesel [10]. Among different alternatives, the esterification of glycerol with propionic acid to yield tripropionin as a valuable transportation fuel additive is such an option.

The research line, described in the present work, is focusing on purification of crude glycerol and the synthesis process for converting partly purified glycerol in to tripropionin. Influences of raw materials (different glycerol qualities), reaction conditions were investigated and optimized.

RESULTS AND DISCUSSION

Purification of crude glycerol

During our experiments we have made some general observations for the purification process:

- The high viscosity of the crude glycerol is hampering the handling of this phase by enhanced force on pumps and agitators. The increase of the processing temperature can be a solution for this problem.
- The presence of methanol and other light components is of advantage to reduce the viscosity.
- A dilution of crude glycerol by ~25% water was found to be optimal for viscosity reduction.

Dilution by water and acid treatment

The effect of dilution of crude glycerol by water was investigated. The glycerol phase was diluted by 20, 25, 30 and 50% water, thereafter heated up to 80°C and the neutralization process with H_3PO_4 was started. The reaction of an acid with the soaps gives free fatty acids (FFA). Since FFA's are insoluble in glycerol, these components will rise to the top so that they can be skimmed off. Some glycerol-insoluble salts will also precipitate out.

The reaction mixture showed heavy foaming between pH 11 and 6. After a stirring time of 30 minutes it was allowed to settle. Thereafter, the reaction mixture formed three layers:

1. a top layer containing free fatty acids
2. a middle layer which is the glycerol-rich layer
3. a bottom inorganic salt rich precipitate.

The layers were separated by simple phase separation.

The quantity of water, used for dilution does not influence the phase separation. The handling of the crude G-phase is easier in case of higher water dilution but it would increase the cost of purification. Nevertheless a dilution by 25% water seemed to be optimal and this quantity was used in the following experiments.

Table 1. Effect of pH on phase separation after acid treatment of G-phase

	pH		
	2	**3**	**4**
Time (min) necessary for phase separation	20	**30**	100
Clearance of phase boundary	++	**+++**	+

Also, the influence of pH was investigated. As Table 1 demonstrates at pH value of 4 a diffuse phase formed at the border of the layers and almost two hours were needed for separation. The clearest phase boundary between the two layers was obtained at pH value of 3, it was found to be the optimum during acid treatment.

Neutralization by $Ca(OH)_2$

The excess of the phosphoric acid was neutralized by a 25 wt% $Ca(OH)_2$ aqueous slurry. The lowest solubilities of phosphates in crude glycerol were seen to exist near a pH value of 5. The effect of pH (pH=6 and pH=7) was investigated, however filtration was more difficult at higher pH values.

Adsorption by activated carbon

Due to the fact that all filtrates showed a yellow to brownish color, it was investigated whether color bodies could be adsorbed by activated carbon (powder). Table 2 contains the results.

Table 2. Effect of activated carbon on color removal of partly purified G-phase

Amount of activated carbon (wt%)	0	1	2	3
Color of filtrate after adsorption (Gardner)	4.8	1.5	1	1

Original color of crude glycerol coming from the biodiesel plant decreased from 6.7 to 4.8 Gardner during the first processing steps (acid treatment and neutralization). Obviously the upper free fatty acid-rich phase removed a lot of color bodies. An addition of 2 wt% of activated carbon allowed to decrease the color of partly purified G-phase, moreover the odour was reduced by activated carbon, as well.

Purification by distillation

The decolorized solution was containing glycerol, water and salts, only. All water was removed by distillation at 62-67°C under vacuum (~ 3 kPa). After the light removal the glycerol content of this partly purified glycerol went up to 91.05 wt%.

Distillation of glycerol is a rather expensive step in the purification process of crude glycerol, moreover under distillation conditions the salt content causes an enormous viscosity increase of the distillation feedstock, which necessitates so called “salt towers”, an expensive type of equipment, both by investment and by operation cost, too. That is the reason why partly purified glycerol containing inorganic salts was also tested as raw material in synthesis of tripropionin.

Material balance of crude glycerol purification

After physical and chemical treatment, per kg crude glycerol 0.443 kg glycerol (average value) was recovered having a purity of 91.05 wt%.

Expensive distillation of glycerol was not necessary to reach this purity. Table 3 summarizes the properties of the purified crude glycerol of this work in comparison with results of other publications [11, 12].

Originally, contaminants correlated to the matter organic non-glycerol (MONG) group material represented the highest level of impurities. Due to the acid treatment, the MONG content could be reduced from 44.95 wt% down to 4.86 wt%.

The majority of ash content of 4.81 wt% correlates with the transesterification catalyst (KOH).

Table 3. Comparison of purified crude glycerol properties obtained from this work with other works

Author	Source of crude glycerol	Glycerol (wt%)		Ash (wt%))		MONG (wt%)		Water (wt%)	
		(a)	(b)	(a)	(b)	(a)	(b)	(a)	(b)
Ooi et al [11]	Palm kernel oil	17.7	51.4	58.7	13.8	17.7	25.9	5.9	8.9
Kongjao et al [12]	Waste used-oil	28.56	93.34	2.65	4.5e-4	56.13	5.16	6.7	1.5
This work	Rape-seed	49.14	91.05	4.81	3.64	44.95	4.86	1.1	0.45

(a) Concentration of glycerol and impurities content in the original crude glycerol
(b) Concentration of glycerol and impurities content in the purified crude glycerol

Figure 1 shows the measured material balance of our crude glycerol refining process. 82 wt% of the original glycerol content was recovered. This seems to be a promising result when considering the numerous purification steps.

Certain purification steps can be eliminated depending on the further utilization. For example the adsorption step on charcoal and filtration could be left out, if the partly purified glycerol still containing inorganic salts is used as raw material in synthesis of a value-added glycerol derivative, whose color needs to be reduced after the reaction.

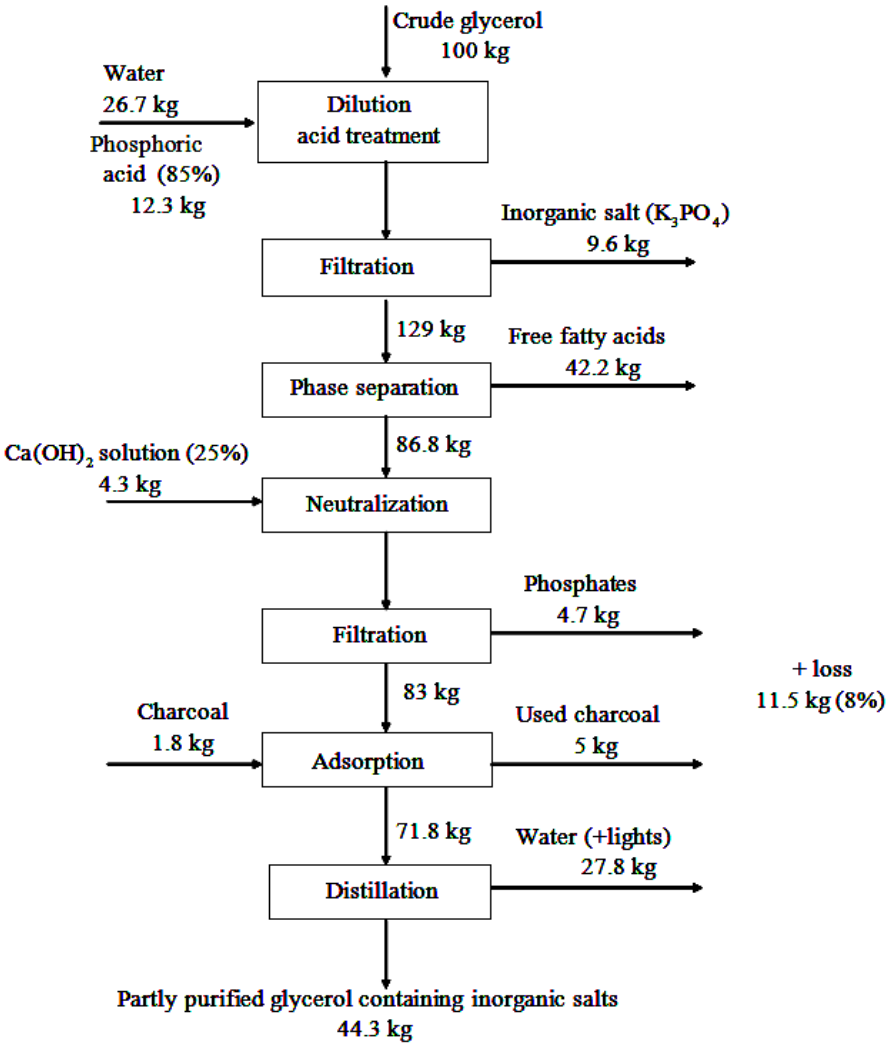

Figure 1. Material balance of crude glycerol purification

Preparation of tripropionin

Triproprionin can be produced in an acid-catalyzed reaction of glycerol with propionic acid (see Scheme 1).

Di- and tri-propyl esters of glycerol are potential oxygenate-additives to diesel fuels because of their good properties as blending components, but also having excellent solubility in diesel fuel. Mono-propyl ester of glycerol is more polar and has a low solubility in diesel fuel and therefore the esterification of glycerol must be directed to the maximum yield of di- and tri-esters.

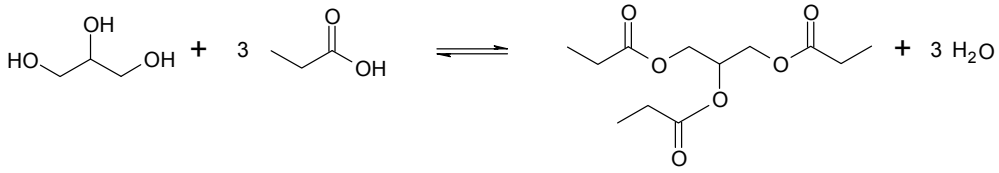

Scheme 1

The boiling point of dipropionin and tripropionin are Bp_{DP}=292°C, Bp_{TP}=290.7°C (Bp_{MP}=n.a.), therefore the separation of tripropionin from mixture containing mono-di and tripropionin by distillation is impossible.

To simplify the process our aim was to synthesize tripropionin by a one-step process with the highest possible selectivity.

The influence of the main reaction parameters, like reaction temperature, quality of raw material and the catalyst on the esterification of glycerol with propionic acid was studied.

The esterification of glycerol (G) with propionic acid (PA) is a complex of three acid catalyzed consecutive equilibrium reactions with formation of monopropionin (MP), dipropionin (DP) and tripropionin (TP).

$$G + PA \leftrightarrow MP + H_2O$$
$$MP + PA \leftrightarrow DP + H_2O$$
$$DP + PA \leftrightarrow TP + H_2O$$

The reaction was carried out in presence of sulfuric acid starting from pure glycerol and partly purified glycerol, still containing inorganic salts. The formed reaction water was removed by straight-forward distillation in absence of entraining solvents. The comparison of the results starting from different raw materials is shown in Table 4.

A better result namely a conversion of 100% and a selectivity of 98 % yield was obtained in case of pure glycerol, as it was predicted before the experiments.

Table 4. Effect of quality of raw material on esterification of glycerol by propionic acid in presence of sulfuric acid (propionic acid/glycerol molar ratio: 6:1, 2-fold excess, reaction temperature: 120-160°C)

Raw material	Catalyst	Entraining solvent	Selectivity %			X_G %	Y_{TP} %
			MP	DP	TP		
Pure glycerol	H_2SO_4	-	0.0	2.0	98.0	100.0	**98.0**
Glycerol cont. salt	H_2SO_4	-	0.0	13.2	86.8	100.0	**86.8**

When the starting glycerol was containing salt the yield of tripropionin dropped down to 86.8% (see Table 4)
The zeotropic removal of water requires a separation tower. Without a separation tower a significant loss of propionic acid was obtained.

Role of entraining solvents and ion exchange resins

Homogeneous catalysts are very effective but require additional handling steps. It is imperative to remove catalysts before distillation, therefore, higher production costs have to be expected [13]. Appropriate fixed-bed catalysts could be incorporated into a packed-bed, continuous flow reactor, simplifying the product separation and purification, but also reducing the waste formation.

In esterification reactions of carboxylic acids with alcohols it is standard to use homogeneous catalysts like sulfuric acid, methane sulfonic acid, hydrofluoric acid, p-toluene-sulfonic acid or the like. Usually, such homogeneous catalysts have to be removed by additional treatment steps during the process.

Therefore, heterogeneous catalysts are becoming more and more in the focus of the industry. The literature is containing numerous publications describing heterogeneous acid catalysts for esterification processes.

So for instance, good results were reported using ion-exchange resins like Amberlyst A15 or Nafion in esterification processes [14, 15]. Generally speaking, the catalytic activity of organic resins is strongly depending on their swelling properties. Resin swelling capacity is fundamental since it controls substrate accessibility to the acid sites and, therefore, affects its overall reactivity. Once swelled, the resin pores usually become macropores. This means that big molecules with long hydrocarbon chains show no diffusion limitations and can readily access the acid sites in the bulk.

Table 5. Characteristics of ion-exchange resins (Amberlyst 15 and 36)

Catalyst (short name)	Cross-linked structure	Acidity (mmol/g)	Average pore diameter (nm)	S_{BET} (m^2/g)	Particle size (mm)	Moisture capacity (%)	T_{max} (°C)
A 15 (Dry)	V	4,7	30	53	-	≤1,6	120
A 36 (Wet)	M	5,4	24	33	0,6-0,85	53-59	150

A: Amberlyst. Crosslinked structure: V-very, M-medium

Despite of the fact that most ion-exchange resins are not stable at temperatures above 140 °C [16], which limits their application to reactions that require higher temperatures, Amberlyst A15 and A36 were investigated.

Physical characteristics of ion-exchange resin catalysts are summarized in Table 5 [17].

The use of entraining agents for the water removal is of great help not to exceed the maximal operation temperature of ion-exchange resins in esterification reactions. Together with ion-exchange resins as esterification catalyst MIBK and n-hexane were tested as entraining agents.

It can be seen from Table 6 the highest yield was reached when raw material was pure glycerol and MIBK was used as entraining solvent in presence of Amberlyst A36 catalyst. Due to the higher boiling point of MIBK-water azeotrope, the temperature of the reaction media was higher (110-120°C) than in case of n-hexane (68-74°C) and higher temperature may be favored by Amberlyst A36.

When raw material was pure glycerol in presence of n-hexane Amberlyst A15 gave better result than Amberlyst A36 which may mean that the optimal working temperature of Amberlyst A15 is lower.

Table 6. Comparison of catalysts, entraining solvents and quality of raw materials for esterification of glycerol (propionic acid/glycerol molar ratio: 6:1, 2-fold excess, reaction temperature: 110-120°C in case of MIBK, 68-74°C in case of n-hexane and 100-124°C in case of toluene)

Raw material	Catalyst	Entraining solvent	Selectivity %			X_G %	Y_{TP} %
			MP	DP	TP		
Pure glycerol	A15	MIBK	8.7	10,1	81,8	100.0	**81.8**
Pure glycerol	A15	n-Hexane	0.0	11.6	88.4	100.0	**88.4**
Glycerol cont. salt	A15	n-Hexane	0.0	74.8	25.2	100.0	**25.2**
Pure glycerol	A36	MIBK	0.0	0.0	100.0	100.0	**100.0**
Pure glycerol	A36	n-Hexane	0.0	42.3	57.7	100.0	**57.7**
*Glycerol cont. salt	A36	n-Hexane	0.0	72.7	7.7	100.0	**7.7**
Glycerol cont. salt	H_2SO_4	Toluene	0.0	4.0	96.0	100.0	**96.0**

* Significant by-product formation was observed

When partly purified glycerol is used as raw material ion-exchange resins are not as effective as in case of pure glycerol. Reaction product contained mainly dipropionin. This could be explained by the desactivation of active sites of ion-exchange resin by salts, present in that raw material.

When partly purified glycerol was used as raw material the best result, 96% yield of tripropionin was achieved in presence of H_2SO_4 catalyst and toluene as entraining solvent.

Distillation of tripropionin

Although, it was known that separation of mono- di- and tripropionin is not possible by distillation. Therefore, a final product purification of tripropionin by distillation was investigated from the point of view of color-removal.

In this case a relatively pure bottom product containing 95% tripropionin was distilled. The distillate contained the components by almost the same ratio as they were present in the raw material. However, the color of material improved significantly (see Table 7).

Considering the material balance of distillation, tripropionin is thermally stable at high temperature (up to ~200°C).

Table 7. Results of distillation of tripropionin under 0.6 kPa vacuum

	Weight (g)	Monopropionin (a%)	Dipropionin (a%)	Tripropionin (a%)	Color (Pt-Co)
Raw material	200.0	0	3.6	95.0	423
Distillate	155.4	0	2.7	96.2	62
Residue	44.6	0	4.3	93.1	n.a.

Material balance of tripropionin synthesis from crude glycerol

A sulfuric acid catalyzed reaction, starting from partly purified glycerol, seems to be the most economical way of tripropionin synthesis. When the reaction water was removed by an azeotropically distillation with toluene, tripropionin yield of >96% was obtained. Considering a technical manufacturing toluene would provide technical and commercial benefit like low solubility in water and low price.

The most difficult problem concerning crude glycerol refining is the removal of salt which is formed during neutralization of the catalyst (KOH, NaOH).

Due to the fact that presence of salts is not disturbing the formation of tripropionin using sulfuric acid, all formed salts can be removed by simple filtration. Such an operation is supported by the facts, that these salts are insoluble in the reaction media, but also easy filterable.

If applications of tripropionin do not require low-color material, an expensive purification step by distillation can be ignored.

Based on the experimental results the following material balance was calculated (see Figure 2 and Table 8).

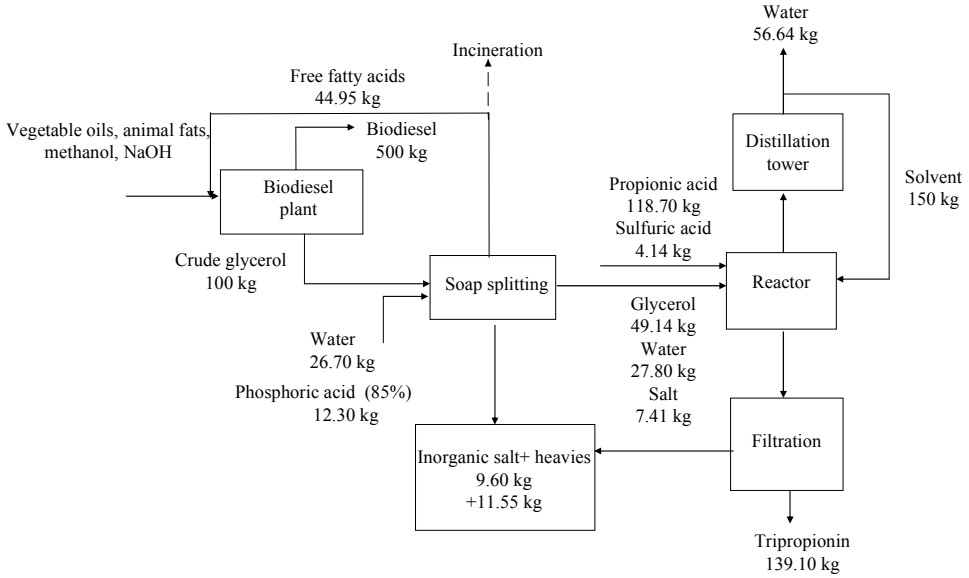

Figure 2. Potential process flow sheet for production of tripropionin from crude glycerol

The manufacture of tripropionin from crude glycerol using entraining agents allows to remove beside the reaction water also water which is remaining from the biodiesel process. Therefore, any earlier dewatering step became obsolete.

Table 8. Mass balance of tripropionin synthesis from crude glycerol

Stream	Input (kg)	Output (kg)
Crude glycerol	**100.00**	-
Water	26.70	56.64
Phosphoric acid	12.30	-
Sulfuric acid	4.14	-
Propionic acid	118.70	-
Solvent (toluene)	150.00	150.00
Free fatty acids	-	44.95
Inorganic salt	-	21.15
Tripropionin	**-**	**139.10**

Any activated-carbon treatment of crude glycerol seems to be unnecessary because tripropionin needs to be decolorized at the end of the process, if the application requires low colored material.

Considering the low prices of raw materials and the severity of the process, tripropionin produced from crude glycerol can be competitive with commercial fuel additives.

Engine performance

Reduction on engine emissions is one major research aspect in engine development because of an increasing concern on environmental protection and strengthening of emission regulations [18]. Diesel engines have the advantages in good fuel economy and low CO_2 emission but may produce high carbon monoxide (CO) and smoke.

Effect of tripropionin blending on engine performance characteristics and environmental repercussions were studied (Table 9). VW-AUDI 1.9 TDI engine was used for the measurements. Blended fuel contained 5 wt% tripropionin.

An increase of total unburned hydrocarbons (THC) in blended fuel was observed which must be in connection with the inadequate burnout of tripropionin. Due to the high oxygen content of tripropionin a decrease of CO, smoke and exhaust temperature was observed.

Table 9. Comparison of reference fuel and blended fuel

	Reference fuel	Blended fuel	Change [%]
THC [ppm]	35.6	37.0	**+3.9**
NO_X	767	768	**+0.1**
CO (V/V%)	0.0174	0.0163	**-6.3**
Smoke [FSN]	1.48	1.29	**-12.8**
Specific fuel consumption [g/kWh]	251	260	**+3.6**
$T_{exhaust}$ [°C]	524	520	**-0.8**

According to the engine performance characteristics and environmental repercussions tripropionin represents a promising material, which can be used as fuel additive. Further studies need to be done to find the optimal ratio of tripropionin in Diesel oil.

CONCLUSIONS

Crude glycerol is a considerable by-product of biodiesel production for which new uses are being sought. Purification of G-phase and esterification of glycerol with propionic acid using sulfuric acid and Amberlyst type strong acid ion-exchance resins were studied. The best result of pure glycerol esterification by propionic acid, 100% yield of tripropionin was obtained in presence of Amberlyst36 catalyst and MIBK entraining solvent.

However a sulfuric acid catalyzed reaction, starting from partly purified glycerol still containing inorganic salts, seems to be the most economical way of tripropionin synthesis. When the reaction water was removed by an azeotropically distillation with toluene, tripropionin yield of >96% was obtained. It has been proven that presence of inorganic salts is not disturbing the formation of esters using the conventional acid catalyst, sulfuric acid. Since all formed salts can be removed by simple filtration, expensive purification of the product by distillation is not necessary.

An economical process for utilization of crude glycerol was created, which can be applied not only for tripropionin production but preparation of other glycerol esters like glyceryl triacetate, glyceryl tributyrate.

Tripropionin represents a promising material, which can be used as fuel additive to improve engine performance characteristics and environmental repercussions. Further studies need to be done to find the optimal ratio of tripropionin in Diesel oil.

EXPERIMENTAL SECTION

Chemicals

Crude glycerol was obtained from a local biodiesel plant - Öko-Line Hungary Ltd. This company utilized rapeseed oil for biodiesel production via alkali (KOH) catalyzed transesterification process.

The wet ion-exchange resin Amberlyst A36 from Sigma-Aldrich was washed with methanol and dried to remove water from the catalyst. Amberlyst A15 strongly acidic, cation exchanger resin (dry, moisture content ~5 wt%) from Sigma-Aldrich was used without pretreatment. Pure glycerol (99.5 wt% purity), activated-carbon powder (Norit) and calcium-hydroxide (95 wt% purity) were obtained from Spektrum-3D Ltd. (Hungary). Propionic acid (>99 wt% purity), methyl isobutyl ketone (>98.5 wt% purity), n-hexane (>96 wt% purity), toluene (>99.8 wt% purity), phosphoric acid (85 wt% purity) and sulfuric acid (95 wt% purity) were obtained from Sigma-Aldrich.

Analytical methods

Glycerol content of samples were analyzed with a Merck LaChrom HPLC equipped with an Ultrahydrogel column (I.D. = 7.8 mm, L= 300 mm) and a Merck LaChrom RI detector. Water was used as eluent (flow rate: 0.8 ml/min, temperature: 30°C).

The water content was determined by volumetric Karl Fischer titration.

Ash content was analyzed by burning 1 g glycerol in muffle furnace at 750 °C for 3 h.

For matter organic non-glycerol (MONG), it was calculated by the difference from a hundred of the previous three compositions (100 − (% glycerol content + % water content + % ash content)).

The samples of reaction products were analyzed with a HP 5890 Series II gas chromatograph equipped with a Restek Rtx-5MS column (30m x 0.25 mm x 0.25 μm) and a HP 5971 MSD detector. Analyses were carried out with temperature program from 60 to 240°C (with a slope of 10°C min^{-1}) and 240°C for 2 min isothermally.

The color of the samples was measured using a Lovibond Colorimeter, model PFX190.

Effect of tripropionin blending on engine performance characteristics and environmental repercussions were tested by a four-cylinder turbocharged direct injection diesel engine (VW-AUDI 1.9 TDI). Blended fuel contained 5 wt% tripropionin which was prepared from partly purified glycerol, entraining solvent was toluene and sulfuric acid was used to catalyze the reaction.

Apparatus and procedure

Procedure A: Purification of crude glycerol

The first step of our refining process was an acid treatment. To make the handling of crude glycerol easier it was diluted by distilled water. Under vigorous stirring phosphoric acid (85 wt%) was added slowly to crude glycerol by pH control. The mixture was stirred at 80 °C, for 30 minutes in a 500 ml three necked round bottomed flask equipped with a thermometer, mechanic stirrer, heating jacket and a reflux condenser. The role of the pH on the product mixture was investigated to check the phase separation conditions.

The reaction of an acid with the soaps will give free fatty acids (FFA). Since FFA's are insoluble in glycerol, these components will rise to the top so that they can be skimmed off. Some glycerol-insoluble salts will also precipitate out. The necessary time of the phase separation was measured. After this treatment salts were filtered by G3 glass filter. The free fatty acids were separated from crude glycerol by simple phase separation.

The next step was the neutralization of excess acid. For that purpose a calcium-hydroxide slurry containing 25 wt% $Ca(OH)_2$ was added to the glycerol phase to reach a pH value of about 5. All precipitated calciumphosphates was eliminated by simple filtration on G3 glass filter.

The filtrate coming from such a neutralization step is yellow or light brown. Pigments and odor bodies were eliminated by adsorption on activated carbon. For that purpose activated charcoal powder was added to the glycerol-containing phase. This mixture was heated to 60°C and stirred for half an hour in a three necked round bottomed flask equipped with a thermometer, mechanic stirrer, heating jacket and a reflux condenser. After the adsorption step activated carbon was filtered off by a G4 glass filter. Different quantities of activated carbon were used to find the best adsorption conditions.

That solution contained glycerol, water and salts, only. The removal of all water contained was done by distillation at 62-67°C under vacuum (~ 3kPa). Most of the reactions were carried out using pure glycerol (>99.5%) to get reference results, but our final aim was to apply partly purified glycerol (containing salt) to produce tripropionin.

Procedure B: Tripropionin synthesis by straight – forward distillation

In a typical run, 46 g (0.5 mol) of glycerol or 50 g partly purified glycerol (~0.5 mol) containing inorganic salts and 222 g (3 mol) propionic acid were used. As catalyst 2 ml H_2SO_4 was used.

The esterification reactions were carried out in a 500 ml glass round bottomed flask equipped with a magnetic stirrer, heating jacket, thermometer and a distillation bridge.

Propionic acid was always used in excess (usually 2-fold molar excess) to shift reaction equilibrium towards the product. Reactions were carried out by straight – forward distillation in absence of entraining solvents.

All water formed during the esterification was removed together with some propionic acid. When temperature reached 141°C, the boiling point of propionic acid, the reaction was stopped.

Homogenous catalyst was neutralized by 50 wt% NaOH aqueous solution.

Inorganic salts formed an easy-filterable precipitation, now. This precipitate was filtered off and the unreacted propionic acid and remaining water were removed by simple distillation under vacuum at 3 kPa.

For the purification of tripropionin by distillation an apparatus was used consisting of a 500 ml glass round bottomed flask equipped with a magnetic stirrer, heating jacket, thermometer and a 30 cm long tower packed by Raschig rings. For fractionation the crude tripropionin was heated up to 200°C bottom temperature at a pressure of 0.6 kPa.

Procedure C: Tripropionin synthesis by azeotropic water removal

In a typical run, 46 g (0.5 mol) of glycerol or 50 g partly purified glycerol (~0.5 mol) containing inorganic salts, 222 g (3 mol) propionic acid were used. As catalyst 2 ml of H_2SO_4 was used, alternatively 10 g of Amberlyst A15 or 12 g of Amberlyst A36 ionexchange resins.

The esterification reactions were carried out in a 500 ml glass round bottomed flask equipped with a magnetic stirrer, heating jacket, thermometer and a calibrated Dean-Stark trap connected to a reflux condenser.

Propionic acid was used in excess (2-fold molar excess) to shift reaction equilibrium towards the product. For the azeotropic removal of the reaction water different entraining solvents like MIBK, n-hexane and toluene were used. The heterogeneous water-solvent azeotropes were phase separated and the solvent recycled to the reaction flask. For product purifications the same method was used as described under procedure B.

REFERENCES

1. W. Xie, Z. Yang, H. Chun, *Industrial & Engineering Chemistry Research*, **2007**, *46*, 7942.
2. F. Ma, M.A. Hanna, *Bioresource Technology*, **1999**, *70*, 1.
3. M. Hájek M, F. Skopal, *Bioresource Technology*, **2010**, *101*, 3242.
4. Y.C. Lin, *International Journal of Hydrogen Energy*, **2013**, *38*, 2678.
5. P. Anand, R.K. Saxena, *New Biotechnology*, **2011**, *00*, 1.
6. F. Yang, M.A. Hanna, R. Sun, *Biotechnology for Biofuels*, **2012**, *5*, 13.
7. B.J. Kerr, W.A. Dozier, K. Bregendahl, Nutritional value of crude glycerin for nonruminants. *In Proceedings of the 23rd Annual Carolina Swine Nutrition Conference*, *Raleigh*, NC, **2007**, 6.
8. M. Slinn, K. Kendall, K. Mallon, J. Andrews, *Bioresource Technology*, **2008**, *99*, 5851.
9. J.A. Meleroa, G. Vicente, M. Paniagua, G. Morales, P. Muñoz, *Bioresource Technology*, **2012**, *103*, 142.
10. Y. Dharmadi, A. Murarka, R. Gonzalez, *Biotechnology and Bioengineering,* **2006**, *94*(5), 821.
11. T.L. Ooi, K.C. Yong, K. Dzulkefly, W.M.Z. Wan Yunus, A.H. Hazimah, *Journal of Oil Palm Research*, **2001**, *13*, 16-22.
12. S. Kongjao, S. Damronglerd, M. Hunsom, *Korean Journal of Chemical Eng*ineering, **2010**, *27*, 944.
13. E. Lotero, Y. Liu, D.E. Lopez, K. Suwannakarn, D.A. Bruce, J.G. Goodwin, *Industrial & Engineering Chemistry Research,* **2005**, *44*, 5353.
14. X. Chen, Z. Xu, T. Okuhara, *Applied Catalysis A: General*, **1999**, *180*, 261.
15. A. Heidekum, M.A. Harmer, W.F. Hoelderich, *Journal of Catalysis*, **1999**, *181*, 217.
16. Z.Y. Zhang, K. Hidajat, A.K. Ray, *Journal of Catalysis,* **2001**, *200*, 209.
17. K. Klepácová, D. Mravec, A. Kaszonyi, M. Bajus, *Applied Catalysis A: General*, **2007**, *328*, 1.
18. X. Wang, C.S. Cheung, Y. Di, Z. Huang, *Fuel,* **2012**, *94*, 317.

STUDIA UBB CHEMIA, LVIII, 2, 2013 (p. 23 – 34)
(RECOMMENDED CITATION)

REMOVAL OF ANIONIC DYE CONGO RED FROM SYNTHETIC WASTEWATER USING IMMOBILISED FIR SAWDUST (*ABIES ALBA*)

CERASELLA INDOLEAN[a], SILVIA BURCĂ[a], ANDRADA MĂICĂNEANU[a], MARIA STANCA[a], DAN RĂDULESCU[b]

ABSTRACT. The purpose of this paper was to establish the optimum experimental conditions for removal of Congo Red (CR) from aqueous solutions by biosorption on alginate immobilized fir tree sawdust *(Abies Alba)* beads. The studies were carried out under various experimental conditions. Dye concentration, fir tree sawdust quantity, stirring rate and working regime were considered in order to assess their influence on the biosorption process. Removal efficiencies up to 97% were reached in the case of immobile phase regime. Also, adsorption capacity increased with a decrease in the sawdust quantity and an increase of the initial dye concentration. The results indicate that this local immobilized material can be an attractive option for dye removal from diluted industrial effluents.

Keywords: *biosorption, Congo red, immobilized fir tree sawdust, alginate beads, kinetics*

INTRODUCTION

Wastewater effluents from many industries such as textile, rubber, paper, leather plastics, cosmetic, painting, etc. contain several kinds of synthetic dyes [1]. This dye-bearing wastewater exhibits high color. Thereby, a very small amount of dye in water is highly visible and therefore, the discharge of these effluents in the environment is worrying for both toxicological and aesthetical reasons [2].

As we know, dyes can be classified into cationic, anionic and nonionic dyes. Cationic dyes are basic dyes while the anionic dyes include direct, acid and reactive dyes [3]. The main problem in treating wastewater containing dyes is related to the high stability of these pollutant species, (they are resistant

[a] *Universitatea Babeş-Bolyai, Departamentul de Inginerie Chimică, Str. Arany Janos nr. 11, RO-400028 Cluj-Napoca, Romania, cella@chem.ubbcluj.ro*
[b] *Universitatea de Medicină şi Farmacie Iuliu Haţieganu, Departamentul de Cardiologie, str. V. Babeş nr.8, RO-400012 Cluj-Napoca, Romania, dan_rad31@yahoo.com*

to moderate oxidizing agents and light, and cannot be removed completely by conventional methods of anaerobic degradation [4]).

Recently, numerous studies have been reported for the adsorption of cationic and anionic dyes by agricultural based adsorbents, such as rice husk [5], tea waste [6], coniferous pins bark powder [7], peanut hull [8], almond shell [9], lemon peel [10], etc.

Adsorption is a very effective separation technique and now it is considered to be superior to other techniques for wastewater treatment in terms of initial cost, simplicity of design, easy of operation and insensitivity to pollutant substances [11-14].

Congo Red (CR, chemical formula = $C_{32}H_{22}N_6Na_2O_6S_2$, FW = 696.68, λ_{max} = 497 nm) is a benzidine-based anionic diazo dye, i.e. a dye with two azo groups. The structure is as illustrated in Figure 1. This anionic dye, in general has been known to cause human allergic reactions and to be metabolized to benzidine, a human carcinogen [15].

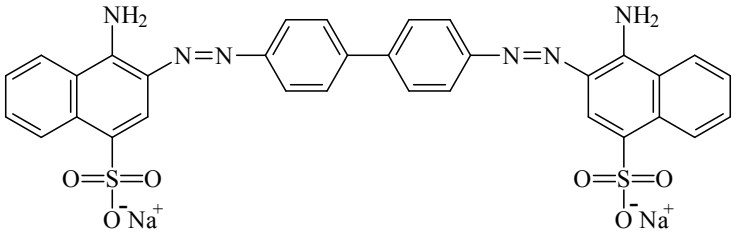

Figure 1. Structure of CR molecule

Abies Alba fir is a common tree from some forest areas in Transylvania (Romania). These trees are the main source for the local wood industry and their sawdust could be a good candidate as a green and economic alternative for Congo Red (CR) removal from wastewater. Previous studies realized on sawdust (timber, pine, *Shorea dasyphylla*, beech wood) showed that they can be used successfully to remove different dyes (methylene blue, direct brown, basic blue, acid blue) from wastewaters [16-19].

Different matrices that can be used for the immobilization of biomass such as alginate [20], chitosan [21], or polyvinylalcohol (PVA) with kaolin [22], etc. are available.

Predicting the rate at which adsorption takes place for a given system is probably the most important factor in adsorption system design, with adsorbate resistance time and the reactor dimensions controlled by the system kinetics [23]. In order to investigate the mechanism of adsorption, various kinetic models have been suggested. Numerous kinetic models have described the reaction order of adsorption system based on solution concentration. These

include first-order [24] and second-order [25] reversible ones, and first-order [26] and second-order [27] irreversible one, pseudo-first-order [28] and pseudo-second-order [29] based on the solution concentration.

The goal of this study was to realize the Congo red biosorption onto immobilized fir tree sawdust (IFTS) from Romanian wood industry and to offer an effective and economical alternative to more expensive adsorption processes (commercial active carbon and resins). Therefore, biosorbent quantity, dye concentration, optimum stirring rate and working regime influence over the biosorption process were investigated in batch conditions. Kinetic models of the considered biosorption process were discussed.

RESULTS AND DISCUSSION

The effect of biomass quantity

The effect of biomass quantity on the biosorption of CR was studied using different masses of sawdust. To establish the optimal dose of adsorbent 100 mL synthetic solution of CR dye, with concentration 50 mg/L was used. Experiments were conducted in batch conditions under magnetic stirring at 300 rpm and room temperature (T = 22°C), using different amounts of sawdust, 1, 2, 3, 4 and 5 g, respectively, immobilized in sodium alginate (IFTS).

Experiments have shown that equilibrium was reached after about 180 minutes when 1, 2 and 3 g of sawdust were used, and after about 150 minutes when 4 or 5 g sawdust were used (Figure 2).

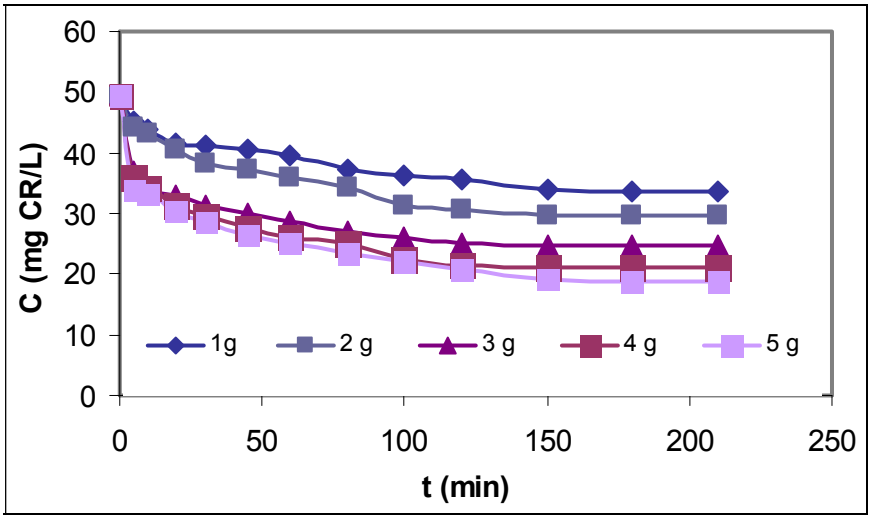

Figure 2. CR concentration time evolution for different initial sawdust quantities (100 mL solution, 50 mg CR/L, 300 rpm, room temperature).

The diagram from Figure 3, gives the maximum removal efficiency E (%) as a function of the biomass quantity. As shown in Figure 3 the maximum removal efficiency varies from 32.35 to 62.04% for 1 and 5 g of sawdust, respectively. The best results were obtained for 4 g (57.66 %) and 5 g (62.04 %). Taking into consideration the fact that the fir tree sawdust is a by-product, therefore is available in large quantities and at very low cost, the experiments were further considered using 5 g for maximum removal efficiency.

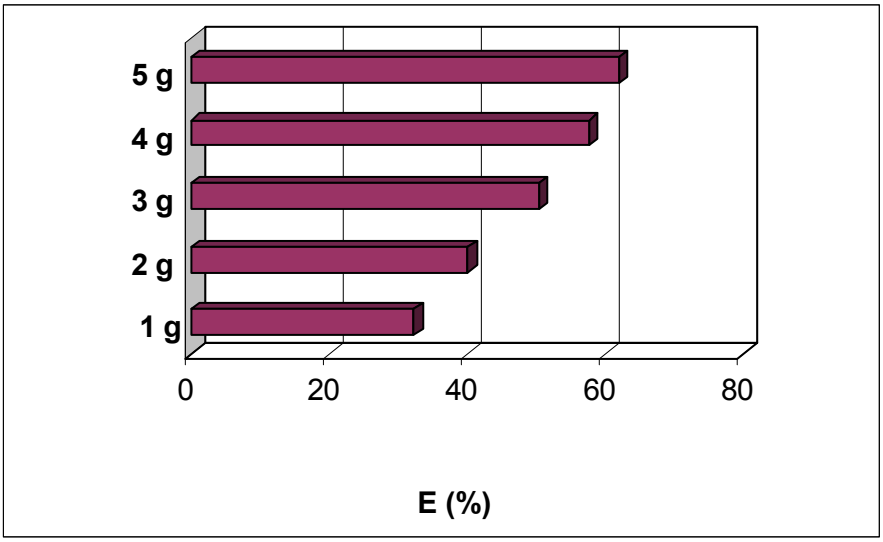

Figure 3. Influence of sawdust quantity over the maximum biosorption process efficiency (100 mL solution, 50 mg CR/L, 300 rpm, room temperature).

The effect of initial CR solution concentration over the biosorption process

Experiments were conducted using volumes of 100 mL CR aqueous solutions with the following concentrations: 50, 105, 150, 200 and 255 mg/L dye and were realized in batch conditions, with magnetic stirring at 300 rpm, at room temperature (T = 22°C) and 5 g of fir tree sawdust, immobilized in sodium alginate.

As the initial concentration decreases, the quantity of dye (CR) retained in the first 30 minutes decreases also due to the smaller difference that exist between the concentration of dye on the adsorbent surface and in the solution. As the initial concentration increases, biosorption process equilibrium was reached more difficult, after about 180 minutes, by comparison with just 80 minutes for small concentrations (50 – 105 mg CR/L) (Figure 4).

The biosorption was noted to occur in two phases of fast and slow rates. This variation could be explained by the easiness with which organic dye gain access to the adsorption sites (favoured by the small stirring rate and macroporosity of the lignocellulosic materials) and by the high activity of the adsorption sites. The formation of a plateau shows a maximum occupation of available biosorption sites, marking thus, the equilibrium achievement of the biosorbate/biosorbent system.

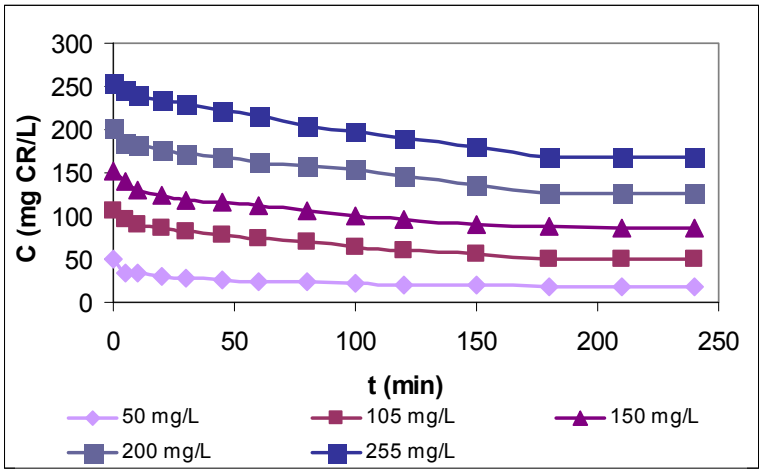

Figure 4. CR concentration time evolution for different initial concentrations (100 mL solution, 5g fir tree sawdust immobilized in alginate beads, 300 rpm, room temperature).

Experimental results showed that biosorption capacity increases with increasing concentration of CR dye in aqueous solution, from 0.51 mg/g when a 50 mg CR/L aqueous solution was used up to 1.43 mg/g when a 255 mg CR/L aqueous solution was used (Figure 5).

Establishing optimum stirring rate

The experiments of biosorption for 5g of fir tree sawdust immobilized in alginate were repeated with varying stirring rate at 300, 500 and 700 rpm, at initial dye concentration of 50 mg CR/L. The efficiency of each experiment is presented in Figure 6. The diagram obtained showed that the biosorption process was intensified with a decrease of stirring rate down to 300 rpm (62.04%). Higher stirring rates, (500 and 700 rpm) will lead to a decrease in efficiency from 45.98% (for 500 rpm) to 29.92% (for 700 rpm), showing that after a certain stirring speed, the minimization of the thin film layer formed at the beads surface will not lead to a further increase in the external diffusion rate.

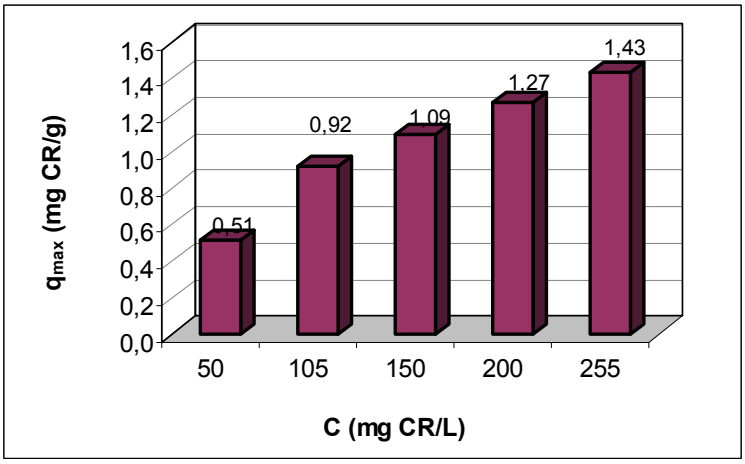

Figure 5. Influence of CR concentration over the biosorption capacity (100 mL solution, 5 g fir tree sawdust immobilized in alginate beads, 300 rpm, room temperature).

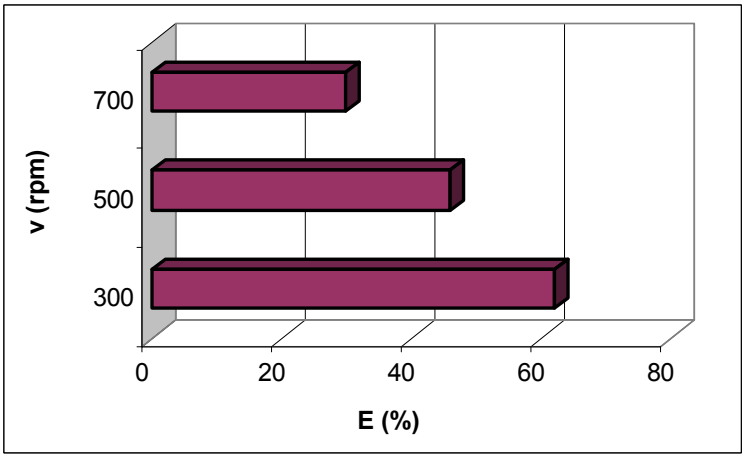

Figure 6. Influence of stirring rate over the maximum biosorption process efficiency (100 mL solution, 50 mg CR/L, 5 g fir tree sawdust immobilized in alginate beads, room temperature).

The influence of working regime on biosorption process

In figure 7, a comparison of maximum removal efficiencies is presented for the experiment conducted in *mobile* and *immobile phases regime*, at different initial concentrations (C_i = 50 – 255 mg CR/L). A closer inspection of this diagram conducts to the conclusion that for all five dye initial concentrations

the *immobile phase regime* is the best solution, leading to the highest removal efficiencies 97.08% (50 mg/L), 96.92% (105 mg/L), 96.41% (150 mg/L), 95.68% (200 mg/L) and 95.14% (255 mg/L). Equilibrium was reached in 250 hours (10 day, approximately), for all five experiments.

In *mobile phase regime*, the same systems were studied and the conclusion was that this type of regime leads to maximum biosorption efficiency between 33.99% (for C_0 = 255 mg CR /L) and 62.04% (for C_0 = 50 mg CR /L), as it can be seen in Figure 7.

These results suggested that due to the size of the CR molecule, diffusion could have an important role in biosorption process, therefore we decided to conduct further experiments in immobile phase regime.

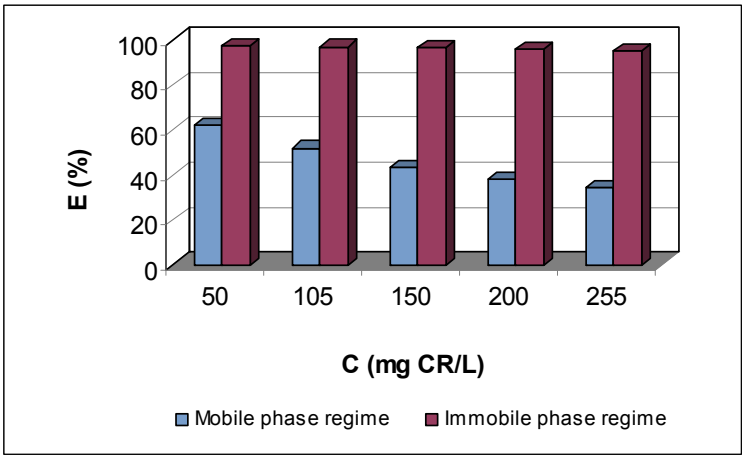

Figure 7. Influence of working regime over the maximum biosorption process efficiency (100 mL solution, 5 g fir tree sawdust immobilized in alginate beads, 300 rpm, room temperature).

Adsorption kinetics

Pseudo-first-order (Lagergren) [30] and pseudo-second-order (Ho) [31] models were used to study the adsorption kinetic of CR onto immobilized sawdust sample. Linear regression was used to determine the best fitting kinetic rate equation (correlation coefficients, R^2) [32].

Lagergren suggested a first order equation for the adsorption of liquid/ solid system based on solid capacity, which can be expressed as follows:

$$\frac{dq_t}{dt} = k_1(q_e - q_t) \quad (1)$$

Integrating equation (1) from the boundary conditions t = 0 to t = t and q_t = 0 to $q_t = q_t$, gives:

$$\ln(q_e - q_t) = \ln q_e - k_1 t \tag{2}$$

where,

q_e and q_t are the amounts of CR adsorbed (mg/g) at equilibrium and time t, respectively

k_1 is the rate constant of first order adsorption (1/min).

In order to determine the rate constant and equilibrium of CR uptake, the straight line plots of $\ln(q_e-q_t)$ against t, eq. (2), were made at five different initial dye concentrations. Because correlation coefficients are modest (between 0.653 and 0.739, figure not shown), CR biosorption onto fir tree sawdust cannot be classified as first order.

The pseudo-second-order kinetic model is derived on the basis of the adsorption capacity of the solid phase, expresses as [27]:

$$\frac{dq_t}{dt} = k_2(q_e - q_t)^2 \tag{3}$$

Integrating eq. (3) from the boundary conditions t = 0 to t = t and q_t = 0 to q_t = q_t, gives:

$$\frac{1}{(q_e - q_t)} = \frac{1}{q_e} + k_2 t \tag{4}$$

where,

q_e and q_t are the amounts of CR adsorbed (mg/g) at equilibrium and time t, respectively

k_2 is the rate constant of first order adsorption (g/mg·min).

Equation (4) can be rearranged in linear form, as follows:

$$\frac{t}{q_t} = \frac{1}{k_2 q_e^2} + \frac{t}{q_e} \tag{5}$$

In order to determine the rate constant and equilibrium of CR uptake, the straight line plots of t/q_t against t, eq. (5), were made at five different initial dye concentrations. Correlation coefficients between 0.921 and 0.997 were obtained (figure 8 and table 1), therefore Congo Red adsorption onto immobilized fir sawdust can be classified as pseudo-second-order.

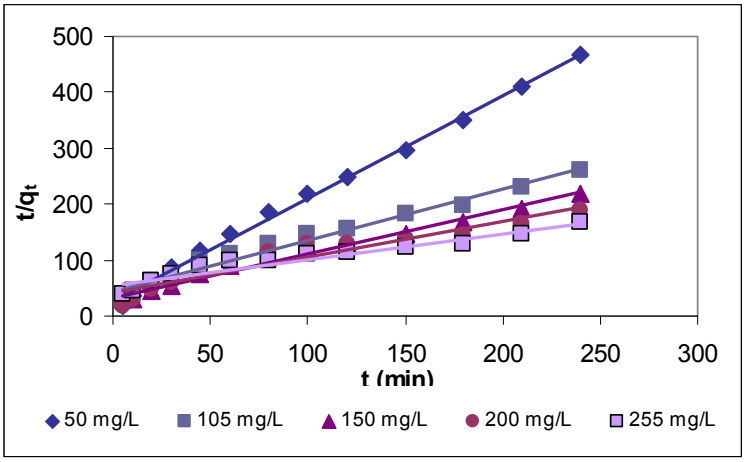

Figure 8. Plots of the second-order model, at different initial CR concentrations (mobile phase regime, 5 g fir tree sawdust immobilized in alginate beads, 100 mL CR solution).

Table 1. Second order adsorption rate constants, and calculated and experimental Q_e values for CR adsorption using different initial concentrations.

Concentration (mg CR/L)	$q_{e,exp}$ (mg/g)	k_2 (g/mg·min)	$q_{e,calc}$ (mg/g)	R^2
50	0.51	$15.04 \cdot 10^{-2}$	0.54	0.997
105	0.92	$4.62 \cdot 10^{-2}$	1.09	0.978
150	1.09	$3.29 \cdot 10^{-2}$	1.27	0.986
200	1.27	$2.43 \cdot 10^{-2}$	1.54	0.921
255	1.43	$1.91 \cdot 10^{-2}$	1.77	0.921

CONCLUSIONS

This study presented results obtained for Congo Red biosoption on popular Romanian fir tree sawdust (*Abies Alba*) from Transylvanian forests, in immobilized form as biosorbent. The biomass was subjected only to mechanical preparation in order to obtain the final biomass (washing, drying and sieving) which was further immobilized in alginate beads. The effects of the initial biomass quantity, initial dye concentration, stirring rate and working regime on biosorption process were studied. Higher biomass quantity, 50 mg CR/L initial dye concentration, reduced stirring rate and immobile phase regime were all favoring the biosorption process. Removal efficiencies up to around 62 % and a maximum adsorption capacity of 0.51 mg/g dye were obtained experimentally, in mobile phase regime, while for immobile phase regime removal efficiencies up to 97% were obtained.

In conclusion, for removal of this bulky anionic dye molecule with immobilized Romanian sawdust, the optimum conditions established experimental are high quantities of biosorbent, immobile phase regime (10 days or probably more, for higher concentrations), solution pH and room temperature.

Kinetics (pseudo-first- and pseudo-second-order) models of the considered biosorption process were discussed. The kinetic of the process was best described by the pseudo-second-order model, suggesting monolayer coverage and a chemisorption process. According to the obtained results it can be concluded that the fir tree (*Abies Alba*) sawdust it is a good biosorbent for Congo Red dye from aqueous solutions, especially in immobile phase regime.

EXPERIMENTAL SECTION

Biosorbent

The fir tree (*Abies Alba*) sawdust was obtained from a local sawmill in Mărgău vilage, Cluj County, Romania. Prior to its utilization the considered biomass was washed several times with distilled water in order to eliminate surface impurities, was dried at 105°C for 24 h. Finally the dried biomass was grinded and sieved (400-600 μm). The sieved sawdust was then stored in an airtight box before its utilization. No further chemical treatments were considered at this stage.

Preparation of Congo Red (CR) solutions

The dye stock solution *(*1000 mg/L) was obtained by dissolving the necessary quantity of solid substance, CR (analytical purity reagent) in distilled water. From this solution were further prepared solutions with known concentration in 50-255 mg CR/L range.

Immobilization of fir sawdust.

Our technique draws inspiration from the methods described by Akar et al., (silica-gel-immobilized waste biomass) [33], Rangsayatorn et al. (cells of *Spirulina platensis* TISTR 8217 immobilized in alginate and silica gel) [35] and Mata et al. (calcium alginate xerogels and immobilized *Fucus vesiculosus*) [35]. In this work, the beads were prepared by mixing 1-5 g of fir sawdust powder to 1 g of sodium alginate and an amount of water varying between 20 and 35 mL according to the quantity of the biosorbent and mixture viscosity. The mixture was blended until was homogeneous and fluid. Then, the mixture was dropped through a syringe using a 1.2 mm in diameter needle into a 0.2 M solution of $CaCl_2$ when beads with diameter between 1.5 and 2.0 mm were formed. Once the beads were formed, stirring was stopped and the beads were let at rest for at least two hours, then removed, washed with water and then conserved in demineralised water, and spin dried before further use.

Biosorption experiments

The Congo Red (CR) biosorption studies were realized using fir tree sawdust (*Abies Alba*) in alginate immobilized form (IFTS).

Biosorption process was conducted in batch conditions, under mobile phase regime (magnetic stirring), and also in immobile phase regime (the biosorbent was contacted with the solution and the process was realized without further stirring), through the contact of a certain amount of biosorbent with a volume of 100 mL dye aqueous solution of various concentrations. The biosorbtion process was realized until equilibrium was reached.

The CR concentration in solution was determined using a Jenway 6305 UV-VIS spectrophotometer at a wavelength of 498 nm and appropriate dilution. Samples were collected at established time intervals.

The influence of the following parameters on the efficiency of biosorbtion process was considered: initial concentration of CR, fir tree sawdust quantity, influence of stirring speed and working regime (with mobile and immobile phases).

All the experiments were repeated three times, the values presented were calculated using averaged concentration values.

Biosorption process efficiency expressed as percentage was calculated with equation (6):

$$E,(\%) = \frac{C_0 - C_t}{C_0} \times 100 \quad (6)$$

where: E – efficiency (%);
C_0 – CR initial concentration (mg/L);
C_t – CR time t concentration (mg/L).

Biosorption capacity was calculated using the equation (7):

$$q = \frac{(C_0 - C_t)}{w} \times \frac{V}{1000} \quad (7)$$

where: C_0 – CR initial concentration (mg/L);
C_t – CR time t concentration (mg/L);
V – aqueous solution volume (mL);
m – biosorbent quantity (g).

Experimental data were used to determine the optimum working conditions and to establish which kinetic model describes better the considered process.

REFERENCES

1. S. Chatterjee, L.S. Lee, M.W. Lee, S.H. Woo, *Bioresource Technology,* **2009**, *100*, 2803.
2. I.A.V. Tan, B.H. Hameed, A.L. Ahmad, *Chemical Engineering Journal,* **2007**, *127*, 111.
3. G. Mishra, M. Triphathy, *Colourage*, **1993**, *40*, 35.
4. W.J. Jr. Weber, *Physiochemical Processes for Water Quality Control*, **1972**, Wiley-Interscience, New York.

5. R. Han, D. Ding, Y. Xu, W. Zou, Y. Li, L. Zou, *J. Bioresource Technol*ogy, **2008**, *99*, 2938.
6. M.T. Uddin, M.A. Islam, S. Mahmud, M. Rukanuzzaman, *Journal of Hazardous Materials*, **2009**, *164*, 53.
7. R. Ahmad, *Journal of Hazardous Materials*, **2009**, *171*, 767.
8. M.Ş. Tanyildizi, *Chemical Engineering Journal*, **2011**, *168*, 1234.
9. F.D. Ardejani, K. Badii, N.Y. Limaee, S.Z. Shafaei, A.R. Mirhabibi, *Journal of Hazardous Materials*, **2008**,*151*, 730.
10. K.V. Kumar, *J. Dye Pig.*, **2007**, *74*, 595.
11. T.K. Sen, S. Afroze, H.M. Ang, *Water Air Soil Pollution,* **2011**, *218*, 499.
12. Z. Yao, L. Wang, J. Qi, *Clean-Soil, Air, Water*, **2009**, *37(8)*, 642.
13. M.M. Abd El-Latif, A.M. Ibrahim, M.F. El-Kady*, Journal of American Science,* **2010**, *6(6)*, 267.
14. M. Mohammad, S. Maitra, N. Ahmad, A. Bustam, T.K. Sen, B.K. Duta, *Journal of Hazardous Materials*, **2010**, *179*, 363.
15. S. Dawood, T.K. Sen, *Water research*, **2012**, *46*, 1933.
16. Y. Djilali, E-H. Elandaloussi, A. Aziz, L.-C. de Menorval, *Journal of Saudi Chemical Society*, **2012**, *http://dx.doi.org/10.1016/j.jscs.2012.10.013*
17. M.A.K.M. Hanafiah, W.S.W. Ngah, S.H. Zolkafly, L.C. Teong, Z.A.A. Majid, *Journal of Environmental Sciences*, **2012**, *24*, 261.
18. D. Politi, D. Sidiras, *Procedia Engineering*, **2012**, *42*, 1969.
19. V. Dulman, S.M. Cucu-Man, *Journal of Hazardous Material*, **2009**, *162*, 1457.
20. S.K. Papageorgiou, E.P. Kouvelos, E.P. Favvas, A.A. Sapalidis, G.E. Romanos, F.K. Katsaros, *Carbohydrates Research,* **2010**, *345,* 469.
21. Y.H. Lin, H.F. Liang, C.K. Chung, M.C. Chen, H.W. Sung, *Biomaterials*, **2005**, 26, 2105.
22. Y. Cheng, H.-Y Lin, Z. Chen, M. Megharaj, R. Naidu, *Ecotoxicology and Environmental Safety,* **2012**, *83,1*08.
23. Y.-S. Ho, *Journal of Hazardous Materials*, **2006**, *B136*, 681.
24. J.E. Saiers, G.M. Hornberger, L. Liang, *Water Resource Research*, **1994**, *30*, 2499.
25. M.A. McCoy, A.I. Liapis, *Journal of Cromatography A*, **1991**, *548*, 25.
26. S.V. Mohan, N.C. Rao, J. Karthikeyan, *Journal of Hazardous Materials*, **2002**, *90*, 189.
27. K. Chu, M. Hashim, *Separation Science and Technology*, **2003**, *38*, 3927.
28. D.J. O'Shannessy, D.J. Winzor, *Analitical Biochemisty*, **1996**, *236*, 275.
29. C.A. Zaror, *Journal of Chemical Technology and Biotechnology.*, **1997**, *70*, 21.
30. S. Lagergren, *Kungliga Svenska Vetenskapsakademien Handlingar*, **1898**, *24*, 1.
31. Y.S. Ho, G. McKay, *Process Biochemistry*, **1999**, ***34***, 451.
32. J. Febrianto, A.N. Kosasih, J. Sunarsao, Y. Ja, N. Indraswati, S. Ismadji, *Journal of Hazardous Materials*, **2009**, *162*, 616.
33. F.N. Acar, Z. Eren, *Journal of Hazardous Materials*, **2006**, *137*, 909.
34. N. Rangsayatorn, P. Pokethitiyook, E.S. Upatham, G.R. Lanza, *Environment International*, **2004**, *30*, 57.
35. Y.N. Mata, M.L. Blazquez, A. Ballester, F. Gonzalez, J.A. Munoz, *Journal of Hazardous Materials*, **2009**, *163*, 555.

STUDIA UBB CHEMIA, LVIII, 2, 2013 (p. 35 – 42)
(RECOMMENDED CITATION)

KINETIC STUDY OF CARROTS DRYING

ADINA GHIRIŞAN[a], SIMION DRĂGAN[a]

ABSTRACT. The present study presents the drying of carrot slices as thin-layer of 4 mm thickness in a laboratory dryer with the drying air temperature in the range of 40–60 ^{0}C. The effect of drying air temperature on the drying kinetics, the drying rates, the effective diffusion coefficients and the activation energy were determined. The effective diffusivity was found to be between $2.6 \cdot 10^{-10}$ and $5.2 \cdot 10^{-10}$ m^2/s. The Newton, Page, modified Page and Henderson & Pabis models available in the literature were fitted to the experimental data using nonlinear regression analysis. The models were compared using the coefficient of determination (R^2). Henderson & Pabis model has shown a better fit to the experimental drying data as compared to other two models.

Keywords: *carrot, thin-layer drying, drying modeling, effective moisture diffusivity*.

INTRODUCTION

The drying operation is frequently used for agricultural products preservation. It is also used for the substantial reduction in weight and volume, minimizes packaging, storage and transportation costs [1].

The basic objective in drying agricultural products is the removal of water or moisture from the surface and from the interior of material up to certain level by evaporation. Thus, the operation involves simultaneous transfer of heat to evaporate the liquid and mass transfer (moisture transfer) as liquid or vapour within the solid and vapour from the surface, usually into a hot carrier gas. The transfer of liquid inside the solid may occur by several mechanisms, such as diffusion in homogeneous solids, capillary flow in granular and porous solids, flow by shrinkage and pressure gradients, and flow caused by a sequence of vaporisation and condensation [2].

[a] *Universitatea Babeş-Bolyai, Facultatea de Chimie şi Inginerie Chimică, Str. Kogălniceanu, Nr. 1, RO-400084 Cluj-Napoca, Romania, ghirisan@chem.ubbcluj.ro*

The evolution of drying can be characterised by the drying curve and drying rate curve. The form of drying rate curve varies with the structure and type of material. There are two typical drying curves: constant-rate drying and falling-rate drying. Drying of fruits and vegetables occurs generally in falling-rate period, the moisture transfer during drying being controlled by internal diffusion [3].

The Fick's second law of unsteady state diffusion (equation 1) was used to calculate the effective moisture diffusivity, considering constant moisture diffusivity, infinite slab geometry, and a uniform initial moisture distribution as equation 2 [4]:

$$\frac{\mathbf{dM}}{\mathbf{dt}} = \nabla\left(\mathbf{D_{eff}}\nabla\mathbf{M}\right) \tag{1}$$

$$\mathbf{M_R} = \frac{\mathbf{M} - \mathbf{M_e}}{\mathbf{M_0} - \mathbf{M_e}} = \mathbf{Ae}^{-\frac{\boldsymbol{\pi}^2\mathbf{D_{eff}}}{4\mathbf{L}^2}\mathbf{t}} \tag{2}$$

where: M is the moisture in kg water/kg dry material at time t, M_R – the moisture ratio, D_{eff} – the effective moisture diffusivity in m^2/s; L – the thickness of the material layer (carrot slab), M_e – the equilibrium moisture content in kg water/kg dry material, and M_0 – the initial moisture content in kg water/kg dry material.

In the simplified form, as equilibrium moisture (M_e) content has negligible effect, the moisture ration becomes:

$$\mathbf{M_R} = \frac{\mathbf{M}}{\mathbf{M_0}} = \mathbf{Ae}^{-\frac{\boldsymbol{\pi}^2\mathbf{D_{eff}}}{4\mathbf{L}^2}\mathbf{t}} \tag{3}$$

The linear form of equation 3, obtained by plotting $\ln(M_R)$ as a function of time offers the possibility to reach the effective diffusivity from experimental data.

The drying rate during experiments was calculated using the following equation:

$$\mathbf{D_R} = \frac{\Delta\mathbf{M}}{\mathbf{A}\cdot\Delta\mathbf{t}} \tag{4}$$

The correlation between the variation of the moisture content and time is a particular dependence for each material and drying conditions, which can not be generalized, but can be experimentally determined.

The present study was undertaken to investigate the thin-layer drying characteristics of carrot slices in a convective dryer and to fit the experimental data to some mathematical models available in the literature.

Carrot was chosen as row material in our research because it is one of the most common vegetables used natural or dried for human nutrition due to the high vitamin and fibre content.

RESULTS AND DISCUSSION

The initial moisture content of carrot slices was found to be 8.10 ± 0.05 (kg water/kg dry matter). The final moisture content of the carrot slices varied with the experimental conditions from 0.25 ± 0.05 to 0.35 ± 0.03 (kg water/kg dry matter).

The variations in the moisture content as a function of drying time at various drying air temperatures and a constant velocity of 0.6 m/s are shown (Figure 1). It can be seen that the moisture content decreases continually with the drying time. The carrot slices of 4 mm will reach the final moisture content within 870-450 min when the air temperature varied from 40^0C to 60^0C.

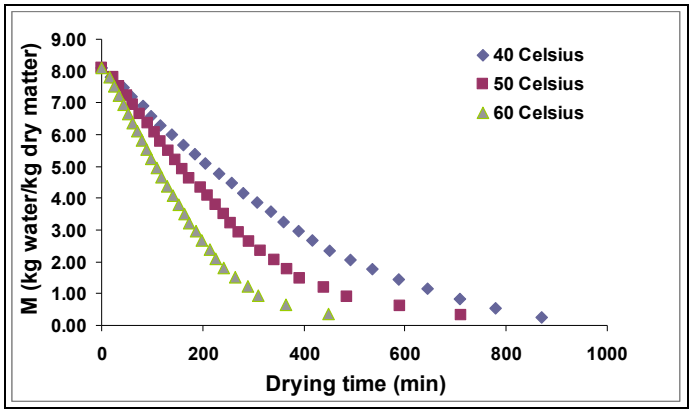

Figure 1. Effect of drying air temperature on moisture content for carrot slices.

Figure 2 show the drying rates, obtained by equation 4, as a function of moisture content at various drying air temperatures.

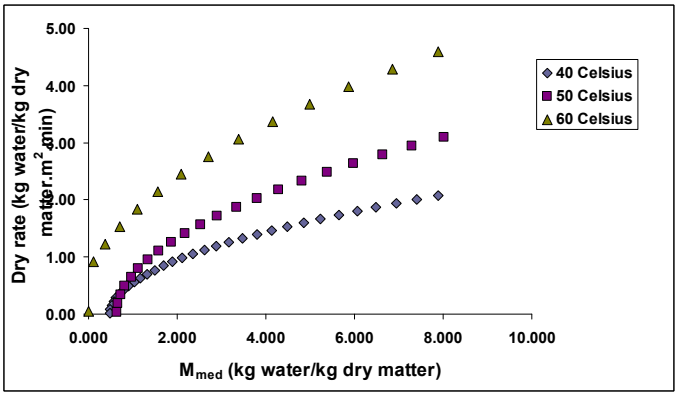

Figure 2. Effect of air temperature on drying rate.

The drying of carrot slices occur in the falling rate period, a continuously decreasing of the drying rate with decreasing moisture content can be seen. In the same time, the increase of drying rates is observed with the increase of drying air temperatures. This means, at high temperatures the transfer of heat and mass is higher and the water loss is more excessive. Similar effects of air temperature are obtained in the drying of apple slices [5].

In order to determine the effective diffusivity the moisture content was converted into the moisture ratio expression M_R. The drying curves for thin layer drying of carrots are shown in Figure 3.

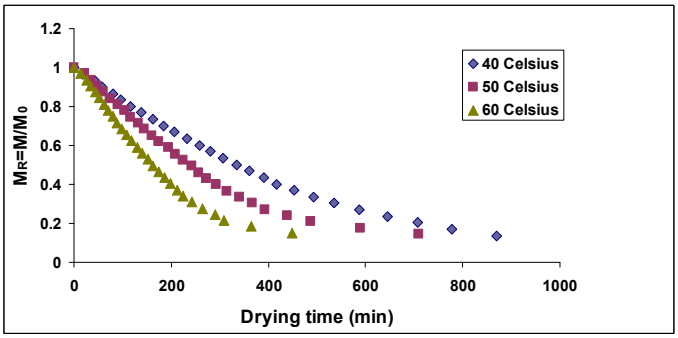

Figure 3. Variation of moisture ratio with the air temperature.

The transport of water during dehydration of carrot is described by applying the Fick's diffusion model. The effective diffusivity can be calculated from the slope of the plot ln(M_R) versus drying time (Fig. 4).

$$\text{slope} = \frac{\pi^2 D_{eff}}{4L^2} \tag{5}$$

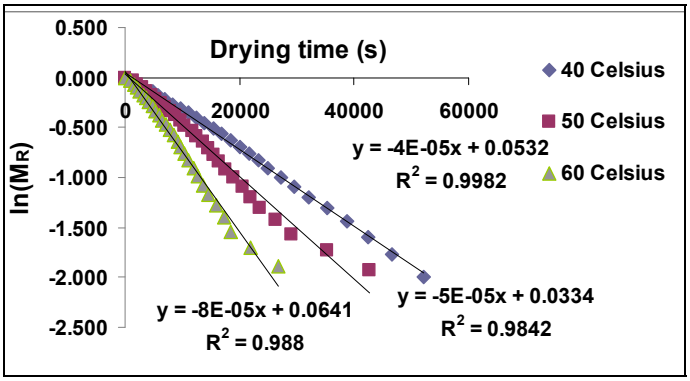

Figure 4. Determination of effective diffusivity coefficient (D_{eff}).

The values of effective diffusivity coefficient obtained by experimental data are shown in Table 1. The values are comparable with those obtained in literature [6]. The effective diffusion coefficient varied with the air temperature from $2.6 \cdot 10^{-10}$ at 40^0C to $5.2 \cdot 10^{-10}$ m^2/s at 60^0C, increasing as temperature increase, which is accordance to the literature mentioned for drying processes of agricultural products. The differences could be due to the differences of drying conditions and drying equipments.

Table 1. Variation of diffusivity coefficient with temperature.

Temperature (^{0}C)	D_{eff} (m^2/s)$\cdot 10^{10}$	1/T
40	2.60	0.0032
50	3.245	0.0031
60	5.20	0.0030

Effect of temperature on effective diffusivity is generally expressed using an Arrhenius-type equation [1, 7]:

$$\mathbf{D_{eff}} = \mathbf{D_0} \exp\left(-\frac{\mathbf{E_a}}{\mathbf{T \cdot R}}\right) \tag{6}$$

where: E_a is the activation energy of the moisture diffusion (kJ/mol), D_0 – the diffusivity value for a infinite moisture content, R- the universal gas constant (kJ/mol·K, and T - the absolute drying air temperature (K).

A plot of $\ln(D_{eff})$ versus 1/T from equation (6) gives a straight line with the slope of E_a/R (Fig. 5).

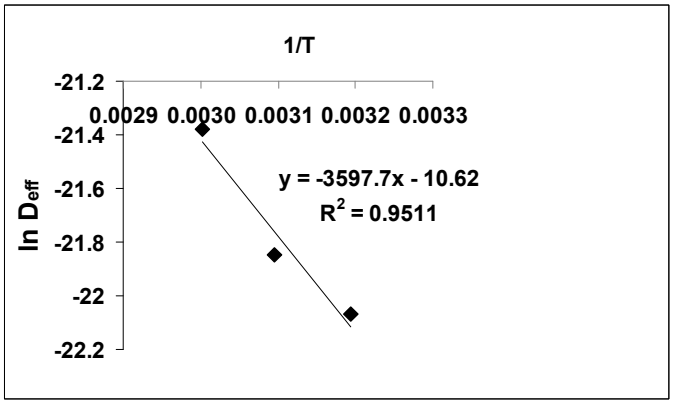

Figure 5. Arrhenius-type representation for activation energy determination.

The obtained value of activation energy of the moisture diffusion was 29.91 kJ/mol and the Arrhenius factor D_0 was $2.44 \cdot 10^{-5}$ m^2/s, which are comparable with the values found in literature [8].

The semi-theoretical models of Newton [3, 9], Page [3, 10] and Henderson & Pabis [3, 10], widely used in thin-layer drying, are considered in the present study to describe the drying behavior of carrots:

$$\mathbf{M_R} = \exp(-\mathbf{kt}) \qquad \text{Newton} \qquad (7)$$

$$\mathbf{M_R} = \exp(-\mathbf{kt^n}) \qquad \text{Page} \qquad (8)$$

$$\mathbf{M_R} = \mathbf{a}\exp(-\mathbf{kt}) \qquad \text{Henderson \& Pabis} \qquad (9)$$

where k is the drying constants, t – the drying time, a and n - the specific drying coefficients.

From each model the drying constant k and the specific drying coefficients determined considering the experimental data are shown in Table 2. As it was expected, the drying coefficient k has increased with the temperature of the drying air. In the same time the models coefficients are affected by the change of air temperature.

Table 2. Drying constant k of model coefficients.

Temperature and relative humidity of drying air	Newton model	Page model	Henderson & Pabis model
40 (^{0}C) RH % = 17.5	k = 0.1332 (h^{-1}) R^2 = 0.995	k = 0.108 (h^{-1}) n = 1.1156 R^2 = 0.999	k = 0.140 (h^{-1}) a = 1.056 R^2 = 0.998
50 (^{0}C) RH % = 11.3	k = 0.180 (h^{-1}) R^2 = 0.983	k = 0.18 (h^{-1}) n = 1.188 R^2 = 0.984	k = 0.184 (h^{-1}) a = 1.034 R^2 = 0.984
60 (^{0}C) RH % = 8.7	k = 0.270 (h^{-1}) R^2 = 0.983	k = 0.252 (h^{-1}) n = 1.245 R^2 = 0.983	k = 0.288 (h^{-1}) a = 1.063 R^2 = 0.988

The models were compared considering the coefficient of determination (R^2) [3, 10]. The Henderson & Pabis model was selected as the best mathematical model for describing the drying kinetics of the carrot slices in our case.

CONCLUSIONS

The experimental results have shown that the carrot slices of 4 mm thick layer were dried between 870 and 450 min when the air temperature was varied from 40^0C to 60^0C.

The moisture content and the drying rate were affected by the air temperature.

The effective diffusion coefficient varied with the air temperature from $2.6 \cdot 10^{-10}$ at 40^0C to $5.2 \cdot 10^{-10}$ m^2/s at 60^0C.

The obtained value of activation energy using Arrhenius type equation was 29.91 kJ/mol and the Arrhenius factor D_0 was $2.44 \cdot 10^{-5}$ m^2/s.

The Henderson & Pabis model was selected as the best mathematical model for describing the drying kinetics of the carrot slices.

EXPERIMENTAL SECTION

Carrots were purchased from the local vegetable market, hand peeled and washed in tap water. The carrots were then cut into slabs with a thickness of 4 mm and putted into the dryer. The initial moisture content of carrot slices of 89 % w. b. (wet basis) was determined drying the sample into a drying stove 70 ^{0}C for 20 h.

The air was supplied by a centrifugal blower, heated to the required temperature with an electrical wire placed inside the heating chamber and connected with a variable transformer which can change the tension. The temperature and the relative humidity in drying chamber were measured with an HD2001.3 - Relative Humidity – Temperature Transmitter. The sample tray with the carrot slices were put into the dryer on the pan of the balance. The loss of each gram from the moisture was recorded as a function of time in order to determine the drying behavior.

REFERENCES

1. I. Doymaz, O. Gorel, N. A. Akgun, *Biosystems Engineering*, **2004**, *88(2),* 213.
2. Geankoplis C.J., “Transport processes and unit operations”, Prentice-hall PTR, Englewood Cliffs, New Jersey, **1993**, chapter 9.
3. A. Kaya, O. Aydin, C. Demirtaş, *Biosystems Engineering*, **2007**, *96(4)*, 517.

4. J. Crank, “Mathematics of Diffusion”, 2nd Edition, Oxford University Press, London, **1975**.
5. K. Sacilik, A.K. Elicin, *Journal of Food Engineering*, **2006**, *73*, 281.
6. J. Srikiatden, J.S. Roberts, *Journal of Food Engineering*, **2008**, *84*, 516.
7. M.C. Gely, S.A. Giner, *Biosystems Engineering*, **2007**, *96(2),* 213.
8. A. Mulet, *Journal of Food Engineering*, **1994**, *22*, 329.
9. S. Erenturk, M.S. Gulabloglu, S. Gultekin, *Biosystems Engineering*, **2004**, *89(2)*, 159.
10. M. Aktaş, I. Ceylan, S. Yilmaz, *Desalination*, **2009**, *239*, 266.

STUDIA UBB CHEMIA, LVIII, 2, 2013 (p. 43 – 52)
(RECOMMENDED CITATION)

THERMODYNAMIC STUDY OF *HYDRANGEA ASPERA* CHLOROPHYLL CATABOLITES BY REVERSE PHASE LIQUID CHROMATOGRAPHY

NINA DJAPIC[a]

ABSTRACT. The *Hydrangea aspera* chlorophyll catabolites present in autumnal leaves were investigated. The thermodynamic study of the *Hydrangea aspera* chlorophyll catabolites was done using reversed phase liquid chromatography on the C_4 and C_8 analytical columns with water (acidified):methanol mobile phase in combination with ultraviolet detection and electrospray ionization mass spectrometry identification. The retention behaviors of *Hydrangea aspera* chlorophyll catabolites over a temperature range of 278-318 K were investigated. The data obtained permitted the construction of the van't Hoff plots. The stationary phase composition influences the thermodynamic retention of the *Hydrangea aspera* chlorophyll catabolites.

Keywords: *Hydrangea aspera; chlorophyll catabolites; Liquid Chromatography-Mass Spectrometry; van't Hoff plot*

INTRODUCTION

The chlorophyll catabolism consists of a great number of steps and, up to know, chlorophyll catabolites that have a chromophore that can absorb the ultraviolet-visible (UV-Vis) light are known. In the plant cell, every step is coordinated, highly regulated and most steps are enzymatically catalyzed. The chlorophyll catabolites found in *Hydrangea aspera* D. Don ssp. sargentiana E. M. McClint autumnal leaves have been isolated from autumnal leaves of *Cercidiphyllum japonicum*, *Spinacia oleracea* and *Nicotiana rustica* [1, 2, 3]. Reverse phase high pressure liquid chromatography (RP-HPLC) methods have been used for the qualitative identification of the chlorophyll catabolites [1]. The hyphenated techniques provided the information on the *m/z* of the

[a] *University of Novi Sad, Technical Faculty "Mihajlo Pupin", Djure Djakovica bb, SRB-23000 Zrenjanin, Serbia, djapic@tfzr.uns.ac.rs*

chlorophyll catabolites and allowed the structural determination of the chlorophyll catabolites by their molecular mass [4]. The temperature plays an important role in the chromatographic separation of the chlorophyll catabolites. The temperature can influence the separation of compounds [5]. The role of temperature in RP-HPLC and RP liquid chromatography (RP-LC) has been used for the analysis of basic pharmaceuticals, water soluble vitamins, small peptides, etc [6, 7, 8]. The retention behavior of the *Hydrangea aspera* chlorophyll catabolites over the temperature range of 278K-318 K was investigated in order to collect the data on the effects of the temperature on the separation of the *Hydrangea aspera* chlorophyll catabolites on the C_4 and C_8 reverse phase (RP) analytical columns. The capacity factor was calculated for the chlorophyll catabolites present in autumnal leaves of *Hydrangea aspera*. The enthalpy and entropy changes of the *Hydrangea aspera* chlorophyll catabolites are reported.

RESULTS AND DISCUSSION

The *Hydrangea aspera* chlorophyll catabolites.

The LC – MS analysis of the *Hydrangea aspera* autumnal leaves dichloromethane and ethyl acetate extracts were subjected on the RP – C_4 and RP – C_8 analytical columns under the same acquisition parameters and elution solvent mixtures. The chromatograms obtained revealed the presence of the chlorophyll catabolites depicted in Fig.1.

The *Hydrangea aspera* autumnal leaves dichloromethane extract revealed the presence of nine chlorophyll catabolites when the separation was done on the RP – C_4 analytical column. The chlorophyll catabolite (**4**) with the m/z 677, eluted at 48.2 min. at the 298 K, assigned as 2 in Fig.2. Two isomers with the m/z 679, assigned 1 and 3 in the Fig.2, refers to the structure **3** in the Fig.1. Two isomers with the m/z 805 refers to the structure **6** in the Fig. 1 and where assigned 4 and 8 in Fig. 2. Two most abundant chlorophyll catabolites were with the m/z 807 (**5**) and were assigned in Fig. 2 with the numbers 5 and 6. The chlorophyll catabolites with the m/z 645 (**1**) and 643 (**2**) were also present and are assigned with the numbers 7 and 9 in the Fig. 2., respectively. The ESI-MS data of the chlorophyll catabolites numerated 3 (**3**) 5 (**5**), 7 (**1**) and 9 (**2**) in the Fig. 2 is depicted in Fig. 4. During the thermodynamical investigations chlorophyll catabolites numeration refers to the numbers they were assigned in Fig. 2.

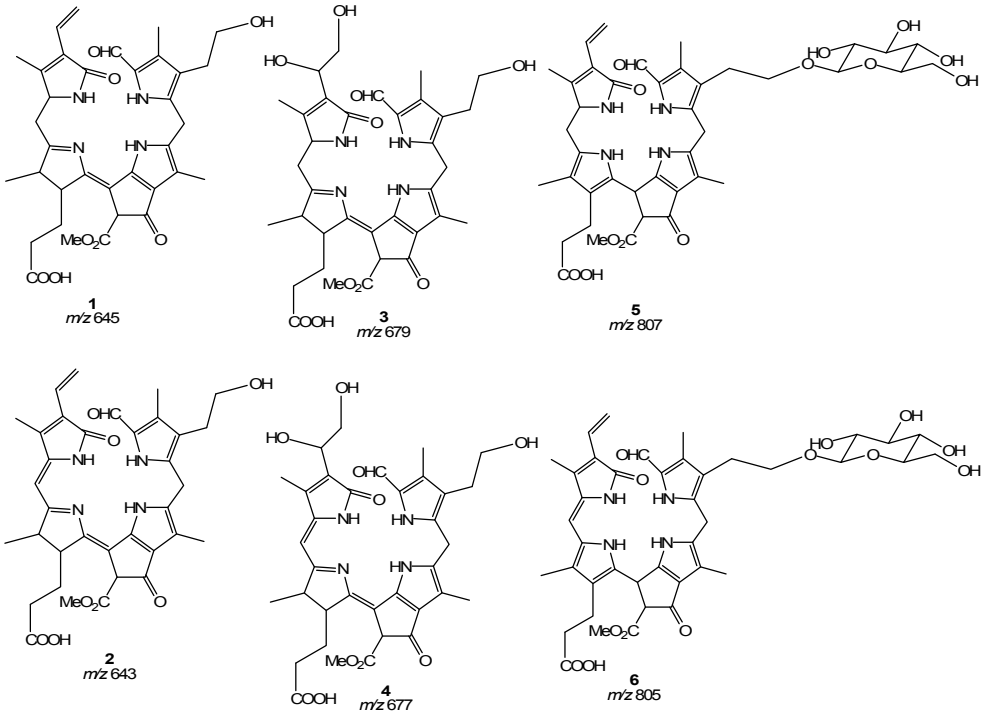

Figure 1. Chlorophyll catabolites present in *Hydrangea aspera* autumnal leaves dichloromethane and ethyl acetate extracts.

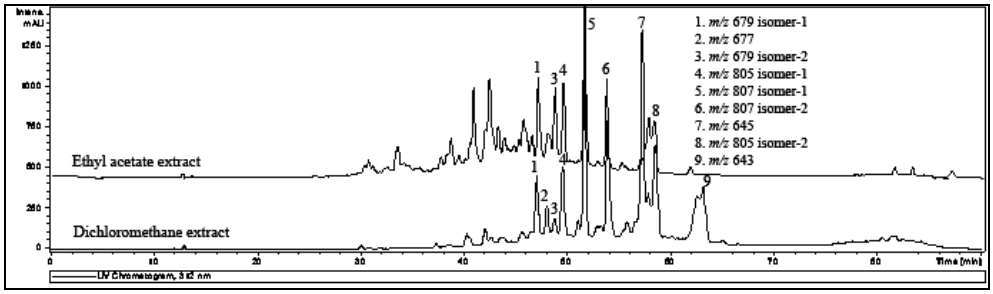

Figure 2. The chromatogram of *Hydrangea aspera* autumnal leaves' dichloromethane and ethyl acetate extract. The LC conditions: Column: Nucleosil 100-5 C_4 4x250 mm. The mobile phase: 90% v/v water (0.1% TFA):methanol to 0% v/v water (0.1%TFA):methanol in 90 minutes. Flow rate: 0.2 ml min^{-1}. UV detection at λ=312. The oven temperature was 298 K.

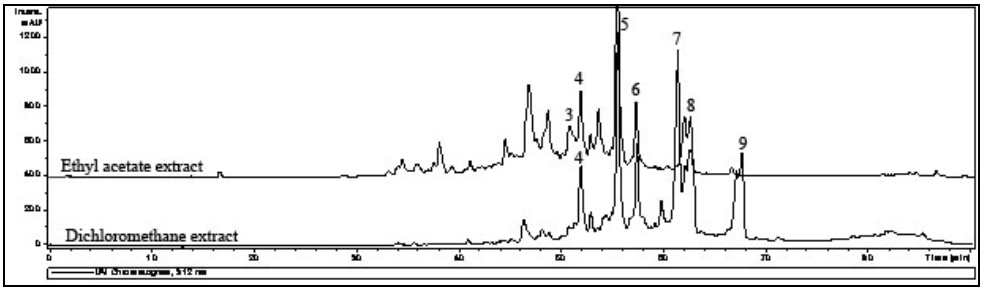

Figure 3. The chromatogram of *Hydrangea aspera* autumnal leaves' dichloromethane and ethyl acetate extract. The LC conditions: Column: Nucleosil 100-5 C_8 4x250 mm. The mobile phase: 90% v/v water (0.1% TFA):methanol to 0% v/v water (0.1%TFA):methanol in 90 minutes. Flow rate: 0.2 ml min-1. UV detection at λ=312. The oven temperature was 298 K. The numeration of chlorophyll catabolites is as in the Fig. 2.

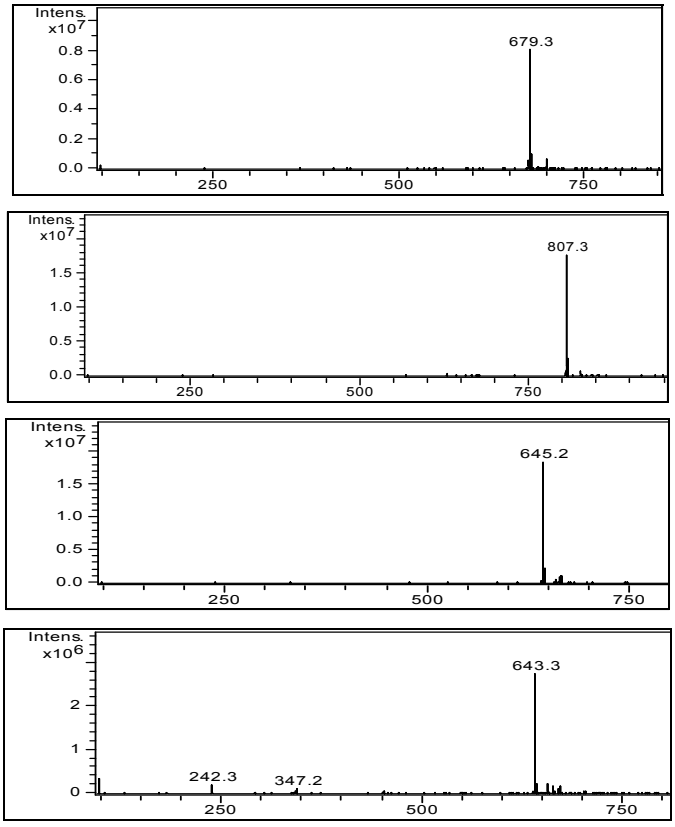

Figure 4. The ESI-MS of the chlorophyll catabolites numerated 3, 5, 7 and 9 in the Figure 2.

The thermodynamic study on the separation of the *Hydrangea aspera* chlorophyll catabolites on the RP – C_4 and RP – C_8 analytical columns. In case, when the separation was done on the RP – C_4 analytical column, the capacity factor k' showed a decrease, with a few exceptions at the temperature of 298K (Table 1). The capacity factor k' increases with the temperature in the case of all the *Hydrangea aspera* chlorophyll catabolites when the separation is done on the RP – C_8 analytical column (Table 2).

Table 1. Capacity factor of *Hydrangea aspera* chlorophyll catabolites on the RP-C_4 analytical column at different temperatures

T [K]	278	288	298	308	318
k' of the m/z 679 isomer-1	0.44	0.41	0.41	0.39	0.38
k' of the m/z 677	0.45	0.42	0.43	0.41	0.40
k' of the m/z 679 isomer-2	0.46	0.43	0.44	0.42	0.41
k' of the m/z 805 isomer-1	0.47	0.44	0.45	0.43	0.42
k' of the m/z 807 isomer-1	0.49	0.46	0.47	0.45	0.43
k' of the m/z 807 isomer-2	0.51	0.49	0.50	0.48	0.47
k' of the m/z 645	0.54	0.52	0.53	0.52	0.51
k' of the m/z 805 isomer-2	0.55	0.53	0.54	0.53	0.52
k' of the m/z 643	0.59	0.57	0.58	0.57	0.57

k' – capacity factor.

Table 2. Capacity factor of *Hydrangea aspera* chlorophyll catabolites on the RP-C_8 analytical column at different temperatures

T [K]	278	288	298	308	318
k' of the m/z 679 isomer-2	0.31	0.31	0.34	0.34	0.35
k' of the m/z 805 isomer-1	0.31	0.31	0.34	0.34	0.36
k' of the m/z 807 isomer-1	0.35	0.35	0.38	0.39	0.40
k' of the m/z 807 isomer-2	0.37	0.38	0.41	0.41	0.43
k' of the m/z 645	0.41	0.42	0.45	0.45	0.47
k' of the m/z 805 isomer-2	0.42	0.43	0.46	0.46	0.48

k' – capacity factor.

The representative graphs of the retention factor logarithm versus the inverse temperature (van't Hoff plots) are shown in Fig. 5 and 6.

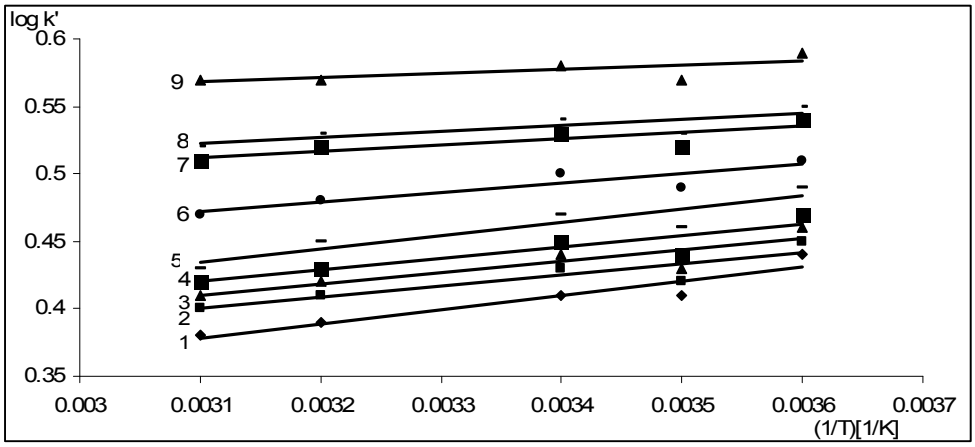

Figure 5. The graphs of the retention factor vs. inverse temperature used to calculate the change in molar enthalpy and entropy of the *Hydrangea aspera* chlorophyll catabolites, the: *m/z* 679 isomer-1 (graph 1), *m/z* 677 (graph 2), *m/z* 679 isomer-2 (graph 3), *m/z* 805 isomer-1 (graph 4), *m/z* 807 isomer-1 (graph 5), *m/z* 807 isomer-2 (graph 6), *m/z* 645 (graph 7), *m/z* 805 isomer-2 (graph 8) and *m/z* 643 (graph 9) on the RP-C_4 analytical column.

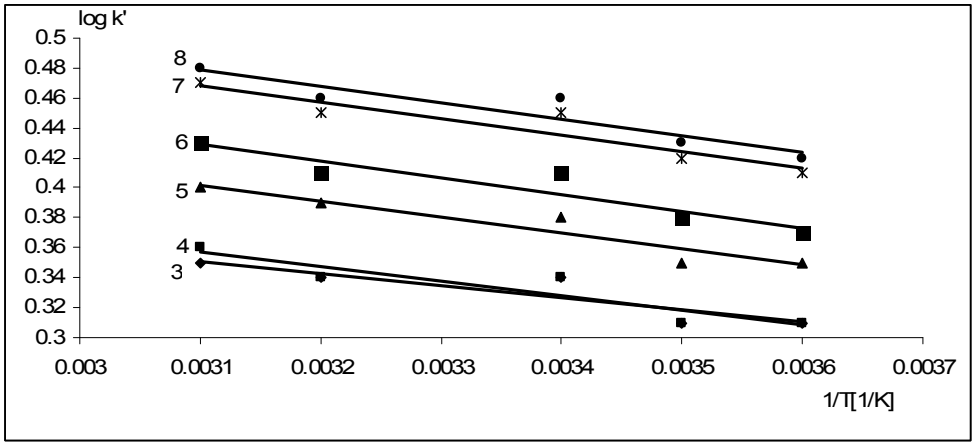

Figure 6. The graphs of the retention factor vs. inverse temperature used to calculate the change in molar enthalpy and entropy of the *Hydrangea aspera* chlorophyll catabolites, the: *m/z* 679 isomer-2 (graph 3), *m/z* 805 isomer-1 (graph 4), *m/z* 807 isomer-1 (graph 5), *m/z* 807 isomer-2 (graph 6), the *m/z* 645 (graph 7) and the *m/z* 805 isomer-2 (graph 8) on the RP-C_8 analytical column.

The obtained graphs were approximated to be linear although the square of the correlation coefficient were variable in case when the separation was done on the RP-C_4 analytical column, while when the separation was done on the RP-C_8, the square of the correlation coefficient were in the range of R^2=0.81 – 0.91 (Table 3 and 4). The linear graph would have indicated that the change in molar enthalpy is constant and that there is no significant change in retention mechanism over the temperature range of 278 – 318 K. The slopes are negative for the separations on the RP – C_8 analytical column indicating a positive change in molar enthalpy suggesting that the transfer from the mobile to the stationary phase is enthalpically unfavorable. The changes in molar enthalpies were calculated from the slopes in Fig. 5 and 6, according to the equation (2) and are depicted in Tables 3 and 4. The phase ratio of the column (Φ) was assumed to be a constant.

Table 3. Capacity factor of *Hydrangea aspera* chlorophyll catabolites on the RP-C_4 analytical column at different temperatures

	ΔH [J mol^{-1}]	ΔS [J mol^{-1}]	R^2
k' of the m/z 679 isomer-1	-2.02	0.97	0.91
k' of the m/z 677	-1.60	2.69	0.81
k' of the m/z 679 isomer-2	-1.60	2.88	0.81
k' of the m/z 805 isomer-1	-1.60	3.07	0.81
k' of the m/z 807 isomer-1	-1.89	2.45	0.84
k' of the m/z 807 isomer-2	-1.33	4.88	0.84
k' of the m/z 645	-0.87	7.11	0.68
k' of the m/z 805 isomer-2	-0.87	7.30	0.68
k' of the m/z 643	-0.58	9.07	0.49

ΔH – molar enthalpy, ΔS – molar entropy, R^2 – the square of the correlation coefficient.

Table 4. Capacity factor of *Hydrangea aspera* chlorophyll catabolites on the RP-C_8 analytical column at different temperatures

	ΔH [kJ mol^{-1}]	ΔS [J mol^{-1}]	R^2
k' of the m/z 679 isomer-2	1.56	11.54	0.81
k' of the m/z 805 isomer-1	1.85	12.55	0.85
k' of the m/z 807 isomer-1	2.02	13.95	0.91
k' of the m/z 807 isomer-2	2.11	14.75	0.87
k' of the m/z 645	2.11	15.51	0.87
k' of the m/z 805 isomer-2	2.11	15.70	0.87

ΔH – molar enthalpy, ΔS – molar entropy, R^2 – the square of the correlation coefficient.

When molar enthalpies are compared during the separation on the RP – C_4 analytical column there is an increase in molar entropy from the first *Hydrangea aspera* chlorophyll catabolite, with the *m/z* 679 isomer-1 to the last eluting *Hydrangea aspera* chlorophyll catabolite, with the *m/z* 643. The only exception was the *Hydrangea aspera* chlorophyll catabolite, with the *m/z* 807 isomer-1.

CONCLUSIONS

The extraction of *Hydrangea aspera* chlorophyll catabolites from the autumnal leaves' methanol extract with dichloromethane and ethyl acetate differs slightly. The identification of *Hydrangea aspera* chlorophyll catabolites on the RP –C_4 column reveals the presence of nine chlorophyll catabolites, while the separation on the RP –C_8 reveals the presence of few less chlorophyll catabolites. The thermodynamic investigations indicated that the retention behaviour of *Hydrangea aspera* chlorophyll catabolites on RP – C_4 and RP – C_8 analytical columns were slightly driven by the enthalpy difference. The van't Hoff curves obtained were approximated to be linear. When the investigations were done on the RP – C_4 the deviation from the linear approximation was great in case of the *Hydrangea aspera* chlorophyll catabolites with the *m/z* 643. The next investigations in reversed – phase liquid chromatography of chlorophyll catabolites are desirable. The search for the optimal mobile phases, modifiers and buffers is necessary in order to find the best separation conditions for the separation of the chlorophyll catabolites.

EXPERIMENTAL SECTION

Hydrangea aspera D. Don ssp. Sargentiana E. M. McClint autumnal leaves (15g dry weight, 20g "fresh" weight) were chilled with liquid nitrogen, grinded and homogenized in a blender with 0.2 dm^3 methanol, at room temperature, for 10 minutes. After centrifugation, the methanol extract was filtered and partitioned between hexane and methanol. Water was added to the methanol. The obtained volume was divided in two parts. From one part *Hydrangea aspera* chlorophyll catabolites were extracted with dichloromethane from the aqueous phase. Evaporation of dichloromethane ($t<40^oC$) yielded 12.53 mg. From the other part *Hydrangea aspera* chlorophyll catabolites were extracted with ethyl acetate from the aqueous phase. Evaporation of ethyl acetate ($t<40^oC$) yielded 10.84 mg. The extracts obtained were dissolved in methanol and subjected to the LC-MS analysis. Methanol and water used for the LC separation were HPLC grade (Acros Organics, Geel, Belgium) and trifluoroacetic acid (TFA) was reagent grade (Fluka, Buch, Switzerland). The LC/UV/ESI – MS analysis were performed on Waters 2695 Separations Module (Milford, MA, USA) coupled to a Waters 2996 PDA UV-Vis detector and connected to Bruker Daltonics esquire HCT (Bruker Daltonik, GmbH, Bremen, Germany) equipped with an electrospray ionization (ESI) source. Nitrogen produced by nitrogen generator (Domnick Hunter Group plc, Durham, England) was used as nebulizer (20 psi) and drying gas (9 L min^{-1} at 320^0C) in ESI experiments. The ESI detection was done in positive mode. The capillary voltage in a ramp ranged from 4.5 to 1.5 kV. Data were acquired by HyStarTM and processed by Bruker Daltonics Data Analysis running under Windows NTTM (Microsoft, Redmond, USA). The LC separations were carried on the reverse phase (RP) EC 250x4 mm Nucleosil® 100-5 C_8 column together with RP CC 8x4 mm Nucleosil® 100-5 C_8 precolumn and the RP column with the stationary phase EC 250x4 mm Nucleosil® 120-5 C_4 column together with CC 8x4 mm Nucleosil® 120-5 C_4 precolumn (Macherey-Nagel, Oesingen, Switzerland). The injection volume was 10μL via autosampler injection and in every sample 10 μL of uracil (0.01 mg mL^{-1}) was dissolved. For the thermodynamical investigations the temperature of the column oven was in a range from 278 K to 318 K. The starting measurement was done at oven temperature of 278 K with the subsequent increase of temperature by 10 K. Mobile phase consisted of methanol and 0.1 % TFA in water. The proportion of methanol was increased linearly from 10% to 100% in 80 minutes with a flow rate of 0.2 mL min^{-1}. After each separation the column was reequilibrated linearly from 100 % methanol to 90% water (0.1% TFA):10% methanol in 10 minutes and additional 5 minutes at 90% water (0.1% TFA):10% methanol. Data were acquired by HyStarTM and processed by Bruker Daltonics Data Analysis running under Windows NT™ (Microsoft, Redmond, USA).

The following formulas were used for the calculation of the capacity factor and the van't Hoff isotherm [9].
The capacity factor (k') was calculated with the equation (1):

$$k' = \frac{t_R - t_0}{t_0} \quad (1)$$

where the t_R is the retention time of one of the *Hydrangea aspera* chlorophyll catabolite and t_0 is the retention time of the unretained compound (uracil).
The van't Hoff equation [10]:

$$\log k' = (-\frac{\Delta H}{2.3\,RT}) + (\frac{\Delta S}{2.3R}) + \log \Phi \quad (2)$$

where ΔH is enthalpy, ΔS is entropy, T is the absolute temperature, R is the universal gas constant and the Φ is the phase ratio of the system. In the van't Hoff plot the log k' versus 1/T is usually a linear curve with the slope of –ΔH/2.3R and an intercept of ΔS/2.3R+log Φ. The value of Φ was assumed to remain constant over the temperature range studied, so that the general trends in ΔS could be analyzed [6].

The values obtained during the experimental measurements represent the means of the triplicate measurements (n=3) ± SD.

REFERENCES

1. M. Oberhuber, J. Berghold, K. Breuker, S. Hoertensteiner, B. Kraeutler, *Proceedings of the National Academy of Sciences USA*, **2003**, 100, 6910.
2. M. Oberhuber, J. Berghold, W. Muehlecker, S. Hoertensteiner, B. Kraeutler, *Helvetica Chimica Acta*, **2001**, 84, 2615.
3. J. Berghold, C. Eichmueller, S. Hoertensteiner, B. Kraeutler, *Chemistry & Biodiversity*, **2004**, 1, 657.
4. T. Mueller, S. Oradu, D. R. Ifa, R.G. Cooks, B. Kraeutler, *Analytical Chemistry*, **2011**, 83, 5754.
5. C.B. Castells, P. W. Carr, *Chromatographia*, **2000**, 52, 535.
6. R.J.M. Vervoort, E. Ruyter, A.J.J. Debets, H.A. Claessens, C.A. Cramers, G.J. de Jong, *Journal of Chromatography A*, **2002**, 964, 67.
7. V.A. Chirkin, S.I. Karpov, V.F. Selemenev, *Russian Journal of Physical Chemistry A*, **2012**, 86, 1903.
8. C.-W. Tsai, C.-I. Liu, Y.-C. Chan, H.-H. Tsai, R.-C. Ruaan, *Chromatographia*, **2010**, 114, 11620.
9. R.E. Ardrey, "Liquid chromatography – mass spectrometry: An Introduction", Wiley, England, **2003**, chapter 2.
10. A. Tchapla, S. Heron, H. Colin, G. Guichon, *Analytical Chemistry*, **1988**, 60, 1443.

STUDIA UBB CHEMIA, LVIII, 2, 2013 (p. 53 – 59)
(RECOMMENDED CITATION)

CHARACTERIZATION OF BUFFALO MILK FAT GLOBULES USING THE CONFOCAL LASER SCANNING MICROSCOPY

ALEXANDRA LĂPUŞAN[a]*, FLAVIU TĂBĂRAN[a]*, SORIN DANIEL DAN[a], ROMOLICA MIHAIU[b], CORNEL CĂTOI[a], MARIAN MIHAIU[a]

ABSTRACT. Milk fat globules are biologically essential components due to their functional and health properties. Milk fat composition has been thoroughly studied in cow milk but still it remains unclear in buffalo milk. We have used confocal laser scanning microscopy (CLSM) to investigate the structure of the fat globules in cow and buffalo milk, using two types of fluorescently-labelled dyes for phospholipid and triglyceride constituents. Using this technique, we have observed heterogeneities in the distribution of these lipids both in the membrane as on the surface relating to the specie and size of the globules. The statistical analysis has shown that there are significant differences ($p<0.05$) among the average fluorescence intensity (13.68±9.98 AU/μm^2) found at buffalo milk fat globules in comparison to cow ones (16.88 ± 4.3 AU/μm^2). The statistical comparison of the phospholipids quantification values in both species revealed the fact that there are no significant differences ($p>0.05$), the average found at cow milk being 31.07 AU/μm^2 and at buffalo 34.85 AU/μm^2. The use of specific dyes may be essential in the evaluation of the unsaturated lipid milk fraction, the buffalo milk fat globules being easily differentiated from cow milk by OilRed quantification.

Keywords: *milk, buffalo, confocal laser scanning microscopy, fluorescence, dye*

INTRODUCTION

Milk fat globules play an essential role in the processing and technology characteristics of dairy products, leading to different particularities according to the specie. The size of these fat globules is essential in milk

[a] *University of Agricultural Sciences and Veterinary Medicine, Faculty of Veterinary Medicine, 3-5 Mănăştur street, 400372, Cluj-Napoca, Romania, email: lapusan_alexandra@yahoo.com*
a authors with equal contribution*
[b] *Babes – Bolyai University, Faculty of Economics and Business Administration, Cluj-Napoca, Romania*

separation, cheese technology and their further processing [1-3]. The protein quantity absorbed per surface unit, the emulsion stability as well as their optical, rheological (colour and viscosity) [4] and conductibility features [5] are influenced by fat globules. On the other hand, the variation in size, distribution, microstructure and rheological properties according to the animal species [6,7] leads to the characteristic of each dairy product.

The distribution of the fat globules' sizes was previously evaluated using various methods such as classical microscopy, turbidity measurements, and electronic impulses [8]. The classical microscopy was mainly used to establish the quality damage degree of milk fat globules. Until now, the heat treated milk or cream was investigated by using the classical [9], electronic [10] and confocal microscopy [11,12,13]. Recently, Evers et al. (2008) [14] have introduced the laser confocal microscopy method (CLSM) as a non-invasive technique for studying the cow fat globule' membrane using lipophilic and lectin colorants. Lopez et al. (2011) [15] has used a fluorescent staining for phospholipids analogue with lectines in order to visualize their distribution in the milk fat globule membrane. In Romania this is the first study performed on buffalo milk that characterizes the biochemical aspects of fat globules through confocal laser microscopy in comparison to cow milk.

RESULTS AND DISCUSSION

The unsaturated lipid fractions evaluation found in the fat globules of buffalo and cow milk was performed by using the lipid fluorescent dye OilRed.

The images presented in figure1 reveal the fluorescence emission of the dispersed dye in the spherical areas of cow milk. The use of this dye with affinity for unsaturated lipid fractions has confirmed the fact that in both species these molecules are found exclusively in the fat globules. This is not very surprising given the fact that the class they belong to, triglycerides, are hydrophobic molecules. This method has allowed the making of 2D and 3D images of these fat globules.

The distribution of fat globules in cow milk was measured also, varying from a 0.10 μm in diameter to 10 μm, with a final average of 4,33 μm. The distribution was revealed in three peaks, corresponding to the diameters: small sized (0,13 – 2,84 μm); average sized (3,5 – 7,87 μm) and large sized globules (much lower in number) with values in between 8 and 10,2 μm.

The fat globules' sizes evaluated in buffalo milk have varied considerably in diameter, registering a minimal value of 0.45 μm and a maximal value of 18.2 μm. The average registered was of 9.41 μm. Our study has revealed a higher value than the one found by El-Zeini (2006) [16] (8,7 μm).

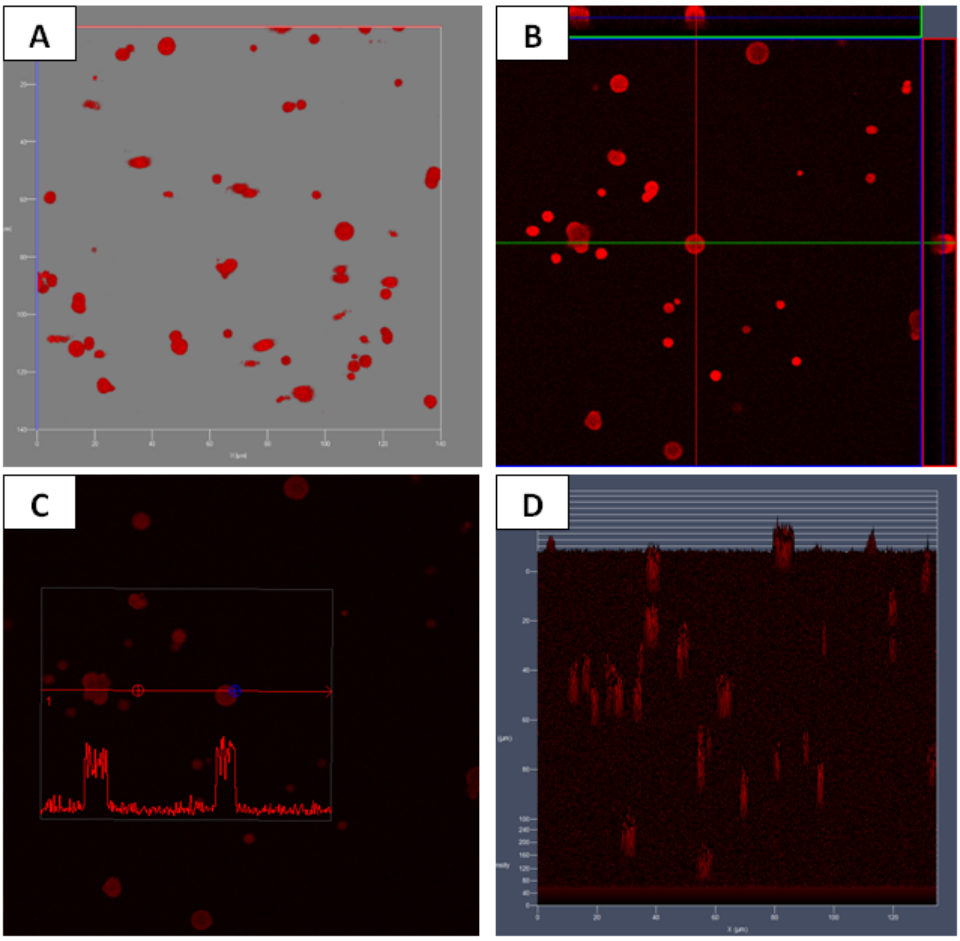

Figure 1. CLSM representing buffalo milk fat globules, colored with selective staining for fats Oil Red (Obx63, Apocromat immersion); A - tridimensional reconstruction; B – section analysis; C- fluorescence peak compared to the minimal background fluorescence; D – 2,5 D triglyceride fluorescence

The use of OilRed dye for these lipid fractions has allowed the statistical evaluation of fluorescence values measured in these stained fat globules and the interpretation of their fluorescence degrees. Their distribution is structurally and chemically heterogeneous in cow and also buffalo milk. Some of the results at the triglycerides' quantification from buffalo milk are shown in table 1.

Table 1. Triglycerides' fluorescence quantification in fat globules of buffalo milk

No.	Mean intensity (AU/Arbitrary units)	SD*	Pixels	Area
1.	4,67	3,95	1188	82,53
2.	3,4	3,57	331	23
3.	4,28	2,1	251	17,44
4.	2,14	3,62	502	34,88
5.	1,78	2,72	483	33,56
6.	2,18	2,31	461	32,03
7.	3,56	7,12	335	23,27
8.	2,85	3,97	326	22,65
9.	6,56	5,82	491	34,11
10.	50,72	9,53	861	59,82
11.	77,03	13,83	343	23,83
12.	8,17	3,67	494	34,32
13.	10,25	1,04	208	14,45

*SD – standard deviation

As shown also in table 1, buffalo milk fat globules have revealed a much lower intensity in the triglycerides' fluorescence. The statistical analysis has shown the fact that there are significant differences ($p<0.05$) among the average fluorescence intensity found at buffalo milk fat globules in comparison to cow ones. The average value of the fluorescence obtained in cow milk samples was 16.88 ± 4.3 AU/μm^2, with a minimum registered of 9.3 AU/μm^2 and a maximum of 32.57 AU/μm^2. In case of buffalo milk, the intensity was lower revealing an average of 13.68±9.98 AU/μm^2 with a minimum of 1.78 AU/μm^2 and a maximum of 77.03 AU/ μm^2. At the comparison of the fat globules' surface area, a significant difference ($p<0.05$) was noticed among the two species. This time, the surface area was higher in the case of buffalo milk (435,89 μm) and lower in the case of cow milk (182.98 μm).

These results are in accordance with other studies made on cow milk fat globules evaluated through the same technique [17,14]. Although there are innovative studies that characterize these fat globules lipid constituents, there aren't any that show a fully detailed comparison among different species. The correlation found in this experiment show that the fat globules' higher degree of fluorescence (OilRed) in the unsaturated lipid fraction at cow milk is due to the higher proportion of unsaturated fatty acids proved previously in our studies [18]. Although at the statistical analysis of the percentages of unsaturated fatty acids in cow milk compared to buffalo milk there were no significant changes revealed, we proved that based on their fluorescence degree quantification there are ($p<0.05$).

Milk fat globules were stained also with Rhodamine, an exogenous dye. This substance is a headgroup labelled phospholipid probe which can be incorporated with minimal perturbation into the phospholipids layer of the milk fat globule membrane.

We observed that the staining of the milk fat globule membrane was heterogeneous. In figure 2 it is also shown that two phases coexist within the buffalo milk fat globule membrane, a phase stained with rhodamine (reddish) and a phase where rhodamine is absent (green) (Figure 2). This fact was also observed in the case of cow milk fat globule, where the structure of the membrane formed by phospholipids were revealed in a disorganized liquid phase coexistent with the organized one. When comparing the intensities of fluorescence at the two species it was revealed the fact that there were no significant differences ($p>0.05$), the average found at cow milk being 31.07 AU/μm^2 and at buffalo 34.85 AU/μm^2. No matter the size of the fat globules, the rhodamine fluorescence dependant on the phospholipids substrate remains in the range at both species (28.05 – 36.9 AU/μm^2).

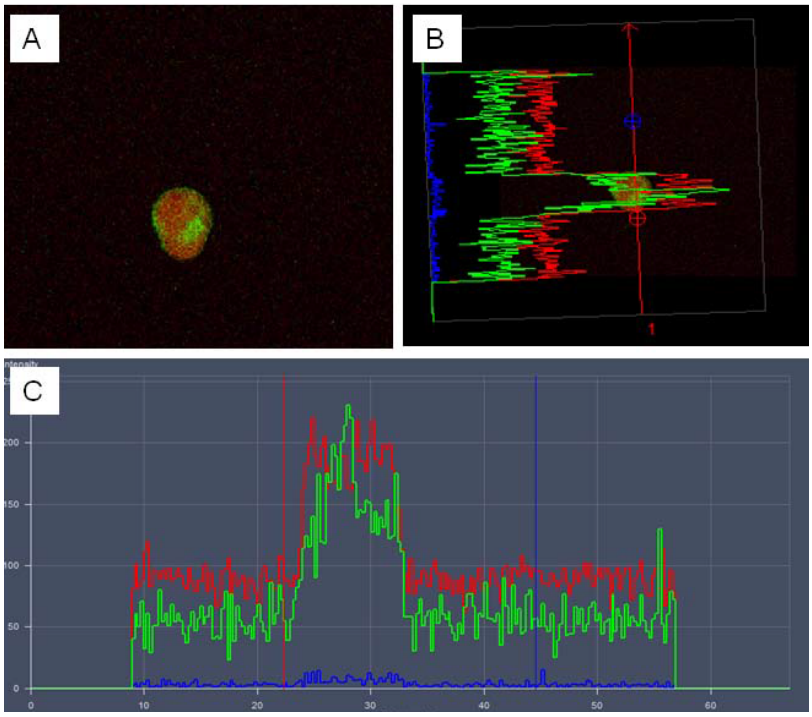

Figure 2. CLSM representing buffalo milk fat globules, stained with selective staining for triglycerides and phospholipids (Obx63, Apocromat immersion); A – plane image; B – fluorescence intensity profile on axis 1; C- Graphical representation of the fluorescence; Ch2 Rhodamine

CONCLUSIONS

The use of specific dyes in the evaluation of the unsaturated lipid fractions has revealed particularities at buffalo milk fat globules. The intensity of tryglicerides' fluorescence found in milk fat globule can be used as a particular marker in assessing the specie. Given the fact that the intensity of fluorescence is dependent on the amount of tryglicerides found in the fat globules we can conclude that in buffalo milk the tryglicerides quantity is lower than in cow milk. Regarding the phospholipids evaluation, the intensity of the fluorescence was not statistically different, being able to affirm that buffalo milk fat globules have similar phospholipids values as cow milk fat globules, not being able to use this method for possible differentiations.

EXPERIMENTAL SECTION

The study was conducted on 84 samples of buffalo milk and 87 cow milk samples, respectively. The samples were collected in sterile recipients and kept at refrigerating temperatures until their further analysis. No samples were kept longer than 6 hours until their analysis.

The confocal laser scanning microscopy analysis

The samples were analysed with the Confocal Laser Zeiss LSM 710 microscope, adjusted to an inversed microscope Acio Observer Z1. The specific visualization of the emitted fluorescence by the complex lipid-Oil red O was made by the laser exciting of the samples at a wave length of 596 nm and the use of an absorption filter between 578 and 637 nm (wave length for exciting/emission of the Texas Red fluorochrome). In order to visualize the Rhodamine 123 fluorescence a fluorochrome excitation of 511 wave length was used and the emission filters were in between 535-623. In order to visualize the entire image spectrum a Zeiss Plan-Apochromat objective (63x/1.40) was used. The images were processed and analysed by using the ZEN software, standard version.

The calibration at the beginning of the experiment was made according to the standard curve provided by the producers of the confocal system.

The quantification of the Oil Red and Rhodamine fluorescent signal

The quantitative assessment of triglycerides and phospholipid was performed with the mentioned dyes: Oil Red and Rhodamine, using the previously published protocol by Bhirde (2009) [19].

REFERENCES

1. M.K. Rowney, M.W. Hickey, P. Roupas, D.W. Everett**,** *Journal of Dairy Science*, **2003**,*86*, 712.
2. D.W. Everett and N.F. Olson**,** *Journal of Dairy Science,* **2003**, 86, 755.
3. Y. Ma and D.M. Barbano**,** *Journal of Dairy Science,* **2000**, 83, 1719.
4. P. Walstra, "Advanced Dairy Chemistry, Lipids", Chapman & Hall, Inc., London, **1995**, chapter 2.
5. M. Clausse, "Encyclopedia of Emulsion Technology", Marcel Dekker, Inc*.,* New York, **1983**, chapter 6.
6. M.A. Mehaia, *Milchwessenschaft,* **1995**, *50*, 260.
7. L.B. Abd El-Hamid and A.E. Khader, *Journal of Dairy Science*, **1982**, *10*, 43.
8. M.C Michalski, M. Ollivon, V. Briard, N. Leconte, C. Lopez, *Chemistry and Physics of Lipids,* **2004**, *132*: 2, 247.
9. J. Hinrichs and H.G. Kessler, *Cork Ireland: International Dairy Federation* **1995**, *9*, 21.
10. W. Buchheim, G. Falk, A. Hinz, *Food Microstructure,* **1986**, *5*, 181.
11. L. Fang**,** The effect of milk fat globule membrane damage in the absence of air on foulding in heat exchangers. MTech Thesis, Palmerston North: Massey University, **1998**.
12. S. Herbert, B. Bouchet, A. Riaublanc, E. Dufour, D.J. Gallant**,** *Lait,* **1999**, *79:6*, 567.
13. J.M Evers, *International Dairy Journal,* **2004**,*14:8*, 661.
14. J.M. Evers, R.G. Haverkamp, S.E. Holroyd, G.B. Jameson, D.D.S. Mackenzie, O.J. McCarthy, *International Dairy Journal,* **2008**,*18*, 1081.
15. C. Lopez and O. Ménard**,** *Colloids and Surfaces B: Biointerfaces,* **2011**, *83:1*, 29.
16. H.M. El-Zeini**,** *Polish Journal Food Nutrition,* **2006**, *15/56:2*, 147.
17. C. Lopez, B. Camier, J.Y. Gassi, *International Dairy Journal,* **2007**,17, 235.
18. M. Mihaiu, A. Lăpuşan, C. Bele, R. Mihaiu, S. D. Dan, Carmen Taulescu, C. Matea, *Roumanian Biotechnological Letters,* **2011**,*16*, 123.
19. A.A. Bhirde, V. Patel, J. Gavard, G. Zhang, A.A. Sousa, A. Masedunskas, R.D. Leapman, R. Weigert, J.S. Gutkind, J.F. Rusling, *ACS Nano,* **2009**, *3(2)*: 307.

STUDIA UBB CHEMIA, LVIII, 2, 2013 (p. 61 – 69)
(RECOMMENDED CITATION)

SITE DIRECTED SPIN LABELING OF HEMERYTHRIN AND HEMOGLOBIN

ISTVÁN MIHÁLY TAKÁCS[a], AUGUSTIN MOT[b], RADU SILAGHI-DUMITRESCU[b], GRIGORE DAMIAN[a*]

ABSTRACT. Site directed spin labeling in combination with electron paramagnetic resonance spectroscopy has become a very effective tool for studying the dynamics and structure of biomolecules in their native environment. This work presents the basics of site directed spin labeling and provides our results obtained in spin labeling hemerythrin and hemoglobin using methanethiosulfonate spin label. Best fit magnetic and libration parameters are obtained by simulation of EPR spectra.

Keywords: *site-directed spin labeling, EPR, proteins, nitroxides*

INTRODUCTION

The concept of site-directed spin labeling (SDSL) in combination with electron paramagnetic resonance (EPR) spectroscopy was developed by Wayne L. Hubbell and coworkers [1, 2]. Often conventional spectroscopic techniques are insufficient for studying structural properties of biomolecules, and EPR spectroscopy has distinguished itself by offering the possibility of studying the behavior of proteins in their native-like environment. The technique is available for studying soluble biomolecules such as proteins and nucleic acids, regardless of the size or complexity of the system [3, 4, 5, 6]. Although the majority of proteins are EPR-silent, SDSL and EPR can be used together, often in conjunction with site directed mutagenesis for creating a specific attachment point for the attachment of a nitroxide spin label, or, in cases where multiple such points already exist, for selecting only one of those for SDSL. Cysteine is a convenient aminoacid to use as target for SDSL, as its thiol group will react with the functional groups of the spin label; methanethiosulfonate, maleimide and iodoacetamide, creating a covalent bond.

[a] *"Babeş-Bolyai" University, Faculty of Physics, Str. Kogalniceanu, No. 1, RO-400084 Cluj-Napoca, Romania*
**corresponding author: grigore.damian@phys.ubbcluj.ro*
[b] *"Babeş-Bolyai" University, Faculty of Chemistry and Chemical Engineering, Str. Arany János, No. 11, RO-400028, Cluj-Napoca, Romania*

The nitroxide spin labels contain the nitroxyl radical (N-O) incorporated in a heterocyclic ring and the unpaired electron localized mostly on the N-O bond. Once attached to the protein their motion is dominated by their environment and the proteins backbone motion. The nitroxide spin label is influenced by his environment, surrounding structures and the motion of the protein, which is reflected in the EPR spectra of the spin label [7, 8].

Among the long list of available spin labels the (1-oxyl-2,2,5,5-tetramethylpyroline-3methyl) methanethiosulfonate spin label (MTSSL) [9] is the most often used, because its small molecular volume and flexibility, due to the link between the piperidine-oxyl group and the protein backbone, minimizing the disturbance of protein folding. After labeling the attached side chain is abbreviated as R1. Although their length, 5-8Å depending on the conformation, MTSSL side chains don't influence or disrupt the structural and functional properties of the protein [10].

The free electron situated on the nitroxyl radical has a strong dipolar interaction with the nitrogen nucleus, due to the nitrogen's nuclear spin state of I=1, the EPR spectral line shape will be formed by three lines each arising from one of the three quantum states of the nitrogen nucleus. The electron is also sensible to the anisotropic environment of the chemical bond. These anisotropies of the surrounding interactions make the label sensitive to its motion.

Continuous wave (cw) EPR spectroscopy of the spin labeled systems gives information about side chain mobility, solvent accessibility, polarity of the spin labels environment and distance between two paramagnetic centers [11].

Side chain mobility is a term used to describe the effect of motional rate, anisotropy and reorientational motion of the spin label on the EPR spectra [12]. At room temperature the EPR spectrum is particularly sensitive to the reorientational motion of the side chain because of the partial motional averaging of the anisotropic components of the g- and hyperfine tensors [10, 13, 14]. When exposed to a motionally less restrictive environment (e.g., water), the nitroxide will gain a faster rotational correlation time, in the ns range. In this case the three-peaked EPR spectra will look sharper, with a small central line width (ΔH_0) and small hyperfine splitting. In case of mobility restriction of the spin label (e.g., due to higher viscosity solvents or buried location of the side chain), the central line width and also the hyperfine splitting will increase and the first and last peaks intensity will also decrease [4, 15].

This paper reports the procedure and our results obtained in site directed spin labeling of *Phascolopsis gouldii* (Peanut worm) hemerythrin (Hr) and *Bos Taurus* (Bovine) hemoglobin (Hb).

RESULTS AND DISCUSSION

In Figure 1 the EPR spectrum of the MTS spin label free in water is presented, where the spin label moves faster and has a fast rotational correlation time of 0.79 ns. The second EPR spectrum represents also unbound MTS spin label, but now in a more viscous environment - 85% glycerol in water. The high viscosity of the glycerol determines the spin label to move slower obtaining a rotational correlation time of 2.12 ns. The difference is noticeable on the spectral lines, and the first and third peak have decreased in the case of 85% glycerol, when the label became more immobile; also, the central line width changes from ΔH_0=1.17 G in water, to 2.05 G in the glycerol/water mixture.

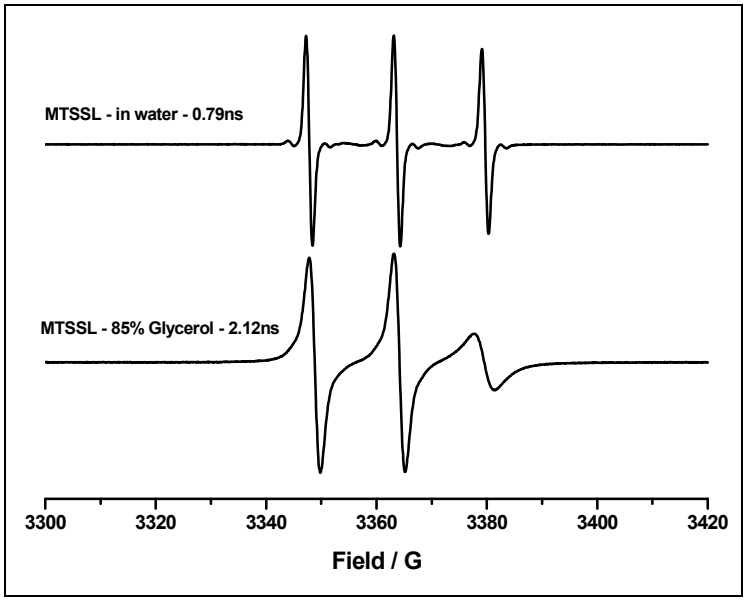

Figure 1. EPR spectra of MTSSL in water and glycerol-water solution.

Hemerythrin is a respiratory protein extracted from the blood of the Peanut worm; the protein is responsible for the oxygen transport in the organism by using a non-heme di-iron site [16, 17, 18]. Hr is a relatively large protein with a homooctameric structure and 108 kDa mass. The subunits are consistent of a four-helix bundle protein backbone, with 114 aminoacids. Every subunit is identical and contains a native cysteine at the 51st position, allowing one to spin label the protein at this selected site; Figure 2 illustrates the position of this cysteine within the monomer.

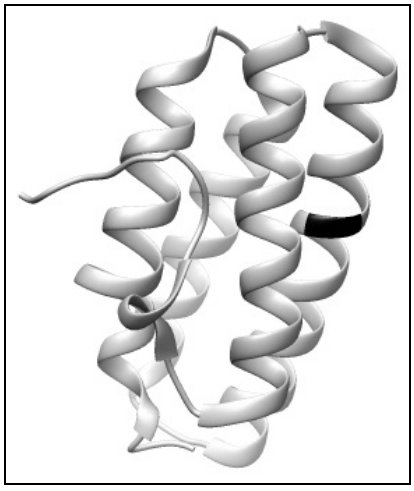

Figure 2. Hemerythrin subunit A with native cysteine at the 51stposition (black)

For a next step the labeling protocol was also applied to bovine hemoglobin. This type of hemoglobin is slightly different from the human one, in that it has only native cysteine in the *beta* (β) subunit at the 92nd position, the protein is composed from two *alpha* subunits and two *beta* subunits, containing in total 2 cysteines available for labeling. After labeling we abbreviated the sample Hb92R1. Figure 3 illustrates the beta subunit of the Hb containing the native cysteine in blacked.

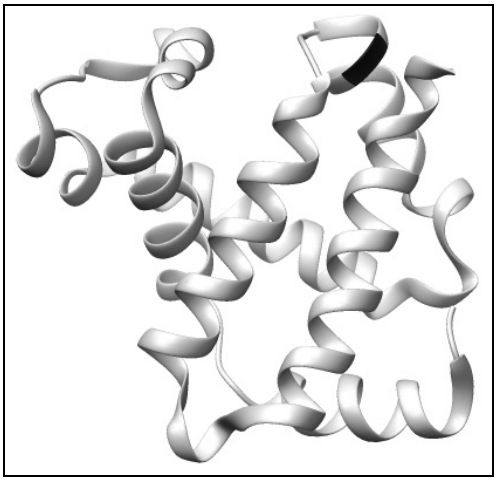

Figure 3. Representation of the Hb beta subunit with native cysteine colored in black.

For a quantification of the successfully bonded spin label to the protein, spin labeling efficiency, the EPR spectra of precisely prepared 100μM MTSSL sample were recorded as control. The double integral area of the EPR spectra of the MTSSL control sample can be used as a reference for the spin quantity corresponding to 100 μM spin units. The concentration of the protein was determined by UV-vis spectroscopy, via the absorption at 330 nm in the case of the Hr and at 430 in case of Hb.

From the double integral area of the EPR spectra of the samples the concentration of spins in the samples could then be determined – which, reported to the protein concentration and taking into account the number of cysteines available per monomer allows one to calculate the spin labeling efficiency.

For the hemerythrin sample prepared without reducing with DTT the labeling efficiency was 82%, whereas for the other sample, in which preparation included the DTT reducing step, a 91% labeling efficiency was attained. The nearly 10% difference observed by using DTT is a considerable advantage and improvement to the procedure. In the case of the hemoglobin the obtained spin labeling efficiency was 97%. Overall, these are very good yields. Indeed, both of the proteins have their native cysteine in a location easily accessible for the spin label; this is known to be one of the major influencing factor in spin labeling.

Upon analysis of the EPR spectra, the g- and hyperfine tensor values for the samples and the rotational correlation time of the spin label along with the component fraction were calculated. Using the simulation software for nitroxide spin labels Multicomponent EPR 495 developed by Christian Altenbach, we simulated the EPR spectra of the Hr with 3 components. The idea in a simulation is to use the minimum number of components possible in a simulation and obtain the best result. In the case of the Hb the simulation was done with 2 components.

Table 1. Best fit simulation parameters for spin labeled hemerythrin EPR spectra

Comp	**Fraction** (%)	$\mathbf{A_{xx}}$ (G)	$\mathbf{A_{yy}}$ (G)	$\mathbf{A_{zz}}$ (G)	$\mathbf{g_{xx}}$	$\mathbf{g_{yy}}$	$\mathbf{g_{zz}}$	**Corr. Time ns**
I	68.34	7.35	7.65	33.02	2.0087	2.0067	2.0032	4.26
II	22.57	8.25	8.55	32.05	2.0085	2.0065	2.0045	3.5
III	9.09	8.55	8.85	31.56	2.0085	2.0065	2.0041	1.16

A possible practical explanation for the three Hr components would be that the largest fraction represents the Hr octameric structure, the smallest fraction would represent the monomeric state of the protein and the third component would represent a multimeric structure of the protein.

As seen in Table 1 the small fractioned component is the fastest one; the explanation that this component represents the monomeric state in the protein fits perfectly, because of the large possible mobility of the spin label on the single subunit, due to his outer side position on the helix of the subunit. This mobility is limited when we talk about the octameric form since in that case the spin label is not at the surface anymore - it is between two subunits, and this fact is observed also in the rotational correlation time.

Table 2 contains the data obtained from simulations on the hemoglobin spectra. The mobility of this protein is quite different from the Hr; the protein is tighter, smaller and more restrictive for the spin label movement as the Hr. In this case the label is not pointing towards the outside as in the case of the Hr subunits, but is rather trapped inside the beta unit; this explains the slower rotational correlation times.

Table 2. Best fit simulation parameters for spin labeled hemoglobin EPR spectra

Comp	**Fraction** (%)	$\mathbf{A_{xx}}$ (G)	$\mathbf{A_{yy}}$ (G)	$\mathbf{A_{zz}}$ (G)	$\mathbf{g_{xx}}$	$\mathbf{g_{yy}}$	$\mathbf{g_{zz}}$	**Corr. Time ns**
I	21.21	9.83	10.13	33.68	2.0070	2.0050	2.0039	3
II	78.79	5.9	6.2	34.76	2.0080	2.0060	2.0022	4.73

By looking at the spectra of the two proteins on the Figure 4 one can clearly see the differences in the shape. The simulation data shows that the Hr is more mobile, and this is noticeable in the EPR spectra as well, with the first peak more intense and sharp. In the Hb spectra, this component is shifted to the left and has less sharpness and intensity. In the case of Hb, due to the tightness of the system, the label is not as mobile as in the case of the Hr, this is reflected in the spectra as well as in the correlation times.

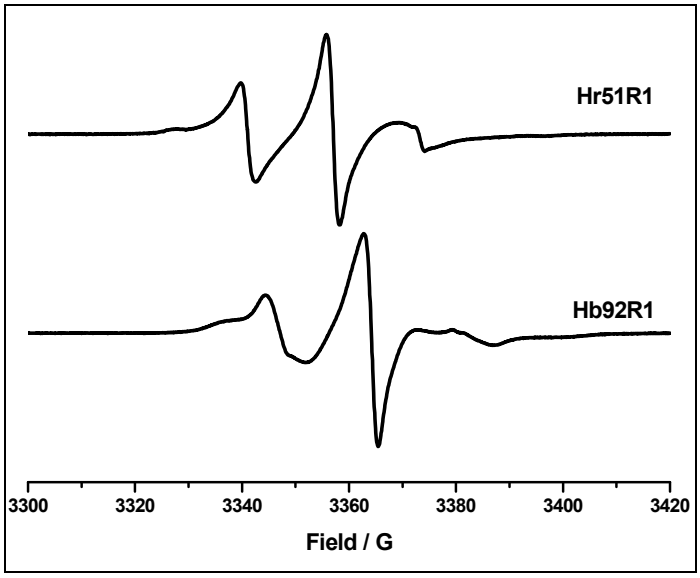

Figure 4. EPR spectra of the spin labeled hemerythrin (top) and spin labeled Hemoglobin (bottom).

CONCLUSIONS

By analysis of EPR spectra of nitroxide radical motion within a labelled protein one can obtain the main dynamic parameters of protein domains and characterizes protein conformation and any changes that may occur in different environments, too. Proof of concept data are shown here for hemerythrin for the first time, in comparison with the more often-studied hemoglobin.

EXPERIMENTAL SECTION

The EPR measurements were carried out on a Bruker EMX EPR spectrometer with continuous wave at X-band (9 GHz), equipped with a Bruker liquid nitrogen temperature controller. The spectra were recorded at room temperature with a microwave frequency of 9.45 GHz, microwave power of 4 mW, modulation frequency of 100 kHz, modulation amplitude of 1 G and microwave attenuation of 17 dB. The samples were measured in quartz capillary tubes containing 15 µL of sample.

The MTS spin label was inquired from Enzo Life Sciences and was dissolved in DMSO (100 mM, stock solution).

Simulation of the EPR spectra of labelled proteins, was performed by Multi-Component EPR Fitting v2 version 495 program, a LabVIEW software, developed by Dr. Christian Altenbach (University of California, Los Angeles, California, *https://sites.google.com/site/altenbach/labview-programs/epr-programs/multicomponent)*

For the purpose of spin labeling, *Phascolopsis gouldii* Hr, purified as previously described [19], was first suspended in PBS buffer and a final concentration of 10 mM DTT was added to the solution. The mixture was incubated and constantly shaken at 4^{o}C for 2 hours. To obtain a good spin labeling efficiency, by preventing the reduction of the disulfide bridge between the cysteine and the side chain, the DTT was removed by washing from the system using a 10kDa Millipore filter in a Beckman J21B centrifuge. The sample was centrifuged 6 times at 4^{o}C, 5000 rpm for 30 minutes. After each step the flow-trough was checked by UV-vis spectroscopy for traces of DTT. After the complete removal of DTT from the system the MTSSL spin label was introduced into the sample with a 10 times excess to each monomer. A second sample of Hr was also prepared, where the DTT part was altogether omitted, on the grounds that Hr does not contain disulfide bonds – and the role of DTT in principle would be precisely to cleave disulfide bonds in order to liberate the thiols for labeling. The two samples were incubated overnight at 4^{o}C.

The next step was to remove the unbound excess spin label from the sample and to determine the efficiency of the spin labeling. The two samples were washed out of the excess spin label by using 10 kDa Millipore filters and were centrifuged at 5000 rpm and 4^{o}C for 5 times. After each step of washing the flow-trough was checked for remnant spin labels by EPR spectroscopy. After the 4th step the flow-through EPR spectra showed no traces of spin label. This was done to both of the samples in the same conditions. The obtained sample after labeling is abbreviated as Hr51R1, 51 representing the 51st position of the subunit where the spin label is bound and R1 is the name of the side chain after labeling, as mentioned before.

ACKNOWLEDGMENTS

IMT acknowledges the financial support of the Sectorial Operational Programme for Human Resources Development 2007-2013, co-financed by the European Social Fund, under the project number POSDRU/107/ 1.5/S/76841 with the title „*Modern Doctoral Studies: Internationalization and Interdisciplinarity*”.

REFERENCES

1. C. Altenbach, S.L. Flitsch, H.G. Khorana, W.L. Hubbell, Biochemistry, **1989**, 28:7806-7812.
2. C. Altenbach, T. Marti, H.G. Khorana, W.L. Hubbell, Science, **1990**, 248:1088-1092.
3. E. Bordignon, H-J.Steinhoff, Membrane protein structure and dynamics studied by site-directed spin labelling ESR. In: M.A. Hemminga, L.J. Berliner (eds) ESR spectroscopy in membrane biophysics, **2007,** Springer Science and Business Media, New York, pp 129-164.
4. W.L. Hubbell, H.S. Mchaourab, C. Altenbach, M.A. Lietzow, Structure, **1996**, 4:779-783.
5. W.L. Hubbell, A. Gross, R. Langen, M.A. Lietzow, Curr. Opin. Struct. Biol. **1998**, 8:649-656.
6. C.S. Klug, J.B. Feix, Methods and applications of site-directed spin labelling EPR spectroscopy, In: J.J. Correia, H.W. Detrich (eds), Methods in cell biology. Biophysical tools for biologists, Volume one: in vitro techniques, **2008**, New York, Academic Press, pp 617-658.
7. S.Cavalu, G.Damian, Biomacromolecules, **2003**, 4(6);1630-1635.
8. S.Cavalu, G.Damian, M.Dansoreanu, Biophysical Chemistry, **2002**, 99(2):181-188.
9. L.J. Berliner, J. Grunwald, H.O. Hankovszky, K. Hideg, Anal. Biochem. **1982**, 119:450-455.
10. J.P.Klare, H-J. Steinhoff, Spin labelling EPR, Photosynth. Res., **2009**, Volume 102, 2-3:377-390.
11. G.F. White, L. Ottingnon, T. Georgiu, C. Kleanthous, G.R. Moore, A.J. Thomson, V.S. Oganesyan, Journal of magnetic Resonance, **2007**, 185:191-203.
12. L.J. Berliner, Spin labeling: theory and applications, **1976**, Academic Press, New York.
13. L.J. Berliner, Spin labeling II: theory and applications, **1979**, Academic Press, New York.
14. L.J. Berliner, J. Reuben, Spin labeling theory and applications, **1989**, Plenum Press, New York.
15. H.S. Mchaourab, M.A. Lietzow, K. Hideg, W.L. Hubbell, Biochemistry, **1996**, 35:7692-7704.
16. C.S. Farmer, D.M. Kurtz Jr, R.S. Phillips, J. Ai, J. Sanders-loeher, J. Biol. Chem., **2000**, 275:17043-17050.
17. S. Jin, D.M. Kurtz Jr, Z.J. Liu, J. Rose, B.C. Wang, J. Am. Chem. Soc., **2002**, 124:9845-9855.
18. S.V. Kryatov, E.V. Rybak-Akimova, S. Schindler, Chem. Rev. **2005**, 105:2175-2226.
19. A.C. Mot, A. Roman, I. Lupan, D.M. Kurtz Jr, R. Silaghi-Dumitrescu, , Protein J, **2010,** 29:387-393.

STUDIA UBB CHEMIA, LVIII, 2, 2013 (p. 71 – 86)
(RECOMMENDED CITATION)

MAXIMAL HARARY INDEX OF UNICYCLIC GRAPHS WITH A GIVEN MATCHING NUMBER

KEXIANG XU[a*], KINKAR CH. DAS[b], HONGBO HUA[c], MIRCEA V. DIUDEA[d]

ABSTRACT. The Harary index is defined as the sum of reciprocals of distances between all the vertex pairs of a connected graph. In this paper we present upper bounds on Harary index of unicyclic graphs with a given matching number and characterize the extremal graphs for which the upper bounds on Harary index are attained.

Key Words: *Graph, Reciprocal distance, Harary Index, upper bound*

INTRODUCTION

The Harary index of a graph, denoted by *H*(*G*), has been introduced in 1993, independently by Ivanciuc *et al*.[1] and by Plavšić *et al*.[2] Even earlier, the QSAR group in Timisoara, Romania, particularly Ciubotariu [3], have used this index to express the decay of interactions between atoms in molecules as the distances between them increased. It has been so named in the honor of Professor Frank Harary, on the occasion of his 70th birthday. The Harary index is defined as

$$H(G) = \sum_{u,v \in V(G)} \frac{1}{d_G(u,v)}$$

where the summation runs over all unordered pairs of vertices of the graph *G* and $d_G(u,v)$ denotes the topological distance between any two vertices *u* and *v* of *G* (i.e., the number of edges in a shortest path connecting *u* and *v*). Mathematical properties and applications of *H* are reported in refs. [4-14].

[a] *College of Science, Nanjing University of Aeronautics & Astronautics, Nanjing, China*
** xukexiang1211@gmail.com (K. Xu)*
[b] *Department of Mathematics, Sungkyunkwan University, Suwon 440-746, Republic of Korea*
[c] *Faculty of Mathematics and Physics, Huaiyin Institute of Technology,Huai'an, Jiangsu, China*
[d] *Faculty of Chemistry and Chemical Engineering, Babes-Bolyai University, Cluj, 400084, Romania*

Chemical applications of this index, in correlating with thermodynamic properties or octane number of alkanes, or in discriminating alkane isomers, are presented in refs. [5,15-18]. Some new interesting properties of other distance-based graph invariants can be seen in refs. [19-21].

Let $\gamma(G,k)$ be the number of vertex pairs of *G* lying to each other at the distance *k*. Then, from refs.[8,12] we have:

$$H(G) = \sum_{k\geq 1} \frac{1}{k} \gamma(G,k). \quad (1)$$

All graphs herein considered are finite and simple ones. Let *G* = (*V;E*) be a graph with the vertex set *V* (*G*) and edge set *E*(*G*). A connected graph *G* is called a unicyclic graph if $|V(G)| = |E(G)|$. Two edges e_1 and e_2 are called independent if they do not have a common vertex. A matching of *G* is a subset of *E*(*G*) with some pairwise independent edges. For a graph *G*, the *matching number* $\beta(G)$ is the maximum cardinality among the independent sets of edges in *G*. For a matching *M* of a graph *G*, if a vertex $v \in V(G)$ is incident to an edge of *M*, then *v* is said *M*-saturated. For a graph *G*, *D*(*G*) denotes the diameter of *G*, or the maximum topological distance between any two vertices in *G*. In the following, we denote by P_n, C_n and S_n the path graph, the cycle graph and the star graph with *n* vertices, respectively. For other notations and terminology in the Graph Theory, the readers may consult refs. [22,23].

Let $\bigcup(n,m)$ be the set of connected unicyclic graphs, of order *n* and having the matching number *m*. Recently, Ilić *et al.* [24] have determined the tree with the maximal Harary index among all the trees of order *n* and having the matching number *m*. Du and Zhou [25] determined the extremal graph of $\bigcup(n,m)$ with the minimal Wiener index. Inspired by the above results, the graphs of $\bigcup(n,m)$, having the maximal Harary index and their characterization, will be presented in the following.

SOME LEMMAS

As preliminaries, let us introduce some basic lemmas. For a graph *G*, with $v \in V(G)$, one defines [12]

$$Q_G(v) = \sum_{u\in V(G)} \frac{d_G(u,v)}{d_G(u,v)+1}.$$

For convenience, we will write $Q_G(v)$ as $Q_{V(G)}(v)$. Note that the function $f(x)=\frac{x}{x+1}$ is strictly increasing for $x>1$.

Let $U_{n,m}$ be a unicyclic graph obtained by attaching $n-2m+1$ pendent edges and $m-2$ pendent paths, of length 2, to one vertex of the triangle C_3, as shown in Figure 1. By equality (1), we can obtain

$$H(U_{n,m})=n+\frac{1}{2}\left[\binom{n-m+1}{2}-1+m-2\right]+\frac{1}{3}[(n-2m+3)(m-2)+(m-2)(m-3)]+\frac{1}{4}\binom{m-2}{2}$$

$$=n+\frac{1}{2}\frac{(n-m)^2+n+m-6}{2}+\frac{1}{3}(n-m)(m-2)+\frac{1}{4}\binom{m-2}{2}$$

$$=\frac{1}{24}(6n^2-4mn+m^2+14n+7m-18). \qquad (*)$$

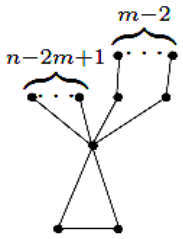

Fig.1 The graph $U(n,m)$

For a vertex *v* of *G*, the *eccentricity ecc*(*v*) is defined as the maximum distance from *v* to any other vertex in *G*.

Lemma 2.1. *Let G be a connected graph of order n* > 4, *with a pendent vertex v adjacent to the vertex u, and let w be a neighbor of u different from v. Then*

$$H(G)-H(G-v)\le\frac{n}{3}+\frac{1}{6}+\frac{1}{6}d_G(v) \qquad (2)$$

with the equality holding if and only if ecc(*u*) = 2. *Moreover, if* $d_G(u)=2$, *then*

$$H(G)-H(G-\{u,v\})\le\frac{7n}{12}+\frac{1}{2}+\frac{1}{4}d_G(w) \qquad (3)$$

with the equality holding if and only if ecc(*w*) = 2.

Proof. Considering that *v* is a pendent vertex of *G*, we have

$$\begin{aligned} H(G)-H(G-v) &= n-1-Q_{G-v}(u) \\ &\le n-1-[\frac{1}{2}(d_G(u)-1)+\frac{2}{3}(n-1-d_G(u))] \\ &= \frac{n}{3}+\frac{1}{6}+\frac{1}{6}d_G(u) \end{aligned}$$

with the equality holding if and only if *ecc*(*u*) = 2.

When $d_G(u)=2$, we have

$$\begin{aligned} H(G)-H(G-\{u,v\}) &= H(G)-H(G-v)+H(G-v)-H(G-\{u,v\}) \\ &= n-1-Q_{G-v}(u)+n-2-Q_{G-\{u,v\}}(w) \\ &\le n-1-[\frac{1}{2}+\frac{2}{3}(d_G(w)-1)+\frac{3}{4}(n-2-d_G(w))] \\ &\quad +n-2-[\frac{1}{2}(d_G(w)-1)+\frac{2}{3}(n-2-d_G(w))] \\ &= \frac{7n}{12}+\frac{1}{2}+\frac{1}{4}d_G(w) \end{aligned}$$

with the equality holding if and only if *ecc*(*w*) = 2.

Lemma 2.2. [26] *Let* $G\in\bigcup(2m,m)$, $m\ge 3$ *and T be a branch of G with the root r. If* $u\in V(T)$ *is a pendent vertex closest to the root r, with* $d_G(u,r)\ge 2$, *then u is adjacent to a vertex of degree two.*

Lemma 2.3. [27] *Let* $G\in\bigcup(n,m)$, *with n > 2m and* $G\ne C_n$. *Then, there is a maximum matching M and a pendent vertex v of G such that v is not M-saturated.*

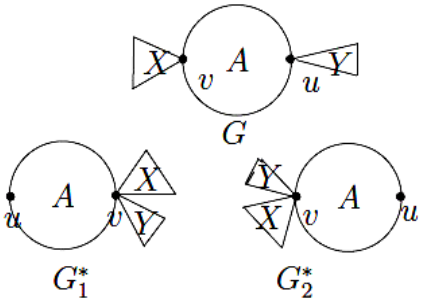

Fig. 2 The graphs G, G_1^* and G_2^* in Lemma 2.4

Lemma 2.4. [10,13] *Let A, X and Y be three connected graphs with disjoint vertex sets. Suppose that u, v are two vertices of A,* v_0 *is a vertex of X and* u_0 *is a vertex of Y . Let G be the graph obtained from A, X and Y by identifying v with* v_0 *and u with* u_0*, respectively. Let* G_1^* *be the graph obtained from A, X and Y by identifying three vertices v,* v_0 *and* u_0*, and let* G_2^* *be the graph obtained from A, X and Y by identifying three vertices u,* v_0 *and* u_0 *(Figure 2). Then we have:*

$$H(G_1^*) > H(G) \text{ or } H(G_2^*) > H(G).$$

From Lemma 2.4, the following corollary is immediate.

Corollary 2.1. *Let G be a connected graph with* $u, v \in V(G)$*. Denote by G(s;t) the graph obtained by attaching s > 1 pendent vertices to vertex u and t > 1 pendent vertices to vertex v. Then, we have*

$$H(G(1, s+t-1)) > H(G) \text{ or } H(G(s+t-1,1)) > H(G).$$

Lemma 2.5. [13] *Let G be a (connected) graph with a cut vertex w such that* G_1 *and* G_2 *are two connected subgraphs of G having w as the only common vertex and* $G_1 \cup G_2 = G$*. Let* $|V(G_i)| = n_i$ *for* $i = 1,2$*. Then*

$$H(G) = H(G_1) + H(G_2) + \sum_{u \in V(G_1)\setminus\{w\}} \sum_{v \in V(G_2)\setminus\{w\}} \frac{1}{d_{G_1}(u,w) + d_{G_2}(w,v)}.$$

Let $C_k(1^{n-k})$ be a graph obtained by attaching $n-k$ pendent edges to a vertex of C_k. Based on equality (1), we can claim that $H(C_k(1^1)) > H(C_{k+1})$, for $k \geq 5$. Denote by $C_k^*(n-k-1,1)$ a unicyclic graph obtained by attaching one pendent vertex and $n-k-1$ pendent vertices, respectively, to two adjacent vertices of a cycle C_k.

Lemma 2.6. *Let* $k \geq 5$ *and* $C_k^*(n-k-1,1)$ *be a unicyclic graph defined as above. Then*

$$H(C_k^*(n-k-1,1)) > H(C_{k+1}^*(n-k-2,1)).$$

Proof. To prove this lemma, we first prove that

$$H(C_k(1^{n-k})) > H(C_{k+1}(1^{n-k-2})).$$

Note that $C_k(1^{n-k})$ is obtained by identifying the unique vertex of degree 3 in $C_k(1^1)$ with the center of star S_{n-k-1}, where the new vertex is labeled as w_1

and $C_{k+1}(1^{n-k-2})$ is obtained by identifying one vertex C_{k+1} with the center of the star S_{n-k-1}, where the new vertex is labeled as w_2. Set $A = H(C_k(1^{n-k})) - H(C_{k+1}(1^{n-k-2}))$. So, by Lemma 2.5, we have

$$H(C_k(1^{n-k-1})) = H(S_{n-k-1}) + H(C_k(1^1)) + (n-k-2)\sum_{v\in V(C_k(1^1))\setminus\{w_1\}} \frac{1}{1+d_{C_k(1^1)}(w_1,v)},$$

$$H(C_{k+1}(1^{n-k-2})) = H(S_{n-k-1}) + H(C_{k+1}) + (n-k-2)\sum_{v\in V(C_{k+1})\setminus\{w_2\}} \frac{1}{1+d_{C_{k+1}}(w_2,v)}.$$

Thus, considering that $H(C_k(1^1)) > H(C_{k+1})$, for $k \geq 5$, from above we get

$$A > (n-k-2)\Big(\sum_{v\in V(C_k(1^1))\setminus\{w_1\}} \frac{1}{1+d_{C_k(1^1)}(w_1,v)} - \sum_{v\in V(C_{k+1})\setminus\{w_2\}} \frac{1}{1+d_{C_{k+1}}(w_2,v)}\Big)$$

$$= (n-k-2)\Big(\frac{1}{2} - \frac{1}{1+\left\lceil \frac{k}{2} \right\rceil}\Big) > 0$$

as expected.

Assume that the unique vertex of degree 3 in $C_k^*(n-k-1,1)$ is u_1 and the unique vertex of degree 3 in $C_{k+1}^*(n-k-2,1)$ is u_2. Suppose that $V(C_k(1^{n-k-1})) = V(C_k^*(n-k-1,1)) \setminus \{v_1\}$ and $V(C_k(1^{n-k-1})) = V(C_k^*(n-k-1,1)) \setminus \{v_1\}$, where v_1 is adjacent to u_1 in $C_k^*(n-k-1,1)$ and v_2 is adjacent to u_2 in $C_{k+1}^*(n-k-2,1)$. Let $B = H(C_k^*(n-k-1,1)) - H(C_{k+1}^*(n-k-2,1))$. Similarly, by Lemma 2.5, we arrive at

$$H(C_k^*(n-k-1,1)) = 1 + H(C_k(1^{n-k-1})) + \sum_{v\in V(C_k(1^{n-k-1}))\setminus\{u_1\}} \frac{1}{1+d_{C_k(1^{n-k-1})}(u_1,v)},$$

$$H(C_{k+1}^*(n-k-2,1)) = 1 + H(C_{k+1}(1^{n-k-2})) + \sum_{v\in V(C_{k+1}(1^{n-k-2}))\setminus\{u_2\}} \frac{1}{1+d_{C_{k+1}(1^{n-k-2})}(u_2,v)}.$$

From above, we get

$$B > \sum_{v\in V(C_k(1^{n-k-1}))\setminus\{u_1\}} \frac{1}{1+d_{C_k(1^{n-k-1})}(u_1,v)} - \sum_{v\in V(C_{k+1}(1^{n-k-2}))\setminus\{u_2\}} \frac{1}{1+d_{C_{k+1}(1^{n-k-2})\setminus\{u_2\}}(u_2,v)}$$

as $H(C_{k+1}(1^{n-k-2})) > H(C_{k+1}(1^{n-k-2}))$

$= \frac{1}{3} - \frac{1}{1+\left\lceil \frac{k}{2} \right\rceil} > 0$, thus ending the proof of this lemma.

MAIN RESULTS

In this section, the graph of $\bigcup(n,m)$, with the maximal Harary index, will be determined. Before presenting the main results, we first will deal with some special cases of this problem.

When *n* = 3, there is only one unicyclic graph, which is just the triangle C_3, with the matching number 1. There is nothing to prove, in this case. Clearly, only C_3 belongs to $\bigcup(n,1)$. Next, we only need to consider the set $\bigcup(n,m)$, with $n \geq 4$ and $m \geq 2$. If *n* = 4, there are exactly two unicyclic graphs, C_4 and $C_3(1^1)$, which belong to $\bigcup(4,2)$, with $H(C_4) = H(C_3(1^1))$. When *n* = 5, we can easily check that (see ref.[11]) only two graphs C_n and $C_3(1^2)$ have the maximal Harary index in $\bigcup(5,2)$. From ref. [17] we find that the unique graph $C_3(1^{n-3})$ has the maximal Harary index in $\bigcup(n,2)$, with $n \geq 6$.

Now we consider the case *n* = 6. Two graphs, $G_6^{(1)}$ and $G_6^{(2)}$ are shown in Fig. 2. It is not difficult to check that there are only five graphs: $U_{6,3}$, $C_5(1^1)$, $G_6^{(1)}$, $G_6^{(2)}$ and C_6, in $\bigcup(6,3)$, and

$$H(C_5(1^1)) = 6 + \frac{1}{2}\times 7 + \frac{1}{3}\times 2 = 10\frac{1}{6}$$
$$> H(U_{6,3}) = H(C_6) = H(G_6^{(1)}) = H(G_6^{(2)})$$
$$= 6 + \frac{1}{2}\times 6 + \frac{1}{3}\times 3 = 10.$$

Thus $C_5(1^1)$ has the maximal Harary index in $\bigcup(6,3)$. In the following we assume that $n \geq 7$ and $m \geq 3$.

$G_6^{(1)}$ $G_6^{(2)}$

Fig. 3 The graphs $G_6^{(1)}$ and $G_6^{(2)}$

Let $\bigcup^{(1)}(m)$ be the set of graphs from $\bigcup(6,3)$ having a pendent vertex whose neighbor is of degree two. Also, let $\bigcup^{(2)}(m) = \bigcup(m) \setminus \bigcup^{(1)}(m)$. Denote by $C_5(1,1,1)$ the graph obtained by attaching three pendent vertices to three consecutive vertices in C_5.

Lemma 3.1. *Let* $G \in \bigcup^{(2)}(m)$, *with* $m \geq 4$. *Then, we have*

$$H(G) \leq \frac{1}{24}(17m^2 + 35m - 18)$$

with the equality holding if and only if $G \cong C_5(1,1,1)$.

Proof. If $G \cong C_5(1,1,1)$, the equality holds immediately. So it suffices to prove that

$H(G) < \frac{1}{24}(17m^2 + 35m - 18)$, when $G \neq C_5(1,1,1)$.

For any graph $G \in \bigcup^{(2)}(m) \setminus \{C_5(1,1,1)\}$, by Lemma 2.2, we find that *G* is the cycle C_{2m} or a graph obtained by attaching some pendent vertices to some vertices of C_k with $m \leq k \leq 2m-1$. Combining the structure of $U_{n,m}$ with *n* = 2*m* and formula (*), we can easily find

$$\frac{17m^2 + 35m - 18}{24} = 2m + \frac{1}{2}\frac{m^2 + 3m - 6}{2} + \frac{1}{3}m(m-2) + \frac{1}{4}\binom{m-2}{2}$$

Moreover, for $m \geq 4$,

$\gamma(C_{2m},2) = 2m < \frac{m^2 + 3m - 6}{2}$, $\gamma(C_{2m},3) = 2m < m(m-2)$ and

$$\gamma(C_{2m},4) \geq m, \ldots, \gamma(C_{2m},m) = m.$$

Therefore, from (1), we have $H(C_{2m}) < \frac{17m^2 + 35m - 18}{24}$.

Now, let us consider the case when *G* is a graph obtained by attaching some pendent vertices to some vertices of C_k, with $m \leq k \leq 2m-1$. To prove this lemma, we need to look at the following three cases.

Case 1: *k* = *m*. In this case, we can easily find that *G* is a graph obtained by attaching

a pendent vertex to each vertex of C_m. If m = 4, we can easily check that $H(G) < H(C_5(1,1,1))$. When $m \geq 5$, we have $\gamma(G,2) = 3m < \frac{m^2+3m-6}{2}$, $\gamma(G,3) = 3m + \gamma(C_m,3) \leq m(m-2)$, $\gamma(G,4) = m + 2\gamma(C_m,4), \cdots,$ $\gamma(G,\left\lfloor \frac{m}{2} \right\rfloor + 2) = \gamma(C_m,\left\lfloor \frac{m}{2} \right\rfloor) = \left\lfloor \frac{m}{2} \right\rfloor > 1.$

Therefore, according to (1), we have $H(G) < \frac{17m^2+35m-18}{24}$.

Case 2. $m+1 \leq k \leq 2m-2$. For this case, by Corollary 2.1, we claim that any graph G of this type can be changed into a graph $C_k(n-k-1,1) = C_k(1,n-k-1)$.

Considering the equality (1), $H(C_k(2m-k-1,1))$ reaches its maximum value when the two vertices of degrees 3 and $2m-k+1$ are adjacent. We denote by C_k^* the type of graph with the maximal Harary index. When m = 4, since $G \neq C_5(1,1,1)$, we have $G \cong C_6^*$. A simple calculation shows that $H(C_6^*) = \frac{97}{6} < \frac{197}{12} = H(C_5(1,1,1))$. In the following, we assume that $m \geq 5$. By Lemma 2.6, we claim that the maximum value of $H(C_k^*)$ is attained at k = m + 1. Moreover,

$$\begin{aligned}
\gamma(C_{m+1}^*,2) &= m+1+2(m-1)+\binom{m-2}{2} \\
&= 3m-1+\frac{(m-2)(m-3)}{2} \\
&\leq \frac{m^2+3m-6}{2}, \\
\gamma(C_{m+1}^*,3) &= \gamma(C_{m+1},3)+2(m-1)+(m-2) \\
&= \begin{cases} 3m-1 & if\ m=5 \\ 4m-3 & if\ m \geq 6 \end{cases} \\
&< m^2-2m, \\
D(C_{m+1}^*) &= \left\lfloor \frac{m+1}{2} \right\rfloor + 1 \geq 4.
\end{aligned}$$

Combining the above arguments with the equality (1), we have

$$H(G) < H(C^*_{m+1}) < \frac{17m^2+35m-18}{24}.$$

Case 3. $k = 2m-1$. In this case, we claim that $G \cong C_{2m-1}(1^1)$. If *m* = 4, it is easy to see that $H(C_7(1^1)) = 16 < \frac{197}{12} = H(C_5(1,1,1))$. For $k \geq 5$, we can find that $\gamma(C_{2m-1}(1^1),2) = 2m+1 < \frac{m^2+3m-6}{2}$,

$\gamma(C_{2m-1}(1^1),3) = 2m+1 < m(m-2)$ and $D(C_{2m-1}(1^1)) = m \geq 5$.

Similarly to the above two cases, we have $H(C_{2m-1}(1^1)) < \frac{17m^2+35m-18}{24}$.

Thus we completed the proof of this lemma.

Lemma 3.2. *Let* $G \in \bigcup(2m,m)$ *and v be any vertex in V* (*G*)*. Then* $d_G(v) \leq m+1$.

Proof. There exists a graph $G \in \bigcup(2m,m)$ with a vertex $v \in V(G)$, of degree $s \geq m+2$. Assume that $v_1, v_2, \cdots, v_s$ are all the neighbors of *v* in *G*. Now there are $2m-s \leq m-2$ edges remained in $G \in \bigcup(2m,m)$.

Therefore, $\beta(G) \leq m-2+1 = m-1$. This is a contradiction to the fact that $G \in \bigcup(2m,m)$, thus proving this lemma.

Lemma 3.3. *Let* $G \in \bigcup(8,4)$. *Then* $H(G) \leq \frac{197}{12}$, *with the equality holding if* $G \cong U_{8,4}$ *or* $G \cong C_5(1,1,1)$.

Proof. If $G \in \bigcup^{(2)}(4)$, by Lemma 3.1, we have $H(G) \leq \frac{197}{12}$ with the equality holding if and only if *G* = C_5(1*;* 1*;* 1). If $G \in \bigcup^{(1)}(4)$, with a pendent vertex $v \in V(G)$ and *u* as the neighbor of *v,* of degree two, then $G-\{u,v\} \in \bigcup(6,3)$. By Lemmas 2.1 and 3.2, we have

$$H(G) \leq H(G-\{u,v\}) + \frac{31}{6} + \frac{1}{4}d_G(w)$$

$$\leq H(G-\{u,v\}) + \frac{31}{6} + \frac{5}{4}$$

with the equality holding if and only if *ecc*(*w*) = 2 and $d_G(w) = 5$.

Considering the structures of $U_{6,3}, C_5(1^1)$, $G_6^{(1)}$, $G_6^{(2)}$ and C_6 (there is only $U_{6,3}$ with the maximum degree 4), we claim that the above equality holds if and only if $G \cong U_{8,4}$. The lemma follows immediately.

In the following, we give a lemma as a starting point for our main results. In this lemma, the graph of $\bigcup(10,5)$, with the maximum Harary index, will be completely characterized.

Lemma 3.4. *Let* $G \in \bigcup(10,5)$. *Then,* $H(G) \le \frac{97}{4}$ *with the equality holding if and only if* $G \cong U_{10,5}$.

Proof. By Lemma 3.1, we have $H(G) \le \frac{97}{4}$ if $G \in \bigcup^{(2)}(5)$. For any graph

$G \in \bigcup^{(1)}(5)$, from Lemmas 2.1, 3.2 and 3.3, we have

$$H(G) \le H(G - \{u,v\}) + \frac{38}{6} + \frac{1}{4} d_G(w)$$

$$\le \frac{197}{12} + \frac{38}{6} + \frac{3}{2} = \frac{97}{4}$$

with the equality holding if and only $G - \{u,v\} \cong U_{8,4}$ or $G \cong C_5(1,1,1)$, *ecc*(*w*) = 2 and $d_G(w) = 6$, that is, $G \cong U_{10,5}$.

Theorem 3.1. *Let* $G \in \bigcup(2m,m)$ *with* $m \ge 5$. *Then we have*

$$H(G) < \frac{17m^2 + 35m - 18}{24} \tag{4}$$

with the equality holding in (4) if and only if $G \cong U_{2m,m}$.

Proof. We prove this theorem by induction on *m*. For *m* = 5, from Lemma 3.4, this lemma follows immediately.

Assume that the result is true for any graphs in $\bigcup(2m-2, m-1)$, with $m \ge 6$.

If $G \in \bigcup^{(2)}(m)$, then by Lemma 3.1, we have $H(G) < \frac{17m^2+35m-18}{24}$. If $G \in \bigcup^{(1)}(m)$, with a pendent vertex $v \in V(G)$ and *u* as the neighbor of *v*, of degree two, we can conclude that $G-\{u,v\} \in \bigcup(2m-2,m-1)$. By Lemma 2.1 and the induction hypothesis, it follows that

$$H(G) \le H(G-\{u,v\}) + \frac{7m+3}{6} + \frac{1}{4}d_G(w)$$
$$\le \frac{17(m-1)^2+35(m-1)-18}{24} + \frac{7m+3}{6} + \frac{m+1}{4} = \frac{17m^2+35m-18}{24}$$

with the equalities holding if and only if $G-\{u,v\} \cong U_{2m-2,m-1}$, *ecc*(*w*) = 2 and $d_G(w) = m+1$; thus, *G* is just $U_{2m,m}$ and the theorem is completely proved.

Theorem 3.2. *Let* $G \in \bigcup(n,m)$ *with* $3 \le m \le \frac{n}{2}$ *and* $n \ge 7$.

Then we have

$$H(G) < \frac{6n^2-4mn+m^2+14n+7m-18}{24} \tag{5}$$

with the equality holding in (5) if and only if $G \cong U_{7,3}$ *or* $C_5(1^2)$ *for* $(n,m) = (7,3)$; $G \cong U_{8,4}$ *or* $C_5(1,1,1)$ *for* $(n,m) = (8,4)$; $G \cong U_{n,m}$ *otherwise.*

Proof. First we define a function

$$f(n,m) = \frac{6n^2-4mn+m^2+14n+7m-18}{24},$$

where n,m are all positive integers. In view of formula (*) we obtain

$$f(n,m) = n + \frac{1}{2}\frac{(n-m)^2+n+m-6}{2} + \frac{1}{3}(n-m)(m-2) + \frac{1}{4}\binom{m-2}{2}.$$

For the cycle C_n, we have $n = 2m+1$ or $n = 2m$. Based on equality (1), using a procedure as that followed in the proof of Lemma 3.1, we can get $H(C_n) < f(n,m)$.

For any graph $G \in \bigcup(n,m)$, with $n > 2m$ different from C_n, by Lemma 2.3, there must be a pendent vertex *v* of *G* and a maximum matching *M* such that *v* is not *M*-saturated in *G*. Clearly, $G-v \in \bigcup(n-1,m)$. Let *u* be the unique neighbor of *v* in *G*. As proved in ref. [25] $d_G(u) \le n-m+1$.

Now we prove this result by induction on *n*. According to the value of *m*, we divide the discussion into the following three cases.

Case 1: *m* = 3. For *n* = 7, $G-v\in\bigcup(6,3)$. If $G-v\cong C_5(1^1)$, we have $d_G(u)\le 4$. Then, by Lemma 2.1, it follows that

$$H(G)\le H(C_5(1^1))+\frac{5}{2}+\frac{1}{6}d_G(u)\le\frac{61}{6}+\frac{5}{2}+\frac{2}{3}=\frac{40}{3}$$

with the equalities holding if and only if $d_G(u)=4$ and *ecc*(*u*) = 2, that is, $G\cong C_5(1^2)$. If $G-v\ne C_5(1^1)$, by Lemma 2.1, we have

$$H(G)\le H(G-v)+\frac{5}{2}+\frac{1}{6}d_G(u)\le 10+\frac{5}{2}+\frac{5}{6}=\frac{40}{3}$$

with the equalities holding if and only if $G\cong U_{6,3}$, C_6, $G_6^{(1)}$, *or* $G_6^{(2)}$ (Fig. 2), $d_G(u)=5$ and *ecc*(*u*) = 2, which implies $G\cong U_{7,3}$. Thus, we claim that $H(G)\le\frac{40}{3}$. When $G\in\bigcup(n,m)$, with $(n,m)=(7,3)$, the equality is holding if and only if $G\cong C_5(1^2)$*; or* $U_{7,3}$.

When *n* = 8, we get $G-v\in\bigcup(7,3)$. By Lemma 2.1,

$$H(G)\le H(G-v)+\frac{17}{6}+\frac{1}{6}d_G(u)\le\frac{40}{3}+\frac{17}{6}+1=f(8,3)$$

with the equalities holding if and only if $G-v\cong U_{7,3}$, $d_G(u)=6$ and *ecc*(*u*) = 2, i.e., $G\cong U_{8,3}$. Assume that the result holds for all graph $G\in\bigcup(n-1,3)$ with $n\ge 9$. By Lemma 2.1 and induction hypothesis, we have

$$H(G)\le H(G-v)+\frac{2n+1}{6}+\frac{1}{6}d_G(u)\le f(n-1,m)+\frac{2n+1}{6}+\frac{n-2}{6}=f(n,3)$$

with the equalities holding if and only if $G-v\cong U_{n-1,3}$, $d_G(u)=n-2$ and *ecc*(*u*) = 2, equivalently, $G\cong U_{n,3}$.

Case 2: *m* = 4. For *n* = 8, the result follows from Lemma 3.3. In case $n=9$, $G-v\in\bigcup(8,4)$. Based on Lemma 2.1, by analogy to the Case 1, we have $H(G)\le\frac{197}{12}+\frac{19}{6}+1=f(9,4)$

with the equality holding if and only if $G \cong U_{9,4}$. Suppose that the result holds for any graph $G - v \in \bigcup(n-1,4)$, with $n \geq 10$; from Lemma 2.1 and induction hypothesis, we have

$$H(G) \leq H(G-v) + \frac{2n+1}{6} + \frac{1}{6} d_G(u) \leq f(n-1,4) + \frac{2n+1}{6} + \frac{n-3}{6} = f(n,4)$$

with the equalities holding if and only if $G - v \cong U_{n-1,4}$, $d_G(u) = n-3$ and *ecc*(*u*) = 2, equivalently, $G \cong U_{n,4}$.

Case 3: $m \geq 5$. When $n = 2m$, the result holds from Lemma 3.4. Assume the result is true for any graph $G \in \bigcup(n-1,4)$ with $\geq 2m$. By a similar procedure, we obtain

$$H(G) \leq H(G-v) + \frac{2n+1}{6} + \frac{1}{6} d_G(u) \leq f(n-1,4) + \frac{2n+1}{6} + \frac{n-m+1}{6} = f(n,m)$$

with the equalities holding if and only if $G - v \cong U_{n-1,m}$, $d_G(u) = n-m+1$ and *ecc*(*u*) = 2, that is, $G \cong U_{n,m}$. Thus, the proof of this theorem is completed.

The cyclomatic number η of *G* is defined as $\eta(G) = |E(G)| - |V(G)| + \omega(G)$, where $\omega(G)$ is the number of connected components of *G*. Denote by $G(n,\eta,m)$ the set of connected graphs of order *n* and by *m* the matching number. Clearly, when $\eta = 0$, $G(n,\eta,m)$ denotes the set of trees of order *n,* of the matching number *m*; if $\eta = 1$, then $G(n,\eta,m) = \bigcup(n,m)$. Considering the main results in this paper (for $\eta = 1$) and those in ref. [24] (for $\eta = 0$), we naturally ask the following problem:

Problem 3.1. *Can we determine the graph of* $G(n,\eta,m)$ *with the maximal Harary index being an integer* $\eta \geq 2$*?*

Even more difficult is to determine the graph of $G(n,\eta,m)$ with the minimal Harary index, even for the case $\eta = 0$. Therefore, we will end this paper with the following interesting problem:

Problem 3.2. *Which graph of* $G(n,\eta,m)$ *has the minimal Harary index for a given integer* $\eta \geq 0$*?*

ACKNOWLEDGEMENT

K. X. is supported by NUAA Research Funding, No. NN2012080 and NNSF of China (No. 11201227). K. Ch. D. and H. H. acknowledge, respectively, for the support of Sungkyunkwan University BK21 Project, BK21 Math Modeling HRD Div. Sungkyunkwan University, Suwon, Republic of Korea and Qing Lan Project of Jiangsu Province, PR China.

REFERENCES

1. O. Ivanciuc, T. S. Balaban, and A. T. Balaban, *J. Math. Chem.* **1993**, *12*, 309.
2. D. Plavšić, S. Nikolić, N. Trinajstić, ad Z. Mihalić, *J. Math. Chem.* **1993**, *12*, 235.
3. D. Ciubotariu, PhD thesis, 1987, Timisoara, Romania; D. Ciubotariu, M. Medeleanu, V. Vlaia, T. Olariu, C. Ciubotariu, D. Dragos, and C. Seiman, *Molecules*, **2004**, *9*, 1053.
4. K.C. Das, B. Zhou, and N. Trinajstic, *J. Math. Chem.* **2009**, *46*, 1369.
5. M.V. Diudea, *J. Chem. Inf. Comput.* Sci. **1997**, 37, 292.
6. E. Estrada, L. Rodriguez, *MATCH Commun. Math. Comput. Chem.* **1997**, *35*, 157.
7. L. Feng and A. Ilic, *Appl. Math. Lett.* **2010**, *23*, 943.
8. I. Gutman, *Indian J. Chem.* **1997**, *36 A*, 128.
9. B. Lucić, A. Miličević, S. Nikolić, and N. Trinajstić, *Croat. Chem. Acta* **2002**, *75*, 847.
10. K. Xu, *Discrete Appl. Math.* **2012**, *160*, 321.
11. K. Xu and K. C. Das, *Bull. Malys. Math. Sci. Soc.***2013**, 36, 373.
12. K. Xu and K. C. Das, *Discrete Appl. Math.* **2011**, *159*, 1631.
13. K. Xu and N. Trinajstić, *Utilitas Math.* **2011**, *84*, 153.
14. B. Zhou, X. Cai, and N. Trinajstić, *J. Math. Chem.* **2008**, *44*, 611.
15. M.V. Diudea, *MATCH Commun*. *Math*. *Comput*. *Chem*. **1995**, *32*, 85.
16. M.V. Diudea and C. M. Pop, *Indian J*. *Chem*. **1996**, *35A*, 257.
17. M.V. Diudea, O. Ivanciuc, S. Nikolić, and N. Trinajstić, *MATCH Commun*. *Math*. *Comput*. *Chem*. **1997**, *35*, 41.
18. M.V. Diudea and I. Gutman, *Croat*. *Chem*. *Acta,* **1998**, *71*, 21.
19. H. Deng, *Math. Comput. Model.* **2012**, *55*, 634.
20. M.H. Khalifeh, H. Yousefi-Azari, and A.R. Ashrafi, *Comput. Math. Appl.* **2008**, *56*, 1402.

21. A. Hamzeh, S. Hossein-Zadeh, and A. R. Ashrafi, *Appl. Math. Lett.* **2011**, *24*, 1099.
22. J.A. Bondy and U.S.R. Murty, *Graph Theory with Applications*, Macillan Press, New York, 1976.
23. M.V. Diudea, I. Gutman, and L. Jäntschi, *Molecular Topology*, NOVA, New York, 2002.
24. A. Ilić, G. Yu, and L. Feng, *Utilitas Math.*, in press.
25. Z. Du and B. Zhou, *MATCH Commun. Math. Comput. Chem.* **2010**, *63*, 101.
26. A. Chang and F. Tian, *Lin. Algebra Appl.* **2003,** *370*, 237.
27. A. Yu and F. Tian, *MATCH Commum. Math. Comput. Chem.* **2004**,*51*, 97.

STUDIA UBB CHEMIA, LVIII, 2, 2013 (p. 87 – 92)
(RECOMMENDED CITATION)

FAST GC-MS METHOD FOR QUANTIFICATION OF GAMMA-BUTYROLACTONE IN BIOLOGICAL MATRICES

ANIKÓ PÉTER[a], TÍMEA DERGEZ[a], IBOLYA KISS[b], FERENC KILÁR[a,b]

ABSTRACT. A sensitive and specific gas chromatography-mass spectrometry analysis using selective ion monitoring for the quantification of γ-butyrolactone in biological matrices was developed. The method includes a simple liquid-liquid extraction and no derivatization procedure before the GC-MS analysis. An internal standard, α-methylene-γ-butyrolactone was applied for the quantitative determination. The method was linear between 0.34 µg/ml (LOD) and 500 µg/ml. The limit of quantification (LOQ) was obtained to be 0.798 µg/ml using 100 µl blood, urine or plasma.

Keywords: *gamma-butyrolactone, gamma-hydroxybutyric acid, GC-MS, blood, urine, plasma*

INTRODUCTION

Gamma-butyrolactone (γ-butyrolactone, GBL) is the chemical precursor of gamma-hydroxybutiric acid (γ-hydroxybutiric acid, GHB). Both are components of the normal mammalian metabolism, as endogenous constituents of the mammalian brain and they have been hypothesized to have a role as neurotransmitters [1]. Gamma-hydroxybutiric acid has been gaining popularity amongst club-goers as a recreational drug [2] . It is a component of “date rape drugs”, due to its euphoric effects [3] and ability to reduce inhibitions [4] or as doping agent (enhancer of muscle growth) [5]. Gamma-butyrolactone, on the other hand, has a hypothetical effect in the fungal metabolism, in filamentous fungi as a signalling molecule [6]. GBL has therapeutic importance, because of its pharmacokinetic and anti-angiogenic activity. Several quantitative analytical methods have been developed for measuring GHB and/or GBL in biological matrices [7-10]. Most of the papers report methods with gas chromatography-mass spectrometry, high performance liquid chromatography

[a] *Institute of Bioanalysis, University of Pécs, Faculty of Medicine, University of Pécs, Szigeti út. 12, H-7624 Pécs, Hungary, ferenc.kilar@aok.pte.hu*
[b] *Department of Analytical and Environmental Chemistry, Faculty of Science, University of Pécs, Ifjúság útja 6., H-7624 Pécs, Hungary*

or capillary electrophoresis procedures. The physiological level of gamma-hydroxybutiric acid is approximately 2 μg/ml in blood, and the normal endogenous concentration in urine is typically less than 10 μg/ml [11, 12]. Studies on the serum level of γ-butyrolactone, however, could not demonstrate its normal presence in significant amount, presumably due to its rapid conversion to γ-butyrolactone by γ-lactonase [13]. The determination of GHB was possible in the form of GBL after its acidic conversion [14]. The expected concentration of GBL in culture media of fungi is between 50-300 μg/ml [15, 16].

The aim of this study was to develop a rapid and simple method, for the quantitative determination of γ-butyrolactone in culture media of fungi, which will be applicable for the investigation of GBL in human blood and urine, as well. No method has previously been published for the determination of gamma-butyrolactone in culture medium.

RESULTS AND DISCUSSION

The gas-chromatography-mass-spectrometry analysis of γ-butyrolactone extracted by organic solvents from different biological matrices was studied. For the quantification of GBL an internal standard, α-methylene-γ-butyrolactone (M-GBL) was applied. Five solvents, chloroform, cyclohexane, dichloromethane, ethyl-acetate and methyl *tert*-butyl ether were examined in the extraction procedure. Care was taken to find the most suitable conditions for concentrating the extracts. A typical chromatogram of the two components after an extraction procedure with methyl *tert*-butyl ether (MTBE) using single ion monitoring is presented in Figure 1. The base peak of GBL at 42 *m*/*z*, and the base peak of M-GBL at 68 *m/z* can be clearly differentiated in the chromatogram, and besides these a fragment of GBL at 68 *m/z* can also be detected. The suggested fragmentation structure for the 42 *m/z* fragment is $[O=C=CH_2]^{+\cdot}$, while the M-GBL looses one carbon, one oxygen, and two hydrogens to form the 68 *m/z* fragment, it means most likely the elimination of $CH_2=O$ neutral molecule.

The quantification of γ-butyrolactone was obtained by using a calibration. The calibration curve for the standard was linear in the 0.34 - 500 μg/ml concentration range. Each correlation coefficient for three independent calibrations was R=0.999. The recovery experiments were carried out with a 500 μg/ml GBL concentration in blood, urine, or fungal culture. Cyclohexane and ethyl-acetate provided a recovery of γ-butyrolactone less than 20 % and 45 %, respectively. Although, the extraction with dichloromethane and chloroform resulted in a recovery higher than 90 %, due to the background noise, the LOD was higher than 200 μg/ml. The best recovery (95 %) was obtained with extraction using MTBE. The limit of quantitation was found to be 0.798 μg/ml (RSD: 20 %), and the limit of detection was obtained to be 0.34 μg/ml (RSD: 33 %).

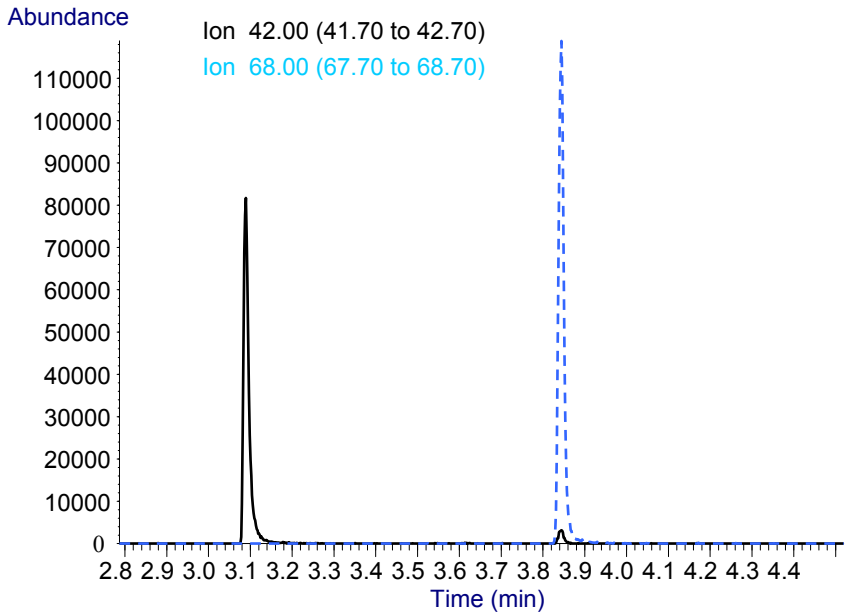

Figure 1. GC-MS chromatogram of a sample containing γ-butyrolactone and α-methylene-γ-butyrolactone. Single ion monitoring (SIM) detection of two fragment ions, 42 *m/z* (solid line) and 68 *m/z* (dashed line) was applied. The culture medium spiked with γ-butyrolactone (500 µg/ml) and α-methylene-γ-butyrolactone (500 µg/ml) was extracted with methyl *tert*-butyl ether. Other experimental conditions are given in the Experimental session.

The within-batch precision, using culture medium in the extraction, was between 1.1 to 3.9 %, the between-batch precision was between 1.7 to 7.3 % (experiments with three replicates). In the case of plasma, the within-batch precision was 4.9-8.1 %; in the case of blood cell suspension 10.1-13.4 %; and using urine the precision was between 0.8-5 %. The limit of detection was 0.34 µg/ml in culture medium and urine, and 0.5 µg/ml in blood. The limit of quantitation was 0.798 µg/ml in culture medium and urine, and 1.6 µg/ml in blood. The ratio of γ-butyrolactone present in the plasma and blood cells after centrifugation was *ca.* 45/55.

It was not possible to detect γ-butyrolactone in blank plasma or in blood cell suspension, which is in accordance to previous results, showing that the concentration of GBL in blank plasma is about 0.1 µg/ml [17].

The most efficient extraction was obtained with methyl *tert*-butyl ether (a low-boiling point solvent), but valid result could be obtained only after satisfactory sample preparation and within 40 min after sampling. The pretreatment procedure has been investigated with different solvents mainly with chloroform [7], but solid-phase extraction methods were also developed for the extraction of GBL [12]. Some publications applies salting-out approach [18], but those techniques are more complicated compared to the one described here.

CONCLUSIONS

The analytical gas-chromatography-mass-spectrometry method developed in this study is sensitive, accurate and precise for the determination of γ-butyrolactone, which participates in signal processes of fungi [15], but possibly occurent in human blood and urine. Only a simple pretreatment of the sample is necessary. The method provides a low LOD for the determination, although, applying special analytical conditions and instrumentation results with lower LOD values can be found in the literature [19]. In the case of following drug administration in human material a cautious interpretation of the data is necessary to avoid false positive results, therefore, it is mandatory to collect blood with EDTA, because the drug is cleared from the blood within 6 h [20].

EXPERIMENTAL SECTION

Reagents

Gamma-butyrolactone (GBL) and α-methylene-γ-butyrolactone (M-GBL) were purchased from Sigma-Aldrich (Darmstadt, Germany). Chloroform, cyclohexane, dichloromethane, ethyl-acetate and methyl *tert*-butyl ether (MTBE) were of GC grade. Stock solutions of GBL (10 mg/ml) were prepared in the organic solvents; M-GBL (10 mg/ml) was dissolved in MTBE. The Difco Potato Dextrose Broth (Difco Laboratories, Le Pont de Claix, France) was used (24 mg/ml) as culture medium. Drug-free human urine and blood were collected from healthy individuals. The blood samples were taken in EDTA tubes, and the biological samples were stored at 4°C.

Extraction

Extraction of GBL was made from aqueous solution, culture medium and from biological matrices containing different amounts of gamma-butyrolactone and 500 μg/ml α-methylene-gamma-butyrolactone, as internal standard. The concentration of GBL in the different solutions were as follows: aqueous solutions: 10 μg/ml or 50 μg/ml GBL; culture medium: 0, 0.4, 0.8, 1, 2.5, 5, 50, 100 and 500 μg/ml; blood or urine: 0, 0.5, 1, 2, 5, 10, 20 and 50 μg/ml.

The extraction procedure of the biological samples was preceded with a purification step, the samples in the culture medium were filtered through a Whatman Syringe Filter (0.45 µm), the urine was filtered with Millipore-Millex filter (0.45 µm), and the blood plasma was separated from the blood cells by centrifugation (3000 rpm, 30 min). The extraction was made applying 100 µl samples and 1 ml organic solvents (chloroform, cyclohexane, dichloromethane, ethyl-acetate or methyl *tert*-butyl ether). A suspension of the blood cells (100 µl) was also used for extraction. After vortexing (1 min. two times) and centrifugation (3000 rpm, 10 min) the organic part was collected and evaporated to *ca.* 100 µl final volume.

Gas chromatography-mass spectrometry

Gas chromatography-mass spectrometry (GC-MS) analyses were performed on an Agilent 6890N GC equipped with a 5975 Inert Mass Selective detector (Agilent Technologies, Waldbronn, Germany). A HP-1 column (25 m x 0.2 mm I.D., 0.33 µm film thickness of polydimethylsiloxane) (Agilent Technologies, Waldbronn, Germany) was used for the separations applying helium as carrier gas at a flow rate of 1.5 ml/min. An HP 7683B automatic sampler was used for the injection. Split injection (20:1) was used with the valve closed for 2.7 min, and 1 µl samples being injected. The operating conditions for the analyses were: inlet temperature 250°C; the detector temperature 300°C; initial oven temperature was 50°C with a hold time of 0.6 minute and with a temperature ramp of 15°C min^{-1} up to 300°C. The mass spectrometer was operated in the selective ion monitoring (SIM) mode, monitoring GBL and M-GBL (the internal standard) by the 42 *m/z* and 68 *m/z* major fragment ions, respectively.

Method validation

The extraction was tested with γ-butyrolactone spiked distilled water (100 µg/ml). A calibration curve was constructed by preparing solutions in MTBE containing 0.5, 2.5, 5, 50, 100, 500 µg/ml GBL. The calibration curves were constructed in the case of the culture media by using 0, 0.4, 0.8, 1, 2.5, 5, 50, 100 and 500 µg/ml final γ-butyrolactone concentrations, and in the cases of blood and urine by using 0, 0.5, 1, 2, 5, 10, 20, 50 µg/ml final GBL concentrations.

ACKNOWLEDGEMENTS

The work was supported by the European Commission grant STREP-FP6-NMP4-CT2006-032811 and by the grants TÁMOP 4.2.2./A-11/1/ KONV-2012-0065, OTKA K-100667 and the Foundation of Faculty of Medicine, University of Pécs.

REFERENCES

1. P.Vayer, P.Mandel, M.Maitre, *Life Sciences* **1987**, *41*, 1547.
2. Z.Nemeth, B.Kun, Z.Demetrovics, *J. Psychopharmacol.* **2010**, *24*, 1281.
3. M.A.Felmlee, S.A.Roiko, B.L.Morse, M.E.Morris, *J. Pharmacol. Exp. Ther.* **2010**, *333*, 764.
4. C.Grov, J.T.Parsons, D.S.Bimbi, *Aids Educ. Prev.* **2008**, *20*, 42.
5. F.Bortolotti, G.De Paoli, R.Gottardo, M.Trattene, F.Tagliaro, *Journal of Chromatography B-Analytical Technologies in the Biomedical and Life Sciences* **2004**, *800*, 239.
6. L.A.Maggio-Hall, T.M.Hammond, N.P.Keller, *Secondary Metabolism in Model Systems* **2004**, *38*, 197.
7. J.T.Lettieri, H.L.Fung, *Biochemical Medicine* **1978**, *20*, 70.
8. S.D.Ferrara, L.Tedeschi, G.Frison, F.Castagna, L.Gallimberti, R.Giorgetti, G.L.Gessa, P.Palatini, *Journal of Pharmaceutical and Biomedical Analysis* **1993**, *11*, 483.
9. J.D.Doherty, O.C.Snead, R.H.Roth, *Analytical Biochemistry* **1975**, *69*, 268.
10. T.B.Vree, E.Vanderkleijn, H.J.Knop, *Journal of Chromatography* **1976**, *121*, 150.
11. D.T.Yeatman, K.Reid, *Journal of Analytical Toxicology* **2003**, *27*, 40.
12. S.P.Elliott, *Forensic Science International* **2003**, *133*, 9.
13. W.A.M.S.Dunn, *Emergency Medicine News* **2001**, *23*, 40.
14. Y.Fukui, E.Matsusima, K.Muramoto, N.Nagai, K.Ohama, K.Yamashita, *Journal of Chromatography B-Analytical Technologies in the Biomedical and Life Sciences* **2003**, *785*, 73.
15. S.Raina, D.De Vizio, M.Odell, M.Clements, S.Vanhulle, T.Keshavarz, *Biotechnology and Applied Biochemistry* **2009**, *54*, 65.
16. S.Raina, M.Odell, T.Keshavarz, *Journal of Biotechnology* **2010**, *148*, 91.
17. K.M.Gibson, S.I.Goodman, F.E.Frerman, A.M.Glasgow, *The Journal of Pediatrics* **1989**, *114*, 607.
18. A.Kankaanpaa, R.Liukkonen, K.Ariniemi, *Forensic Sci. Int.* **2007**, *170*, 133.
19. F.Tateo, M.Bononi, *Journal of Food Composition and Analysis* **2003**, *16*, 721.
20. M.Villain, V.Cirimele, B.Ludes, P.Kintz, *Journal of Chromatography B-Analytical Technologies in the Biomedical and Life Sciences* **2003**, *792*, 83.

STUDIA UBB CHEMIA, LVIII, 2, 2013 (p. 93 – 104)
(RECOMMENDED CITATION)

HETEROCYCLES 34. SYNTHESIS AND ANTI-INFLAMMATORY ACTIVITY OF NEW POLYHETEROCYCLIC SCHIFF BASES AND MANNICH BASES

ALEXANDRA TOMA[a], DENISA HAPĂU[a], MARA NAGHI[b], LAURIAN VLASE[c], CRISTINA MOGOŞAN[d*], VALENTIN ZAHARIA[a]

ABSTRACT. New polyheterocyclic Schiff bases and Mannich bases containing 5-(pyridin-4-yl)-2H-1,2,4-triazole-3-thione moiety have been synthesized. The structures of the newly obtained compounds were confirmed by spectral analysis IR, ^{1}H NMR, ^{13}C NMR and MS. The obtained Schiff bases and Mannich bases were screened for their anti-inflammatory activity using the carrageenan-induced rat paw oedema test. Compounds 6c, 6f, 7b, 7c, 7d, 8a, 8c, 8d, 8f and 10 showed significant anti-inflammatory activity.

Keywords: *polyheterocyclic compounds, Schiff bases, Mannich bases, anti-inflammatory activity*

INTRODUCTION

Heterocyclic ring systems thiazole, 1,2,4-triazole and pyridine can be commonly found in the structure of many compounds of medicinal interest, presenting a diverse array of biological activities, including antimicrobial [1,2], anti-inflammatory [2c,3,4] enzyme inhibitory [5] and anticancer [6] properties. Moreover, the condensed ring system thiazolo-triazole was also found to be responsible for antimicrobial [7] and anti-inflammatory activity [7b,8].

[a] *Iuliu Haţieganu University of Medicine and Pharmacy Cluj-Napoca, Department of Organic Chemistry*
[b] *Babeş-Bolyai University of Cluj-Napoca, Department of Biochemistry and Biochemical Engineering, Ro-400028 Cluj-Napoca, Arany János 11, Romania*
[c] *Iuliu Haţieganu University of Medicine and Pharmacy Cluj-Napoca, Department of Pharmaceutical Technology and Biopharmacy*
[d] *Iuliu Haţieganu University of Medicine and Pharmacy Cluj-Napoca, Department of Pharmacology, Pysiology and Physiopathology, Ro-400012 Cluj-Napoca, Victor Babeş 41, Romania, *corresponding author: cmogosan@umfcluj.ro*

Schiff bases and Mannich bases are important classes of pharma cologically and chemically useful compounds due to their therapeutic potential and to the reactivity of their functional groups. In particular, Schiff bases and Mannich bases derived from 1,2,4-triazole were recently reported as potent anticancer [9], antimicrobial [10], anti-inflammatory and analgesic [11,12] agents. Consequently, polyheterocyclic Schiff bases and Mannich bases rejoining the above mentioned ring systems are becoming even more important in medicinal research.

As a part of our interest for the synthesis of new biologically active compounds containing azolic rings, herein we report the synthesis, charac terization and anti-inflammatory evaluation of some new polyheterocyclic Schiff bases and Mannich bases.

Mannich reaction has found broad application in synthetic organic chemistry, as a key step for new C-C and C-N bond forming. Besides the classical variant, which involves the use of an enolisable carbonyl compound as CH-acidic substrate, atypical Mannich reactions involving other compounds with mobile hydrogen have been already described. Encouraged by the recently reported regioselective aminoalkylation of 2H-1,2,4-triazole-3-thione derivatives [12], which afforded the corresponding N-Mannich bases in good yields, we decided to apply the N-aminoalkylation reaction in the series of azolic derivatives and Schiff bases containing the 5-(pyridin-4-yl)-2H-1,2,4-triazole-3-thione moiety, in order to obtain new biologically active polyheterocyclic Mannich bases.

RESULTS AND DISCUSSION

Synthesis of polyheterocyclic compounds

As illustrated in Scheme 1, the heterocyclic precursors **1-4** were obtained as previously described in the literature [13], starting from isonicotinic hydrazide.

Condensation of 4-amino-5-(pyridin-4-yl)-2H-1,2,4-triazole-3-thione 4 with various thiazole and thiazolo-triazole aldehydes **5a-f [14,15]**, in glacial acetic acid [10a], afforded the corresponding Schiff bases **6a-f** in good yield.

Mannich bases **7a-f, 8a,c,d,f, 9-12** were obtained by the amino methylation of 4-substituted-5-(pyridine-4-yl)-2H-1,2,4-triazole-3-thiones **1-3** and **6a-f** with formaldehyde and secondary amines (pyrrolidine and piperidine) [10].

The structures of all newly synthesized polyheterocyclic compounds were established by their spectral analysis IR, ^{1}H NMR, ^{13}C NMR and MS.

The IR spectra of Schiff bases **6a-f** revealed the presence of the N-H absorption band in the range of 3446-3482 cm^{-1} and the C=S stretching

at 1263-1286 cm^{-1}, due to the existence of the thione tautomeric form. The absorption bands for the primary amino group -NH_2 were not observed, indicating the formation of the Schiff base. The -C=N- stretching vibration appeared in the range of 1603-1611 cm^{-1}. In the IR spectra of the Mannich bases **7a-f**, **8a,c,d,f**, **9-12**, the absence of the -NH- absorption band confirmed the formation of N-Mannich bases.

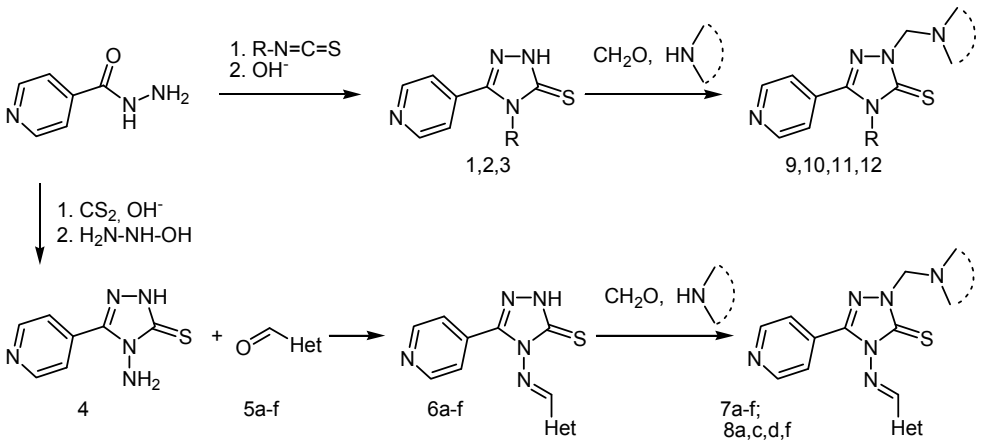

Compound	Het
5,6,7a-f, 8a,c,d,f	C_6H_5 (a); *p*CH_3-C_6H_4 (b); *m*CH_3-C_6H_4 (c); *p*Cl-C_6H_4 (d); *p*Br-C_6H_4 (e); C_6H_5 (f)
Compound	—N
7a-f	—N
8a,c,d,f	—N

Compound	R	—N
1	$-CH_3$	–
2		–
3		–
9	$-CH_3$	—N
10		—N
11		—N
12		—N

Sheme 1. The synthesis of polyheterocyclic compounds

Previously reported spectral studies have already confirmed that 4-amino-5-(pyridine-4-yl)-2H-1,2,4-triazole-3-thione exists in the thione tautomeric form [13b]. In the ^{1}H NMR spectra of compounds **6a-f**, the NH proton resonated as a singlet at δ 14.53 ppm, indicating also in this case the existence of the thione tautomeric form. The formation of the Schiff bases **6a-f** was confirmed by the presence of the -N=CH- proton as a singlet at δ 9.93-9.97 ppm, whereas the signal due to the NH_2 protons was completely absent.

In the ^{1}H NMR spectra of products **7a-f**, **8a,c,d,f**, **9-12**, the signal at δ 14.53 ppm due to the NH proton was absent and the >N-CH_2-N< protons appeared as a singlet at δ 5.26-5.53 ppm, confirming the formation of the corresponding Mannich bases. The presence of the pyrrolidine/piperidine ring was confirmed by other characteristic signals in the aliphatic region.

In the ^{13}C NMR spectra of Schiff bases **6a-f**, the C=S carbon belonging to the thione tautomeric form was recorded at δ 168.52-169.26 ppm. For compounds **7a-f**, **8a,c,d,f**, **9-12,** formation of Mannich bases was confirmed by the presence of a characteristic signal around δ 65.94-71.18 ppm due to the >N-CH_2-N< carbon and by other aliphatic signals due to the pyrrolidine ring (2 signals at δ 23.84-23.95 ppm and 50.34-50.67 ppm), respectively the piperidine ring (3 signals at δ 23.77-23.98 ppm, 25.95-26.23 ppm and 51.89-52.13 ppm), which are absent in ^{13}C spectra of the precursors **1,2,3** and **6a-f**. The C=S carbon signal remained present in all ^{13}C spectra of Mannich bases, at δ 168.32-171.17 ppm.

The anti-inflammatory activity

The anti-inflammatory activity of the tested compounds was found to be in the inflammatory oedema inhibition range of 10.74% - 58.87%, while standard drug Diclofenac showed 62.61% inhibition, after 4h (**Table 1**).

Among the tested compounds, Schiff base **6f** and Mannich bases **7b, 7d, 10, 8d** and **8f** displayed the most potent anti-inflammatory activity, the percentages of oedema inhibition being close to those of diclofenac. A moderate anti-inflammatory activity was observed for the Schiff base **6c** and the Mannich bases **7c, 8a** and **8c**.

Compounds **6c, 10, 8d** and **8f** proved to be more potent than diclofenac 1 hour after inducing inflammation (**Table 1**). Schiff base **6f** displayed anti-inflammatory activity comparable to diclofenac 2 and 3 hours after inducing inflammation, while the corresponding Mannich base **8f** displayed a better profile after 3 and 4 hours.

Table 1. Anti-inflammatory activity of Schiff bases and Mannich bases

Compound	Oedema volume in ml (average±SD) % inhibition			
	1h	2h	3h	4h
Control	0.69±0.16	1.48±0.21	1.78±0.28	2.14±0.37
Diclofenac	0.40±0.14* 42.02%	0.61±0.11* 58.78%	0.85±0.23* 52.24%	0.80±0.24* 62.61%
6a	0.55±0.12 20.28%	1.24±0.39 16.21%	1.25±0.28* 29.77%	1.87±0.47 12.61%
6b	0.71±0.23 -2.89%	1.12±0.39 24.32%	1.18±0.41* 33.70%	1.49±0.27* 30.37%
6c	**0.39±0.14*** **43.47%**	**0.98±0.3*** **33.78%**	1.40±0.36 21.34%	**1.47±0.38*** **31.3%**
6d	0.54±0.16 21.74%	1.37±0.41 7.43%	1.65±0.51 7.30%	1.82±0.27 14.95%
6e	0.51±0.14 26.08%	1.01±0.42* 31.75%	1.27±0.51 28.65%	1.32±0.45* 38.31%
6f	0.49±0.19 28.98%	**0.68±0.28*** **54.05%**	**0.86±0.27*** **51.68%**	**1.22±0.35*** **42.99%**
7a	0.69±0.31 0%	1.11±0.47 25%	1.33±0.44 25.28%	1.91±0.65 10.74%
7b	0.43±0.25 37.68%	**0.86±0.43*** **41.89%**	**1.02±0.38*** **42.69%**	**1.46±0.35*** **31.77%**
7c	0.57±0.15 17.39%	**1.21±0.13*** **18.24%**	**1.19±0.21*** **33.14%**	**1.31±0.3*** **38.78%**
7d	0.62±0.27 10.14%	**0.79±0.24*** **46.62%**	**1.07±0.35*** **39.88%**	**1.10±0.43*** **48.59%**
7e	0.49±0.06* 28.98%	1.26±0.43 14.86%	1.34±0.56 24.71%	1.12±0.46* 47.66%
7f	0.58±0.22 15.94%	1.03±0.34* 30.40%	1.33±0.43 25.28%	1.3±0.42* 39.25%
9	0.44±0.24 36.23%	1.47±0.30 0.67%	1.53±0.31 14.04%	1.48±0.35* 30.84%
10	**0.31±0.05*** **55.07%**	**0.90±0.32*** **39.18%**	**1.12±0.28*** **37.07%**	**1.03±0.18*** **51.86%**
11	0.51±0.24 26.08%	1.47±0.30 0.67%	1.35±0.31* 24.15%	1.28±0.40* 40.18%
8a	**0.36±0.13*** **47.82%**	**0.97±0.41*** **34.45%**	**1.26±0.37*** **29.21%**	**1.45±0.31*** **32.24%**
8c	**0.47±0.16*** **31.88%**	**1.18±0.25*** **20.27%**	**1.25±0.25*** **29.77%**	**1.39±0.29*** **35.04%**
8d	**0.38±0.15*** **44.92%**	**0.73±0.12*** **50.67%**	**1.00±0.25*** **43.82%**	**1.13±0.28*** **47.19%**
12	0.67±0.26 2.89%	1.64±0.65 -10.81%	1.82±0.70 -2.24%	1.85±0.59 13.55%
8f	**0.39±0.22*** **43.47%**	**0.73±0.26*** **50.67%**	**0.88±0.37*** **50.56%**	**0.88±0.32*** **58.87%**

* $p<0.05$ t-test

CONCLUSIONS

A serie of new polyheterocyclic compounds representing Schiff bases and Mannich bases containing the 5-(pyridine-4-yl)-2H-1,2,4-triazole-3-thione moiety have been synthesized, characterized and evaluated for their anti-inflammatory activity. Schiff bases **6c**, **6f** and Mannich bases **7b**, **7c**, **7d**, **8a**, **8c**, **8d**, **8f**, **10** significantly reduced the inflammatory response, their maximum percent inhibition ranging from 30 to 58.87%. Derivatization of Schiff bases **6a-f** at NH (2^{th} position of the 1,2,4-triazole ring) into the corresponding N-Mannich bases enhanced in most cases the anti-inflammatory activity.

EXPERIMENTAL SECTION

All chemicals (solvents and reagents) were purchased from Merck. ^{1}H NMR and ^{13}C NMR spectra were recorded in $CDCl_3$ and DMSO-D_6 solution on a Brucker Avance DPX spectrometer operating at 300 MHz and respectively 75 MHz. Chemical shifts are expressed in ppm values (δ scale) from TMS as internal standard. Mass Spectra were recorded on Agilent 1100 Ion Trap mass spectrometer operating at 70 eV, while IR spectra were recorded on a Brucker Equinox 55 FT-IR spectrometer. Melting points were determined on open glass capillaries using an Electrothermal IA 9000 digital melting point apparatus.

General procedure for the synthesis of Schiff bases 6a-f

To a solution of 4-amino-5-(pyridine-4-yl)-2H-1,2,4-triazole-3-thione (**4**, 1 mmol) in 10 ml glacial acetic acid, the thiazolic aldehyde **5a-f** (1,5 mmol) was added. The mixture was refluxed for 2 h. The formed precipitate was isolated by filtration and washed with water and then with ethanol.

4-((2-phenylthiazol-4-yl)methyleneamino)-5-(pyridin-4-yl)-2H-1,2,4-triazole-3-thione (6a): Yield 86%; solid; m.p. 307.7-309.7^{0}C; IR (KBr, cm^{-1}): v = 3450 cm^{-1} (N-H secondary); 3085 cm^{-1} (C-H aromatic); 1603 cm^{-1} (C=N); 1271 cm^{-1} (C=S); ^{1}H NMR (300 MHz, DMSO-D_6): δ = 7.54-7.56 (m, 3H); 7.93 (d, J = 6.0 Hz, 2H); 8.01-8.03 (m, 2H); 8.67 (s, 1H); 8.76 (d, J = 5.8 Hz, 2H); 9.96 (s, 1H); 14.53 (s, 1H); ^{13}C NMR (75 MHz, DMSO-D_6): δ = 122.41; 127.02; 128.00; 129.90; 131.48; 132.71; 133.14; 147.06; 149.83; 150.76; 159.77; 163.77; 169.18; ESI$^+$-MS: M^+ found (M^+ calculated for $C_{17}H_{12}N_6S_2$): 365.2 (364.4).

4-((2-*p*-tolylthiazol-4-yl)methyleneamino)-5-(pyridin-4-yl)-2H-1,2,4-triazole-3-thione (6b): Yield 78%; solid; m.p. 313.3-315.5^{0}C; IR (KBr, cm^{-1}): v = 3450 cm^{-1} (N-H secondary); 3082 cm^{-1} (C-H aromatic); 1603 cm^{-1} (C=N); 1269 cm^{-1} (C=S); ^{1}H NMR (300 MHz, DMSO-D_6): δ = 2.37 (s, 3H); 7.35 (d, J = 7.6 Hz, 2H); 7.89-7.92 (m, 4H); 8.63 (s, 1H); 8.76 (d, J = 4.4 Hz, 2H); 9.93 (s, 1H); 14.52 (s, 1H); ^{13}C NMR (75 MHz, DMSO-D_6): δ = 21.46; 122.41; 126.95; 127.60; 130.14; 130.42; 133.15; 141.18; 147.06; 149.70; 150.76; 159.88; 163.27; 169.27; ESI$^+$-MS: M^+ found (M^+ calculated for $C_{18}H_{14}N_6S_2$): 379.3 (378.5).

4-((2-*m*-tolylthiazol-4-yl)methyleneamino)-5-(pyridin-4-yl)-2H-1,2,4-triazole-3-thione (6c): Yield 89%; solid; m.p. 310.3-314.7^{0}C; v = 3450 cm^{-1} (N-H secondary); 3055 cm^{-1} (C-H aromatic); 1611 cm^{-1} (C=N); 1263 cm^{-1} (C=S); ^{1}H NMR (300 MHz, DMSO-D_6): δ= 2.39 (s, 3H); 7.34 (d, J = 7.5 Hz, 1H); 7.42 (t, J = 7.6 Hz, 1H); 7.78-7.82 (m, 2H); 7.92 (dd, J = 4.6 Hz, 1.5 Hz, 2H); 8.64 (s, 1H); 8.76 (d, J = 6.0 Hz, 2H); 9.96 (s, 1H); 14.53 (s, 1H); ^{13}C NMR (75 MHz, DMSO-D_6): δ= 21.32; 122.41; 124.22; 127.34; 127.75; 129.76; 132.13; 132.66; 133.14; 139.31; 147.05; 149.78; 150.74; 159.63; 163.29; 169.26; ESI$^+$-MS: M^+ found (M^+ calculated for $C_{18}H_{14}N_6S_2$): 379.3 (378.5).

4-((2-*p*-chlorophenylthiazol-4-yl)methyleneamino)-5-(pyridin-4-yl)-2H-1,2,4-triazole-3-thione (6d): Yield 97%; solid; m.p. 307.3-308.4^{0}C; v = 3446 cm^{-1} (N-H secondary); 3058 cm^{-1} (C-H aromatic); 1604 cm^{-1} (C=N); 1276 cm^{-1} (C=S); ^{1}H NMR (300 MHz, DMSO-D_6): δ= 7.62 (d, J = 8.1 Hz, 2H); 7.92 (d, J = 4.5 Hz, 2H); 8.05 (d, J = 7.9 Hz, 2H); 8.70 (s, 1H); 8.77 (d, J = 4.5 Hz, 2H); 9.97 (s, 1H); 14.53 (s, 1H); ^{13}C NMR (75 MHz, DMSO-D_6): δ = 120.20; 123.88; 126.97; 129.98; 133.29; 135.36; 137.52; 146.30; 149.16; 150.76; 162.83; 165.06; 168.52; ESI$^+$-MS: M^+ found (M^+ calculated for $C_{17}H_{11}ClN_6S_2$): 399.2 (398.9).

4-((2-*p*-bromophenylthiazol-4-yl)methyleneamino)-5-(pyridin-4-yl)-2H-1,2,4-triazole-3-thione (6e): Yield 87%; solid; m.p. 296.1-298.3^{0}C; v = 3482 cm^{-1} (N-H secondary); 3055 cm^{-1} (C-H aromatic); 1604 cm^{-1} (C=N); 1277 cm^{-1} (C=S); ^{1}H NMR (300 MHz, DMSO-D_6): δ= 7.76 (d, J = 8.4 Hz, 2H); 7.92 (d, J = 5.7 Hz, 2H); 7.98 (d, J = 8.4 Hz, 2H); 8.71 (s, 1H); 8.77 (d, J = 5.5 Hz, 2H); 9.97 (s, 1H); 14.53 (s, 1H); ^{13}C NMR (75 MHz, DMSO-D_6): δ = 121.84; 124.35; 127.57; 128.44; 131.44; 132.39; 132.82; 146.60; 149.57; 150.27; 158.60; 162.92; 167.43; ESI$^+$-MS: M^+ found (M^+ calculated for $C_{17}H_{11}BrN_6S_2$): 443.3 (443.3).

4-((2-phenylthiazolo[3,2-*b*][1,2,4]-triazol-6-yl)methyleneamino)-5-(pyridin-4-yl)-2H-1,2,4-triazole-3-thione (6f): Yield 77%; solid; m.p. 285.3-288.2^{0}C; v = 3461 cm^{-1} (N-H secondary); 3067 cm^{-1} (C-H aromatic); 1604 cm^{-1} (C=N); 1286 cm^{-1} (C=S); ^{1}H NMR (300 MHz, DMSO-D_6): δ= 7.51-7.56 (m, 3H); 8.12-8.16 (m, 2H); 8.29 (dd, J = 4.6 Hz, 1.5 Hz, 2H); 8.40 (s, 1H); 8.65 (d, J = 5.9 Hz, 2H); 9.97 (s, 1H); 14.53 (s, 1H); ^{13}C NMR (75 MHz, DMSO-D_6): δ= 121.42; 122.93; 123.95; 126.69; 127.04; 129.59; 130.32; 136.83; 137.42; 147.55; 148.45; 150.47; 151.64; 161.91; ESI$^+$-MS: M^+ found (M^+ calculated for $C_{17}H_{11}BrN_6S_2$): 404.3 (404.5).

General procedure for the synthesis of Mannich bases 7a-f; 8a,c,d,f; 9-12

1 mmol of the previously obtained 1,2,4-triazole derivatives (Schiff bases **6a-f** and triazole derivatives **1-3**) was suspended into a mixture of 2.5 ml DMF and 1 ml of absolute ethanol. To the obtained mixture were added 0.15 ml of formaldehyde solution 37% and 1 mmol of secondary amine (pyrrolidine, piperidine). The reaction mixture was stirred at room temperature for 48 h and then kept for 12h at 0ºC. The formed precipitate was filtered and washed with ethanol.

4-((2-phenylthiazol-4-yl)methyleneamino)-5-(pyridin-4-yl)-2-((pyrrolidin-1-yl)methyl)-2H-1,2,4-triazole-3-thione (7a): Yield 50%; solid; m.p. 145.2-143.8^{0}C; v = 3093 cm^{-1} (C-H aromatic); 2964 cm^{-1} (C-H aliphatic); 1676 cm^{-1} (C=N); 1268 cm^{-1} (C=S); ^{1}H NMR (300 MHz, $CDCl_3$): δ = 1.77 (m, 4H); 2.95 (m, 4H); 5.36 (s, 2H); 7.46-7.48 (m, 3H); 7.98-8.02 (m, 5H); 8.76 (d, J = 6 Hz, 2H); 10.46 (s, 1H); ^{13}C NMR (75 MHz, $CDCl_3$): δ = 24.02; 50.50; 66.10; 122.32; 124.61; 126.95; 129.21; 130.99; 132.80; 133.00; 145.95; 150.36; 150.43; 156.53; 164.33; 169.88.

4-((2-*p*-tolylthiazol-4-yl)methyleneamino)-5-(pyridin-4-yl)-2-((pyrrolidin-1-yl)methyl)-2H-1,2,4-triazole-3-thione (7b): Yield 69%; solid; m.p. 151.2-153.9^{0}C; v = 3090 cm^{-1} (C-H aromatic); 2971 cm^{-1} (C-H aliphatic); 1676 cm^{-1} (C=N); 1266 cm^{-1} (C=S); ^{1}H NMR (300 MHz, $CDCl_3$): δ = 1.78 (m, 4H); 2.43 (s, 3H); 2.97 (m, 4H); 5.38 (s, 2H); 7.29 (d, J = 6.7 Hz, 2H); 7.92 (d, J = 8.1 Hz, 2H); 8.01-8.02 (m, 3H); 8.76 (d, J = 6.1 Hz, 2H); 10.45 (s, 1H); ^{13}C NMR (75 MHz, $CDCl_3$): δ = 21.62; 24.03; 50.50; 66.10; 122.32; 124.40; 126.89; 129.89; 130.19; 133.01; 141.42; 145.96; 150.21; 150.44; 156.67; 164,40; 169.93.

4-((2-*m*-tolylthiazol-4-yl)methyleneamino)-5-(pyridin-4-yl)-2-((pyrrolidin-1-yl)methyl)-2H-1,2,4-triazole-3-thione (7c): Yield 69%; solid; m.p. 177.6-178.9^{0}C; v = 3031 cm^{-1} (C-H aromatic); 2967 cm^{-1} (C-H aliphatic); 1679 cm^{-1} (C=N); 1282 cm^{-1} (C=S); ^{1}H NMR (300 MHz, $CDCl_3$): δ = 1.77 (m, 4H); 2.43 (s, 3H); 2.95 (m, 4H); 5.36 (s, 2H); 7.29-7.38 (m, 2H); 7.78 (d, J = 7.5 Hz, 1H); 7.84 (s, 1H); 7.98-8.01 (m, 3H); 8.76 (d, J = 6.1 Hz, 2H); 10.45 (s, 1H); ^{13}C NMR (75 MHz, $CDCl_3$): δ = 21.32; 23.87; 50.34; 65.94; 122.17; 124.03; 124.48; 127.31; 128.93; 131.66; 132.54; 132.85; 138.91; 145.79; 150.11; 150.26; 156.39; 164.24; 169.82.

4-((2-*p*-chlorophenylthiazol-4-yl)methyleneamino)-5-(pyridin-4-yl)-2-((pyrrolidin-1-yl)methyl)-2H-1,2,4-triazole-3-thione (7d): Yield 57%; solid; m.p. 170.2-172.8^{0}C; v = 3031 cm^{-1} (C-H aromatic); 2972 cm^{-1} (C-H aliphatic); 1674 cm^{-1} (C=N); 1267 cm^{-1} (C=S); ^{1}H NMR (300 MHz, $CDCl_3$): δ = 1.79 (m, 4H); 2.96 (m, 4H); 5.38 (s, 2H); 7.46 (d, J = 8.0 Hz, 2H); 7.94-8 (m, 4H); 8.05 (s, 1H); 8.76 (d, J= 4.3 Hz, 2H); 10.49 (s, 1H); ^{13}C NMR (75 MHz, $CDCl_3$): δ = 23.94; 50.43; 66.06; 122.24; 124.54; 128.05; 129.39; 131.20; 132.89; 136.94; 145.87; 150.35; 150.44; 156.27; 164.30; 168.39.

4-((2-*p*-bromophenylthiazol-4-yl)methyleneamino)-5-(pyridin-4-yl)-2-((pyrrolidin-1-yl)methyl)-2H-1,2,4-triazole-3-thione (7e): Yield 58%; solid; m.p. 168.8-171.3^{0}C; v = 3035 cm^{-1} (C-H aromatic); 2972 cm^{-1} (C-H aliphatic); 1673 cm^{-1} (C=N); 1266 cm^{-1} (C=S); ^{1}H NMR (300 MHz, $CDCl_3$): δ =1.79 (m, 4H); 2.97 (m, 4H); 5.38 (s, 2H); 7.63 (d, J = 8.5 Hz, 2H); 7.90 (d, J = 8.5 Hz, 2H); 7.99 (d, J = 6.1 Hz, 2H); 8.06 (s, 1H); 8.77 (d, J = 6.1 Hz, 2H); 10.50 (s, 1H); ^{13}C NMR (75 MHz, $CDCl_3$): δ = 23.95; 50.43; 66.07; 122.24; 124.52; 125.31; 128.25; 131.63; 132.35; 132.89; 145.88; 150.36; 150.48; 156.08; 164.25; 168.38.

4-((2-phenylthiazolo[3,2-*b*][1,2,4]-triazol-6-yl)methyleneamino)-5-(pyridin-4-yl)-2-((pyrrolidin-1-yl)methyl)-2H-1,2,4-triazole-3-thione (7f): Yield 50%; solid; m.p. 208.5-210.7^{0}C; v = 3043 cm^{-1} (C-H aromatic); 2964 cm^{-1} (C-H aliphatic); 1672 cm^{-1} (C=N); 1274 cm^{-1} (C=S); ^{1}H NMR (300 MHz, $CDCl_3$): δ = 1.79 (m, 4H); 2.97 (m,

4H)); 5.38 (s, 2H); 7.48-7.51 (m, 3H); 7.66 (s, 1H); 8.19-8.22 (m, 2H); 8.38 (dd, J = 4.6 Hz, 1.6 Hz, 2H); 8.77 (dd, J = 4.6 Hz, 1.6 Hz, 2H); 11.16 (s, 1H); ^{13}C NMR (75 MHz, $CDCl_3$): δ = 24.20; 50.62; 66.11; 121.54; 122.66; 127.01; 128.05; 129.03; 130.42; 130.92; 132.84; 145.99; 146.68; 150.70; 157.53; 163.95; 168.36.

4-((2-*p*henylthiazol-4-yl)methyleneamino)-5-(pyridin-4-yl)-2-((piperidin-1-yl)methyl)-2H-1,2,4-triazole-3-thione (8a): Yield 87%; solid; m.p. 188.3-188.9^{0}C; v = 3031 cm^{-1} (C-H aromatic); 2944 cm^{-1} (C-H aliphatic); 1669 cm^{-1} (C=N); 1270 cm^{-1} (C=S); ^{1}H NMR (300 MHz, $CDCl_3$): δ = 1.42 (m, 2H); 1.61 (m, 4H); 2.84 (m, 4H); 5.27 (s, 2H); 7.49 (m, 3H); 8.01-8.04 (m, 5H); 8.78 (d, J = 4.8 Hz, 2H); 10.47 (s, 1H); ^{13}C NMR (75 MHz, $CDCl_3$): δ=23.77; 26.01; 51.89; 70.87; 122.25; 124.54; 126.88; 129.13; 130.91; 132.73; 132.96; 145.67; 150.29; 150.36; 156.51; 164.40; 169.64.

4-((2-*m*-tolylthiazol-4-yl)methyleneamino)-5-(pyridin-4-yl)-2-((piperidin-1-yl)methyl)-2H-1,2,4-triazole-3-thione (8c): Yield 67%; solid; m.p. 151.8-155.5^{0}C; v = 3023 cm^{-1} (C-H aromatic); 2933 cm^{-1} (C-H aliphatic); 1676 cm^{-1} (C=N); 1270 cm^{-1} (C=S); ^{1}H NMR (300 MHz, $CDCl_3$): δ = 1.42 (m, 2H); 1.61 (m, 4H); 2.45 (s, 3H); 2.84 (t, J = 5.1 Hz, 4H); 5.27 (s, 2H); 7.28-7.40 (m, 2H); 7.80 (d, J = 7.5 Hz, 1H); 8.01-8.03 (m, 3H) overlapped with 7.81 (s, 1H); 8.79 (dd, J = 4.7 Hz, 1.5 Hz, 2H); 10.45 (s, 1H); ^{13}C NMR (75 MHz, $CDCl_3$): δ = 21.39; 23.78; 26.01; 51.90; 70.65; 122.25; 124.12; 124.57; 127.40; 129.02; 131.73; 132.63; 132.97; 138.89; 145.67; 150.20; 150.30; 156.54; 164.41; 169.91.

4-((2-*p*-chlorophenylthiazol-4-yl)methyleneamino)-5-(pyridin-4-yl)-2-((piperidin-1-yl)methyl)-2H-1,2,4-triazole-3-thione (8d): Yield 58%; solid; m.p. 187.3-187.9 ^{0}C; v = 3103 cm^{-1} (C-H aromatic); 2930 cm^{-1} (C-H aliphatic); 1669 cm^{-1} (C=N); 1273 cm^{-1} (C=S); ^{1}H NMR (300 MHz, $CDCl_3$): δ = 1.42 (m, 2H); 1.60 (m, 4H); 2.84 (t, J = 5.0 Hz, 4H); 5.26 (s, 2H); 7.45 (d, J = 8.5 Hz, 2H); 7.94-8.00 (m, 4H); 8.05 (s, 1H); 8.78 (d, J = 6.0 Hz, 2H); 10.47 (s, 1H); ^{13}C NMR (75 MHz, $CDCl_3$): δ = 23.84; 26.07; 51.96; 70.96; 122.29; 124.60; 128.12; 129.45; 131.27; 132.99; 137.00; 154.73; 150.43; 150.51; 156.38; 164.45; 168.32.

4-((2-phenylthiazolo[3,2-*b*][1,2,4]-triazol-6-yl)methyleneamino)-5-(pyridin-4-yl)-2-((piperidin-1-yl)methyl)-2H-1,2,4-triazole-3-thione (8f): Yield 60%; solid; m.p. 212.4-215.7^{0}C; v = 3055 cm^{-1} (C-H aromatic); 2932 cm^{-1} (C-H aliphatic); 1670 cm^{-1} (C=N); 1261 cm^{-1} (C=S); ^{1}H NMR (300 MHz, $CDCl_3$): δ = 1.42 (m, 2H); 1.61 (m, 4H); 2.84 (t, J = 5.1 Hz, 4H); 5.26 (s, 2H); 7.49-7.51 (m, 3H); 7.66 (s, 1H); 8.19-8.22 (m, 2H); 8.38 (dd, J = 4.6 Hz, 1.6 Hz, 2H); 8.77 (dd, J = 4.6 Hz, 1.6 Hz, 2H); 11.16 (s, 1H); ^{13}C NMR (75 MHz, $CDCl_3$): δ = 23.98; 26.23; 52.13; 70.96; 121.50; 122.67; 127.03; 128.08; 129.04; 130.42; 130.93; 132.88; 145.94; 146.96; 150.72; 159.18; 164.31; 168.42.

4-methyl-5-(pyridin-4-yl)-2-((pyrrolidin-1-yl)methyl)-2H-1,2,4-triazole-3-thione (9): Yield 59%; solid; m.p. 140.3-142.8^{0}C; v = 2964 cm^{-1} (C-H aliphatic); 1220 cm^{-1} (C=S); ^{1}H NMR (300 MHz, $CDCl_3$): δ = 1.71-1.75 (m, 4H); 2.90 (t, J = 6.4 Hz, 4H); 3.71 (s, 3H); 5.27 (s, 2H); 7.54 (dd, J = 4.5, 1.5 Hz, 2H); 8.79 (dd, J = 4.5, 1.5 Hz, 2H); ^{13}C NMR (75 MHz, $CDCl_3$): δ = 23.86; 33.24; 50.47; 66.27; 122.17; 133.39; 147.95; 150.79; 169.88.

4-allyl-5-(pyridin-4-yl)-2-((pyrrolidin-1-yl)methyl)-2H-1,2,4-triazole-3-thione (10): Yield 40%; solid; m.p. 110.5-111.9^{0}C; v = 3036 cm^{-1} (C-H vinyl); 2975 cm^{-1} (C-H aliphatic); 1267 cm^{-1} (C=S); ^{1}H NMR (300 MHz, $CDCl_3$): δ= 1.73-1.78 (m, 4H); 2.91 (t, J = 5.5 Hz, 4H); 4.78-4.80 (m, 2H); 5.30 (s, 2H); 5.93-6.05 (m, 1H); 7.58 (dd, J = 4.5 Hz, 1.5 Hz, 2H); 8.77 (dd, J = 4.5 Hz, 1.5 Hz, 2H); ^{13}C NMR (75 MHz, $CDCl_3$): δ = 23.85; 47.85; 50.50; 66.24; 118.52; 122.20; 130.87; 133.33; 148.18; 150.73; 169.78.

4-phenyl-5-(pyridin-4-yl)-2-((pyrrolidin-1-yl)methyl)-2H-1,2,4-triazole-3-thione (11): Yield 61%; solid; m.p. 160.5-161.5^{0}C; v = 3031 cm^{-1} (C-H aromatic); 2957 cm^{-1} (C-H aliphatic); 1151 cm^{-1} (C=S); ^{1}H NMR (300 MHz, $CDCl_3$): δ= 1.77-1.81 (m, 4H); 2.97 (t, J = 5.5 Hz, 4H); 5.35 (s, 2H); 7.18 (dd, J = 4.6 Hz, 1.5 Hz, 2H); 7.29-7.32 (m, 3H); 7.52-7.54 (m, 2H); 8.54 (dd, J = 4.6 Hz, 1.5 Hz, 2H); ^{13}C NMR (75 MHz, $CDCl_3$): δ = 23.92; 50.67; 66.54; 121.59; 129.21; 130.04; 130.29; 132.92; 134.72; 146.83; 150.34; 170.98.

4-phenyl-5-(pyridin-4-yl)-2-((piperidin-1-yl)methyl)-2H-1,2,4-triazole-3-thione (12): Yield 60%; solid; m.p. 204.5-206.30C; v = 3029 cm^{-1} (C-H aromatic); 2932 cm^{-1} (C-H aliphatic); 1273 cm^{-1} (C=S); ^{1}H NMR (300 MHz, $CDCl_3$): δ = 1.42-1.46 (m, 2H); 1.59-1.66 (m, 4H); 2.86 (t, J = 5.2 Hz, 4H); 5.27 (s, 1H); 7.21 (dd, J = 4.6 Hz, 1.5 Hz, 2H); 7.31-7.34 (m, 2H); 7.55-7.57 (m, 3H); 8.57 (dd, J = 4.6 Hz, 1.5 Hz, 2H); ^{13}C NMR (75 MHz, $CDCl_3$): δ =23.77; 25.95; 51.91; 71.18; 121.61; 128.24; 130.04; 130.29; 132.99; 134.75; 146.61; 150.32; 171.17.

The anti-inflammatory activity

All synthesized compounds were evaluated in order to determinate their anti-inflammatory activity, by performing the rat paw oedema test, according to the method of Winter et al (1962) modified by the introduction of a commercially available plethysmometer from Ugo Basile, Varese, Italy [16]. Male rats Winstar breed with an average weight around 175g were divided into 22 groups of 6 rats. All animals were housed in standard conditions with food and water *ad libitum*. The first group which represents the control one was injected intraperitoneally (i.p.) with 1 ml vehicle (Tween 80 and distilled water). The second group which represents the standard one was injected i.p. with diclofenac 20mg/kg as reference drug. In the 20 treated groups, all tested compounds were injected i.p. with doses of 20mg/kg. For all 22 groups the volume of the solution used for intraperitoneal administration was 1ml.

The inflammation was induced thirty minutes after intraperitoneal injection by administrating 0.1 ml carrageenan solution 1% intraplantar. Rats oedema were evaluated by measuring the rat hind left paw volume at hourly intervals from 1 to 4 hours. The rats paw volume was also measured before inducing inflammation.

The inhibition percent was calculated according to the following formula: % Inhibition of oedema = (1-Ēt/Ēm)x100, where Ēt represents the average value of the oedema in all treated groups 1 – 4 hours after the induced inflammation (in ml) and Ēm represents the average value of the oedema in control group 1 – 4 hours after after the induced inflammation (in ml).

Statistical analysis was performed by Student's 't' test, and *p*-value was choosen less than 0.05 for statistical significance.

The biological experiment was conducted according to the EC Directive 2010/63/EU, which regulates the use of laboratory animals.

ACKNOWLEDGMENTS

The present study was conducted with the financial support of the European Social Fund under the project POSDRU number 107/1.5/S/78702. The authors are grateful to Mr. Mircea Dan Puia for providing the IR spectra.

REFERENCES

1. P.C. Lv, K.R. Wang, Y. Yang, W.J. Mao, J. Chen, J. Xiong, et al, *Bioor. Med. Chem. Lett.,* **2009**, *19*, 6750; (b) V. Padmavathi, C.P. Kumari, B.C. Venkatesh, A. Padmaja, *Eur. J. Med. Chem.,* **2011**, *46*, 5317; (c) N.C. Desai, K.M Rajpara, V.V. Joshi, J. Fluorine Chem., **2013**, 1*45*, 102.
2. S. Shelke, G. Mhaske, S. Gadakh, C. Gill, *Bioor. Med. Chem. Lett.,* **2010**, *20*, 7200; (b) N.B. Patel, I.H. Khan, S.D. Rajani, *Eur. J. Med. Chem.,* **2010**, *45*, 4293; (c) S.G. Kucukguzel, I. Kucukguzel, E. Tatar, S. Rollas, F. Sahin, M. Gulluce, et al, *Eur. J. Med. Chem.,* **2007**, *42*, 893.
3. P.X. Franklin, A.D. Pillai, P.D. Rathod, S. Yerande, M. Nivsarkar, H. Padh, et al, *Eur. J. Med. Chem.,* **2008**, *43*, 129; (b) O. Kouatly, A. Geronikaki, C. Kamoutsis, D.L. Hadjipavlou, P. Eleftheriou, *Eur. J. Med. Chem.,* **2009**, *44*, 1198; (c) R. Aggarwal, S. Kumar, P. Kaushik, D. Kaushik, G.K. Gupta, *Eur. J. Med. Chem.,* **2013**, *62*, 508; (d) N. Singh, S.K. Bhati, A. Kuma, *Eur. J. Med. Chem.,* **2008**, *43*, 2597; (e) S.H. Shelke, P.C. Mhaske, M. Nandave, S. Narkhade, N.M. Walhekar, V.D. Bobade, *Bioor. Med. Chem. Lett.,* **2012**, *22*, 6373.
4. M.A. Al-Omar, A.E.Amr. El-Galil, R.A. Al-Salahi*, Arch. Pharm. Chem. Life Sci.*, **2010**, 10, 648; (b) A.M.A. Megged, H.M.A. Rahman, g.E.S. Alkaramany, M.A.El-Gendy, *Eur. J. Med. Chem.,* **2009**, *44*, 117.
5. K. Imtiaz, A. Sajid, H. shahid, R.H. Nasim, M.T. Hussain, A. Wadood et al, *Eur. J. Med. Chem.,* **2010**, *45*, 5200; (b) T. Sato, N. Ashizawa, T. Iwanaga, H. Nakamura, K. Matsumoto, T. Inoue, et al, *Bioor. Med. Chem. Lett.,* **2009**, *19*, 184; (c) T. Sato, N. Ashizawa, K. Matsumoto, T. Iwanaga, H. Nakamura, , T. Inoue, et al, *Bioor. Med. Chem. Lett.,* **2009**, *19*, 6225.

6. G.S. Hassan, S. M. El-Messery, F. A. M. Al-Omary, H. I. El-Subbagh, *Bioor. Med. Chem. Lett.,* **2012**, *22*, 6318; (b) V. Zaharia, A. Ignat, N. Palibroda, B. Ngameni, V. Kuete, C. N. Fokunang, M.L. Moungang, B.T. Ngadjui, *Eur. J. Med. Chem.* **2010**, 45, 5080; (c) D.S. Prasannaa, C.V. Kavithab, K. Vinayaa, S.R. Ranganathab, S.C. Raghavanb, K.S. Rangappa, *Eur. J. Med. Chem.,* **2010**, *45*, 5331; (d) R. Romagnoli, R.G. Baraldi, M.K. Salvador, M.E. Camacho, D. Preti, M.A. Tabrizi et al, *Bioor. Med. Chem.,* **2012**, *20*, 7083.
7. M.R. Shireadkar, K.K. Murahari, H.R. Gangadasu, T. Suresh, C.A. Kalyan, D. Panchal et al, *Bioor. Med. Chem. Lett.,* **2007**, *15*, 3997; (b) M.S. Karthikeryan, *Eur. J. Med. Chem.,* **2009**, *44*, 827; (c) S.F. Barbuceanu, G.L. Almajan, I. Samaret, C. Draghici, A.I. Tarcomnicu, G. Bancescu, *Eur. J. Med. Chem.,* **2009**, *44*, 4752.
8. A.U. Baran, B.C. Tel, D. Sarigol, E.I. Ozturk, I. Kazkayasi, G. Okay, et al, *Eur. J. Med. Chem.,* **2012**, *57*, 398; (b) B. Tozkoparan, S.P. Aytac, S. Gursony, G. Aktany, *Med. Chem. Res.*, **2012**, *21*, 192.
9. D. Sunil, A.M. Isloor, P. Shetty, B. Chandraakantha, K. Satyamoorthy, *Med. Chem. Res.*, **2011**, *20*, 1024; (b) D. Sunil, A.M. Isloor, P. Shetty, P.G Nayak, K.S.R. Pai, *Arabian J. Chem.*, **2013**, 6, 25.
10. G.L. Almajan, S.f. Barbuceanu, E.R. Almajan, C. Draghici, G. Samaret, *Eur. J. Med. Chem.,* **2009**, *44*, 3083; (b) H. Bayrak, A. Demirbas, N. Demirbas, S.A. Karaoglu, *Eur. J. Med. Chem.,* **2009**, *44*, 4362; (c) G.V.S. Kumar, Y.R. Prasad, B.P. Mallikarjuna, S.M. Chandrashekar, *Eur. J. Med. Chem.,* **2010**, *45*, 5120; (d) T. Plech, M. Wujec, A. Siwek, U. Kosikowska, A. Malm, *Eur. J. Med. Chem.,* **2011**, *46*, 241; (e) Y.L.N. Murty, B. Govindh, B.S. Diwakar, K. Nagalakshmi, K.V.R. Rao, *Med. Chem. Res.*, **2012**, *21*, 3104; (f) T. Plech, M. Wujec, M. Majewska, U. Kosikowska, A. Malm, *Med. Chem. Res.*, **2013**, *22*, 2531.
11. K.V. Sujith, J.N. Rao, P. Shetty, B. Kalluraya, , *Eur. J. Med. Chem.,* **2009**, *44*, 3697; (b) S.M. Sondhi, a. Surbhi, R. Reshma, K. Nikhil, R. Partha, *Med. Chem. Res.*, **2011**, *21*, 3620.
12. Nithinchandra, B. Kalluraya, S. Aamir, A.R. Shabaraya, *Eur. J. Med. Chem.,* **2012**, *54*, 597.
13. S.O. Yildirim, M. Akkurt, A. Cetin, Ar. Cansiz, M. Sekerci, C. Kazak, *Acta Cryst*., **2005**, *61*, 619. (b) A.A. Creanga, V.N. Bercean, V. Badea, A.I. Patras, A.I. Cocarta, C.A. Tatu et al, *Rev. Chim.*, **2010**, *61*, 1169.
14. Silberg, I. Simiti, H. Mantsch, *Chem. Ber*., **1961**, *94*, 2887.
15. V. Zaharia, M. Palage, I.Simiti, *Farmacia*, **2000**, *XLVIII (6)*, 57.
16. C.A. Winter, E.A. Risley, G.W. Nuss, Proc. Soc. Exp. Biol. Med., **1962**, *111*, 544; (b) T. Griesbacher, R.L Suttlif, F. Lembeck, Br. J. Pharmacol., **1994,** *112*, 1004.

STUDIA UBB CHEMIA, LVIII, 2, 2013 (p. 105 – 114)
(RECOMMENDED CITATION)

ELECTROCHEMICAL BEHAVIOR OF THE HEMIN MODIFIED GRAPHITE ELECTRODE FOR H_2O_2 DETECTION

GEORGETA MARIA MARES[a], GRAZIELLA LIANA TURDEAN[a*], IONEL CĂTĂLIN POPESCU[a]

ABSTRACT. Aiming to detect amperometrically H_2O_2, iron (III) protoporphyrin IX (hemin; Hm) was immobilized by simple adsorption on the surface of a graphite (G) electrode. The electrochemical behavior of the G/Hm modified electrode was investigated by using cyclic voltammetry (CV) and square-wave voltammetry (SWV) under different experimental conditions (scan rate or frequency and pH). The catalytic current measured at G/Hm was found to depend linearly on the H_2O_2 concentration from ~0.01 mM up to 0.04 mM H_2O_2 (R/N = 0.987 / 4) and from ~0.01 mM up to 0.08 mM H_2O_2 (R/N = 0.973/14) for CV and SWV measurements, respectively. For both methods the detection limit was ~10 μM, while the sensitivity was much higher for SWV [(276 ± 12) mA/M] than for CV [(13.5 ± 1.6) mA/M].

Keywords: *iron(III) protoporphyrin (IX), hydrogen peroxide, cyclic voltammetry, square wave voltammetry, electrocatalysis.*

INTRODUCTION

As defined by IUPAC, a chemically modified electrode (CME) "is an electrode made of a conducting or semiconducting material that is coated with a selected monomolecular, multimolecular, ionic, or polymeric film of a chemical modifier and that by means of faradaic (charge-transfer) reactions or interfacial potential differences (no net charge transfer) exhibits chemical, electrochemical, and/or optical properties of the film" [1]. Usually, the chemically modified electrodes can be obtained by one of the following approaches: (i) chemisorption, (ii) covalent bonding, (iii) polymer film coating, and (iv) entrapment in a conductive material. Among these, the simplest way exploiting the

[a] *Department of Physical Chemistry, "Babes-Bolyai" University, Arany Janos 11, RO-3400 Cluj-Napoca, Romania,*corresponding author: gturdean@chem.ubbcluj.ro*

adsorption of the modifier on the electrode surface, generates a stable film. Usually, this approach yields monolayer modified electrodes with high electrocatalytic activity.

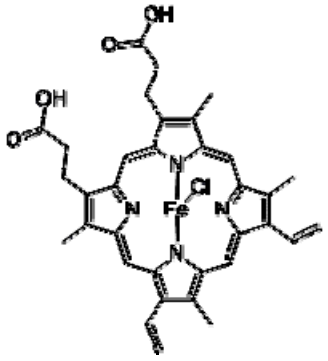

Scheme 1

Hemin (iron protoporphyrin IX; Hm) is one of the most important biological substances. It corresponds to the active center of several families of heme proteins, for example C-type cytocromes, peroxidase and oxygen–carrying proteins such as hemoglobin (Hb) and myoglobin (Mb) [2]. Hemin dissolved in an aqueous solution, adsorbed on the electrode surface or incorporated within a polymeric film immobilized on the electrode surface, maintains its electrochemical activity [3].

Hemin, due to its peculiar chemical structure (Scheme 1), is strongly adsorbed on the carbonaceous electrode materials, especially on pyrolytic graphite (PG) [4, 5]. The so obtained modified electrodes were used for the amperometric detection of H_2O_2 [6], superoxide [7], nitritc oxide [8], 4-aminophenol [9] and tryptophan or its derivates [10].

In this work we report on the preparation, by simple adsorption, of a hemin modified graphite electrode. The electrochemical behavior of G/Hm was examined by using two complementary electrochemical methods: cyclic voltammetry (CV) and square-wave voltammetry (SWV). Finally, the G/Hm modified electrode was used for the amperometric detection of H_2O_2 and the electroanalytical and kinetic parameters were estimated.

RESULTS AND DISCUSSION

Electrochemical behavior of G/Hm electrode

In figure 1 are showed the CV and SWV responses, recorded at G/Hm modified electrodes. In both cases, stable and well-defined peaks pairs corresponding to the immobilized hemin were observed. Also, the CV measurements show that the peak potentials shift progressively towards higher absolute values when the scan rate increases, suggesting a quasi-reversible electrochemical process.

The cyclic voltammogram recorded at 50 mV/s (Figure 1A) was used to evaluate the formal standard potential [$E^{0'} = (E_{pa} + E_{pc})/2$, where E_{pa} and E_{pc} stand for the anodic and cathodic peak potentials, respectively] of the hemin redox couple. The calculated value (-0.33 V *vs.* Ag/AgCl,KCl_{sat}) was found in good agreement with that already reported (-0.34 V *vs*. Ag/AgCl,KCl_{3M}) for hemin [11]. Additionally, the peak potentials separation ($\Delta E_p = E_{p,a} - E_{p,c}$ = 0.034 V, at 50 mV/s), confirms that the investigated redox process corresponds

to a quasi-reversible one [8]. Additionally, the I_{pa}/I_{pc} ratio is very close to 1 (0.955, at 50 mV/s). Finally, it can be concluded that the adsorbed hemin exhibits the characteristic features for a quasi-reversible redox couple [12].

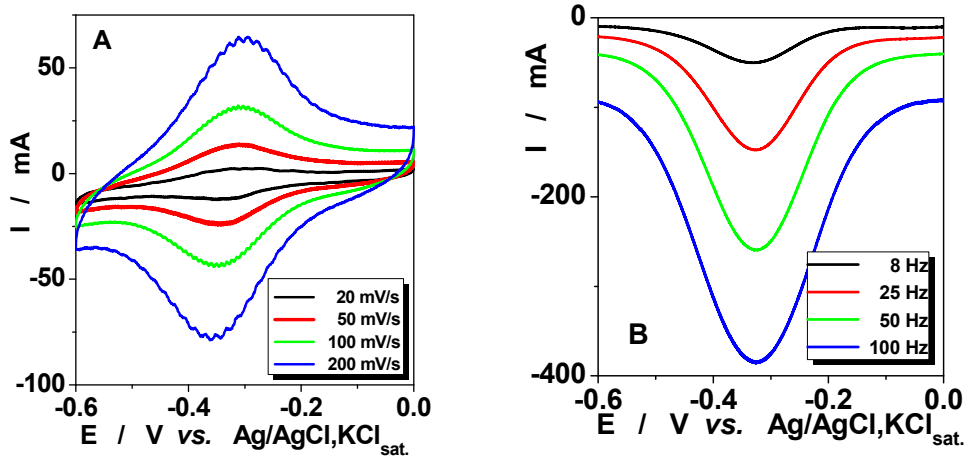

Figure 1. Cyclic (**A**) and square-wave (**B**) voltammograms recorded at G/Hm modified electrode. Experimental conditions: supporting electrolyte, 0.1 M phosphate buffer (pH 7.0); starting potential, -0.6 V *vs*. Ag/AgCl,$KCl_{sat.}$ (A) and 0 V *vs*. Ag/AgCl,KCl_{sat} (B); SWV amplitude, 20 mV; deaerated solution (Ar)

As expected for a surface confined redox couple [13], in the investigated range of potential scan rate (20 – 200 mV/s), the anodic (I_{ap}) and cathodic (I_{cp}) peak currents depend linearly on the potential scan rate (v) (Figure 2A).

Within the limits of the experimental error, this conclusion was confirmed by the slope values obtained from the $\log(I_p)$ - log(v) dependencies (Table 1).

Table 1. The slopes of the $\log(I_p)$ *vs.* log(v) dependencies for G/Hm electrode.

Redox process	Slope	R / No. of exp. points
anodic	1.18 ± 0.05	0.990 / 6
cathodic	0.82 ± 0.02	0.997 / 7

For CV measurements, this parameter is considered a relevant criterion helping to distinguish between the adsorbed (slope ~1) or dissolved (slope ~0.5) redox couples. Furthermore, it is worth to mention that SWV measurements confirm that hemin behaves as a redox couple strongly immobilized on the graphite surface. Thus, the I_{cp} depends linearly on the square root of the applied frequency (*f*) (Figure 2B).

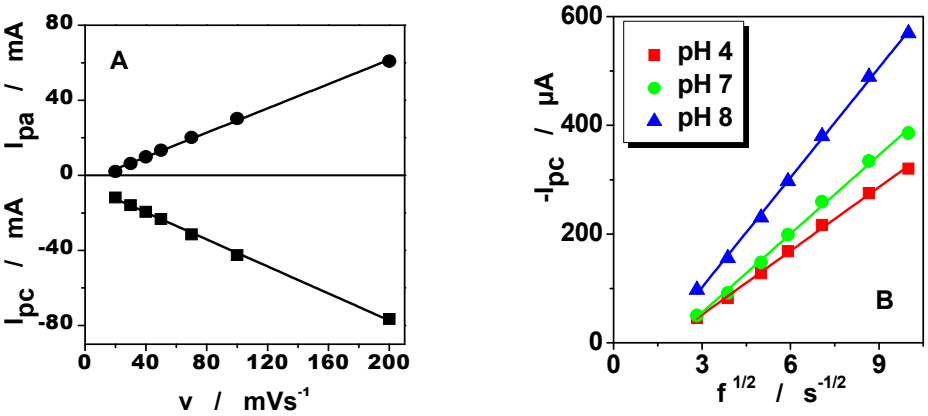

Figure 2. The I_p *vs.* potential scan rate (**A**) and I_{pc} *vs.* $\nu^{1/2}$ (**B**) dependencies recorded at G/Hm modified electrode. Experimental conditions: see figure 1.

Both methods (CV and SWV) used to investigate the electrochemical behavior of the G/Hm modified electrode showed that, when the pH of the supporting electrolyte increases, a negative shift of the recorded cyclic voltammograms can be clearly observed (Figure 3).

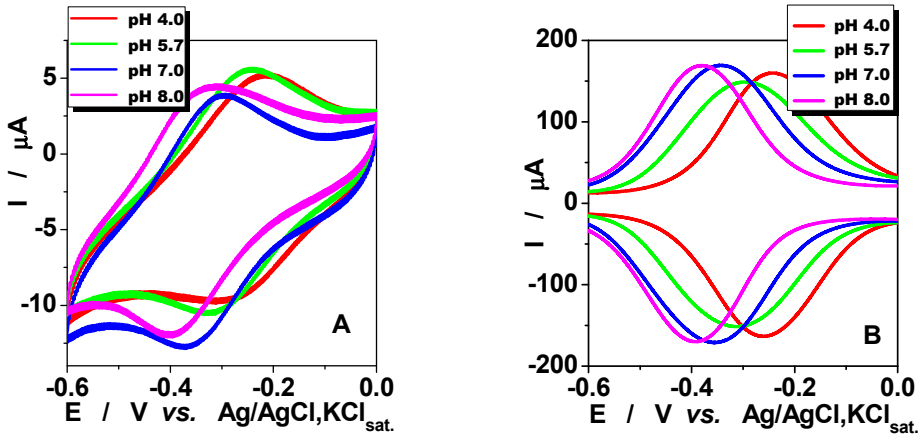

Figure 3. pH influence on the electrochemical response of G/Hm modified electrode recorded using CV (**A**) and SWV (**B**) measurements. Experimental conditions: supporting electrolyte, 0.1 M phosphate buffer; starting potential, -0.6 V *vs*. Ag/AgCl,KCl$_{sat}$ (A) and 0 V *vs*. Ag/AgCl,KCl$_{sat}$ (B); scan rate, 20 mV/s (A); frequency 25 Hz (B); amplitude, 20 mV (B); deaerated solution (Ar).

The $E^{0'}$ values, estimated from the CV and SWV measurements illustrated in figures 3A and 3B, respectively, were found to depend linearly on the pH of supporting electrolyte (results not shown). However, in the pH range from 4 up to 8, the values of the slopes calculated for these dependencies [CV: (-0.041 ± 0.005) V/pH, with R = 0.962 and n = 4; SWV: (-0.033 ± 0.001) V/pH, with R = 0.99 and n = 4], do not agree with the theoretical value (0.059 V/pH) expected for a redox process involving the transfer of $1e^-/1H^+$. This peculiar behavior was already observed for hemin [14, 15] and was attributed to the protonation states of the *trans* ligands of the heme iron, combined with the protonation of the amino acids surrounding the heme or the protonation of the water molecule coordinated to the iron atom [16, 17, 18].

The stability of the modified electrode is a very important characteristic because it provides information on the electrode life-time, a decisive parameter for its future applications. For this reason, the short-time stability of G/Hm was evaluated by continuous cycling of the electrode potential when it was in contact with the supporting electrolyte (0.1 M PB, pH 7). Figure 4A shows qualitatively that for both cathodic and anodic peak currents no significant variation in time can be observed after 12 repetitive full potential scans.

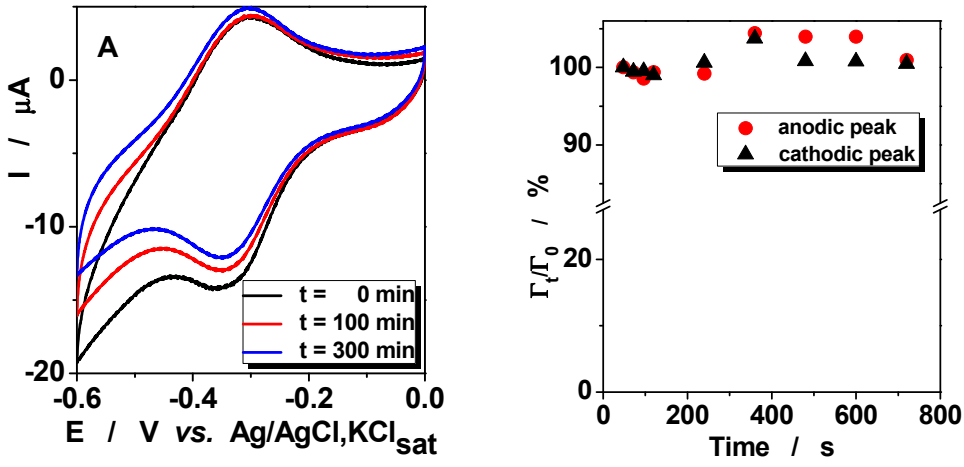

Figure 4. Repetitive CV measurements performed at G/Hm modified electrode (**A**) and the time dependence of the relative surface coverage (Γ_t/Γ_0) (**B**). Experimental conditions: supporting electrolyte, 0.1 M PB (pH 7.0); starting potential, -0.6 V *vs.* Ag/AgCl,$KCl_{sat.}$; scan rate, 50 mV/s; deaerated solution (Ar)

The variation in time of the electrode surface coverage [$\Gamma(mol/cm^2) = Q/(nFA)$, where Q(Coulomb) is the amount of charge corresponding to the cathodic or anodic under-peak area, estimated after the background current correction; n(=1) is the number of electrons transferred during the redox process, which generates the voltammetric peak; F (Coulomb) is the Faraday's constant; $A(cm^2)$ is the electrode geometric area] confirms that hemin is strongly adsorbed on the graphite surface (Figure 4B).

The tables 2-4 summarized the data concerning the variation in time of the surface coverage (Table 2) and the peak parameters (Tables 3 and 4) of the voltammetric response recorded at G/Hm modified electrode. Between measurements the G/Hm electrodes were stored at 4°C, in a water saturated atmosphere. All data prove the high stability of the G/Hm modified electrode. This behavior was related to the hemin insolubility under acidic and neutral conditions [19], associated with the strong π-π interaction between hemin and graphite [20].

Table 2. Short time stability of G/Hm modified electrode.

Time (s)	Γ_c (nmol/cm^2)	Γ_a (nmol/cm^2)	$\Delta\Gamma_c$ (%)	$\Delta\Gamma_a$ (%)
48	76.2	129	-	-
240	76.6	128	0.53	0.08
480	76.8	135	0.79	4.65
720	76.5	130	0.39	0.08

$\Delta\Gamma_c = 100(\Gamma_{c,t} - \Gamma_{c,t=48})/\Gamma_{c,t=48}$; $\Delta\Gamma_a = 100(\Gamma_{a,t} - \Gamma_{a,t=48})/\Gamma_{a,t=48}$

Table 3. Short time variation of the peak parameters for the voltammetric response of G/Hm modified electrode.

Time (s)	E_{pc} (V*)	E_{pa} (V*)	ΔE_p (V)	$E^{0'}$ (V*)	I_{ap}/I_{cp}
48	-0.346	-0.306	0.040	0.020	1.38
240	-0.348	-0.306	0.042	0.021	1.36
480	-0.348	-0.306	0.042	0.021	1.38
720	-0.348	-0.306	0.042	0.021	1.37

*E_{pc}, E_{pc} and $E^{0'}$ were measured *vs.* the Ag/AgCl,KCl_{sat} reference electrode

Table 4. Long time variation of the peak parameters for the voltammetric response of G/Hm modified electrode.

ΔI_{ap} (%)	ΔI_{cp} (%)	$\Delta\Gamma_c$ (%)	$\Delta\Gamma_a$ (%)	ΔE_p (mV)	I_{ap}/I_{cp}
7.6	2.4	6.5	9.3	23	1.15

where: $\Delta I_{cp} = 100(I_{cp,\,t=305} - I_{cp,\,t=0})/I_{cp,\,t=0}$; $\Delta I_{ap} = 100(I_{ap,\,t=305} - I_{ap,\,t=0})/I_{ap,\,t=0}$

$\Delta\Gamma_c = 100(\Gamma_{c,t=305} - \Gamma_{c,t=0})/\Gamma_{c,t=0}$; $\Delta\Gamma_a = 100(\Gamma_{a,t=305} - \Gamma_{a,t=0})/\Gamma_{a,t=0}$

Electrocatalytic behavior of G/Hm modified electrode

Taking into account that H_2O_2 is a product of the biochemical reactions catalyzed by oxidases, its detection is of considerable importance in clinical, food, pharmaceutical and environmental analysis [2, 21]. In this context, the electrocatalytic behavior of the G/Hm modified electrode was investigated for H_2O_2 electrocatalytic reduction by using CV and SWV measurements (Figure 6). As can be seen from figure 6 and table 6, the SWV measurements provided better analytical and kinetic parameters than those obtained from CV measurements. Probably, this difference is due to the higher resolution of SWV technique, associated with the easier and better correction for the background current in the case of SWV measurements.

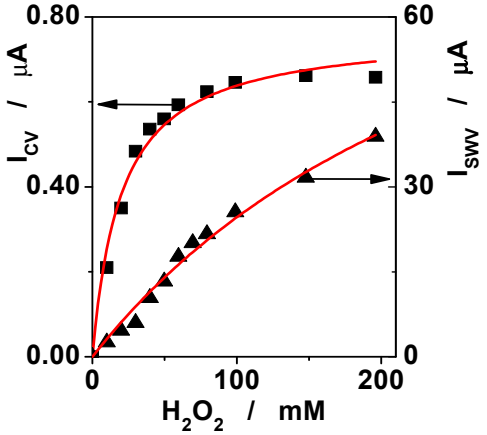

Figure 6. Calibration curve of the G/Hm modified electrode for H_2O_2 detection using CV and SWV measurements. Experimental conditions: supporting electrolyte, 0.1 M PB (pH 7.0); starting potential, -0.6 V *vs*. Ag/AgCl,$KCl_{sat.}$(CV), 0 mV *vs*. Ag/AgCl,$KCl_{sat.}$ (SWV); scan rate, 20 mV/s; amplitude, 20 mV; frequency, 25 Hz; deaerated solution (Ar).

Table 5. Analytical and kinetic parameters of G/Hm modified electrode.

Method	CV	SWV
Parameters	Michaelis-Menten fitting	
I_{max} (µA)	0.77 ± 0.02	101.4 ± 16.1
K_M^{app} (mM)	20.2 ± 2.5	311.6 ± 68.3
Sensitivity (mA/M)	0.038	0.325
R / N	0.9836 / 11	0.9861 / 12
	Linear fitting	
Slope (A/mM)	16.0 ± 1.3	276.3 ± 11.9
Detection limit /mM	0.011	0.012
Linear range (mM)	10 - 40	10 - 80
R / N	R = 0.979 / n = 5	R = 0.993 / n = 9

***Sensitivity = I_{max}/K_M^{app}**

CONCLUSIONS

This work describes a simple and reproducible way to prepare a modified electrode for H_2O_2 detection, based on the hemin adsorption on the graphite surface. The electrochemical characterization of the G/Hm electrode, performed by using CV and SWV measurements, allowed establishing the influence of the experimental conditions (scan rate, pH and duration of use) on the electrode performances. Additionally, it was confirmed that the immobilized hemin is involved in a quasi-reversible $1e^-/1H^+$ redox process, with the features of a surface confined species. The electrocatalytic behavior of G/Hm modified electrode for H_2O_2 electroreduction recommends it as a promising transducer for sensors and biosensors construction.

EXPERIMENTAL SECTION

Reagents

Hemin, iron (III) protoporphyrin (IX) chloride (Hm), tris(hydroxymethyl) aminomethane (TRIS) and H_2O_2 (30%) were purchased from Fluka, Sigma and Merck, respectively. A stock solution of 5 mM Hm was prepared by dissolving the appropriate amount of salt in 0.05 M TRIS chloride buffer (pH 10.5). The 0.1 M phosphate buffer solution (PB, pH 8.0) was prepared from 0.05 M KH_2PO_4 and 0.05 M K_2HPO_4 (Sigma). The pH of PB was adjusted by using HCl and NaOH (Reactivul-Bucharest). Deionized water was used for preparing all solutions.

Equipments

All electrochemical measurements were carried out using a computer controlled voltammetric analyzer (Autolab-PGSTAT 10 EcoChemie, The Netherlands).

A standard single-compartment three electrode cell was equipped with a Pt counter electrode, a $Ag/AgCl,KCl_{sat}$ reference electrode (Radiometer, France), and the working electrode made of spectral graphite (Ringsdorff-Werke Gmbh, Bonn-Bad Godesberg, Germany).

In order to remove the dissolved oxygen, highly purified argon gas was purged into the working solution for at least 15 minutes prior to the experiment. Additionally, the argon flow was kept over the solution during all time of measurements. All experiments were performed at room temperature (25 ± 2 °C).

A combined glass electrode connected to a digital pH meter (Hanna Instruments HI 1230) was used for the pH measurements.

Preparation of G/Hm modified electrode

Before Hm deposition, the graphite disc electrode (3 mm diameter) was polished by using wet emery paper (320 and P1200C grit), until a smooth surface was obtained. Then, the electrodes were ultrasonicated for 2 minutes. The cleanness of the graphite electrode surface was validated by performing CV measurements in 0.1 M PB (pH 7), between -0.6 and 0 V *vs*. Ag/ $AgCl,KCl_{sat}$ and using a scan rate of 20 mV/s.

The G/Hm modified electrode was prepared by dropping 5 μL of 5 mM Hm solution on the graphite surface. Further, the electrode was dried in air by keeping it during the night. Between measurements, the modified electrodes were at 4 °C.

ACKNOWLEDGEMENTS

The authors acknowledge the financial support from ID_PCCE_ 129/2008 (NANOBIOFUN) grant.

REFERENCES

1. R.A. Durst, A.J. Baumner, R.W. Murray, R.P. Buck, C.P. Andrieux, *Pure and Applied Chemistry*, **1997**, *69*, 1317.
2. G.L. Turdean, I.C. Popescu, A. Curulli, G. Palleschi, *Electrochimica Acta*, **2006**, *51*, 6435.
3. T. Sagara, S. Takeuchi, K. Kumazaki, N. Nakashima, *Journal of Electroanalytical Chemistry,* **1995,** *396*, 525.
4. J. Chen, U. Wollenberger, F. Lisdat, B. Ge, F.W. Scheller, *Sensors and Actuators B*, **2000,** *70*, 115.
5. P. Bianco, J. Haladjian, K. Draoui, *Journal of Electroanalytical Chemistry,* **1990,** *279*, 305**.**
6. J. Chen, L. Zhao, H. Bai, G. Shi, *Journal of Electroanalytical Chemistry,* **2011**, *657*, 34.
7. H. Zejli, J.L.H.-H. de Cisneros, I. Naranjo-Rodríguez, K.R. Temsamani, J.-L. Marty, *Talanta*, **2010**, *80*, 1805.
8. R.M. Santos, M.S. Rodrigues, J. Laranjinha, R.M. Barbosa, *Biosensors and Bioelectronics*, **2013**, *44*, 152.
9. J.R.M. Neto, W.J.R. Santos, P.R. Lima, S.M.C.N. Tanaka, A.A. Tanaka, L.T. Kubota, *Sensors and Actuators B*, **2011**, *152*, 220.

10. C.G. Nan, Z.Z. Feng, W.X. Li, D.J. Ping, C.H. Qin, *Analytica Chimica Acta*, **2002**, *452*, 245.
11. J.-S. Ye, Y. Wen, W.D. Zhang, H.-F. Cui, L.M. Gan, G.Q. Xu, F.-S. Sheu, *Journal of Electroanalytical Chemistry*, **2004**, *562*, 241.
12. A.J. Bard, L.R. Faulkner, "Electrochemical Methods", Wiley-VCH, New York, **1980**, p. 522.
13. R.W. Murray, in: A.J. Bard (Ed.), "Electroanalytical Chemistry", Marcel Dekker, New York, **1983**, vol. 13, p. 191.
14 J.-J. Sun, K.–Y. Huang, S.-F. Zhao, Y. Fan, Z.-W. Wu, *Bioelectrochemistry*, **2011**, *82*, 125.
15 C.P. Baron, H. J. Andersen, *Journal of Agricultural and Food Chemistry*, **2002,** *50*, 3887.
16 I. Yamazaki, T. Araiso, Y. Hayashi, H. Yamada, R. Makino, *Advances in Biophysics*, **1978**, *11*, 249.
17. J.–J. Feng, J.–J. Z. Xu, H.-Y. Chen, *Biosensors and Bioelectronics,* **2007,** *22*, 1618.
18. J. Yang, N. Hu, J.F. Rusling, *Journal of Electroanalytical Chemistry,* **1999**, *463*, 53.
19. N. Zheng, Y. Zeng, P.G. Osborne, Y. Li, W. Chang, Z. Wang, *Journal of Applied Electrochemistry*, **2002**, *32*, 129.
20. X. Wang, Y. Liu, W. Qiu, D. Zhu, *Journal of Materials Chemistry*, **2002**, *12*, 1636.
21. J.-T. Zhu, C.-G. Shi, J.-J. Xu, H.-Y. Chen, *Bioelectrochemistry,* **2007,** *71*, 243.

STUDIA UBB CHEMIA, LVIII, 2, 2013 (p. 115 – 125)
(RECOMMENDED CITATION)

DETERMINATION OF COBALT AND NICKEL AFTER MODIFIED-COLD-INDUCED AGGREGATION MICROEXTRACTION BASED ON IONIC LIQUID IN HAIR AND WATER SAMPLES

FARIBA TADAYON[a]* AND MAHNOOSH HANASAEI[a]

ABSTRACT. Modified-cold-induced aggregation microextraction(M-CIAME) as a separation and preconcentration method for Co^{+2} and Ni^{+2} ions determination based ionic liquid (IL) coupled to UV-Vis spectrophotometry is proposed. Cobalt and nickel were complexed with4-(2-pyridylazo)-resorcinol (PAR) as a chelating at pH 6. Then 60µL of 1-Hexyl-3-methylimidazoliumhexafluorophosphate [CMIM][PF_6] was injected to 10mL of sample solution. Afterward, the mixture was cooled in an ice bath and complex extracted in to ionic liquid phase. After centrifuging the extractant phase was analyzed using a spectrophotometric detection method.Several factors influencing the microextraction efficiency of Co^{+2} and Ni^{+2} ions such as: pH, concentration of chelating agent, extractant phase volume, extraction time and interfering effect, have been investigated. Under the optimum conditions, the detection limits (LODs) of the method were5.9 and 5.87 ngL^{-1} for Co^{+2} and Ni^{+2}, with the relative standard deviations (RSDs) for 59 ngL^{-1} (n=4) of Co^{+2} and Ni^{+2} were 1.85% and 1.24%. The developed method was applied to the determination of trace cobalt and nickel in water and hair samples with satisfactory results.

Keywords: *Cold-induced aggregation microextraction, Ionic Liquid, Cobalt, Nickel, UV-Vis spectrophotometry.*

1. INTRODUCTION

The determination of trace amounts of cobalt and nickel in biological and environmental samples are getting increasingly important in contamination monitoring studies. Nickel is the metal component of the enzymeurease [1] and a necessary partaker of metabolism of plants and some animals [2].

[a] *Department of Chemistry, North Tehran Branch, Islamic Azad University, Tehran, Iran.*
** Email:F_tadayon@iau-tnb.ac.ir. Fax:(98)(21)22949650; Tel(98)(21)22222263*

Also, cobalt is an essential trace element in nature,having an important role in many body functions, as a component of vitamin B_{12}[3]. However, if both of metals ingest in high levels, these could be harmful to human health. UV-Vis spectrophotometry is relatively simple, cheap and available technique in many laboratories for heavy metal determinations. In the determination of traces of cobalt and nickel in biological and environmental samples, serious interferences often occur owing to matrix components. Therefore, several preconcentration methods have been reported for the separation and preconcentration of Co and Ni ions, such as: dispersive liquid–liquid microextraction (DLLME) [4-5], in situsolvent formation microextraction(ISFME) [6], classical liquid–liquid extraction(LLE) [7-8], Solidified floating organic drop microextraction (SFODME) [9], solid phase extraction(SPE) [10-12], cloud point extraction(CPE) [13-16] and liquid phase microextraction (LPME) [17]. Also preconcentration is a very important issue for obtaining of low limits of detection. Modified-cold-induced aggregation microextraction(M-CIAME) is a highly sensitive, efficient and rapid method for the preconcentration and determination of traces of organic and inorganic compounds in several samples. So it can easily settle a salt content of up to40% [18-19]. This procedure can effectively decrease the detection limit while eliminating matrix interferences [20-21].

Ionic liquids (ILs) are salts that are usually composed of organic or an inorganic anions and either large asymmetric organic cations. They as replacement solvents in the sample preparation, due to their unique chemical and physical properties, such as: negligible vapor-pressure, high stability, good extractability for metal ions [22-24]. ILs are regarded to have the potential to be alternative reaction media for" Green Chemistry"[25]. In this work, a green preconcentration and extraction of $Co^{+2}$and Ni^{+2}ions with complexation were carried out using 4-(2-pyridylazo)-resorcinol(PAR) as a chelating and an ion liquid(1-hexyl-3-methylimidazolium hexafluorophosphate [CMIM][PF_6]) as an extractant solvent based on modified-cold-induced aggregation microextraction (M-CIAME). This was followed by UV-Vis spectrophotometry.

2. RESULTS AND DISCUSSION

In this study, one variable at a time optimization was used to obtain the optimum conditions for the M-CIAME based IL. These conditions for preconcentration and determination of cobalt and nickel ions were: pH, volume of IL as an extractant, the concentration of the chelating agent, extraction time, centrifuge condition, salts concentration, which were investigated and optimized in order to achieve a high recovery and enrichment factor.

2.1. Effect of pH

pH plays an important and unique role on complex formation and subsequent extraction, as it defines the charge of the complex. The effect of pH on the formation of complex for cobalt and nickel was studied in the range of 2–9. Absorbance increased in the range 2-6 and then started to decrease, because PAR activity decreases in the acidic qualification due to protonation of oxygen and nitrogen. The results illustrated in Fig.1 showed that the absorbance at pH of 6was much stronger. Therefore, samples and standards were adjusted at pH6 before M-CIAME based IL procedure.

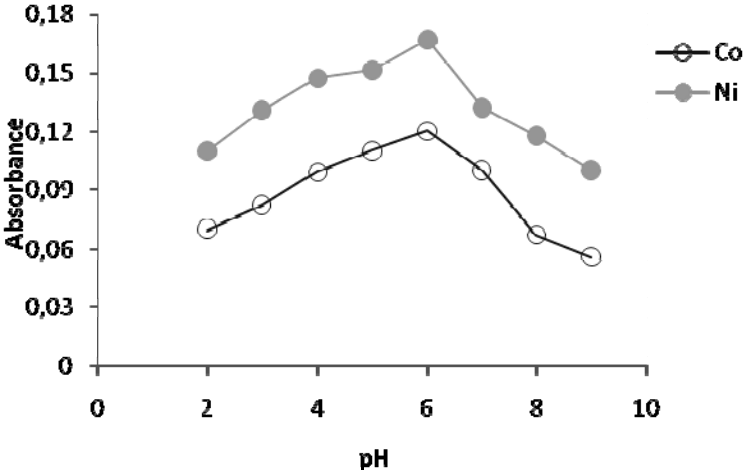

Figure 1. Effect of pH on cobalt and nickel extraction: sample volume, 10 mL; cobalt and nickel concentration, 59 ngL^{-1}.;PAR concentration,10^{-4} M; IL volume, 65µL;extraction time, 10min.

2.2. Effect of chelating agent concentration and IL volume

The influence of the amount of PAR on extraction efficiency of Co^{+2} and Ni^{+2} were studied and the experimental results are shown in Fig2. The absorbance Co^{+2} and Ni^{+2} incised by increasing the PAR concentration up to 4×10^{-4} $molL^{-1}$ of PAR and then decreased. So, a concentration of 4×10^{-4} $molL^{-1}$ was chosen as the optimum PAR concentration in order to achieve the highest possible extraction efficiency.

The volume of [CMIM][PF_6] that is used in this preconcentration procedure is a critical factor to obtain high extraction efficiency. Therefore, the effect of [CMIM][PF_6] volume on the performance of the microextraction procedure was studied within the range of 10-100 µL. By increasing the [CMIM][PF_6] volume, the absorbance of Co^{+2} and Ni^{+2} initially increased up

to about 60-70µL of [CMIM][PF_6] and then started to decrease(Fig. 3). Thus, in order to achieve a good enrichment factor, low viscosity, 60 and70 µLof IL as optimum were chosen for Co^{+2} and Ni^{+2} respectively.

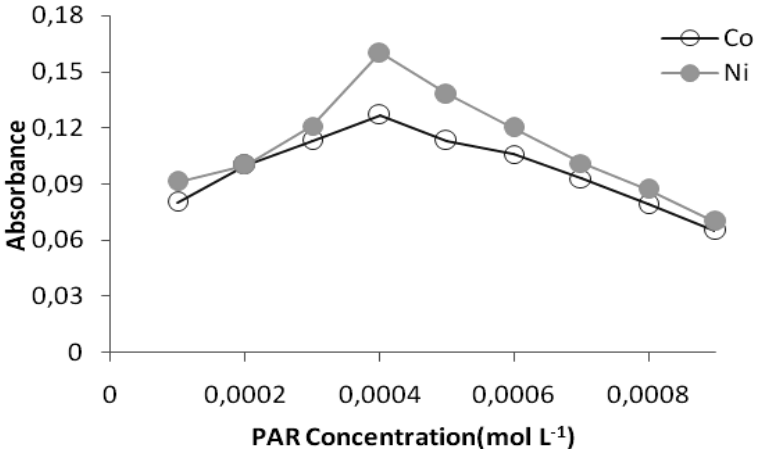

Figure 2. Effect of concentration PAR on cobalt and nickel extraction: sample volume, 10 mL;cobalt and nickel concentration, 59 ngL^{-1}; pH 6; IL volume, 65µL; extraction time, 10min**.**

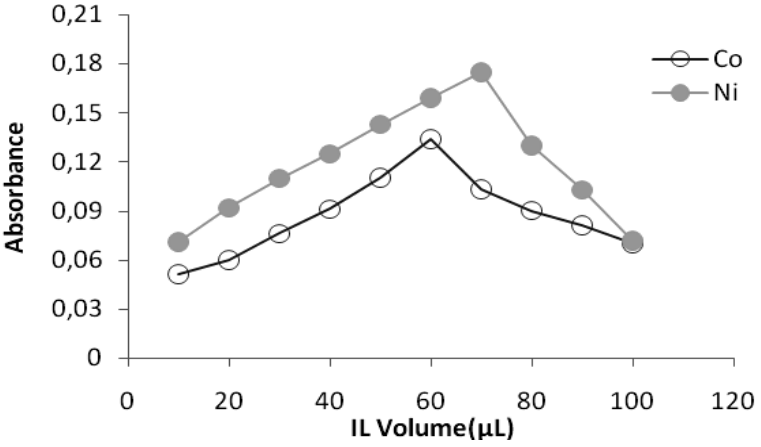

Figure 3. Effect of IL volume on cobalt and nickel extraction: sample volume, 10 mL; cobalt and nickel concentration, 59 ngL^{-1}.; pH6; PAR concentration, 4×10^{-4} M; extraction time, 10min.

2.3. Effect of temperature and extraction time

Optimal temperature is necessary to complete reactions, and to achieve easy and complete phase separation and preconcentration as efficient as possible [26]. Before shaking a solution containing IL, they were heated in the range of 20–60°C. So the temperature of 50°C for 4min was chosen. Because that the increase of temperature has no suitable effect up on the extraction efficiency.

In M-CIAME based IL, the extraction time is defined as the interval time between finishing the disruption of[CMIM][PF_6] and starting to centrifuge. Hence, extraction time plays an important role in this new procedure. In order to have excellent precision and high speed, it is essential; to select an extraction time that guarantees the attainment of equilibrium between aqueous and IL phase and maximize the extraction of analyte. The effect of extraction time was evaluated in the range of 5–25min. Fig.4 shows that the amount of complex extracted into IL phase increased with the increase of extraction time to15min. Therefore, a extraction time of 15min was selected in this work.

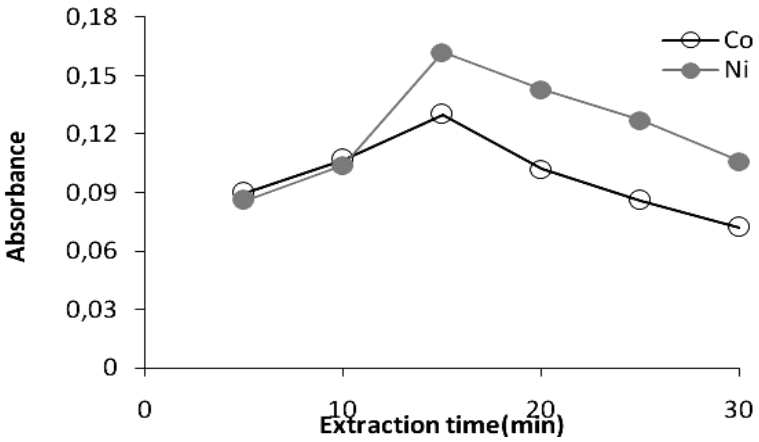

Figure 4. Effect of extraction time on cobalt and nickel extraction: sample volume,10 mL;cobalt and nickel concentration, 59 ngL^{-1}.; pH6; PAR concentration, 4×10^{-4} M; IL volume, 60µL.

2.4. Effect of centrifuge condition and salt content

The effect of centrifugation rate on the absorbance was studied in the range of 1000–6000rpm. It was found that over 4000rpm, IL-phase completely settled and a centrifugation time of 5 min at 5000rpm was selected for subsequent experiments, due to complete separation occurred at this time.

The effect of salt concentration on the extraction of Co^{+2} and Ni^{+2} was studied in the presence of $NaNO_3$ (10-60%W/V). Absorbance of Co^{+2} and Ni^{+2} decreased rapidly by increasing the salt concentration due to increase in solubility of [CMIM][PF_6]. Thus, concentration of 10% and 20% $NaNO_3$ (wv^{-1}) were selected for Co^{+2} and Ni^{+2}respectively in this work (Fig.5).

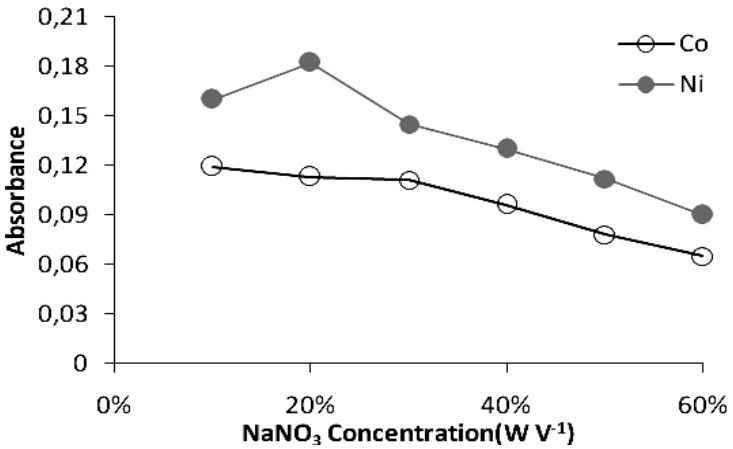

Figure 5. Effect of $NaNO_3$ on cobalt and nickel extraction:sample volume, 10 mL; cobalt and nickel concentration, 59 ngL^{-1}.; pH6; PAR concentration, 4×10^{-4} M;IL volume, 60µL; extraction time, 15min.

2.5. Interference study

The effect of diverse ions on the determination of Co^{+2} and Ni^{+} were studied according to the abovedescribed procedure. For this purpose, solution of 59 ngL^{-1} of studied analyte containing the corresponding interfering ions were prepared and operated according to the suggested procedure. The tolerable limit were defined the largest amount of foreign ions that produced an error not exceeding5% in the determination of Co^{+2} and Ni^{+2}. Most of cations and anions examined did not interference with the microextraction and determination of Co^{+2} and Ni^{+2}. The recoveries of Co^{+2} and Ni^{+2} were almost quantitative in the presence of all interfering ions in experiments, shown in Table1. All studied ions were found not interference from the coexisting ions for the determination of Co^{+2} and Ni^{+2}. Only Mn^{+2} interfered with the determination of Ni^{+2} in this experiment.

Table 1. Effect of foreign ions the recovery of cobalt and nickel(59 ngL^{-1})

Ni recovery(%)	Molar ratio(Ion/Ni^{+2})	Foreign ion	Co recovery(%)	Molar ratio(Ion/Co^{+2})	Foreign ion
92.3	1	Cr^{3+}	92.69	1	Cr^{3+}
88	1	Mn^{2+}	97.46	1	Mn^{2+}
91.42	100	Mg^{2+}	104	100	Mg^{2+}
98.81	1	Co^{2+}	98.41	1	Ni^{2+}
99.4	10	Cu^{2+}	96.82	10	Cu^{2+}
93.19	1000	Na^{+}	95.23	1000	Na^{+}
94.97	100	K^{+}	101	100	K^{+}
94.37	1	Pb^{2+}	95.87	1	Pb^{2+}
98.81	10	Fe^{3+}	102	10	Fe^{3+}
103	100	Hg^{2+}	101	100	Hg^{2+}
97.63	100	Cl^{-}	103	100	Cl^{-}
90	100	NO_3^-	104	100	NO_3^-
98.22	100	SO_4^{2-}	95.2	100	SO_4^{2-}

Table 2.1. Determination of Co^{+2} and Ni^{+2}inTap water

Metal	Added(ngL^{-1})	Found mean± SD[a] UV-Vis(ngL^{-1})	Recovery (%)	Found mean±SD (ET-AAS) (ngL^{-1})
Co	0	0. 59±0.017	-	-
	59	61.06±0.06	102.4	63.18
Ni	0	0.587±0.026	-	-
	58.7	60.5±0.064	102	59.11

[a]Standard deviation (n=4)

Table 2.2. Determination of Co^{+2} and Ni^{+2} in human and cow hairs(n=4)

Metal	Sample	Found mean± SD UV-Vis(μgg^{-1})	Found mean±SD (ET-AAS) (μgg^{-1})
Co	Human hair	1.65±0.07	1.70
	Cow hair	1.21±0.095	1.18
Ni	Human hair	1.83±0.054	1.82
	Cow hair	1.42±0.086	1.46

2.6. Figures of merit

Under the optimized experimental conditions,some parameters were investigated. The calibration curves were observed to be linear in the concentration range of(0.058-590μgL^{-1}) of Co^{+2} and Ni^{+2}. The correlation coefficient of the calibration curve equations was higher than0.990 for all elements. The detection limits calculated according to three times the standard deviation of the blank signals with the preconcentration step were 5.9 and 5.87 ngL^{-1}for Co^{+2} and Ni^{+2}respectively. Extraction recovery(ER) was calculatedaccording to the following given equation [29]:

Equation.1

$$\%ER=\frac{C_{ILPhase} \times V_{ILPhase}}{C_{aq} \times V_{aq}} \times 100$$

Enhancement of factors was obtained from the slope ratio of the calibration curve after and before preconcentration. The analytical characteristics of the methods are summarized in Table 3.

Table 3. Analytical characteristics of modified CLAME method

Parameter	Co^{+2} with preconcentration	Ni^{+2} with preconcentration
Correlation coefficient(R^2)	0.997	0.995
Limit of detection (ngL^{-1})	5.9	5.87
Enrichment factor(EF)	74	79.05
RSD % (n=4)	1.85	1.24
Extraction recovery (ER)	94	101

3. CONCLUSIONS

In this study, a new method of Modified-cold-induced aggregation microextraction(M-CIAME) based- ionic liquid solvent was successfully used for preconcentration and determination trace of cobalt and nickel by UV-Vis spectrophotometry in environmental and biological samples with good accuracy and reproducibility. This method is simple, environmentally friendly, selective, fast, safe and robust against very high content of salt (upto40%). Also our proposed method requires smallest volume of solvent while having good LOD and enhancement factor. This developed method was employed to determine cobalt and nickel ions in biological and environmental samples with satisfactory recovery.

4. EXPERIMENTAL SECTION

4.1. Apparatus

A lambda 25 UV-Vis spectrometer was purchased from Perkin-Elmer (USA). A100µL microsyringe(Hamilton) was employed to inject ionic liquid extracting phase to the sample solution. A (H-11 n) Kokusan Japan centrifuge was used to accelerate the phase separation process and aJeio Tech BW-05G water bath was used.

4.2. Reagents and materials

Standard stock solutions of Co^{+2} and Ni^{+2} at a concentration 1000 ppm were prepared by dissolving appropriate amounts of the pure nitrate salts in 100mL double distilled water. Solutions of lower concentrations were prepared daily by a suitable dilution of the stock solution with distilled water. Buffer solution with pH6 was prepared from 1.8 $molL^{-1}$sodium acetate solution and 0.1$molL^{-1}$ acetic acid solution by mixing the appropriate volumes of the two solutions and diluting to100mL. Acetic acid, sodium acetate and metal salts are all of analytical grade and purchased from Merck Chemical Company. A $4\times10^{-4}molL^{-1}$ PAR solution was prepared in deionized water and ethanol 50:50(v/v) (Aldrich Com) and also appropriate amounts of [CMIM][PF_6] was prepared in acetonitrile(Aldrich).

4.3. Modified CIAME procedure

For M-CIAME procedure 10mLof the sample solution containing Co^{+2} or Ni^{+2} and PAR (4×10^{-4} $molL^{-1}$) were adjusted to pH6 (acetate/acetic acid buffer) in a glass test tube with a conical bottom. Then, 60µL of [CMIM][PF_6] with a microsyringe was added to the solution. The tube was placed in a thermo stated bath at 50°C for 4min. The next step, the mixture was cooled in an ice bath for 10min, cloudy solution was immediately formed and metal ions was extracted in to the fine droplets of IL . Then separation of two phases was obtained by centrifugation for 5min at 5000rpm and IL-phase was diluted with 100µL ethanol and transferred to 350µL quartz cell for UV-Vis spectrophotometry determination.

4.4. Real samples preparation

The method was applied to tap water, human hair and cow hair sample from Tehran city. Standard hair samples were washed with 1% (w/v) (DDTC), 0.1M HCl and deionized water. The hair samples were firstly washed with HCL then one time with deionized water then with acetone and again one time with deionized water. Afterwards, the hair sample dried in oven at 70°C for 8 hours

and then digested the next day [27]. Then 1g of washed hair samples were weighted and transferred to a teflon bombs and 10mL of concentrated HNO_3(65%) was added. The samples were heated on a plate about 100°C for 2h. After dissolution, the solution was allowed to cool and 5mL of H_2O_2 (30%) was added. The mixture was heated at(80°C for 2h). After digestion, the sample was diluted to final volume with deionized water and was treated according to the given procedure[28]. The results are show in Table2.

ACKNOWLEDGMENTS

With special thanks of Ms. Vahideh Mohajeri and Ms. Mahtab Rezazadeh that supported us in this project.

REFERENCES

1. C. Arpa Sahin, M. Efecinar, N. Satiroglu, Journal of Hazardous Materials, **2010**, 176, 672.
2. S. Dadfarnia, A.M. Haji Shabani, M. Shirani Bidabadi, A.A. Jafari, Journal of Hazardous Materials, **2010**, 173, 534.
3. D. Lison, G.F. Nordberg, B.A. Fowler, M. Nordberg, L. Friberg, ״Hand book on the Toxicology of Metals״, Third Edition, Academic Press Inc., United States Of America, **2007**, Chapter 25.
4. N. Shokoufi, F. Shemirani, Y. Assadi, Analytica Chimica Acta, **2007**, 597, 349.
5. P.X. Baliza, L.S. Gomes Teixeira, V.A. Lemos, Microchemical Journal, **2009**, 93, 220.
6. M.R. Jamali, B. Soleimani, R. Rahnama, S.H.A. Rahimi, Arabian Journal Of Chemistry, **2012**.
7. Z. Fan, B. Hu, Z. Jiang, Talanta, **2006**, 68, 1359.
8. K. Minakata, M. Suzuki, O. Suzuki, Analytica Chimica Acta, **2008**, 614, 161.
9. M. Shirani Bidabadi, S. Dadfarnia, A.M. Haji Shabani, Journal of Hazardous Materials, **2009**, 166, 291.
10. A. Rajabi Khorrami, H. Naeimi, A.R. Fakhari, Talanta, **2004**, 64, 13.
11. V. Kaur, J.S. Aulakh, A.K. Malik, Analytica Chimica Acta, **2007**, 603, 44.
12. M. Tuzen, M. Soylak, D. Citak, H.S. Ferreira, M.G.A. Korn, M.A. Bezerra, Journal of Hazardous Materials, **2009**, 162, 1041.
13. J. Chen, Kh. Ch. Teo, Analytica Chimica Acta, **2001**, 434, 325.
14. G.L. Donat, C.C. Nascentes, A.R.A. Nogueira, M.A.Z. Arruda, J.A. Nobrega, Microchemical Journal, **2006**, 82, 189.
15. N. Shokoufi, F. Shemirani, F. Memarzadeh, Analytica Chimica Acta, **2007**, 601, 204.

16. M. Ghaedi, A. Shokrollahi, KH. Niknam, E. Niknam, M. Soylak, Central European Journal Of Chemistry, **2009**, 7, 148.
17. N. Yoshikuni, T. Baba, N. Tsunoda, K. Oguma, Talanta, **2005**, 66, 40.
18. M. Baghdadi, F. Shemirani, Analytica Chimica Acta, **2008**, 613, 56.
19. M. Baghdadi, F.Shemirani, Analytica Chimica Acta, **2009**, 634, 186.
20. SH. Mahpishanian, F. Shemirani, Minerals Engineering, **2010**, 23, 823.
21. M. Vaezzadeh, F. Shemirani, B. Majidi, Food and Chemical Toxicology, **2010**, 48, 1455.
22. E. Molaakbari, A. Mostafavi, D. Afzali, Journal of Hazardous Materials, **2011**, 185, 647.
23. R. Khani, F. Shemirani, B. Majidi, Desalination, **2011**, 266, 238.
24. M. Zeeb, M.R. Ganjali, P. Norouzi, M.R. Kalaee, Food and Chemical Toxicology, **2011**, 49, 1086.
25. P. Wasserscheid, R. V. Hal, A. Bosmann, Green Chemistry, **2002**, 4, 400.
26. H. Abdolmohammad Zadeh, G.H. Sadeghi, Analytica Chimica Acta, **2009**, 649, 211.
27. F. Tadayon, M.S. Tehrani, S. Rajabi Nia, Academic Research International, **2012**, 2, 11.
28. M. Saber-Tehrani, F. Tadayon, Asian journal Of Chemistry, **2009**, 21, 3660.
29. P. Berton, R.G. Wuilloud, Analytica Chimica Acta, **2010**, 662, 155.
30. L. Xia, X. Li, Y. Wu, B. Hu, R. Chen, Spectrochimica Acta Part B, **2008**, 63, 1290.
31. M. Gharehbaghi, F. Shemirani, M. Davudabadi Farahani, Journal of Hazardous Materials, **2009**, 165, 1049.
32. J. Abulhassani, J.L. Manzoori, M. Amjadi, Journal of Hazardous Materials, **2010**, 176, 481.
33. H. Jiang, Y. Qin, B. Hu, Talanta, **2008**, 74, 1160.

STUDIA UBB CHEMIA, LVIII, 2, 2013 (p. 127 – 132)
(RECOMMENDED CITATION)

SECOND-CONNECTIVITY INDEX OF CAPRA-DESIGNED PLANAR BENZENOID SERIES $Ca_n(C_6)$

MOHAMMAD REZA FARAHANI[a*], KATALIN KOLLO[b], MIRANDA PETRONELLA VLAD[c]

ABSTRACT. The benzene is a key molecule in organic chemistry. In this paper, we focus on the structure of the *Capra*-designed planar benzenoid series $Ca_n(C_6)$ and compute the 2-connectivity index in the general case of this family of benzenoids.

Keywords: *Randić connectivity index, Sum-connectivity index, Benzenoid, Capra, Second connectivity index.*

INTRODUCTION

Let $G=(V,E)$ be a simple connected graph with the vertex set $V(G)$ and the edge set $E(G)$. Molecular connectivity indices are related to the accessibility to the reaction centres. In identifying the accessibility perimeters, we have to recognize the atom degrees. The generalized connectivity index is the *m-connectivity* index, defined as:

$$^{m}\chi(G)=\sum_{v_{i_1}v_{i_2}..v_{i_{m+1}}}\frac{1}{\sqrt{d_{i_1}d_{i_2}..d_{i_{m+1}}}}$$

where $v_{i_1}v_{i_2}\ldots v_{i_{m+1}}$ runs over all paths of length m in G and d_i is the degree of vertex $v_i \in V(G)$. In particular, 1-connectivity index (the original *Randić* index) can be written as

$$\chi(G)=\sum_{e=(i,j)\in E(G)}\frac{1}{\sqrt{d_i d_j}}$$

[a] *Department of Mathematics of Iran University of Science and Technology (IUST), Narmak, Tehran 16844, Iran. Mr_Farahani@Mathdep.iust.ac.ir*
[b] *Faculty of Chemistry and Chemical Engineering, Babes-Bolyai University, 400028, Aranj Janos 11, Cluj, Romania. katalinkollo@gmail.com*
[c] *Dimitrie Cantemir University, Bucharest, Faculty of Economic Sciences, No 56 Teodor Mihali Street, 400591, Cluj Napoca, Romania, mirandapv@yahoo.com*

The Randić Connectivity Index was introduced by *Milan Randić* [1, 2] in 1975. For more study, see references [3-9]. The *2-connectivity index* is defined as follows:

$$^2\chi(G) = \sum_{v_{i_1}v_{i_2}v_{i_3}} \frac{1}{\sqrt{d_{i_1}d_{i_2}d_{i_3}}}$$

The Randić and second-order connectivity indices (or 2-connectivity index) represents the molecular accessibility areas and volumes, respectively.

The *benzene* is a usual chemical molecule in chemistry with a distinctive structure. The benzene is a key molecule in chemistry and related sciences, with various applications in different fields.

We use the *Capra-designed operation* to generate new structures called benzoids. This operation was introduced by *M.V. Diudea* and used in many papers [10-19], see Figure 1.

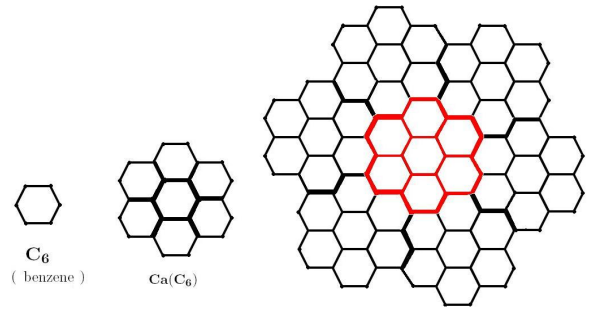

Figure 1. The first two graphs $Ca_1(C_6)$ and $Ca_2(C_6)$ from the Capra of planar benzenoid series and molecular graph benzene $C_6=Ca_0(C_6)$.

RESULTS AND DISCUSSION

Let d_{ij} denote the number of edges in G connecting vertices of degrees i and j; clearly, $d_{ij}=d_{ji}$. Define d_{ijk} as a number of 2-edges paths with 3 vertices of degree i, j and k, respectively. It is obvious that $d_{ijk}=d_{kji}$ and the number of 2-edge paths for all possible i, j and k is denoted by $d_2(G)$.

Theorem 1. [16] Consider the graph $G=Ca_k(C_6)$, $k \in N$ is the Capra-designed planar benzenoid series. Then Randić connectivity index $\chi(Ca_k(C_6))$ is equal to $\frac{2(7^k)+(4\sqrt{6}-1)3^{k-1}+1}{2}$.

Theorem 2. Second-connectivity index of $Ca_k(C_6)$ is computed as:

$$^2\chi(Ca_k(C_6)) = \frac{2\sqrt{3}}{3}7^k + \left(\frac{7\sqrt{2}}{6} - \frac{5\sqrt{3}}{18}\right)3^k + \left(\sqrt{3} - \frac{3\sqrt{2}}{2}\right).$$

Proof of Theorem 2. Let $G=Ca_k(C_6)$ be the Capra-designed planar benzenoid series. Since, this graph has $2\times7^k+3^{k+1}+1$ vertices and $3\times7^k+3^{k+1}$ edges (denoted by n_k and e_k, respectively). At the first, we determine the number of 2-edge paths $d_2^{(k)}(G)$ in $G=Ca_k(C_6)$. So, we attend to d_{ijk} for every arbitrary vertices *i, j* and *k*; and obviously the number of d_{ijk} is dependent of the degree of vertex *j* (denoted by d_j). On the other hand, the number of 2-edge paths passing the vertex *j* of *G* is equal to $(d_j-1)+(d_j-2)+\ldots+(2)+(1)=\frac{d_j(d_j-1)}{2}$ and obviously $d_2^{(k)}(G)=\sum_{v\in V(G)}\frac{d_v(d_v-1)}{2}$. There are two partitions $V_2=\{v\in V(Ca_k(C_6))\,|\,d_v=2\}$ and $V_3=\{v\in V(Ca_k(C_6))\,|\,d_v=3\}$, with size $v_2^{(k)}=|V_2|=3^{k+1}+3$ and $v_3^{(k)}=|V_3|=2(7^k-1)$ respectively. Then,

$$\begin{aligned} d_2^{(k)}(Ca_k(C_6)) &= \sum_{v\in V(Ca_k(C_6))}\frac{d_v(d_v-1)}{2} \\ &= \sum_{v\in V_3}\frac{3(3-1)}{2}+\sum_{v\in V_2}\frac{2(2-1)}{2} \\ &= 3\times2(7^k-1)+1\times3(3^k+1) \\ &= 6\times7^k+3^{k+1}+3 \end{aligned}$$

Now, according to the Capra-designed structure (Figure 2), we see that there exist two kinds of 2-edge paths $d_2^{(k)}(Ca_k(C_6))$: *internal 2-edge paths* and *external 2-edge paths*. Thus we have:

$$d_2^{(k)}(Ca_k(C_6)) = \underbrace{\underbrace{6(7^k)}_{6\zeta_k}}_{internal\ 2-edge\ paths} + \underbrace{\underbrace{3^{k+1}-3}_{v_2^{(k)}-6}}_{external\ 2-edge\ paths}$$

where ζ_k is the number of cycles with length six and is equal to 7^k. Alternatively, the number of internal 2-edge paths of $Ca_k(C_6)$ is equal to $d_{2\ (in)}^{(k)}=6\ \zeta_k=6(7^k)$. The number of external 2-edge paths of $Ca_k(C_6)$ is equal to $d_{2\ (ex)}^{(k)}=3^{k+1}-3$, being obtained from the sequence:

$$0,\ 6,\ 24,\ 6\times13,\ldots,\ d_{2\ (ex)}^{(k)}=6\left(\frac{d_{2\ (ex)}^{(k-1)}}{2}+1\right).$$

In proving theorem 2 we have to calculate the number of 2-edges paths $d_{223}^{(k)}$, $d_{333}^{(k)}$ from internal 2-edge paths and $d_{323}^{(k)}$, $d_{232}^{(k)}$ from external 2-edge paths:

$$d_2^{(k)}(Ca_k(C_6)) = \underbrace{d_{223}^{(k)}+d_{333}^{(k)}}_{internal\ 2-edges\ paths} + d_{233}^{(k)} + \underbrace{d_{232}^{(k)}+d_{323}^{(k)}}_{external\ 2-edges\ paths}$$

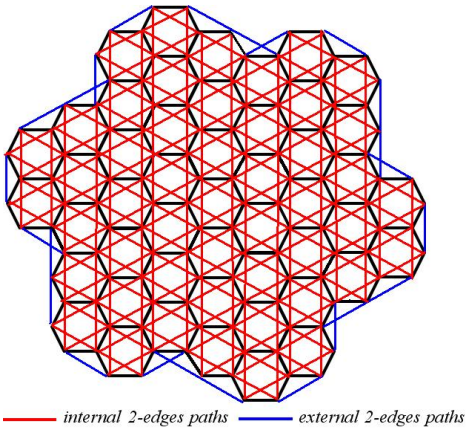

Figure 2. The internal 2-edges paths and external 2-edges paths of $Ca_2(C_6)$.

It is obvious that, in $C_6=Ca_0(C_6)$, $d^{(0)}_{223}= d^{(0)}_{323}= d^{(0)}_{232}= d^{(0)}_{233}= d^{(0)}_{333}=0$, $d^{(0)}_{222}=6$ and $${}^2\chi(Ca_0(C_6)) = \frac{6}{\sqrt{2\times 2\times 2}} = 2.1213$$

Next, for $Ca_1(C_6)$, $d^{(1)}_{223}=2\times 6$, $d^{(1)}_{323}=0$, $d^{(1)}_{232}=6$, $d^{(1)}_{233}=2\times 6$ and $d^{(1)}_{333}=18$. Thus

$${}^2\chi(Ca_1(C_6)) = \frac{12}{\sqrt{2\times 2\times 3}} + \frac{6}{\sqrt{2\times 3\times 2}} + \frac{12}{\sqrt{2\times 3\times 3}} + \frac{0}{\sqrt{3\times 2\times 3}} + \frac{18}{\sqrt{3\times 3\times 3}} = 11.4886.$$

Now, by simple calculation and induction on $n=1,2,3,\ldots,k$, (see Figure 1., 2. and 3.) we show that for $G=Ca_k(C_6)$

$$d^{(0)}_{223}=0,\ d^{(1)}_{223}=12,\ d^{(2)}_{223}=24,\ d^{(3)}_{223}=2(3^3+3)=60,\ \ldots,\ \underbrace{d^{(k)}_{223}}_{internal}=2(3^k+3)=2e^{(k)}_4.$$

$$d^{(0)}_{323}=0,\ d^{(1)}_{323}=0,\ d^{(2)}_{323}=12,\ d^{(3)}_{323}=24,\ \ldots,\ \underbrace{d^{(k)}_{323}=v^{(k)}_2-2e^{(k)}_4}_{external}=3^{k+1}+3-2(3^k+3)=3^k-3.$$

$$d^{(0)}_{232}=0,\ d^{(1)}_{232}=6,\ d^{(2)}_{232}=12,\ d^{(3)}_{232}=6(\frac{12}{2}-1)=30,\ \ldots,\ d^{(k)}_{232}=6(\frac{d^{(k-1)}_{232}}{2}-1)=3d^{(k-1)}_{232}-6=3^k+3.$$

$$d^{(0)}_{233}=0,\ d^{(1)}_{233}=\underbrace{0}_{ex}+\underbrace{2\times 6}_{in}=12,\ d^{(2)}_{233}=\underbrace{2\times 6}_{ex}+\underbrace{6\times 6}_{in}=48,\ d^{(3)}_{232}=\underbrace{8\times 6}_{ex}+\underbrace{18\times 6}_{in}=156,$$

$\ldots,\ d^{(k)}_{233}=d^{(k)}_{233(ex)}+d^{(k)}_{233(in)}=6(3^k-1)$

where
$$\begin{cases} d^{(k)}_{233\,(ex)} = d^{(k)}_{323\,(ex)} - d^{(k)}_{232\,(ex)} = 3^{k+1}-3-(3^k+3) = 6(3^{k-1}-1) \\ d^{(k)}_{233\,(in)} = 6(\dfrac{d^{(k-1)}_{233\ \ (in)}}{2}) = 3d^{(k-1)}_{233\ \ (in)} = 4(3^k) \end{cases}$$

$$d_{333}^{(0)}=0, \qquad d_{333}^{(1)}=18, \qquad d_{333}^{(2)}=228, \qquad d_{333}^{(3)}=1866, \qquad \ldots,$$

$$\underbrace{d_{333}^{(k)}}_{internal}=d_2^{(k)}-d_{233\,(ex)}^{(k)}-d_{233\,(in)}^{(k)}-d_{232\,(ex)}^{(k)}-d_{323\,(ex)}^{(k)}-d_{223\,(in)}^{(k)}$$

$$=6(7^k)+3^{k+1}-3-2(3^k)-6-3^k+3-6(3^k)+6-3^k-3 \text{ =6×7}^k\text{-7(3}^k\text{)-3}$$

In totally,

$$d_{ijk}^{(k)}=\begin{cases}6(7^k)-7(3^k)-3 & ijk=333\\ 2e_4^{(k)}=2(3^k+3) & ijk=223\end{cases}\ internal\ 2-edge\ paths$$

$$\begin{cases}6(3^{k-1}-1)+4(3^k)=6(3^k-1) & ijk=233\\ v_2^{(k)}-2e_4^{(k)}=3^k-3 & ijk=323\\ 3^k+3 & ijk=232\end{cases}\ external\ 2-edge\ paths$$

where $e_4^{(k)}=3^k-3$ is the number of edge of $Ca_k(C_6)$ with end-point and first-point of degree 2. Therefore:

$${}^2\chi(Ca_k(C_6))=\sum_{v_{i_1}v_{i_2}v_{i_3}}\frac{1}{\sqrt{d_{i_1}d_{i_2}d_{i_3}}}$$

$$=\frac{2(3^k+3)+3^k+3}{\sqrt{12}}+\frac{3^k-3+6(3^k)-6}{\sqrt{18}}+\frac{6(7^k)-7(3^k)-3}{\sqrt{27}}$$

$$=\frac{3^{k+1}+9}{6}\sqrt{3}+\frac{7(3^k)-9}{6}\sqrt{2}+\frac{6(7^k)-7(3^k)-3}{9}\sqrt{3}$$

$$=\frac{(3^{k+2}+27+12(7^k)-14(3^k)-6)\sqrt{3}+(7(3^{k+1})-27)\sqrt{2}}{18}$$

$$=\frac{((12(7^k)-5(3^k)+21)\sqrt{3}+(7(3^{k+1})-27)\sqrt{2})}{18}.$$

The second-connectivity index of $Ca_k(C_6)$ is equal to

$${}^2\chi(Ca_k(C_6))=\frac{2\sqrt{3}}{3}7^k+\left(\frac{7\sqrt{2}}{6}-\frac{5\sqrt{3}}{18}\right)3^k+\left(\sqrt{3}-\frac{3\sqrt{2}}{2}\right).$$

Thus, we completed the proof of Theorem 2.

We can use formula for ${}^2\chi(Ca_k(C_6))$ to compute some numerical examples:

$$\hat{}$$

$${}^2\chi(Ca_k(C_6))=1.1547(7^k)+1.1688(3^k)-0.3892.$$

Examples for ${}^2\chi(Ca_k(C_6))$ for *k=1, 2, 3, 4, 5, 10, 20, 30, 40, 50, 100* are given in Table 1.

Table 1. Values of second-connectivity index $^{2}\chi(Ca_k(C_6))$

k	**Number of Vertices**	**Number of edges**	**2-connectivity index**
1	*24*	*30*	*11. 2001*
2	*123*	*174*	*66. 7103*
3	*768*	*1110*	*427. 2305*
4	*5046*	*7446*	*2866. 7183*
5	*34344*	*51150*	*19690. 6721*
10	*565127646*	*847602894*	*326243186. 1023*
20	*1. 5958454306×10^{17}*	*2. 3937680935×10^{17}*	*9. 2136133969×10^{16}*
30	*4. 5078680582×10^{25}*	*6. 6718020873×10^{25}*	*2. 602617623×10^{25}*
40	*1. 2733611522×10^{34}*	*1. 9100417283 ×10^{34}*	*7. 3517506121 ×10^{33}*
50	*3. 596330085×10^{42}*	*5. 3953951279 ×10^{42}*	*2. 0766875847 ×10^{42}*
100	*6. 4689530192×10^{84}*	*9. 7034295289 ×10^{84}*	*6. 4689530192 ×10^{84}*

REFERENCES

1. M. Randić and P. Hansen. J. Chem. Inf. Comput. Sci. **1988***, 28*, 60.
2. M. Randić. J. Am. Chem. Soc. **1975,** *97,* 6609.
3. N. Trinajstić. Chemical Graph Theory. CRC Press, Boca Raton, FL, 1992.
4. P. Yu. J. Math. Study Chinese. **1998,** *31*, 225.
5. M.R. Farahani. Acta Chim. Slov. **2012,** *59, 779–783.*
6. E. Estrada. J. Chem. Inf. Comput. Sci. **1995***, 35*, 1022.
7. E. Estrada. Chem. Phys. Lett. **1999,** *312*, 556.
8. Z. Mihali and N. Trinajstić. J. Chem. Educ. **1992***, 69*(9), 701.
9. D. Morales and O. Araujo. J. Math. Chem. **1993***, 13*, 95.
10. M. Goldberg. Tohoku Math. J. **1937,** *43*, 104.
11. A. Dress and G. Brinkmen. MATCH Commun. Math. Comput. Chem. **1996***, 33***,** 87.
12. M.V. Diudea, M. Ştefu, P.E. John, and A. Graovac, Croat. Chem. Acta, **2006***, 79,* 355.
13. M.V. Diudea, J. Chem. Inf. Model, **2005,** *45*, 1002.
14. M.R. Farahani and M.P.Vlad. Studia Universitatis Babes-Bolyai Chemia. **2012,** *57(4),* 55-63.
15. M.R. Farahani. J. Applied Math. & Info. **2013,** *31(5-6)*, in press.
16. M.R. Farahani and M.P.Vlad. Studia Universitatis Babes-Bolyai Chemia. **2013,** *58(2),* accepted.
17. M.R. Farahani. Polymers Research Journal. **2013,** *7(3),* In press.
18. M.R. Farahani. Advances in Materials and Corrosion. **2012,** *1*, 61-64.
19. M.R. Farahani. Chemical Physics Research Journal. **2013,** In press.

STUDIA UBB CHEMIA, LVIII, 2, 2013 (p. 133 – 142)
(RECOMMENDED CITATION)

COMPUTING FIRST AND SECOND ZAGREB INDEX, FIRST AND SECOND ZAGREB POLYNOMIAL OF CAPRA-DESIGNED PLANAR BENZENOID SERIES $Ca_n(C_6)$

MOHAMMAD REZA FARAHANI[a], MIRANDA PETRONELLA VLAD[b]

ABSTRACT. In graph theory, various polynomials and topological indices are known, as invariants under graph automorphism. In this paper, we focus on the structure of *Capra*-designed planar benzenoid series $Ca_k(C_6)$, $k\geq 0$ and compute on it several topological indices and polynomials: first and second Zagreb polynomials and their corresponding indices.

Keywords: *Capra Operation, benzenoid series, First Zagreb index, second Zagreb index, First Zagreb polynomial, second Zagreb polynomial.*

INTRODUCTION

Let *G=(V,E)* be a molecular graph with the vertex set *V(G)* and the edge set *E(G). |V (G)|=n, |E(G)|=e* are the number of vertices and edges. A molecular graph is a simple finite graph such that its vertices correspond to the atoms and the edges to the chemical bonds. The distance *d(u,v)* in the graph *G* is the number of edges in a shortest path between two vertices *u* and *v*. The number of vertex pairs at unit distance equals the number of edges. A topological index of a graph is a number related to that graph and is invariant under graph automorphism.

Wiener index W(G) is the oldest topological index [1-5], which has found many chemical applications. It is defined as:

$$W(G)=\frac{1}{2}\sum_{u\in V(G)}\sum_{v\in V(G)} d(u,v)$$

[a] *Department of Mathematics of Iran University of Science and Technology, (IUST), Narmak, Tehran 16844, Iran. Mr_Farahani@Mathdep.iust.ac.ir*
[b] *Dimitrie Cantemir University, Bucharest, Faculty of Economic Sciences, No 56 Teodor Mihali Street, 400591, Cluj Napoca, Romania, mirandapv@yahoo.com*

Hyper-Wiener index is a more recently introduced distance-based molecular descriptor [6]:

$$WW(G)=\frac{1}{2}\sum_{u\in V(G)}\sum_{v\in V(G)}\left(d(u,v)+d(u,v)^2\right)=\frac{1}{2}W(G)+\frac{1}{2}\sum_{u\in V(G)}\sum_{v\in V(G)}d(u,v)^2.$$

Denote by *d(G,k)* the number of vertex pairs of *G* lying at distance k to each other and by *d(G)* the topological diameter (i.e, the longest topological distance in *G)*. Then Wiener and hyper-Wiener indices of *G* can be expressed as [7, 8]:

$$W(G)=\frac{1}{2}\sum_{i=1}^{d(G)} i\,d(G,i)$$

$$WW(G)=\frac{1}{2}\sum_{i=1}^{d(G)} i\,(i+1)d(G,i).$$

Other oldest graph invariant is the *First Zagreb index*, which was formally introduced by *Gutman* and *Trinajstić* [9, 10]. It is denoted by $M_1(G)$ and is defined as the sum of squares of the vertex degrees:

$$M_1(G)=\sum_{v\in V(G)}d(v)^2=\sum_{e=uv\in E(G)}\left[d(u)+d(v)\right]$$

where d_v is the degree of vertex *v*. Next, *Gutman* introduced the *Second Zagreb index* $M_2(G)$ as:

$$M_2(G)=\sum_{e=uv\in E(G)}\left[d(u)\times d(v)\right]$$

Some basic properties of $M_1(G)$ can be found in ref. [9]. For a survey on theory and applications of Zagreb indices see ref. [10]. Related to the two above topological indices, we have the first Zagreb Polynomial $M_1(G,x)$ and second Zagreb Polynomial $M_2(G,x)$, respectively. They are defined as:

$$M_1(G,x)=\sum_{e=uv\in E(G)}x^{d(u)+d(v)}$$

$$M_2(G,x)=\sum_{e=uv\in E(G)}x^{d(u)d(v)}$$

There was a vast research concerning Zagreb indices and Wiener index with its modifications [6] and relations between Wiener, hyper-Wiener and Zagreb indices [9-26].

WHAT IT IS THE CAPRA OPERATION?

A mapping is a new drawing of an arbitrary planar graph *G* on the plane. In graph theory, there are many different mappings (or drawing); one of them is *Capra operation*. This method enables one to build a new structure of a planar graph *G.*

Let *G* be a cyclic planar graph. Capra map operation is achieved as follows:

(i) insert two vertices on every edge of G;

(ii) add pendant vertices to the above inserted ones and

(iii) **c**onnect the pendant vertices in order (-1,+3) around the boundary of a face of G. By runing these steps for every face/cycle of *G,* one obtains the Capra-transform of *G Ca(G)*, see Figure 1.

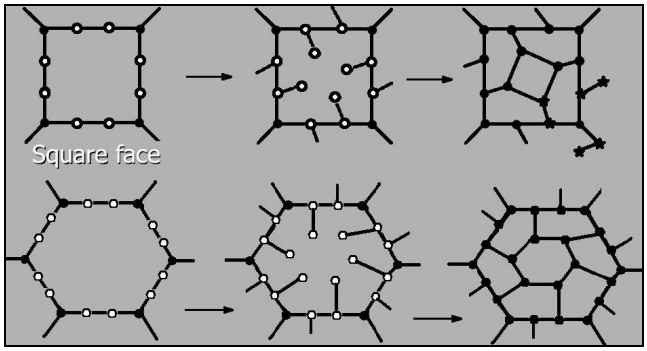

Figure 1. Examples of Capra operation on the square face (top row) and mapping Capra of planar hexagon (bottom row).

By iterating the Capra-operation on the hexagon (i.e. benzene graph C_6) and its Ca-transforms, a benzenoid series (Figures 2 and 3) can be designed. We will use the Capra-designed benzene series to calculate some connectivity indices (see below).

This method was introduced by *M.V. Diudea* and used in many papers [27-36]. Since Capra of planar benzenoid series has a very remarkable structure, we lionize it.

We denote Capra operation by *Ca*, in this paper, as originally *Diudea* did. Thus, Capra operation of arbitrary graph *G* is *Ca(G),* iteration of Capra will be denoted by *CaCa(G)* (or we denote $Ca_2(G)$) (Figures 2 and 3).

The benzene molecule is a usual molecule in chemistry, physics and nano sciences. This molecule is very useful to synthesize aromatic compounds. We use the Capra operation to generate new structures of molecular graph benzene series.

Theorem 1. Let $Ca(C_6)$ be the first member of Capra of benzenoid series. Then, *Hosoya polynomial* of $Ca(C_6)$ is equal to:

$$H(Ca(C_6),x)=24+30x^1+48x^2+57x^3+x54x^4+45x^5+30x^6+12x^7$$

and the Wiener index of $Ca(C_6)$ is equal to 1002.

Hosoya polynomial H(G) is equal to $\frac{1}{2}\sum_{u\in V(G)}\sum_{v\in V(G)} x^{d(u,v)}$. It is easy to see that Wiener index is obtained from Hosoya polynomial as the first derivative, in *x=1*.

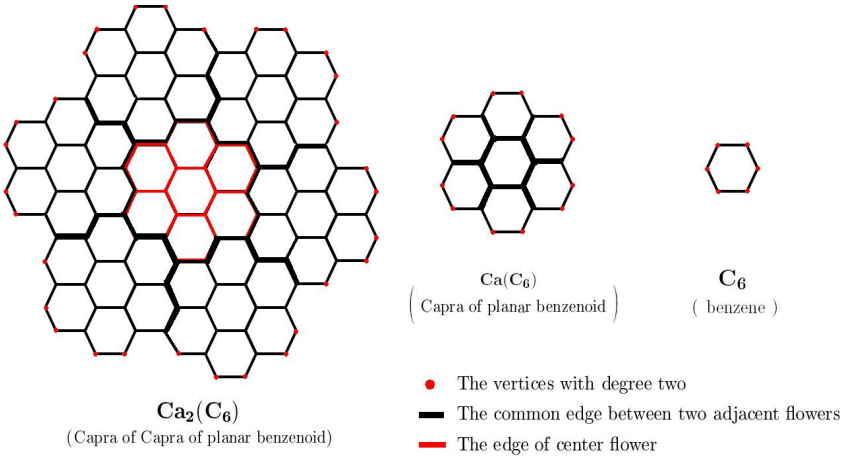

Figure 2. The first two graphs *Ca*(C_6) and *Ca*$_2$(C_6) from the Capra of planar benzenoid series, together with the molecular graph of benzene (denoted here *Ca*$_0$(C_6))

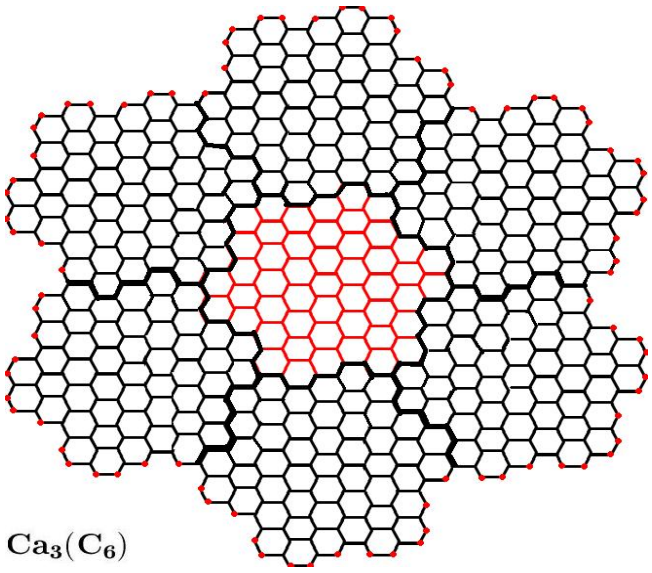

Figure 3. Graph *Ca*$_3$(C_6) is the third member of Capra planar benzenoid series.

By these terminologies, we have the following theorem:

Theorem 2. Consider the graph $G=Ca_k(C_6)$ as the iterative Capra of planar benzenoid series. Then:
First Zagreb polynomial of G is equal to

$$M_1(Ca_k(C_6),x)=(3(7^k)-2(3^k)-3)x^6+4(3^k)x^5+(3^k+3)x^4$$

and the First Zagreb index is $M_1(Ca_k(C_6))=18(7^k)+12(3^k)-6$.
Second Zagreb polynomial of G is equal to

$$M_2Ca_k(C_6),x)=(3(7^k)-2(3^k)-3)x^9 4(3^k)x^6(3^k+3)x^4$$

and the Second Zagreb index of G is $M_2(Ca_k(C_6))=27(7^k)+10(3^k)-15$.

RESULTS AND DISCUSSION

Capra transforms of a planar benzenoid series is a family of molecular graphs which are generalizations of benzene molecule C_6.

In other words, we consider the base member of this family is the planar benzene, denoted here $Ca_0(C_6)=C_6=benzene$. It is easy to see that $Ca_k(C_6)=Ca(Ca_{k-1}(C_6))$ (Figures 2 and 3) [27-36]. In addition, we need the following definition.

Definition 3. [21] Let G be a molecular graph and d_v is the degree of vertex $v \in V(G)$. We divide vertex set $V(G)$ and edge set $E(G)$ of graph G to several partitions, as follow:

$$\forall i, \delta < i < \Delta, V_i = \{v \in V(G) \mid d_v = i\},$$

$$\text{and } \forall k, \delta^2 \le k \le \Delta^2, E_k^* = \{e = uv \in E(G) \mid d_v \times d_u = k\}.$$

Obviously, $1 \le \delta \le d_v \le \Delta \le n-1$ such that $\delta = Min\{d_v \mid v \in V(G)\}$ and $\Delta = Max\{d_v \mid v \in V(G)\}$. Now, we start to proof of the above theorem.

Proof of Theorem 2. Let $G=Ca_k(C_6)$ $(k\ge 0)$ be the Capra planar benzenoid series. By construction, the structure $Ca_k(C_6)$ collects seven times of structure $Ca_{k-1}(C_6)$ (we call "flower" the substructure $Ca_{k-1}(C_6)$ in the graph $Ca_k(C_6)$). Therefore, by simple induction on k, the vertex set of $Ca_k(C_6)$ will have $7\times|V(Ca_k(C_6))|-6(2\times 3^{k-1}+1)$ members. Because, there are $3^{k-1}+1$ and 3^{k-1} common vertices between seven flowers $Ca_{k-1}(C_6)$ in $Ca_k(C_6)$, marked by full black color in the above figures. Similarly, the edge set $E(Ca_k(C_6))$ have $7\times|E(Ca_k(C_6))|-6(2\times 3^{k-1}+1)$ members. Since, there are 3^{k-1} and 3^{k-1} common edges (full black color in these figures).

Now, we solve the recursive sequences $|V(Ca_k(C_6))|$ and $|E(Ca_k(C_6))|$. First, suppose $n_k=|V(Ca_k(C_6))|$ and $e_k=|E(Ca_k(C_6))|$ so $n_k = 7n_{k-1} - 4\underbrace{(3^k)}_{\grave{o}_k} - 6$ and $e_k = 7e_{k-1} - 4\underbrace{(3^k)}_{\grave{o}_k}$. Thus, we have

$$\begin{aligned}
n_k &= 7n_{k-1} - 4\grave{o}_k - 6 \\
&= 7(7n_{k-2} - 4\grave{o}_{k-1} - 6) - 4\grave{o}_k - 6 \\
&= 7^2 n_{k-2} - 7(4\grave{o}_{k-1} + 6) - (4\grave{o}_k + 6) \\
&= 7^3 n_{k-3} - 7^2(4\grave{o}_{k-2} + 6) - 7(4\grave{o}_{k-1} + 6) - (4\grave{o}_k + 6) \\
&\vdots \\
&= 7^i n_{k-i} - 7^{i-1}(4\grave{o}_{k-(i-1)} + 6) - \ldots - 7(4\grave{o}_{k-1} + 6) - (4\grave{o}_k + 6) \\
&= 7^i n_{k-i} - \sum_{j=0}^{i-1} 7^j (4\grave{o}_{k-j} + 6) \\
&\vdots \\
&= 7^k n_{k-k} - \sum_{i=0}^{k-1} 7^i (4\grave{o}_{k-i} + 6) \\
&= 7^k n_0 - 4\sum_{i=0}^{k-1} 7^i 3^{k-i} - 6\sum_{i=0}^{k-1} 7^i . \qquad (1)
\end{aligned}$$

where $n_0=6$ is the number of vertices in benzene C_6 (Figure 2) and $6\sum_{i=0}^{k-1} 7^i$ is equal to $\frac{6(7^k-1)}{7-1} = 7^k - 1$. On the other hand, since

$$(\alpha - \beta)\sum_{i=0}^{n} \alpha^i \beta^{n-i} = (\alpha - \beta)(\alpha^0\beta^n + \alpha^1\beta^{n-1} + \ldots + \alpha^{n-1}\beta^1 + \alpha^n\beta^0) = (\alpha^{n+1} - \beta^{n+1}).$$

Hence $\sum_{i=0}^{k-1} 7^i 3^{k-i} = (7^0 3^k + 7^1 3^{k-1} + \ldots + 7^{k-2}3^2 + 7^{k-1}3^1) + 7^k 3^0 - 7^k 3^0$

$$\begin{aligned}
&= \frac{7^{k+1} - 3^{k+1}}{7^1 - 3^1} - 7^k 3^0 \\
&= \frac{7^{k+1} - 3^{k+1} - 4(7^k)}{4} \\
&= \frac{3(7^k) - 3(3^k)}{4} \\
&= \frac{3}{4}(7^k - 3^k). \qquad (2)
\end{aligned}$$

Therefore, by using equations (1) and (2), we have

$n_k = 6\times 7^k - \left(4\left(\frac{3}{4}(7^k - 3^k)\right) + (7^k - 1)\right)$ and $\forall\, k \geq 0, n_k = |V(Ca_k(C_6))| = 2\times 7^k + 3^{k+1} + 1$.

By using a similar argument and (1), we can see that

$$e_k = 7e_{k-1} - 4\grave{o}_k = 7^2 e_{k-2} - 7(4\grave{o}_{k-1}) - 4\grave{o}_k$$
$$\vdots$$
$$= 7^k e_{k-k=0} - 4\sum_{i=0}^{k-1} 7^i \grave{o}_{k-i} = 7^k e_0 - 4\sum_{i=0}^{k-1} 7^i 3^{k-i}.$$

It is easy to see that, the first member of recursive sequence e_k is $e_0=6$, (Figure 2). Now, by using (2), we have $e_k = 6\times 7^k - 4\left(\frac{3}{4}(7^k - 3^k)\right)$ and the size of edge set $E(Ca_k(C_6))$ is equal to: $e_k = |E(Ca_k(C_6))| = 3(7^k + 3^k),\ \forall k \geq 0$.

Also, according to Figures 2 and 3, we see that the number of vertices of degree two in the graph $Ca_k(C_6)$ (we denote by $v_2^{(k)}$) is equal to $6\times 3\left(\frac{v_2^{(k-1)}}{6}\right) - 6$. The six removed vertices are the common ones between the six flowers *"$Ca_{k-1}(C_6)$"* with degree three. By using a similar argument and simple induction, we have $v_2^{(k-1)}$ the numbers of edges of graph $Ca_k(C_6)$, which are in the set E_4 or E_4^* (denoted by $e_4^{(k)}$).

Now, we solve the recursive sequence $v_2^{(k)} = 6(3\left(\frac{v_2^{(k-1)}}{6}\right) - 1)$ and we conclude $v_2^{(k)} = 3v_2^{(k-1)} - 6 = 3(3v_2^{(k-2)} - 6) - 6 = \ldots = 3^k v_2^{(0)} - 6\sum_{i=0}^{k-1} 3^i$.

It is obvious that, according to the structure of benzene, $v_2^{(0)} = n_0 = 6$.

Thus, $v_2^{(k)} = 6\times 3^k - 6\left(\frac{3^k - 1}{3-1}\right) = \mathbf{3^{k+1}} + \mathbf{3}$.

Also, $e_4^{(k)} = |E_4| = |E_4^*| = v_2^{(k-1)} = \mathbf{3^k} + \mathbf{3}$ and according to the above definition, it is obvious that, for Capra of planar benzenoid series $G=Ca_k(C_6)$ we have two partitions:

$V_2 = \{v \in V(Ca_k(C_6)) \mid d_v = 2\}$ and $V_3 = \{v \in V(Ca_k(C_6)) \mid d_v = 3\}$, with the size $3^{k+1} + 3$ and $2(7^k - 1)$, respectively.

On the other hand, according to the structure of Capra planar benzenoid series $Ca_k(C_6)$, there are $2v_2^{(k)}$ edges, such that the first point of them is a vertex with degree two. Among these edges, there exist $v_2^{(k-1)}$ edges, of which the first and end point of them have degree 2 (the members of E_4 or E_4^*).

Thus, $e_5^{(k)} = |E_5| = |E_6^*| = 2v_2^{(k)} - 2e_4^{(k)} = 2v_2^{(k)} - 2v_2^{(k-1)}$. So, the size of edge set E_5 and E_6^* is equal to $e_5^{(k)} = 2(3^{k+1} + 3 - 3^k - 3) = 4(3^k)$

Now, it is obvious that:

$$\begin{aligned} e_6^{(k)} &= |E_6| = |E_9^*| = 3\left(7^k + 3^k\right) - e_5^{(k)} - e_4^{(k)} \\ &= 3\times 7^k + 3^{k+1} - 4\times 3^k - 3^k - 3 \\ &= 3\times 7^k - 2\times 3^k - 3 \\ &= \mathbf{3(7^k - 2(3^{k-1}) - 1)}. \end{aligned}$$

Now, we know the size of all sets $V_2, V_3, E_4, E_4^*, E_5, E_6^*, E_6$ and E_9^*. So, we can calculate the First and Second Zagreb Polynomial of Capra planar benzenoid series $G=Ca_k(C_6)$, as follow:

First Zagreb Polynomial of $G=Ca_k(C_6)$:

$$\begin{aligned} M_1(G,x) &= \sum_{e\in E(G)} x^{d(u)+d(v)} \\ &= \sum_{e\in E_6} x^6 + \sum_{e\in E_5} x^5 + \sum_{e\in E_4} x^4 \\ &= |E_6|x^6 + |E_5|x^5 + |E_4|x^4 \\ &= 3(7^k - 2(3^{k-1}) - 1)x^6 + 4(3^k)x^5 + 3(3^{k-1} + 1)x^4 \end{aligned}$$

Second Zagreb Polynomial of $G = Ca_k(C_6)$:

$$\begin{aligned} M_2(G,x) &= \sum_{e\in E(G)} x^{d(u)d(v)} = \sum_{e\in E_9^*} x^9 + \sum_{e\in E_6^*} x^6 + \sum_{e\in E_4^*} x^4 \\ &= 3(7^k - 2(3^{k-1}) - 1)x^9 + 4(3^k)x^6 + 3(3^{k-1} + 1)x^4. \end{aligned}$$

Also, according to definition of First and Second Zagreb index, we have:

$$\begin{aligned} M_1(G) = \frac{\partial M_1(G,x)}{\partial x}|_{x=1} &= 18(7^k - 2(3^{k-1}) - 1) + 20(3^k) + 12(3^{k-1} + 1) \\ &= 18(7^k) + 12(3^k) - 6 \end{aligned}$$

and $M_2(G) = \frac{\partial M_2(G,x)}{\partial x}|_{x=1} = 27(7^k - 2(3^{k-1}) - 1) + 24(3^k) + 12(3^{k-1} + 1)$

$$= 27(7^k) + 10(3^k) - 15$$

Of course, by using $|V_2|$ and $|V_3|$, we have

$$M_1(G) = (3^{k+1} + 3)2^2 + 2(7^k - 1)3^2 = 18(7^k) + 12(3^k) - 6.$$

Thus, we completed the proof of the theorem 3.

ACKNOWLEDGMENTS

The first author is thankful to Dr. M. Alaeiyan and Dr. A. Aghajani of Department of Mathematics, Iran University of Science and Technology (IUST) for their precious support and suggestions.

REFERENCES

1. H. Wiener. *J. Am. Chem. Soc*. **1947**, *69,* 17.
2. A.A. Dobrynin, R. Entringer and I. Gutman. *Acta Appl. Math*. **2001**, *66,* 211.
3. D.E. Needham, I.C. Wei and P.*G.* Seybold. *J. Am. Chem. Soc*. **1988,** *110,* 4186.
4. *G.* Rucker and C. Rucker. *J. Chem. Inf. Comput. Sci*. **1999**, *39,* 788.
5. B. Zhou and I. Gutman, *Chemical Physics Letters*. **2004**, *394,* 93.
6. I. Gutman, *Indian J. Chem*, **1997**, *36,* 128.
7. D.J. Klein, I. Lukovits and I. Gutman. *J. Chem. Inf. Comput. Sci*. **1995**, *35,* 50.
8. B. Zhou and I. Gutman, *Chemical Physics Letters*. **2004**, *394,* 93.
9. I. Gutman and N. Trinajstić*, Chem. Phys. Lett*. **1972**, *17,* 535.
10. I. Gutman, B. Ruscic, N. Trinajstić and C.F. Wilcox, *J. Chem. Phys*. **1975**, *62,* 3399.
11. I. Gutman and K.C. Das, *MATCH Commun. Math. Comput. Chem*. **2004**, *50,* 83.
12. S. Nikolic, *G.* Kovacevic, A. Milicevic and N. Trinajstić*, Croat. Chem. Acta*. **2003**, *76,* 113.
13. A. Behtoei, M. Jannesari and B. Taeri, *Appl. Math. Lett*. **2009**, *22,* 1571.
14. K.C. Das, I. Gutman and B. Zhou, *Journal of Mathematical Chemistry*. **2009**, *46,* 514.
15. M.H. Khalifeh, H. Yousefi-Azari and A.R. Ashrafi, *Comput. Appl. Math*. **2008**, *56,* 1402.
16. S. Li and H. Zhou, *Appl. Math. Lett*. **2010**, *22,* 128.
17. M. Liu and B. Liu, *MATCH Commun. Math. Comput. Chem*. **2010**, *63,* 151.
18. M. Ghorbani and M. Ghazi, *Digest. J. Nanomater. Bios*. **2010**, *5(4),* 1107.
19. M. Ghorbani and M. Ghazi, *Digest. J. Nanomater. Bios*. **2010**, *5(4),* 837.

20. M.R. Farahani. Int. J. Chem. Model. **2013**, *5(4),* Inpress.
21. M.R. Farahani. Acta Chim. Slov. **2012**, *59,* 779–783.
22. M.R. Farahani. Adv. Mater. Corrosion. **2012**, *1,* 57-60.
23. M.R. Farahani. Int. J. Nanosci. Nanotech. **2012**, Accepted for publish.
24. M.R. Farahani. Adv. Mater. Corrosion. **2013**, *2,* 16-19
25. M.R. Farahani. Chemical Physics Research Journal. **2013**, In press.
26. M.R. Farahani. J. Chem. Acta. **2013**, *2,* 70-72.
27. M. Goldberg. *Tohoku Math. J.* **1937**, *43,* 104.
28. A. Dress and *G.* Brinkmen, *MATCH Commun. Math. Comput. Chem*. **1996**, *33,* 87.
29. M.V. Diudea, *J. Chem*. *Inf*. *Model,* **2005**, *45,* 1002.
30. M.V. Diudea, M. Ştefu, P.E. John, and A. Graovac, C*roat. Chem. Acta,* **2006,** *79,* 355.
31. M.R. Farahani and M.P.Vlad. Studia UBB Chemia. **2012,** *57(4),* 55-63.
32. M.R. Farahani. Adv. Mater. Corrosion. **2012,** *1*, 61-64.
33. M.R. Farahani. J. Applied Math. & Info. **2013,** *31(5-6)*, In press.
34. M.R. Farahani and M.P.Vlad. Studia UBB Chemia. **2013,** *58(2),* accepted.
35. M.R. Farahani. Polymers Research Journal. **2013,** *7(3),* In press.
36. M.R. Farahani. Chemical Physics Research Journal. **2013,** In press.

STUDIA UBB CHEMIA, LVIII, 2, 2013 (p. 143 – 150)
(RECOMMENDED CITATION)

ASSESSMENT OF AIR POLLUTION WITH SULPHUR DIOXIDE FROM ELECTRIC ARC FURNACES

DANA – ADRIANA ILUȚIU – VARVARA[a*], DAN RĂDULESCU[b]

ABSTRACT. The purpose of the paper constitutes the assessment of air pollution with sulphur dioxide (SO_2) from the electric arc furnaces. Experimental procedure for determining SO_2 emission levels during the steelmaking and the sulphur dioxide concentrations variation diagrams with the melting temperature of the three types of charges are presented. Sulphur dioxide has a negative impact on the quality of the air, being responsible for generating acid rain. The negative impact of sulphur dioxide manifests itself on the steel works and on the population.

Keywords: *air pollution, sulphur dioxide, electric arc furnace.*

INTRODUCTION

The steelmaking in the electric arc furnace belongs to the category of industrial processes with high degree of pollution because the following pollutants are transferred in the air: carbon oxides, sulphur oxides, nitrogen oxides, volatile organic compounds (VOC), particulate matter, dioxins and furans [1].

Sulphur dioxide (SO_2) forms sulphate aerosols that are thought to have a significant effect on global and regional climate. Sulphate aerosols reflect sunlight into space and also act as condensation nuclei, which tend to make the clouds more reflective and change their lifetimes [2].

Sulphur emissions have grown rapidly and extensive researches have documented a variety of effects on the environment [3]. Sulphur dioxide is the primary cause of acid precipitation, which adversely affects natural systems, agriculture and building materials. The sulphate aerosol particles formed as a consequence of these emissions impair visibility and affect human health.

[a] *Universitatea Tehnică din Cluj – Napoca, Str. Memorandumului, Nr. 28, RO-400114 Cluj-Napoca, Romania, *corresponding author: dana.varvara@gmail.com*
[b] *Universitatea de Medicină şi Farmacie Iuliu Haţieganu Cluj – Napoca, Facultatea de Medicină, Str. Emil Isac, Nr. 13, RO-400023 Cluj-Napoca, Romania*

Sulphur dioxide, dissolves in the water vapors from the air to form acids and interacts with other gases and particles in the air to form particles known as sulphates and other products that can be harmful to people and their environment [4].

In Table 1, there are presented the health effects of respiratory exposure to sulphur dioxide.

Table 1. Health effects of respiratory exposure to sulphur dioxide [5, 6, 7]

Exposure limits [ppm]	Health Effects
1-5	Threshold for respiratory response in healthy individuals upon exercise or deep breathing
3-5	Gas is easily noticeable. Fall in lung function at rest and increased airway resistance
5	Increased airway resistance in healthy individuals
6	Immediate irritation of eyes, nose and throat
10	Worsening irritation of eyes, nose and throat
10-15	Threshold of toxicity for prolonged exposure
>20	Paralysis or death occurs after extended exposure
150	Maximum concentration that can be withstood for a few minutes by healthy individuals

Sulphur dioxide has a negative impact on the human health. Sulphur dioxide penetrates the human organism through the respiratory system. At high concentrations its absorption reaches up to 90% in the upper respiratory tract and less in the lower parts of the respiratory system. During short-term exposure to sulphur dioxide the respiratory system is mainly affected. Population groups sensitive to sulphur dioxide exposure are children, elderly, asthmatic patients, people suffering from cardiovascular diseases or chronic lung diseases. Sulphur dioxide health effects are expressed in respiratory disorders, lung diseases, lung immune protection disorder, aggravation of existing lung and cardiovascular diseases. The asthmatic patients are ten times more sensitive and sulphur dioxide than healthy people. Children, suffering from asthma are particularly sensitive, and sulphur dioxide exposure may lead to inflammatory lung diseases [1, 6, 8, 9].

The European Union (EU) defines the obligations to be met by industrial activities with a major pollution potential. The objective is to avoid or minimize polluting emissions in the atmosphere, water and soil, as well as waste from industrial and agricultural installations, with the aim of achieving a high level of environmental and health protection [10, 11, 12, 13].

The sources with sulphur dioxide generating potential in the electric arc steelmaking are [9]: the metallic charge; additions of auxiliary materials; first fusion pig iron (0.05 – 0.07% S); electric arc furnace atmosphere, when using fuels containing sulphur.

RESULTS AND DISCUSSION

The composition of the charge I is presented in Table 2.

Table 2. The composition of the charge I

Charge	Composition [%]	Weight [g]
Painted plate	50	5
Zincked plate	20	2
First fusion pig iron	27	2.7
Plastics	3	0.3
Total	100	10

In Fig. 1 sulphur dioxide concentration variation and maximum concentration variation of sulphur dioxide for charge I is represented. The graph shows that the sulphur dioxide concentration increased with the increasing of temperature in the interval 350-450^{o}C, so that at the temperature of 450^{o}C reaches the maximum value of 95 [ppm], after which the SO_2 concentration decreases with the increasing of the temperature.

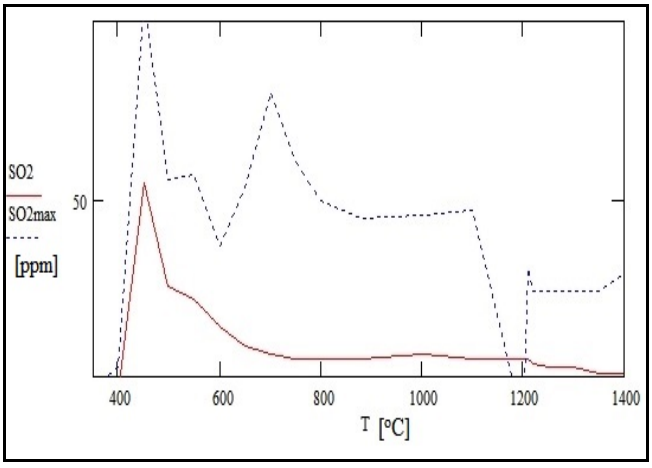

Figure 1. Variation with temperature of sulphur dioxide concentration and maximum concentration variation of sulphur dioxide for charge I

The composition of the charge II is presented in table 3.

Table 3. The composition of the charge II

Charge	Composition [%]	Weight [g]
Painted plate	40	4
Zincked plate	40	4
First fusion pig iron	15	1.5
Plastic and vaseline	5	0.5
Total	100	10

In Fig. 2 sulphur dioxide concentration variation and maximum concentration variation of sulphur dioxide for charge II is represented. The graph shows that the sulphur dioxide concentration decreases with the increasing of temperature in the 520–750°C, 800–860°C and 900-1070°C intervals, and in the intervals 750-800°C and 860 - 900°C sulphur dioxide concentration increases with the increasing of the temperature.

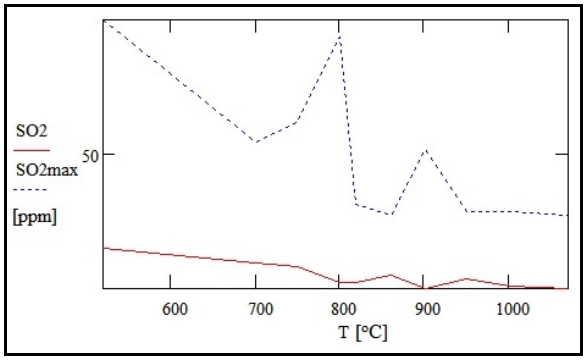

Figure 2. Variation with temperature of sulphur dioxide concentration and maximum concentration variation of sulphur dioxide for charge II

The composition of the charge III is presented in table 4.

Table 4. The composition of the charge III

Load	Composition [%]	Weight [g]
Painted plate	15	1.5
Zincked plate	45	4.5
First fusion pig iron	33	3.3
Plastic and vaseline	7	0.7
Total	100	10

In Fig. 3 sulphur dioxide concentration variation and maximum concentration variation of sulphur dioxide for charge III is represented. The graph shows that in the 680-780°C, 800-850°C and 900-950°C intervals, the maximum sulphur dioxide concentration increases as long as the temperature increases, and in the 780-800°C, 850-900°C and 950-1100°C intervals, decreases as the temperature increases.

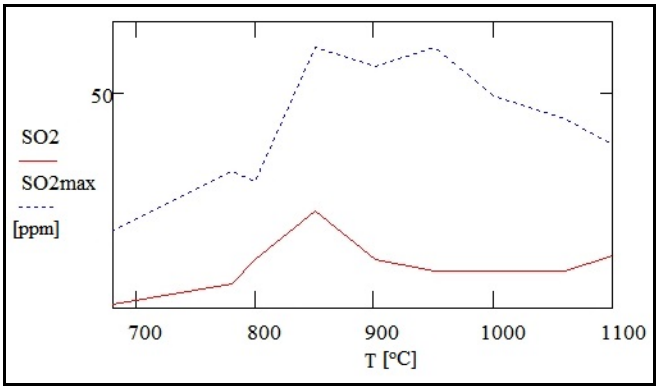

Figure 3. Variation with temperature of sulphur dioxide concentration and maximum concentration variation of sulphur dioxide for charge III

Based on the sulphur dioxide concentrations recorded by the burned gases computer analyzer – MAXILYZER, there were computer the average sulphur dioxide concentrations for the three types of charges analyzed were calculated. Average values are 17.45, 14.90 and 15.00 ppm for the three charges, respectively.

From the analysis of the sulphur dioxide concentrations recorded for the three types of charges, we concluded that the intervention threshold value for SO_2 (13.36 ppm according to the reference [14]) was exceeded by 1.3 times for the first charge, by 1.11 times for the second charge and by 1.12 times for the third charge.

CONCLUSIONS

After analyzing the SO_2 and SO_{2max} concentrations variation graphs for the three charges, it results that: in all the three charges it the presence of sulphur dioxide was detected the presence; the greatest concentration was detected for the charge I (95 ppm); the recorded SO_2 concentrations decreased with the increasing of the temperature; the average concentrations of sulphur dioxide exceed the intervention threshold.

The emissions level of the sulphur dioxide and maximum sulphur dioxide registered for the three charges are influenced by the sulphur contained in the charge components.

In order to reduce sulphur dioxide emissions it is necessary to select the charge and to preheat the furnace. The charge components selection process refers to the reduction/elimination of the sources having a potential to generate sulphur dioxide. The techniques to reduce the air pollution with sulphur dioxide from electric arc furnaces include the followings: the selection of raw materials (first fusion pig iron; scrap with low sulfur content); the usage of fuel with low sulfur content, such as natural gas; flue gas desulphurization (absorption, adsorption, catalytic oxidation and catalytic reduction).

The original aspects of the article are: conception of three types of charge for determining the sulphur dioxide concentrations; identification of air pollution sources with sulphur dioxide from electric arc furnaces; identification of techniques to reduce the sulphur dioxide concentration; assessment of air pollution with sulphur dioxide from electric arc furnaces.

Also for monitoring sulphur dioxide emissions from steelmaking plants it is necessary to achieve a database containing charge compositions, which will make possible the prediction of the emissions concentrations.

EXPERIMENTAL SECTION

In order to determine the sulphur dioxide emissions, which are transferred during steelmaking, three charge types were considered.

In order to realize these determinations, the following equipments were used: an analytical balance; a contact thermometer MICROTEC DIGITEMP 01K; nacelles; a mono-phased electric furnace with chamber type resistance with spirals (model WG/ r01/1522/ 2 VEB) having the following characteristics: P = 2 KV, Umax = 250 V, Imax = 9A, Tmax = 1650^{o}C and transformer of type RFT/SST / 250 V / 20A; a computer for burned gases analysis MAXILYZER.

The nacelle which contains the considered charge was introduced in the furnace with chamber type resistance with spirals, without prior heating, for charges I and III and with preliminary heating at 520^{o}C.

Sulphur dioxide emissions were determined in the 350-1400^{o}C interval (T_1 = 350^{o}C, T_2 = 400^{o}C, T_3 = 450^{o}C, T_4 = 500^{o}C, T_5 = 550^{o}C, T_6 = 600^{o}C, T_7 = 650^{o}C, T_8 = 700^{o}C, T_9 = 750^{o}C, T_{10} = 800^{o}C, T_{11} = 880^{o}C, T_{12} = 1000^{o}C, T_{13} = 1100^{o}C, T_{14} = 1200^{o}C, T_{15} = 1210^{o}C, T_{16} = 1220^{o}C, T_{17} = 1250^{o}C, T_{18} = 1300^{o}C, T_{19} = 1350^{o}C and T_{20} = 1400^{o}C), 520-1070^{o}C (T_1 = 520^{o}C, T_2 = 700^{o}C, T_3 = 750^{o}C, T_4 = 800^{o}C, T_5 = 820^{o}C, T_6 = 860^{o}C, T_7 = 900^{o}C, T_8 = 950^{o}C, T_9 = 1000^{o}C and T_{10} = 1070^{o}C) and 680-1100^{o}C (T_1 = 680^{o}C, T_2 = 780^{o}C, T_3 = 800^{o}C, T_4 = 850^{o}C, T_5 = 900^{o}C, T_6 = 950^{o}C, T_7 = 1000^{o}C, T_8 = 1060^{o}C and T_9 = 1100^{o}C) for charge I, II and III, respectively.

The concentrations of the sulphur dioxide were red every two minutes.

The variation diagrams for the three types of charges were made using MathCAD 7 Professional software.

REFERENCES

1. D.A. Iluțiu-Varvara, "The Generation and Transfer of Pollutant Substances in Industrial Processes", Tehn. Univ. Publishing, Cluj-Napoca, **2007**.
2. P. Forster, V. Ramaswamy, P. Artaxo, T. Berntsen, R. Betts, D.W. Fahey, J. Haywood, J. Lean, D.C. Lowe, G. Myhre, J. Nganga, R. Prinn, G. Raga, M. Schulz, R. Van Dorland, Changes in atmospheric constituents and in radiative forcing. Climate Change, 2007. The Physical Science Basis, "Contribution of Working Group I to the Fourth Assessment Report of the Intergovernmental Panel on Climate Change", Edited by: S.D. Solomon, Qin, M. Manning, Z., M. Chen, K.B. Marquis, M. Averyt, M. Tignor, and H.L. Miller, Cambridge University Press, Cambridge, UK, New York, NY, USA, **2007,** 129–234.
3. US Environmental Protection Agency (USEPA), National Air Pollutant Emission Trends, 1900–1995. EPA-454/R-96-007, Washington, DC, **1996**.
4. L.G. Chestnut, Human Health Benefits From Sulfate Reductions Under Title IV of the 1990 Clean Air Act Amendments, Final Report, U.S. EPA, Office of Atmospheric Programs, Acid Rain Division, **1995**.
5. B. Nemery, P.H.M. Hoet, A. Nemmar, "The Meuse Valley fog of 1930: an air pollution disaster", The Lancet 357(9257), 704-708, **2001**.
6. National Institute for Occupational Safety and Health (NIOSH), "Occupational Health Guidelines for Chemical Hazards", DHHS (NIOSH) Publication No. 81-123, **1981**.
7. A. Wellburn, "Air Pollution and Climate Change: the biological impact", Addison Wesley Longman Limited, Harlow, **1994**, 268.
8. WHO (World Health Organization), “Sulfur Oxides and Suspended Particulate Matter.” *Environmental Health Criteria* 8. Geneva, **1979**.
9. D.A. Varvara, "Studies Concerning the Substances Transfer between the Steelmaking Phases", PhD Thesis, TUC-N, **2007**.
10. Directive 2008/1/EC of the European Parliament and of the Council of 15 January 2008 concerning “Integrated Pollution Prevention and Control”, **2008**.
11. Directive 2001/81/EC of the European Parliament and of the Council of 23 October 2001 on national emission ceilings for certain atmospheric pollutants. Official Journal of the European Communities L 309: 22-30, **2001**.

12. Directive 2001/80/EC of the European Parliament and of the Council of 23 October 2001 on the limitation of emission from certain pollutants into the air from large combustion plants. Official Journal of the European Communities L 309: 1-20, **2001**.

13. Directive 2010/75/EU of the European Parliament and of the Council of 24 November 2010 on industrial emissions (integrated pollution prevention and control), **2010**.

14. "Concerning Atmosphere Protection and Emission Norms for the Determination of Air Pollutants Produced by Stationary Sources", MAPPM Order no. 462/**1993**.

STUDIA UBB CHEMIA, LVIII, 2, 2013 (p. 151 – 160)
(RECOMMENDED CITATION)

EQUILIBRIUM AND THERMODYNAMIC STUDY OF COMPLEXES OF THALLIUM WITH URACIL AT DIFFERENT TEMPERATURES AND CONSTANT IONIC STRENGTH

ELHAM HEIATIAN[a], FARHOUSH KIANI[b], SASAN SHARIFI[a], AZAR BAHADORI[a], AND FARDAD KOOHYAR*[b]

ABSTRACT. In aqueous solution, the protonation equilibria of uracil and their complex formation with thallium(I) ion were investigated using a combination of potentiometric and spectrophotometric methods at different temptatures (283.15, 288.15, 293.15, 298.15, 303.15 and 308.15) K and constant ionic strength (0.1mol dm^{-3} sodium perchlorate). A careful and accurate method based on chemometrical concepts was used in order to determine stability constants. For this purpose, spectral titration data were used and the spectra were recorded in the range (200-500 nm). The stability constants of thallium(I) ion with all the heterocyclic bases were calculated at various temperatures by means of computer fitting of the pH-absorbance data with appropriate mass balance equations. The computer program equispec was used to extract the desired information from the spectral data. The outputs of the fitting processes were protonation and stability constants, spectral profiles of pure forms, distribution diagrams, and other factor analysis data. The composition of the formed complexes were determined and it was shown that thallium(I) forms a mononuclar 1:1 species with the uracil, of the type TlL in the pH range of study (1.0-12.4), where L represents each heterocyclic base. Finally, The effect of temprature on the protonation and stability constants were studied and thermodynamic functions such as change in enthalpy (ΔH), change in entropy (ΔS) and change in gibbs energy (ΔG) have been obtained for the complexes of thallium(I) ion with the heterocyclic bases from the stability constants values and their temperature dependence.

Key words: *Equispec, Thallium(I) complexe, Uracil, Temperature, Constant ionic strengh.*

[a] *Chemistry Department, Islamic Azad University of Arak, Arak, Iran*
[b] *Department of chemistry, Faculty of Science, Islamic Azad University, Ayatollah Amoli Branch, Amol, Iran, *Corresponding Author: E-mail: FardadKoohyar@yahoo.com*

INTRODUCTION

In our life today, the physico-chemical data of biological and organic molecules are very important due to their usages in various fields of industry such as food, pharmacy, cosmetic and detergents. Also, these data help us to better understanding of interaction between molecules in their solutions [1-8].

Uracil is one of the four nucleobases in the nucleic acid of RNA. In the body Uracil help to carry out the synthesis of many enzymes necessary for cell function through bonding with riboses and phosphates [9]. It can be used for drug delivery and as a pharmaceutical [10].

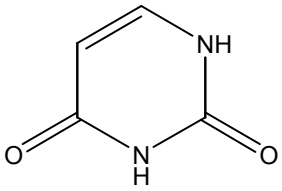

Scheme 1. Structures of the uracil

On the otherhand, thallium is a toxic element and acts on the central nervous system and induces inflammatory response. Since thallium(I) shows marked similarities to that of potassium cation, its interaction with nucleotides, the monomeric units of DNA and RNA, in aqueous would be of a major biochemical interest [11].

Aqueous solutions of Metal complex were studied by various techniques [12]. Also, there are several methods for the determination of acidity constants [13-18]. Spectroscopic methods are in general highly sensitive and are frequently used to analyze chemical equilibria in solution. In among of various properties of analyte, the physical property is measured (in most of these methods) as a function of the pH of the solution and the resulting data are used for the determination of the dissociation constants [19].

In the present work, the protonation and stability constants of uracil with Tl(I) were determined spectropotometrically at six different temperatures in ionic strength 0.1 mol dm^{-3} $NaClO_4$.

The stability constants of the formed complexes at different tempratures were evaluted by the Equispec program using the corresponding spectral absorption-pH data and these values have been compared with similar systems and interpreted. Then, thermodynamic functions have been obtained from the stability constants values and their temperature dependence.

RESULTS AND DISCUSSION

All measurements were carried out at six different temperatures (283.15, 288.15, 293.15, 298.15, 303.15 and 308.15) K. The ionic strength was maintained to 0.1 mol dm^{-3} with sodium perchlorate. The pH meter was calibrated for the revalent H^+ concentration with a solution of 0.01 mol dm^{-3} perchloric acid solution containing 0.09 mol dm^{-3} sodium perchlorate (for adjusting the ionic strength to 0.1 mol dm^{-3}). For this standard solution, we set –log $[H^+]$=2.00 [20]. Junction potential corrections have been calculated from the bellow equation:

$$-\log[H^+]_{real} = -\log[H^+]_{measured} + a + b[H^+]_{measured} \quad (1)$$

where a and b were determined by measuring hydrogen ion concentration for two different solutions of $HClO_4$ or NaOH with sufficient $NaClO_4$ to adjust the ionic strength in solutions.

The species $M_pH_qL_r^{(np+q+r)+}$ formed is characterized by it stoichiometry (x:y:z), where M and L represent the metal ion and each ligand, respectively. To determine the stability constant of the complexation or protonation, eq 2 is defined by β_{pqr} [21]:

$$pM^{n+} + qH^+ + rL^- \Leftrightarrow M_pH_qL_r^{(np+q+r)+} \quad (2)$$

$$\beta_{pqr} = \frac{[M_pH_qL_r^{(np+q+r)+}]}{[M^{+n}]^p[H^+]^q[L^-]^r} \quad (3)$$

The protonation constants of the heterocyclic bases have been used for computation of the stability constant, β_{pqr}, of the metal-ligand. For thallium (I)-uracil system a linear relation between logβ and 1/T is observed in Figure 1. In addition, all these linear diagrams (logβ vs 1/T) have the high R^2 ($R^2 \approx 0.99$).

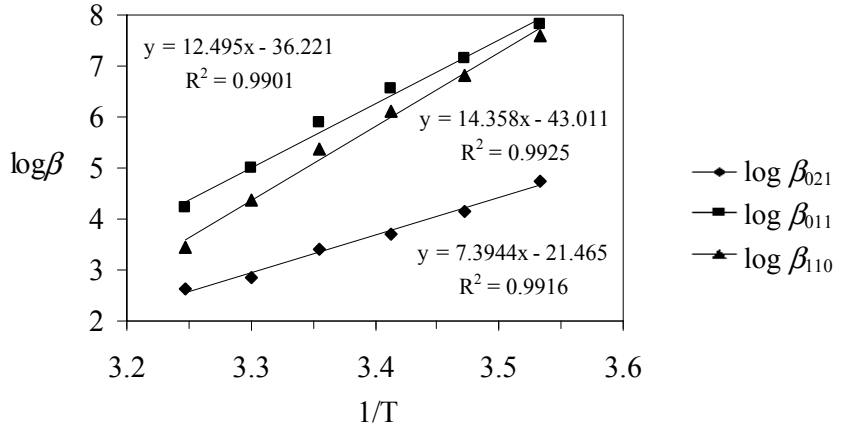

Figure 1. Cureve logβ versus 1/T for Tl(I)-uracil system in ionic strength 0.1 mol dm^{-3} $NaClO_4$.

In this work, the electronic absorption spectra of uracil were recorded in different tempratures and at various pH values. The protonation constants of the uracil were determined using a potentiometric technique and calculated using a computer program which employs a nonlinear least-squares method (Microsoft Excel Solver) [22, 23]. These values are listed in Table 1 (the values reported in the literature are, $pK_1 = 0.6$ and $pK_2 = 9.46$) [24].

Determination of the formation constant was employed using the method mentioned before. Absorbance, A, and -log $[H^+]$ were measured by successive addition of an alkali solution of the ligand to the acidic metal ion solution in the UV range (200 to 500) nm; see Experimental Section. Treatment of the spectrophotometric data (every 5 nm) obtained during the titrations, as a function of H^+ concentration, was conducted with the computer program Equispec (by using the matrix based in the Matlab environment) [25].

Table 1. Average values of the protonation constants of the uracil at different tempratures and constant ionic strength, I, (0.1 mol dm^{-3} $NaClO_4$)

T(ºK)	logβ_{021}	Δ*H* (Kj.mol^{-1})	Δ*S* (j.mol^{-1})	Δ*G* (Kj.mol^{-1})	log β_{011}	Δ*H* (Kj.mol^{-1})	Δ*S* (j.mol^{-1})	*Δ*G *(Kj.mol^{-1})*
283.15	4.74 ± 0.44				7.80 ± 0.53			
288.15	4.16 ± 0.39				7.15 ± 0.50			
293.15	3.71 ± 0.32				6.55 ± 0.45			
298.15	3.40 ± 0.22	-142.10	-412.43	-19.12	5.90 ± 0.12	-248.53	-724.91	*-32.40*
303.15	2.86 ± 0.23				4.98 ± 0.41			
308.15	*2.61 ± 0.34*				*4.20 ± 0.21*			

The stoichiometric formation constants were computed from the data using the computer program. The number of experimental points (absorbance vs pH) was more than 30 for each titration. It is most convenient to arrange a series of the measured absorption spectra at different wavelengths and various pH values as the rows of a matrix Y. According to Beer-Lambert's law, **Y** can be decomposed into the product of a concentration matrix **C** and a matrix **A** of molar absorptivities. The concentration profiles of the absorbing species form the columns of **C** and the molar absorption spectra form the corresponding rows of **A**. Due to the instrumental and experimental errors, this decomposition is not perfect, the difference being the matrix E of residuals. A matrix equation can be written as:

$$Y = CA + E \quad (4)$$

Data fitting consists of determining those unknown parameters for which the sum of the squares over all the elements of the matrix **E** of residuals is minimal. Initially, the unknown parameters including the equilibrium constants, a vector p of nonlinear parameters, overall formation constants, and all the molar absorptivities of all the components, i.e., the complete matrix **A** of linear parameters, were determined. **C** is defined by the model and the appropriate equilibrium constants and is calculated numerically using the law of mass action and the analytical (total) concentration of each componentin solution [26, 27]. If the spectra are measured at many wavelengths, the total number of parameters could be very high, and it is crucial to reduce this number by separation of the linear and nonlinear parameters. For any set off nonlinear parameters, **p**, which defines the concentration matrix C, the best set of linear parameters, the matrix **A**, is an explicit least-squares calculation

$$A = C^{+}Y \tag{5}$$

$\mathbf{C^+}$ is the pseudoinverse which can be calculated as $\mathbf{C^+ = (C^tC)^{-1}C^t}$ or preferably using a numerically more stable algorithm (i.e., an algorithm which guarantees to reach physically meaningful final results) [28]. **A** is now defined as a function of **p** and consequently **E,** and sums of the squares (ssq) are defined as a function of the nonlinear parameters only

$$\mathrm{ssq} = \sum\sum \mathrm{E(i,j)}^2 = \mathrm{f(Y, model, parameters)} = \mathrm{f(P)} \tag{6}$$

In the equilibrium condition, the model is a collection of equilibria between the component species, and the parameters are the equilibrium constants. The computation of the pseudo-seems to be a trivial task. In equilibrium studies, inverse $\mathbf{C^+}$ generally the concentration matrix **C** has, at least theoretically, full rank; i.e., the chemical and mathematical ranks are equal, and the concentration profiles for all species are linearly independent. $\mathbf{C^+}$ can be computed, and **A** is determined by eq 5. This is, however, not always the case, and near linear dependency (i.e., when the distribution diagram of some species can be expressed as a linear combination of some other species) and (or) species with only very low concentrations result in deficiencies in the equilibrium model. In this status, **C**, then, does not have full rank, and the pseudoinverse, $\mathbf{C^+}$, is not or is only poorly defined, which can render its computation difficult to impossible and thus corrupt the resulting **A** as well as the residuals, **E,** and the sum of squares. There are powerful algorithms such as the Newton-Gauss-Levenberg/Marquardt algorithm available for this task [29].

The output of Equispec comprises the spectrum, pk_a values and diagrams of the concentration distribution of each assumed species. From inspection of the experimantal spectra, it is hard to guess even the number of protolytic species involved.

Considering eq 2, different models including ML, MHL and several polynuclear and protonated species were tested by the program. As expected, polynuclear complexes were systematically rejected by the computer program, as also were, MH_2L, and MHL_2, ML_2 and MH_2L_2. Values for some species were calculated by the program, but the species were not considered further because the estimated error in its formation constant was unacceptable, and its inclusion does not improve the goodness of the fit. The models finally chosen, formed by ML for the studied system, resulted in a satisfactory fitting.

Also, the thermodynamic functions for the heterocyclic base have been obtained from the protonation and stability constants values and their temperature dependence.

The calculated average values of the protonation and stability constants for different experiments are listed in Tables 1, 2. In Figure 2 the equilibrium distributions of various species of Tl(I) with uracil system are shown as a function of –log $[H^+]$, respectively. The most important features of the distribution diagrams are the pH limits of the evolving and disappearing of components.

Table 2. Avrage values of the formation constants of Tl(I) with uracil at different temperature and constant ionic strength (0.1 mol dm^{-3} $NaClO_4$) some thermodynmic Parameters at Different Temperatures

T (ºK)	$\log\beta_{101}$	ΔH (Kj.mol^{-1})	ΔS (j.mol^{-1})	ΔG (Kj.mol^{-1})
283.15	7.60±0.65			
288.15	6.82±0.65			
293.15	6.10±0.65			
298.15	5.36±0.65	-275	-823.52	-29.52
303.15	4.38±0.65			
308.15	3.44±0.72			

The calculations shown are based on the stability constant values given in Tables 1 and 2. The curves clearly demonstrate that an increase of the pH is accompanied by an increase in the formation of deprotonated complex species.

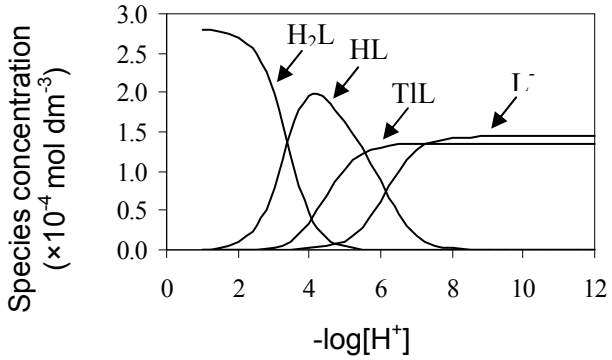

Figure 2. The equilibrium distribution of the species for the system Tl(I)-uracil as a function of log[H^+] at 298.15 K and constant ionic strength 0.1 mol dm^{-3} $NaClO_4$.

CONCLUSION

The stability constants of thallium(I) with uracil were calculated with spectrophotometric titrations using a chemometric method. The striking advantage of the proposed method is using of the whole spectral information in the computation process which enable us to have more precise and accurate thermodynamic constants in comparison to the classical methods such as single wavelength approach. The effect of the temprature on the acid dissociation and stability constants is investigated and it reveals the complex relations of the acid dissociation and stability constants to temprature. The results show good consistency with the previous reported results. However, the differences are mostly due to the different techniques, various ionic strengths with different background electrolytes, and different temperatures that were used.

EXPERIMENTAL

Chemicals

All the chemicals used were of analytical reagent grade. Uracil ($C_4H_4N_2O_2$) was obtained from Merck. The aqueous stock solutions of the uracil were freshly prepared daily. The NaOH solution was prepared from a titrisol solution (Merck), and its concentration was determined by several titrations with standard HCl. Perchloric acid and thallium (I) nitrate were from Fluka and were used without further purification. Dilute perchloric acid solutions were standardized against standard NaOH solution. Sodium perchlorate was purchased from Merck and was kept in a vacuum at least 72 h before use.

All The reagents were used without furthere purification and dilute solutions were prepared from double-distilled water with specific conductance equal to (1.8 ± 0.1) $\mu\Omega^{-1}$ cm^{-1}.

Apparatus and software

The pH values were measured with a HORIBA M-12 pH-meter using a combined glass electrode. The glass electrode was calibrated on the basis of the proton concentration at constant ionic strength (0.1 mol dm^{-3}) according to the procedure described elsewhere [30]. The calibration was repeated at each specific temperature (t ± 0.1) °C by circulation of thermostated water through the jacket. Nitrogen purge gas was used to remove CO_2. An Eppendorf micropipette (±0.6%) was used for the addition of a standard base to the solution. The calibration procedure was as recommended by the IUPAC for glass electrodes [31].

A HP-8453 spectrophotometer controlled by a computer and equipped with a 1 cm path length quartz cell was used for UV-Vis spectra acquisition. Spectra were acquired between 200 and 500 nm (5 nm resolution). The measurement cell was of a flow type. A Masterflex pump allowed circulation of the solution under study from the potentiometer cell to the spectrophotometer cell, so the absorbance and the pH of the solution could be measured simultaneously.

The data were preprocessed using MATLAB software, version 6.5 (Mathworks, Natick, U.S.A) and the deconvolution of the obtained data matrix was performed using Equispec version 3.1.

Procedure

Volumes of 10 cm^3 acidic solution of Tl^+ [(3.85×10^{-5} to 2.8×10^{-4} mol dm^{-3})] was titrated with an alkali solution (0.1 mol dm^{-3} NaOH) of the uracil [(8.05×10^{-5} to 1.6×10^{-4} mol dm^{-3}). Titration of each the heterocyclic base was carried out at 6 temperatures (283.15, 288.15, 293.15, 298.15, 303.15 and 308.15) K in ionic strength 0.1mol dm^{-3}. Ionic strength fixed with $NaClO_4$ solution. The starting points of pH titrations were pH 1.0, which were set using concentrated solutions of HCl and NaOH. The concentrated NaOH solution was also used for titrations, to avoid dilution of the working solutions. The -log [H^+] and absorbance were measured after addition of a few drops of titrant, and the procedure was extended up to required -log [H^+]. A purified nitrogen atmosphere was maintained in the vessel during the titrations.

ACKNOWLEDGMENTS

Thanks are gratefully extended to the Chemistry Department of Islamic Azad University, Arak and Ayatollah Amoli Branch, for its **invaluable** help of this work.

REFERENCES

1. C. Yang, W. Xu, P. Ma, *Journal of Chemical & Engineering Data*, **2004**, *49*, 1794.
2. F. Koohyar, A.A. Rostami, M.J. Chaichi, F. Kiani, *Journal of Solution Chemistry*, **2011**, *40*, 1361.
3. M. Kondaiah, D.S. Kumar, K. Sreekanth, D. Krishna Rao, *Journal of Chemical Thermodynamics*, **2011**, *43*, 1850.
4. F. Koohyar, H. Ghasemnejad-Bosra, M. Sharifirad, *Studia UBB Chemia*, **2012**, *4*, 217.
5. F. Kiani, A. Bahadori, S. Sharifi, F. Koohyar, M. Sharifirad, *European Online Journal of Natural and Social Sciences*, **2013**, *2*, 140.
6. Y.F. Hu, *Journal of Physical Chemistry B*, **2003**, *107*, 13168.
7. A. Niazi, M. Ghalie, A. Yazdanipour, J. Ghasemi, *Journal of Spectrochimica Acta, Part A*, **2006**, *64*, 660.
8. J. Ghasemi, S. Ghobadi, B. Abbasi, M. Kubista, *Journal of Korean Chemical Society*, **2005**, *49*, 269.
9. R.H. Garrett, C.M. Grisham, "Principals of Biochemistry with a Human Focus", United States: Brooks/Cole Thomson Learning, **1997.**
10. M.A. Zajac, A.G. Zakrzewski, M.G. Kowal, S. Narayan, *Synthetic communications*, **2003**, *33*, 3291.
11. F. Gharib, M. Monajjemi, S. Ketabi, *Main Group Metal Chemistry*, **2004**, *27*, 71.
12. F. Garib, K. Zare, A. Tahghvamanesh, A. Shamel, G. Shafiee, *Main Group Metal Chemistry*, **2002**, *25*, 647.
13. A. Safavi, H. Abdollahi, *Talanta*, **2001**, *53*, 1001.
14. J. Barbosa, D. Barron, E. Jimenez-Lozano, V. Sanz-Nebot, *Analytica Chimica Acta*, **2001,** *437*, 309.
15. M.T. Ramírez-Silva, M. Gómez-Hernández, M. L. Pacheco-Hernández, A. Rojas-Hernández, L. Galicia, *Spectrochimica Acta Part A*, **2004**, *60*, 781.
16. A. Niazi, A.A. Rezaei, F. Shahhosseini, *Annali di Chimica* (Rome), **2007**, *97*, 199.
17. E. Fernández, L. García-Río, J. C. Mejuto, M. Parajó, *Spectrochimica Acta, Part A*, **2007***, 66,* 1102.
18. D. Kara, M. Alkan, *Spectrochimica Acta, Part A*, **2000**, *56*, 2753.
19. J.L. Beltrán, N. Sanli, G. Fonrodona, D. Barrón, G. Özkan, J. Barbosa, *Analytica Chimica Acta*, **2003***, 484*, 253.
20. P. Lagrange, M. Schneider, K. Zare, J. Lagrange, *Polyhedron*, **1994**, *13*, 861.
21. M.T. Beck, I. Nagypal, "Chemistry of complex equilibria", Ellis Harwood: New York, **1990**.

22. N. Maleki, B. Haghighi, A. Safavi, *Microchemical Journal*, **1999**, *62*, 229.
23. S. Sharifi, D. Nori-shargh, A. Bahadory, *Journal of Brazilian Chemical Society*, **2007**, *18*, 1011.
24. J.A. Dean, "Lange's Handbook of Chemistry", 15th ed.; McGraw-Hill, New York, **1999**.
25. P.R. Bevington, "Data reduction and error analysis for the physical sciences", McGraw-Hill: New York, **1969**.
26. M. Meloun, J. Havel, E. Hogfeldt, "Computation of solution equilibria", Ellis Harwood: New York, **1988**.
27. J. Polster, H. Lachmann, "Spectrometric titrations", Verlag Chemie: Weinheim, **1989**.
28. G.H. Golub, C.F. Van Loan, "Matrix computations", 2nd ed.; John Hopkins Univ. Press: Baltimore, **1989**.
29. W.H. Press, W.T. Vetterling, S.A. Teukolsky, B.P. Flannery, "Numerical recipes in C", Cambridge Univ. Press: Cambridge, **1995**.
30. A. Braibanti, G. Ostacoli, P. Paoleti, D. Petit, S. Smmartano, Pure *and* Applied Chemistry, **1987**, *59*, 1721.
31. D.E. Metzler, "Biochemistry, The chemical reaction of living cells", Academic press: New York, **2001**.

STUDIA UBB CHEMIA, LVIII, 2, 2013 (p. 161– 174)
(RECOMMENDED CITATION)

KINETICS AND MECHANISM OF OXIDATION OF MALIC ACID BY N-CHLORONICOTINAMIDE (NCN) IN THE PRESENCE OF A MICELLAR SYSTEM

LAKSHMINARASIMHAN PUSHPALATHA[a]

ABSTRACT The oxidation of malic acid by N-chloronicotinamide in the presence of $HClO_4$ is studied. First order kinetics with respect to NCN is observed. The kinetics results indicate fractional order in hydroxy acid. Rate of the reaction increases with a decrease in the percentage of acetic acid. Inverse first order in $[H^+]$ and [nicotinamide] are noted. Decrease in the rate constant was observed with the increase in [SDS]. The values of rate constants observed at four different temperatures were utilized to calculate the activation parameters. A suitable mechanism consistent with the experimental findings has been proposed.

Keywords: *Malic acid, N-Chloronicotinamide, kinetics, oxidation, micelles*

INTRODUCTION

The kinetics of the oxidation of hydroxy acids has been studied with a number of oxidizing agents like potassium bromate, hexamethylene-tetraminebromine, sodium N-chlorobenzenesulfonamide, N-bromoacetamide, ditelluratocuprate(III), 2,2- bipyridium chlorochromate, benzo-dipteridine etc. The presence of micelles can have marked effects on thermodynamic favorability and reaction kinetics as well as on many physical properties[1]. Organic reactions involving ionic, polar and neutral reactants in micellar solution are generally believed to occur in the Stern layer of a micelle of an ionic surfactant. The catalysis and inhibition by ionic micelles is due to ionic micellar incorporation of both the reactants. Due to these facts a significant amount of systematic kinetic results have been reported on the effect of micelles on various organic reactions during past few decades.

A.K. Singh[1] studied the kinetics and mechanism of oxidation of some hydroxy acids by N-bromoacetamide. Chand Waqar[2] investigated the

[a] *Postgraduate and Research Department of Chemistry, National College, Trichy — 620 001, Tamil nadu, India. lathaa_ramesh@yahoo.com*

mechanism of Ru(III)-catalysed oxidation of glycollic and mandelic acids with N-bromosuccinimide in acidic media**.** Pradeep K. Sharma[3] reported the oxidation of some α-hydroxy acids by tetraethylammonium chlorochromate. Ajaya Kumar Singh[4] followed the kinetic and mechanistic study on the oxidation of hydroxy acids by N-bromophthalimide in the presence of a micellar system. E.V. Sundaram[5] explained the oxidation of α-hydroxy acids with Quinolinium Dichromate. Asim K Das[6] studied the micellar effect on the reaction of Chromium(VI) oxidation of some representative alpha-hydroxy acids in the presence and absence of 2,2'-bipyridyl in aqueous acid media.

A perusal of literature shows that the reactivity of N-chloronicotinamide (NCN) could be compared with other N-haloimide such as N-bromosuccinimide (NBS) and N-bromosaccharin (NBSa). There are several reports available in the literature on the oxidation of alpha-hydroxy acids by oxidants such as N-bromosuccinimide, N-bromoacetamide, potassium bromate, N-bromobenzenesulphonamide, and iodate[7]. However, the details of oxidation of malic acid by NCN are yet to be explored. This prompted the micellar effect on the kinetics of the oxidation of the malic acid by NBN in the acidic medium.

RESULTS AND DISCUSSION

The kinetic results for the oxidation of malic acid by N-Chloronicotinamide (NCN) in the presence of surfactant (SDS) can be summarized as follows. The kinetic studies were carried out under pseudo-first order conditions with [malic acid] >> [NCN]. The kinetics of the oxidation of malic acid by NCN in presence of surfactant (SDS) and $HClO_4$ was investigated at several initial concentrations of the reactant. The reaction was of first order linearity of a plot of log [NCN] versus time for malic acid. The rate constants at different initial [NCN] are reported. Table 1 summarizes the pseudo first order rate constant's dependence on the NCN concentration. It was observed that, with the increase in initial NCN concentration, the value of rate constant decreased (Fig. 1).

At a constant value of NCN, surfactant (SDS) and $HClO_4$ the rate constant was determined at different initial concentrations of malic acid ranging from 5×10^{-3} to 50×10^{-3} mol dm^{-3}. Table 2 summarizes the pseudo first order rate constant's dependence on malic acid concentration. The rate constant, increased with increasing [malic acid]. The plot of log k versus log [malic acid] was linear with a slope of less than unity showing fractional order dependence on [malic acid] (Fig. 2).

Furthermore, a plot of log k versus malic acid was linear with an intercept on y axis, confirming the fractional order concentration dependence on substrate. The rate constant k decreased with increase in [$HClO_4$] from 5×10^{-3} to 50×10^{-3} mol dm^{-3} (Table 2) (Fig. 3).

Table 1. Effect of variation of [NCN] on reaction rate
[Malic acid]=0.03mol dm^{-3} [$HClO_4$]=0.01 mol dm^{-3}, [$NaClO_4$]=0.1mol dm^{-3}, AcOH:H_2O (1:4) Temp. =308 K [SDS]=0.01 mol dm^{-3}

[NCN] 10^4 moldm^{-3}	10^5 k_{obs} sec^{-1}
1.0	38.96
1.5	28.43
2.0	22.86
2.5	19.69
3.0	17.71
4.0	14.76
5.0	13.09

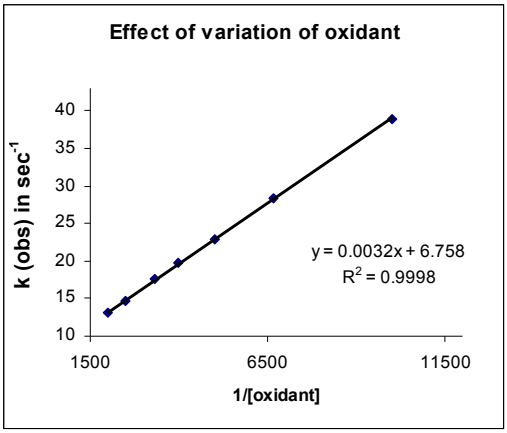

Figure 1. Effect of variation of [NCN] on reaction rate

This may be due to protonation of the substrate. The plot of log k versus log[$HClO_4$] is linear with negative slope. The slope being less than unity indicates inverse fractional order dependence on [$HClO_4$]. Successive addition of nicotinamide (as one of the oxidation products of NCN) to the reaction mixture showed a decreasing effect on the rate of oxidation of malic acid. Addition of $NaClO_4$ (to study the effect of ionic strength) in the reaction mixture showed an insignificant effect on the rate of oxidation. In order to find the effect of dielectric constant (polarity) of the medium on the rate, the oxidation of malic acid by NCN was studied in aqueous acetic acid mixtures of various compositions (Table 2) (Fig.4). The data clearly reveal that the rate of reaction increases with a decrease in the percentage of acetic acid, i.e., increasing dielectric constant or polarity of the medium leads to the inference that there is a charge development in the transition state involving a more polar activated complex than the reactants[11].

Table 2. Effect of variation of [Malic acid], [$HClO_4$] and the dielectric constant on reaction rate

10^3[MA]	10^3[$HClO_4$]	CH_3COOH %(v/v)	10^5 $k_{(obs)}$ sec^{-1}
5	10	20	9.76
10	10	20	15.39
20	10	20	24.12
25	10	20	28.15
30	10	20	31.30
40	10	20	38.29
50	10	20	44.58
30	5	20	46.38
30	10	20	28.87
30	20	20	18.11
30	25	20	15.73
30	30	20	13.86
30	40	20	11.21
30	50	20	9.72
30	10	20	27.89
30	10	25	25.15
30	10	30	22.18
30	10	40	16.17
30	10	50	10.66

[NCN]=0.00015 mol dm^{-3} [$NaClO_4$]=0.1mol dm^{-3}, Temp. =308K, [SDS]=0.01 mol dm^{-3}

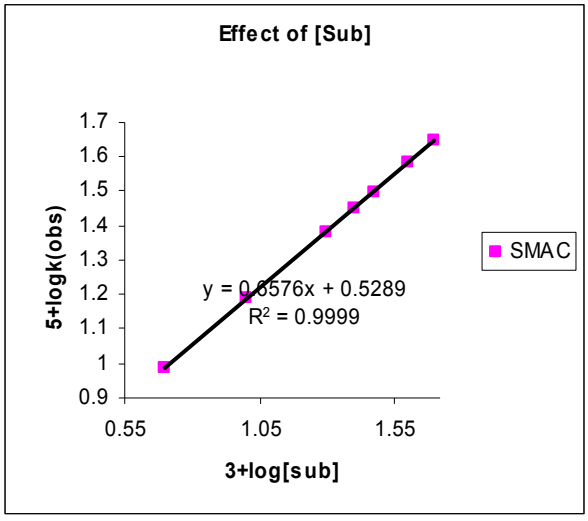

Figure 2. Effect of variation of [malic acid] on reaction rate

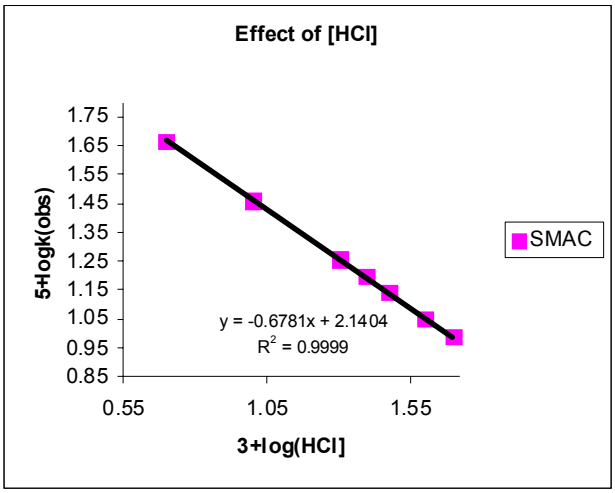

Figure 3. Effect of variation of $[HClO_4]$ on reaction rate

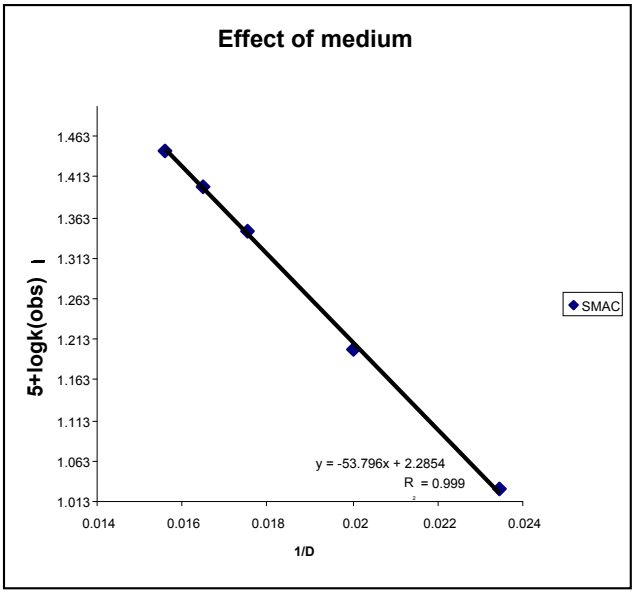

Figure 4. Effect of variation of medium on reaction rate

The effect of added salts on the rate of reaction was also explored because salts as additives, in micellar systems, acquire a special ability to induce structural changes which may, in turn, modify the substrate–surfactant interaction. In the present case, KBr has no effect whereas with the increasing concentration of KCl, rate of reaction increased.

Test for Free Radicals

To test for the presence of free radicals in the reaction, the reaction mixture containing acrylamide was kept for 24 h in an inert atmosphere. When the reaction mixture was diluted with methanol, the formation of a precipitate was not seen. This suggests that there is no possibility of formation of free radicals in the reaction.

Mechanism

It has been reported [11-16] earlier that NCN is a stable oxidizing and chlorinating agent because of the large polarity of the N–Cl bond. NCN, like other similar N-haloimides, may exist in various forms in an acidic medium, that is, free NCN, protonated NCN, Cl^+, HOClr, $(H_2OCl)^+$ according to the following equilibria[17-22].

$$NCN + H_2O \rightleftharpoons HOCl + NA \quad (1)$$

$$NCN + H^+ \rightleftharpoons NA + Cl^+ \quad (2)$$

$$NCN + H^+ \rightleftharpoons [NCNH]^+ \quad (3)$$

$$HOCl + H^+ \rightleftharpoons [H_2OCl]^+ \quad (4)$$

Addition of nicotinamide to the reaction mixture decreases the rate of oxidation in acidic media suggesting that the pre-equilibrium step involves a process in which nicotinamide is one of the products. When NCN or $(NCNH)^+$ is assumed as the reactive species, the derived rate laws fail to explain the negative effect of nicotinamide, hence neither of these species can be considered as reactive species. When $(H_2OCl)^+$ is taken as the reactive species, the rate law obtained shows first order kinetics with respect to hydrogen ion concentrations contrary to the observed negative fractional order in $HClO_4$; although it fully explains the negative effect of nicotinamide. Therefore, the possibility of cationic chlorine (Cl^+) as a reactive species is also ruled out. Thus, the only choice left is HOCl, which, when considered as the reactive species of NCN, leads to a rate law capable of explaining all the kinetics observations and other effects. Hence, in the light of kinetic observations, HOCl can safely be assumed to be the main reactive species of NCN for the present reaction. On the basis of the above experimental findings and taking HOCl to be the most reactive species of NCN, the following scheme can be proposed for the kinetics of oxidation of malic acid by NCN in acidic medium.

$$NCN + H_2O \overset{K_1}{\rightleftharpoons} HOCl + NA \quad (5)$$

$$HOCl + NA \underset{k}{\overset{K_2}{\rightleftharpoons}} X^- + (H_3O)^+ \quad (6)$$

$$X^- \xrightarrow[\text{Rate controlling step}]{} (HO)CH(CH_2COOH) + NA + CO_2 + HCl \quad (7)$$

The rate of disappearance of NCN is given as

$$-\frac{d[NCN]}{dT} = \frac{kK_1K_2[MA][NCN]_{TOTAL}}{[NA][HCl] + K_1K_2[MA]}$$

where

$[NCN]_{TOTAL} = [NCN] + [NA] + [X^-]$

The above rate law is in good agreement with the experimental results.

Influence of SDS on k_{obs}

A continuous decrease in the rate constant was observed with the increase in [SDS] at constant [MA] and [NCN] (Table 4). The inhibition effect is due to the fact that N-chloronicotinamide has N -Cl bond which it binds to SDS micelles in Stern layer, while ionized malic acid, bearing negative charge is repelled by the head group of negatively charged SDS micelles.

$$nD + S \rightleftharpoons D_nS$$

$$D_nS \xrightarrow{K_m} \text{Products}$$

$$S \xrightarrow{k_w} \text{Products}$$

Piszkiewicz[23] model assumes that '*n*' number of surfactant molecules (D) and substrate (S) aggregate to yield the catalysis aggregate D_nS which then reacts to yield the product (P). This is represented by the above scheme where K_D is the dissociation constant of micelle back to its free components and k_m is the rate of reaction within the micelle. As per the above scheme the observed rate constant (k_{obs}) is expressed as a function of surfactant concentration D, by the equation:

$$k(obs) = \frac{k_m[D]^n + kwK_D}{K_D + [D]^n}$$

$$\log\frac{k(obs) - k_w}{k_m - k(obs)} = n\log[D] - \log K_D$$

Table 3. Effect of [SDS] on reaction rate

10^3 **SDS**	10^5 $k_{(obs)}$ sec^{-1}
0	25.65
2	22.32
2.5	20.01
4	18.28
5	16.83
6	14.59
8	13.48
10	12.59
20	-
30	-
40	-
50	-
60	-
70	-
80	-
100	-
110	-
120	-
130	-

[Malic acid]=0.03 mol dm^{-3} [$HClO_4$]=0.01mol dm^{-3},[NCN]=0.0015 mol dm^{-3}
[$NaClO_4$]=0.1mol dm^{-3},AcOH:H_2O (1:4) Temp. =308K

Effect of temperature

Increase in temperature increases the rate of oxidation and plot of log k_{obs} Vs reciprocal of temperature is linear. The oxidation of malic acid by NCN was studied at different temperatures in the presence and absence of SDS (308 to 323K) (Table 4) (Fig.5) and the activation parameters were evaluated (Table 5) (Fig.6). Activation parameters are believed to provide useful information regarding the environment in which chemical reactions take place.

Table 4. Effect of Temperature on reaction rate

Temperature K	10^5 k_{obs} sec^{-1}
308	27.98
313	31.65
318	35.67
323	40.04

[Malic acid]=0.03 mol dm^{-3} [$HClO_4$]=0.01mol dm^{-3},
[NCN]=0.0015 mol dm^{-3} [$NaClO_4$]=0.1mol dm^{-3}, AcOH:H_2O (1:4)

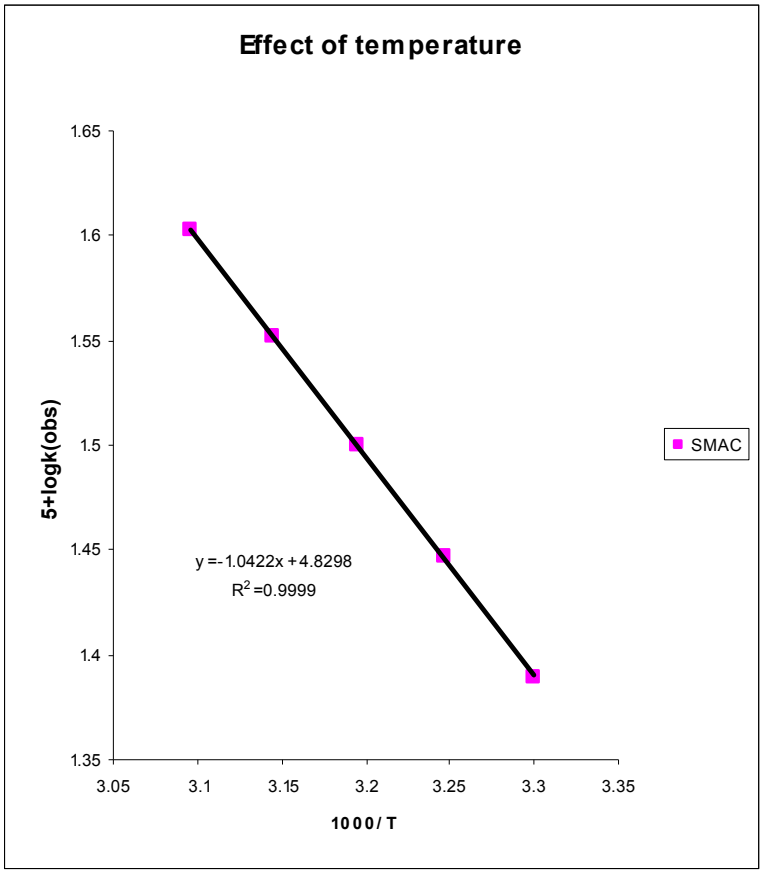

Figure 5. Effect of Temperature on reaction rate

Table 5. Effect of Temperature on reaction rate in the presence of SDS

Temperature K	10^5 k_{obs} sec^{-1}
308	25.75
313	30.02
318	34.58
323	39.79

[SDS]=0.01 mol dm^{-3}

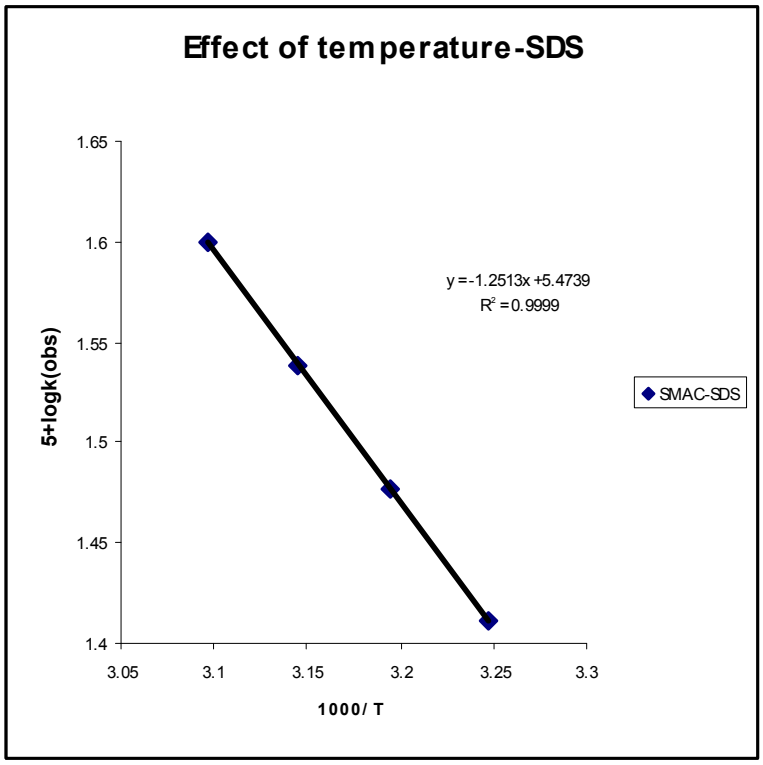

Figure 6. Effect of Temperature on reaction rate in presence of SDS

Table 6. Activation Parameters

Substrate	**E_a kJmol^{-1}**	**$\Delta H^{\#}$ kJmol^{-1}**	**$\Delta S^{\#}$ J K^{-1}mol^{-1}**	**$\Delta G^{\#}$kJmol^{-1}**
Malic acid	11.14	8.58	– 186.5	66.04
Malic acid+SDS	12.95	10.39	–180.9	66.14

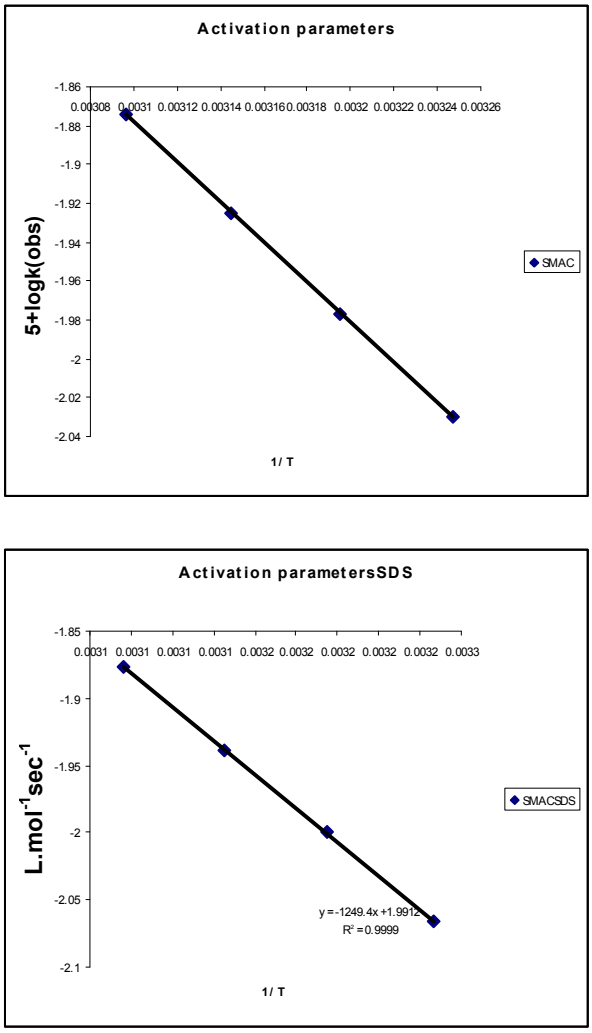

Figure 7. Activation parameters

EXPERIMENTAL

Materials and methods

N-Chloronicotinamide (NCN) was prepared by the reported method[8]. Standard solution of NCN was prepared afresh in water and its purity was checked iodometrically. Standard solutions of SDS (GR) and malic acid (Merck) were prepared using double distilled water. $HClO_4$ (A.R. grade) was diluted with double distilled water and was standardized via acid–base

titration. All other standard solutions of $NaClO_4$, KCl, KBr and nicotinamide were prepared using double distilled water. Double distilled water was distilled over $KMnO_4$ in an all glass (Pyrex) distillation set up. Distilled acetic acid was used throughout the experiment (Table 1).

Kinetic measurements

The solution of malic acid and oxidant were kept in black coated bottles separately. These solutions were kept in the thermostat to attain the thermostatic temperature. The appropriate quantity of oxidant was added to the substrate containing surfactant and other reagents and the reaction bottle was shaken well. The reaction was followed potentiometrically by setting up a cell made up of the reaction mixture into which the platinum electrode and reference electrode(SCE) were dipped. The e.m.f of the cell was measured periodically using a Equip-Tronics (EQ-DGD) potentiometer. The reactions were studied at constant temperature 35°C. Different studies such as variation of malic acid, oxidant (NCN), perchloric acid, sodium perchlorate, nicotinamide, surfactant and temperature were carried out. The reaction was carried out under pseudo-first order condition ([malic acid] >>[NCN]). The pseudo-first order rate constants were computed from the linear ($r^2 > 0.9990$) plots of log (E_t–E_∞) against time. Duplicate kinetic runs showed that the rate constants were reproducible within ±3%. The course of the reaction was studied for more than two half-lives.

Stoichiometry

The reaction mixture containing a known excess of [NCN] >> [malic acid] was kept in the presence of $HClO_4$ and at 40°C for 72 h. After completion of the reaction, the unconsumed NCN was calculated iodometrically. It was found that nearly 2 moles of NCN were consumed for each mole of malic acid.

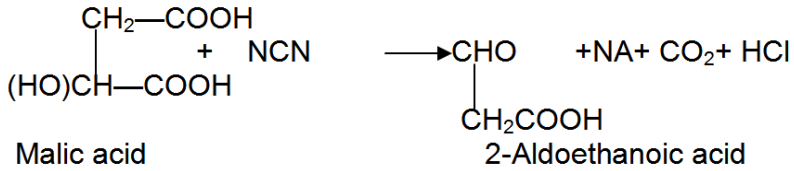

Product analysis

The presence of carbonyl compound (2-aldoethanoic acid) as the main product of oxidation was detected by the spot test [9] and the 2,4-dinitrophenylhydrazine method [10].

CMC determination

Surfactants spontaneously aggregate above a certain concentration called critical micelle concentration (CMC) to form micelle, whose determination has considerable practical importance, normally to understand the self-organizing behavior of surfactants in exact ways. Micelles act as microreactors, which can both speed or inhibit the rate of uni- and bimolecular reactions. Micelle aggregates affect chemical reactivity primarily by binding or excluding reactants and only secondarily by changing the free energy of activation. The critical micelle concentration values of the surfactant (SDS) was determined conductometrically (Digital conductivitymeter, model 611E, Electronic India Company) in the presence and absence of reactants at 40°C. The CMC value was determined from plot of the specific conductivity versus surfactant concentration. The breakpoints of nearly straight-line portions in the plot are taken as an indication of micelle formation, and these correspond to the CMC of surfactant. The CMC values of SDS in different experimental conditions at 40°C are summarized in Table 8. The CMC value is lower than that given in the literature for aqueous solutions of SDS without added electrolyte, which was found to be approximately about 3.21×10^{-3} mol dm^{-3} in reaction mixture for malic acid.

Table 8. Critical micelle concentration (CMC values of SDS in different experimental conditions)
[Malic acid]=0.03mol dm^{-3} [$HClO_4$] = 0.01 mol dm^{-3}, [$NaClO_4$]=0.1mol dm^{-3}, AcOH:H_2O (1:4) Temp. =308 K

Solutions	10^3 CMC mol dm^{-3} **SDS**
Water	7.9
Water+NCN	7.1
Water+malic acid	4.2
Water+malic acid+NCN+ $HClO_4$+20% v/v AcOH	2.8

CONCLUSIONS

In the light of kinetic observations for the micellar effect on the kinetics of oxidation of malic acid by N-chloronicotinamide in the presence of perchloric acid, the following conclusions can be easily drawn: the reactive species of oxidant NCN is HOCl not NCN itself, the reaction rates are enhanced by increase in [malic acid] and temperature. Added nicotinamide retards the rate. 2-Aldoethanoic acid is the product of oxidation. Activation parameters were evaluated for both catalyzed and unanalyzed reactions. The critical micelle concentration is much lower than values that given in the literature for aqueous solutions of SDS without added electrolyte. The rate of oxidation slightly

decreases with increasing concentration of SDS. The micellar effect can be correlated with the nature of the reducing substrates and the reactions conditions. These micellar effects are quite important to understand and to substantiate the proposed mechanistic pathways. This may widen the applicability of NCN as oxidant in organic synthesis.

ACKNOWLEDGEMENTS

The author gratefully acknowledges her husband Mr. A. Ramesh for the moral support.

REFERENCES

1. Madhu Saxena, Ranjana Gupta; Amar Singh; Bharat Singh; Singh, A.K. *Journal of Molecular Catalysis*, **1991**, 65(3), 317.
2. Chand Waqar, Bharat Singh, Sharma, J.P. *Journal of Molecular Catalysis*, **1990**, 60(1), 49.
3. D. Preeti Swami, P. Yajurvedi, Mishra, Pradeep K. Sharma, *International Journal of Chemical Kinetics*, **2010**, 42(1), 50.
4. Patil Sangeeta, Y.R. Katre, Ajaya Kumar Singh, *Journal of surfactants and detergents,* **2007**,10(3),175.
5. Kailasa Aruna, Prerepa Manikyamba, Embar Venkatachari Sundaram, *Collection of Czechoslovak Chemical Communications*, **1978,** 58(7), 1624.
6. Ruhidas Baeyen, Mohirul Islam, Asim K. Das, *Indian Journal of chemistry*, **2009**, 48A, 1055.
7. Sangeeta Patil, Y.R. Katre, Ajaya Kumar Singh, *Colloids and Surfaces. A: Physicochem. Eng. Aspects,* **2007**, 308, 6.
8. K, Vivekanandan, K, Nambi, *Indian J. Chem., Sect. B*, **1996**, 35, 1117.
9. F. Feigl, *Spot test in Organic Analysis,* Elsevier, New York, **1975**,425.
10. A. Mathur, V.Sharma, K.K.Banerji, *Ind. J. Chem.,* **1988**, 27A, 123.
11. L. Pushpalatha, K. Vivekanandan, *J. Indian Chem. Soc*., **2009,** 86, 475.
12. L. Pushpalatha, K. Vivekanandan, *Oxid. Commun*., **2009,** 32(1), 85.
13. L. Pushpalatha, K. Vivekanandan, *Oxid. Commun*., **2008**, 31(3), 598.
14. L. Pushpalatha, K. Vivekanandan, *J. Indian Chem. Soc.,* **2008**, 85, 1027.
15. L. Pushpalatha, K. Vivekanandan, *Oxid. Commun*., **2010**, 33(4), 851.
16. L. Pushpalatha, *Oxid. Commun*., (in press).
17. L. Pushpalatha, K. Vivekanandan, *Oxid. Commun*., (in press).
18. L. Pushpalatha, K. Vivekanandan, *Oxid. Commun*., (in press).
19. L. Pushpalatha, K. Vivekanandan, J. Indian Chem. Soc., **2010**, 87, 1221.
20. L. Pushpalatha, *Afinidad,* **2011**, 68, 551.
21. L. Pushpalatha, *International Journal of Chemistry,* **2012**,1(2), 199.
22. L. Pushpalatha, K. Vivekanandan, M.N.Abubacker, *J. Indian Chem. Soc*., **2013***,* 90, 1027.
23. D.J. Piszkiewicz, *J. Am. Chem. Soc.* **1977**, 99, 7695. A.V. Hill, *J. Physiol*. **1910**, 40, 4.

STUDIA UBB CHEMIA, LVIII, 2, 2013 (p. 175 – 183)
(RECOMMENDED CITATION)

THE ANTIOXIDANT ACTIVITY OF TEA INFUSIONS TESTED BY MEANS OF BRIGGS-RAUSCHER OSCILLATORY REACTION

NORBERT MUNTEAN[a], GABRIELLA SZABÓ[a]

ABSTRACT. The antioxidant capacity of tea extracts was determined by means of Briggs-Rauscher oscillating system in batch conditions. This method consists in the measurement of the inhibition time caused by the addition of tea extract to the oscillating system. The inhibition time vs. the concentration of tea extract shows linear dependence.

Keywords: *Briggs-Rauscher oscillating reaction, inhibitory effect, analytical method, tea extract*

INTRODUCTION

The tea is one of the most popular worldwide beverages and a major source of dietary antioxidants.

In 2011, researchers have conducted a trial to test the effects of rooibos tea on various biological markers, considered to be indicative of risk for cardio-vascular disease and other degenerative diseases. A high intake of rooibos tea resulted in significant reductions in lipid peroxidation, LDL cholesterol, triglycerides, and an increase in HDL cholesterol levels compared with the control group. The researchers concluded that rooibos lowered the risk factor [18].

The main flavonoids found in fresh tea leaves are the catechins (flavan-3-ols, or flavanols) and the flavonols. These flavonoids represent usually more than 30% of the dry weight of the leaves. Two flavonoids were found in rooibos, the quercetin and luteolin, and they are used in cancer therapy [1]. The rooibos leaves do not contain the antioxidant catechins [2]. The differences between the white, green and black tea is the processing method of them. In order to prepare white tea the leaves are collected in spring, when the leaves are covered with white dust. White tea and green

[a] *Department of Chemistry and Chemical Engineering, "Babeş-Bolyai" University, Cluj-Napoca,11 Arany Janos Str, Romania, RO-400028, E-mail: gszabo@chem.ubbcluj.ro.*

tea are produced using thermal processes, such as steaming or dry heating, to inactivate polyphenol oxidase that oxidize catechins to more complex oligomeric flavonoids characteristic of oolong and black teas.

During the manufacture of black and red teas, the colorless, monomeric catechins are converted to orange-yellow- and red-brown-colored oligomeric flavonoids. Additionally, oxidation of amino acids and lipids occurs with the generation of numerous volatile flavor compounds. These oxidative changes are reflected in the red-amber color, reduced bitterness, and increased astringency and more complex flavor of black teas. Green and white tea beverages contain 30–130 mg Epigallocatechin gallate (EGCG) per cup of tea, while black tea beverages 0–70 mg EGCG per cup of tea. The flavonols, such as quercetin, kaempferol, myricetin, and their glycosides, are present in much lower concentrations than the catechins and are found in comparable quantities in black, green, and oolong tea beverages (5–15 mg/cup) [3-6].

Tea polyphenols, especially the catechins, are possible antimicrobial and antioxidant agents, with positive effects on human health. The antioxidant activity can be determined by some well known analytical methods. All these methods are based on the generation of free radicals in the reaction mixture followed by their detection. In the presence of antioxidants, the amount of the free radicals detected is much less in comparison with that of a reference mixture. These are for example: *Franckel, Pryor* rapid screening, TEAC (trolox equivalent antioxidant capacity), TRAP (total radical-trapping antioxidant parameter) method, the FRAP (ferric reducing-antioxidant power) method [7].

The Briggs-Rauscher (BR) reaction, one of the few reactions showing long lived oscillations in batch conditions, was discovered by Briggs and Rauscher. Its classical version is the oscillatory oxidation and iodination of malonic acid (MA) by hydrogen peroxide and iodate, catalyzed by Mn^{2+} ions in acidic medium. The reaction was studied by many research groups, including that lead by Noyes, Furrow, Cervellati and Sørensen [8-10]. Recently a new method was developed based on the inhibition of the well known oscillatory system, the BR reaction [14]. An oscillating reaction is very sensitive -because it is far away from chemical equilibrium - and this behavior is used in analytical determinations.

Oscillations can be demonstrated by vivid color changes in the presence of a starch indicator or usually they are monitored by recording platinum or iodide selective electrode potentials vs. a reference electrode. Kinetically important intermediates are I_2, I^-, I_3^-, O_2, CO_2, CO, HOI, HOO° and iodomalonic acid (IMA) [10-13].

The basis of this analytical method consists in the fact that various antioxidants (mono- and polyphenolic compounds), change the dynamics of the BR reaction fundamentally by suppressing the oscillations even in a surprisingly low concentration (usually in a few micromoles/liter).

This kind of micro-analytical technique is used to determine the antioxidant capacity of various chemical compounds or plant extracts. Cervellati *et al*.[14] reported that the addition of mono- and polyphenolic compounds to the active mixture causes a temporary but instant cessation of oscillations. The time elapsed between the cessation and the subsequent regeneration of the oscillatory regime is the so called inhibition time. A linear correlation was found between the concentration and the inhibition time for numerous phenolic substances added to the BR-mixture

The inhibitory effect was accounted for a fast reaction involving the phenol compound and HOO• radical. Since polyphenols are known free radical scavengers, they can reduce the concentration of HOO• in the BR-mixture [15-17].

According to the suggested mechanism, as soon as the antioxidant is consumed, the HOO• concentration rises to a critical level where the oscillations can reappear.

In this study was made a comparison of white, green, black and rooibos tea's activity. The first three were prepared from the processed young leaves of *Camellia sinensis*, and the last one from the leaves of *Calicotome villosa*.

The study presented in this article is divided in two parts; first the development of the optimal composition of the BR mixture, and in the second part is presented the determination of antioxidant activity of white, green, black and rooibos tea.

It is worth mentioning that, no studies have been published so far, in which the antioxidant capacity of tea was determined by means of BR method.

RESULTS AND DISCUSSION

The optimal composition of the BR mixture

By varying the concentrations of iodate, hydrogen peroxide and H_2SO_4, we expected to obtain a better composition of the mixture with higher amplitude of the oscillations and a longer inhibition time.

These two factors are the most important characteristics of the oscillations; the higher the values of these parameters, the larger the domain of the applications of oscillatory reactions.

Increasing the amplitude of the oscillations the switch between oscillation and inhibition is sharper. On the other hand, the oscillation period is a limitative factor for the inhibition time. In the figure 1 are presented the variations of these parameters vs. the concentration of one of BR mixture's component, and the optimal ones are encircled. The concentrations of the other components in the reactor was kept constant and they were $[Mn^{2+}]$ = 65 mM, [MA] = 50 mM, $[H_2SO_4]$ = 25 mM, $[KIO_3]$ = 67 mM, if it's not mentioned otherwise.

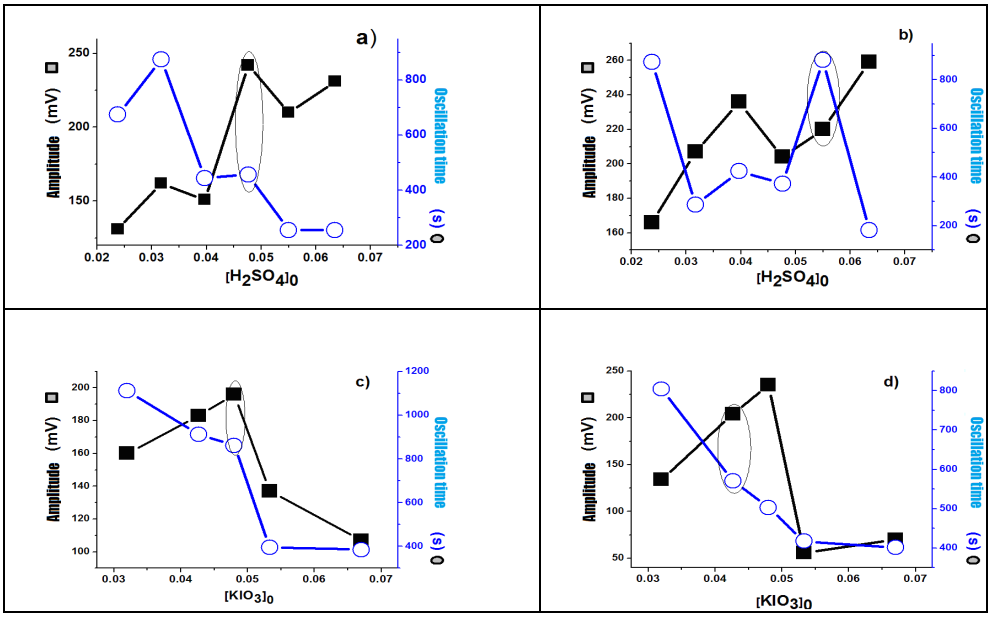

Figure 1 The values of amplitude and the duration of the oscillations as a function of initial concentration of H_2SO_4, figs. a) and b), The values of amplitude and the duration of the oscillations as a function of initial concentration of KIO_3 figs. c) and d) The H_2O_2 concentration was 0.65 M in figs. a) and c) and in figs. b) and d) it was 1.32 M

It can be concluded, that the optimal concentrations for BR method are $[H_2SO_4]_0$= 55 mM, $[KIO_3]_0$= 45 mM, $[MA]_0$= 50 mM, $[MnSO_4]_0$= 65 mM, $[H_2O_2]_0$= 1.32 M

The antioxidant activity of teas

Perturbation of the oscillatory BR system with a tea extract causes the immediate cessation of the oscillations; the time elapsed between the cessation and returns of the oscillations, the so called inhibition time is illustrated in Figure 2.

Using the optimal composition for the BR, the different tea extracts antioxidant activity was determined for several dilutions and the calibration curves were drawn for each of them. Variation of the inhibition time in function of the antioxidant concentration was found to be linear as can be seen in figure 3.

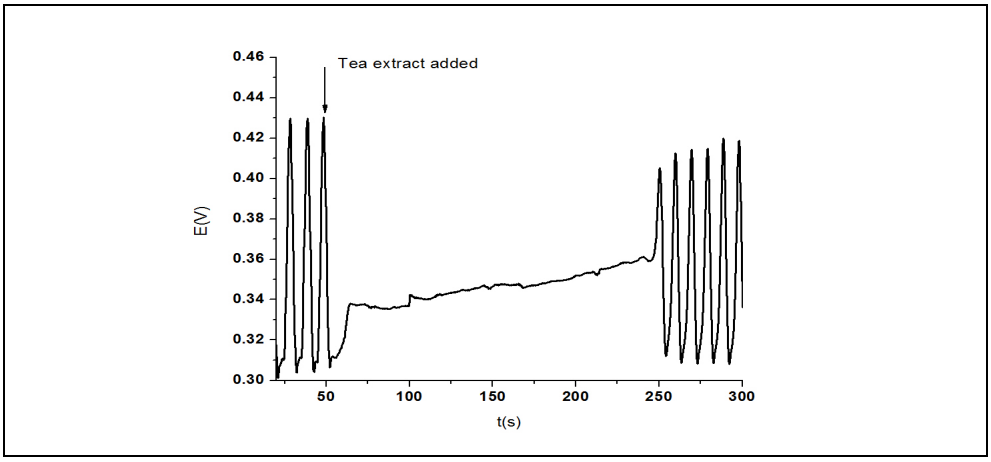

Figure 2. The effect of the roiboos tea extract on the active BR mixture. At the moment indicated by the arrow 0.35 ml of extract was added to the mixture

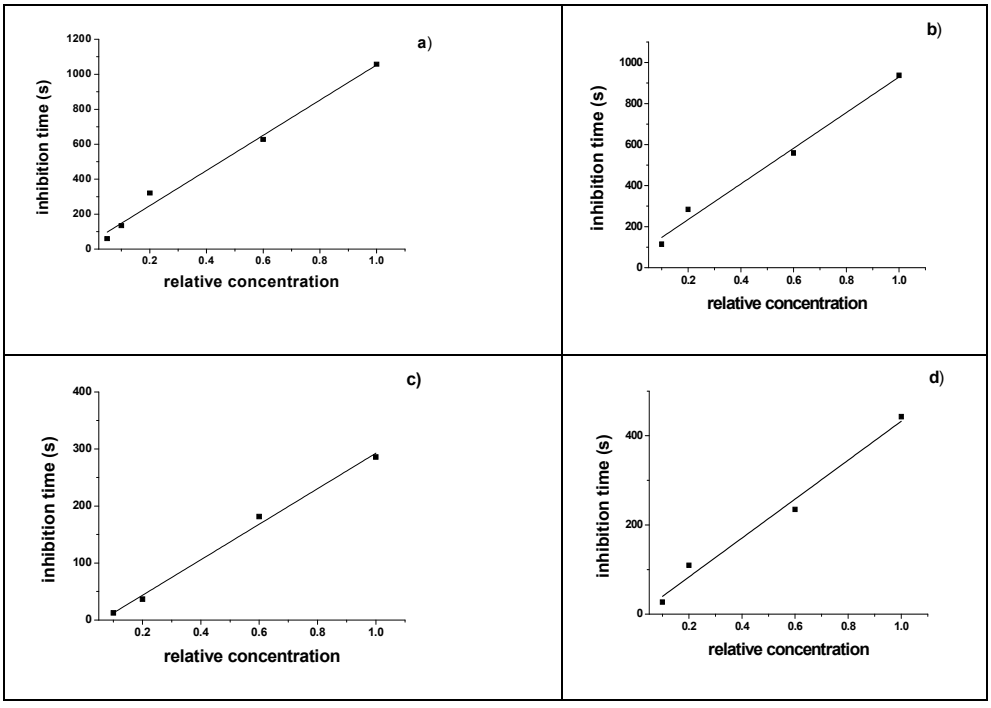

Figure 3. The calibration curves of the tea extracts: a) green tea; b) white tea; c) black tea; d) roiboos tea;

The following equations can be achieved after applying the linear fitting.

t_{inh}=47(±3.29) +1006.6(±6.18) *[green tea]

t_{inh}=60(±3.80) +868.9(±6.41) *[white tea]

t_{inh}=-3.8(±2.28) +436.5(±3.84) *[black tea]

t_{inh}=-18.8(±0.98) +311.4(±1.63) *[roiboos tea]

The antioxidant activity of the extracts was compared with that of the chosen standard (green tea) and R.A.C (relative antioxidant activity related to concentration) was calculated: the ratio between the concentrations of a sample and that of the chosen standard (*green tea*) that give the same inhibition time.

R.A.C. = [standard]/[sample]

R.A.S (relative activity with respect to slopes): the ratio between the slope of the straight line of the sample and that of the chosen standard (*green tea*).

R.A.S. = slope(sample)/slope(standard).

The results are presented in table 1.

Table 1. Values R.A.C and R.A.S for investigated sorts of tea

	R.A.C			
Relative concentration	**Green tea**	**White tea**	**Black tea**	**Roiboos tea**
0.1	1	0.85	0.20	0.10
0.2		0.88	0.34	0.10
0.6		0.89	0.37	0.29
1		0.89	0.42	0.27
R.A.C medium		**0.88**	**0.33**	**0.19**
R.A.S		***0.86***	***0.43***	***0.31***

CONCLUSIONS AND OUTLOOK

The active BR system was used as an analytical method to determine the antioxidant activity of some tea extracts. The analytical sign was the inhibition time which shows linear dependence vs. the concentration. Using the calibration curves two type of relative antioxidant activity was calculated. The R.A.C value show us the sample amount with the same antioxidant activity as the chosen reference (in our case the green tea), the R.A.S show to us the increase of the antioxidant activity with the concentration. The following order of antioxidant activity was found:

Green tea >white tea>black tea> rooibos tea

It can be concluded (using the R.A.C medium value) that approximately three cups of black tea or five cups of roiboos tea has the same antioxidant activity as one cup of green tea, white tea has almost the same activity as green tea. However the advantage of the roiboos tea is due to the absence of caffeine in its composition and because of this can be consumed by peoples with cardio-vascular disease history.

It is to be mentioned that the same order was established by means of TEAC method of determining the antioxidant capacity.

Our future investigation will be focused on the synergetic effect of them.

EXPERIMENTAL SECTION

The instrumental set-up used to implement the proposed method consisted of a double walled glass vessel of 10 mL capacity. Connection to a FALC FA 90 thermostat ensures a constant temperature by water circulation through the temperature jacket. We have chosen a value of 20°C.

Oscillations were monitored with a Pt electrode and an Ag/AgI indicator electrode, both handmade. In the BR reaction both the Platinum and the Ag/AgI electrodes are so called “indicator “ electrodes i.e. their potential oscillate with respect to a reference electrode.

Such a reference electrode should be connected to the system via a double junction salt bridge. To fit a double junction salt bridge into the reactor, however, increases the reactor volume considerably.

Moreover the liquid–liquid junction of a salt bridges always a source of contamination and “memories”.

To keep the reactor volume at a minimum and to avoid memory effects we applied two indicator electrodes. The voltage between these electrodes in the BR reaction was found to be still oscillatory thus the dynamic state of the reactor can be followed by recording that voltage. Potentiometric traces recorded this way were quite reproducible. [19]

They were connected to a PC through a PCI 6036 E data-acquisition interface.

Tea extracts were made using boiled distilled water. Each plant (0.15 g) was mixed with 100 mL of boiling water for 5 min, with constant shaking and the samples were filtered through filter paper. These extracts were considered the stock solutions, and different dilutions were made (for example 10 mL of the stock solution was diluted to 100 mL). The concentration of the diluted solutions –presented in table 1- is related to these ones.

Chemicals and procedure

All chemicals were of analytical grade and were used without further purification. Stock solutions with the following concentration were made: $[H_2SO_4]_0$=220 mM, $[KIO_3]_0$= 180 mM, $[MA]_0$=200 mM, $[MnSO_4]_0$=260 mM, $[H_2O_2]_0$=5.28 M by using double distilled water. In the reactor they were diluted 4 time.

The mixing order was: malonic acid, $MnSO_4$, H_2SO_4, KIO_3, and H_2O_2. Oscillations start after the addition of H_2O_2. At the third oscillation 0.35 mL of tea extract was added to the reactor using a micropipette. The experimental dates were processed by Origin 8 software.

ACKNOWLEDGMENTS

The research was made with the financial support of: POSDRU 89/1.5/S/60189.

REFERENCES AND NOTES

1. Harbowy M, Balentine DA. Tea chemistry: *Crit Rev Plant Sci* **1997***; 16:415–480.*
2. Marongiu, B., Porcedda, S., Piras, A., Rosa, A., Deiana, M., & Dessi, M.A.: *Phyt. Res.,* **2004,** *18(10), 789–792.*
3. Peterson, J., Dwyer, J., Bhagwat, S., Haytowitz, D., Holden, J., Eldridge, A.L.: *J. of Food Comp. and Analy.,* **2005***, 18(6), 487–501.*
4. Wang, H.; Cao, G.; Prior, R. L.: *J. Agric. Food Chem.* **1996***, 44, 701-705.*
5. Ehlenfeldt, M.K.; Prior, R.L.: *J. Agric. Food Chem.* **2001***, 49, 2222-2227.*
6. Connor, A.M. **Variation and heritability of antioxidant activity and its relationship to anthocyanin content and total phenolic content in blueberry** (*Vaccinium* subspecies *Cyanococcus*): Ph.D Dissertation, **2001**, Department *of Horticultural Science, University of Minnesota, St. Paul, MN*.
7. Kalt, W.; McDonald, J.E.; Donner, H. *J. Food Sci*. **2000**, *65*, *390-393*.
8. L. Onel, G. Bourceanu, M. Wittmann, Z. Noszticzius, G. Szabó: *J. Phys. Chem. A*., **2008**, *112, 11649-11655*.
9. T. Lawson, J. Fülöp, M. Wittmann, Z. Noszticzius, N. Muntean, G. Szabó, L. Onel: *J. Phys. Chem. A*., **2009**,*113, 14095-14098*.
10. N. Muntean, G. Szabó, M. Wittmann, T. Lawson, Z. Noszticzius, J. Fülöp, L. Onel: *J. Phys. Chem. A.* **2009** *113*, *9102-9108*.
11. S.K.Scott, **Oscillations waves and chaos in chemical kinetics,** *Oxford* **1998.**
12. R. Epstein, J.A. Pojman, **An introduction to nonlinear chemical dynamics,** *Oxford* **1998.**

13. R. Cervellati, N. Crespi-Perellino, S.D. Furrow, M. Anacleto: *Helv.Chim.Acta*, **2000**, *83: 12, 3179 – 3190*.
14. R. Cervellati, K. Hoener, S. D. Furrow, C. Neddens, S. Costa: *Helv.Chim.Acta,* **2001,** *84: 12 3533 – 3547*.
15. R. Cervellati, C. Renzulli, M.C. Guerra, E. Speroni: *J. Agric. Food Chem.*, **2002,** *50, 7504-7509*.
16. R Cervellati, K. Hoener, S.R. Furrow, F. Mazzanti F: *Helv.Chim.Acta,* **2002***, 85: 8 2523 – 2537*.
17. Marnewick, J.L.; Rautenbach, F.; Venter I.; Neethling H.; Blackhurst, Dee M.; Wolmarans P.; Macharia M: *J. of Ethnopharm.,* **2011,** *133 (1): 46–52.*
18. Norbert Muntean, Lawson Bich Thuy, Kristóf Kály-Kullai, Maria Wittmann, Zoltán Noszticzius, Lavinia Onel, Stanley D. Furrow: *J. Phys. Chem. A* **2012**, *116, 6630−6642.*